SACLANTCEN
Conference Proceedings No. 32

PART 1
Pages 1 to 12-10

SACLANT ASW
RESEARCH CENTRE

UNDERWATER AMBIENT NOISE

Proceedings of a conference held at SACLANTCEN
on 11-14 May 1982

VOL. II UNCLASSIFIED PAPERS

Organized by

RONALD A. WAGSTAFF and OREST Z. BLUY

15 JUNE 1982

NORTH
ATLANTIC
TREATY
ORGANIZATION

LA SPEZIA, ITALY

Compiled and Published by

SACLANTCEN

SACLANTCEN
CONFERENCE PROCEEDINGS NO. 32

NORTH ATLANTIC TREATY ORGANIZATION
SACLANT ASW Research Centre
Viale San Bartolomeo 400, I-19026 San Bartolomeo (SP), Italy.

tel. national 0187 560940
international + 39 187 560940

telex: 271148 SACENT I

UNDERWATER AMBIENT NOISE

Proceedings of a Conference held at SACLANTCEN
on 11-14 May 1982

VOL. II UNCLASSIFIED PAPERS
(Part 1: Pages 1 to 12-10)

Organized by
Ronald A. Wagstaff and Orest Z. Bluy

15 June 1982

LIST OF PARTICIPANTS

CANADA

Fraser, I.A.
Canadian Defence Research
Establishment, Atlantic
Dartmouth, NS

Kennedy, J.S.
Canadian Defence Research
Establishment, Pacific
Victoria, B.C.

Sloboda, R.S.
Canadian Defence Research
Establishment, Pacific
Victoria, B.C.

DENMARK

Bjørnø, L.
Technical Univ. of Denmark
Lyngby

Dahl, P.
Naval Materiel Command
Copenhagen

FRANCE

Bienvenu, G.
Thomson-CSF
Cagnes-sur-Mer

de Raigniac, B.
Société AERO
Paris

Laval, R.
Societé AERO
Paris

Lucas,
GERDSM, DCAN,
Toulon

Pene, J.
Centre d'analyse de défense
Arcueil

Plaisant, A.
Thomson CSF DASM
Cagnes-sur-Mer

FRANCE (Cont'd)

Roy, J.
GERDSM, DCAN
Toulon

Tanguy, A.
GERDSM
Le Brusc
Six-Fours

GERMANY

Bachor, W.
ERPST 71
Eckernfoerde

Bendig, H.
Krupp Atlas-Elektronik
Bremen

Geyer, D.
Forschungsanstalt der Bundeswehr
fur Wasserschall- und Geophysik
Kiel

Maass, G.
BWB
Koblenz

Rottpeter, O.H.
Erprobungsstelle, 71
der Bundeswehr
Eckerntoerde

Scholz, B.
Forschungsanstalt der Bundeswehr
fur Wasserschall- und Geophysik
Kiel

Urban, H.
Krupp Atlas-Elektronik
Bremen

Wille, P.
Forschungsanstalt der Bundeswehr
fur Wasserschall- und Geophysik
Kiel

Ziehm, G.
Forschungsanstalt der Bundeswehr
fur Wasserschall- und Geophysik
Kiel

ITALY

Diamanti, E.
MARIPERMAN
La Spezia

Tacconi, G.
University of Genova
Genova

NETHERLANDS

Blok, H.
LEOK TNO
Oegstgeest

Schippers, P.
TNO Physics Laboratory
The Hague

NORWAY

Grenness, Ø
Norwegian Defence Research Est.
Horten

Johnsen, J.
Norwegian Defence Research Est.
Horten

Sevaldsen, E.
Norwegian Defence Research Est.
Horten

UK

Bourke, R.M.
Scott Polar Research Institute
Cambridge

Evans, P.
Admiralty Underwater Weapons Est.
Portland

Lindop, P.H.
Admiralty Underwater Weapons Est.
Portland

Nicholas, P.J.
MOD
London

Pyett, J.S.
Admiralty Underwater Weapons Est.
Portland

UK (Cont'd)

Roe, J.N.
18 Group, RAF
Northwood

US

Achee, E.
Rockwell International
Arlington, VA

Anderson, A.
US Naval Ocean Research and
Development Activity
Bay St. Louis, MS

Andrews, J.
US Naval Ocean Research and
Development Activity
Bay St. Louis, MS

Blumenthal, I.S.
Rand Corporation
Santa Monica, CA

Bond, J.W.
US Naval Ocean Systems Center
San Diego, CA

Cavanagh, R.C.
Planning Systems Incorporated
McLean, VA

Chaika, E.
US Naval Ocean Research and
Development Activity
Bay St. Louis, MS

Dentino, M.
Rockwell International
Arlington, VA

Di Loreto, E.
US Naval Ocean Systems Center
San Diego, CA

Diachok, O.K.
US Naval Research Laboratory
Washington, DC

Dwyer, R.F.
US Naval Underwater Systems Center
New London, Conn.

US (Cont'd)

Ficarra, J.
Norden Systems
New York, NY

Floyd, E.R.
US Naval Ocean Systems Center
San Diego, CA

Hanrahan, J.J.
US Naval Underwater Systems Center
New London, CT

Heine, J.C.
Bolt Beranek and Newman Inc.
Cambridge, MA

Holland, J.P.
Applied Research Laboratory
State College, PA

Ingenito, F.
US Naval Research Laboratory
Washington DC

Jennings, C.
Rockwell International
Arlington, VA

Lange, D.M.
Norden Systems
Melville, NY

McCloskey, T. (Capt USN)
Chief of Staff
Cmdr Area ASW Forces
US 6th Fleet

Magaraci, A.
Sonalysts Inc.
Waterford, CT

Marshall, S.
US Naval Ocean Research and
Development Activity
Bay St. Louis, MS

Medwin, H.
US Naval Postgraduate School
Monterey, CA

Mosely, W.
US Naval Research Laboratory
Washington D.C.

US (Cont'd)

Nuttal, A.H.
US Naval Underwater Systems Center
New London, CT

Owsley, N.L.
US Naval Ocean Research
and Development Activity
Bay St. Louis, MS

Picard
ASW Forces
US 6th Fleet

Ross, D.
Donanco, Inc.
La Jolla, CA

Sevik, M.M.
David Taylor Naval Ship R&D Center
Bethesda, MD

Shanahan, W.J.
Norden Systems
Melville, NY

Shonting, D.H.
US Naval Underwater Systems Center
Newport, RI

Solomon, L.P.
US Naval Ocean Research
and Development Activity
Bay St. Louis, MS

Strasberg, M.
David Taylor Naval Ship R&D Center
Bethesda, MD

Thoma, D.C.
Mantech Int. Corp.
Arlington, VA

Tyce, R.C.
Scripps Institution of Oceanography
San Diego, CA

Wheatley, B.N.
US Naval Ocean Research and
Development Activity
Bay St. Louis, MS

Williams, Bruce R.
Scripps Institution of Oceanography
San Diego, CA

US (Cont'd)

Wilson, J.H.
Science Applications, Inc.
Canoga Park, CA

Wolf, S.N.
US Naval Research Laboratory
Washington, DC

Young, E.T.
Office of Navy Technology
Bay St. Louis, MS

SACLANTCEN (presenting papers)

Berrou, J.L.
Bluy, O.Z.
Goudriaan, E.
Groen, M.
Hamson, R.
Schmalfeldt, B.
Van Asselt, H.
Wagstaff, R.A.

TABLE OF CONTENTS

Table of Contents (Cont'd)

Table of Contents (Cont'd)

INTRODUCTION

This document is one of two* that reproduce the papers given at a conference on underwater ambient-noise held at the SACLANT ASW Research Centre during the period 11-14 May 1982. The participants were from nine NATO nations and 2 NATO Commands. The objective of the conference was to provide a mechanism for the NATO nations to compare notes on research related to undersea ambient noise and to help establish a common basis for future research. Thirty eight papers were presented on ambient noise and related topics, which included

- Needs of the ASW operational community
- The role of acoustic propagation
- Sources of noise
- Measurement results
- Noise modelling
- Applications in signal processing

For presentation at the conference the papers were grouped into sessions according to the contents given to the organizers in the abstracts. However, because of the limited information available in their abstracts some papers were inappropriately categorized. The categories chosen for publication are therefore as follows:

I	Background
II	Mechanisms
III	Low-Frequency Phenomena
IV	Measurements and Measurement Techniques
V	Processing Techniques
VI	Modelling: development and use
VII	Acoustic Propagation effects

The specific role of certain of the papers presented requires a few lines of explanation, as follows:

---

*WAGSTAFF, R. and BLUY, O.Z. eds. Underwater ambient noise: Classified papers presented at a conference held at SACLANTCEN, 11-14 May 1982, SACLANTCEN CP-31, NATO CONFIDENTIAL. La Spezia, Italy, SACLANT ASW Research Centre, 1982.

*WAGSTAFF, R. and BLUY, O.Z. eds. Underwater ambient noise: Unclassified papers presented at a conference held at SACLANTCEN, 11-14 May 1982, SACLANTCEN CP-32. La Spezia, Italy, SACLANT ASW Research Centre, 1982.

a) The Role of Propagation

Dr Donald Ross of Donanco, Inc. was invited to present a paper on the role of propagation, because the conference organizers are firmly convinced that one must have a good general understanding of acoustic propagation in order to understand ambient noise. There are many acoustic propagation mechanisms that play a dominant role in ambient noise, such as the effects of bathymetric shielding on the depth dependence of noise and down-slope enhancement of the noise in the SOFAR channel. While it may not be necessary to be able to derive and solve the equations that govern these mechanisms, it is necessary to realize their importance and to be able to turn to the literature for more detail when needed. This paper helps to provide such an understanding.

b) Signal Processing

Because signal-processing techniques designed for ASW purposes must operate against a background of ambient noise, the organizers encouraged the participation of signal processors in the conference. The signal-processing researcher often assumes that the ambient noise can be characterized in a given way, such as having a gaussian distribution. These assumptions may not be correct and may be responsible for the ultimate failure of the signal-processing technique. It is up to the ambient-noise community to provide the signal-processing community with the characteristics of the noise field and noise models in forms useful to them. This, of course, cannot be done unless there is communication between the two communities on what is needed, what can be done, and what is the desired format. The papers presented at the conference help to bridge this gap.

c) Operational Research

It was the belief of the conference organizers, and was a general impression at the end of the conference, that the ambient-noise community has not succeeded very well in getting its products to the ASW operational community in a format that is useful to them. The ASW operators are really interested in addressing issues that the ambient-noise community is not equipped to tackle, such as the optimum deployment of ASW assets. The ambient-noise products are a small but important part of the total solution. However, ambient-noise results are just raw data to them and it requires a lot of effort and a high level of expertise to use them correctly. The role of the operational research people is to bridge this gap. This can be done effectively only when they receive the necessary inputs from the ambient-noise community. The ambient-noise community can respond with the required inputs in a useful format (which might include noise models) only if there is understanding between the two communities of what is needed and what is or can be made available. The invited paper by E. Goudriaan of SACLANTCEN gives an example of how some ambient-noise products are used to help address an important issue facing the operational ASW community.

SUMMARY OF THE CONFERENCE

by

R. Wagstaff

Although there was no intention to produce an in-depth summary of the conference, popular opinion seemed to support the idea of a summary of some of the general impressions gained by many of the participants at the end of the conference.

One of the most important impressions resulting from the conference was that the ambient-noise research community, as a whole, fails to satisfy the needs of the ASW operational community. The products that ultimately get to the latter often do not apply to the situations in which they are interested, or are not in formats that are useful to them. It was quite evident that the research community does not understand the decisions that the operational community must make, how they make them, nor why they have made a certain decision. Researchers need to be more familiar with the constraints that operators must work within and must provide products in formats that are useful to them and can help them to do their job. It may be that ambient noise is not what operators need, but some other parameter that has the ambient noise buried within it.

Some of the issues that operators must address are: where should each ASW asset be placed, is there a prefered orientation or tactic to maximize detection and tracking, what will be the detection ranges? The optimum deployment of multiple ASW units of similar and different types is also important. It is obvious that knowing the ambient noise alone will not solve these problems.

It is only one component of the puzzle that must ultimately be put together by someone – perhaps the operational research people – and given to the operational community. However, it is up to the ambient-noise people to provide ambient-noise data in meaningful formats. This is most likely to be achieved by presenting the data as functions of such system parameters as beamwidth, bandwidth, and integration time.

Somewhat related to this problem is the impression that the ambient-noise models are in general not as comprehensive as they should be. This is not in terms of the physics in the models, but in terms of the systems considerations. Provided that the correct input data are available, current ambient-noise models are capable of calculating the noise field in a detail and accuracy that far exceeds our current ability to measure it. Unfortunately, knowing the noise field to this detail and accuracy does not guarantee that the user will be able to translate this knowledge into a correct description of system performance. In most cases the improved resolution increases the difficulty of using the model results.

The ambient-noise models need to be more user-oriented than they are at present. This means that the sonar system must be included in the model and the output given in a format that is system oriented. In some cases the manner in which the system and the signal processing operate may have

to be simulated by the model. Even this may not be going far enough for some applications. It may be necessary to carry the results to the point of signal-to-noise ratio.

There were some interesting discussions about "measurements" versus "experiments". "Measurement" is defined as collecting ambient-noise data to add to the existing data base. "Experiments" are defined as investigations conducted to study particular phenomena such as down-slope enhancement, depth dependence, or noise-stripping. The general feeling was that experiments help understand the noise, which in turn helps in better modelling and prediction.

Future work should concentrate on the multiple-dimension aspects of the noise, such as its properties in frequency/azimuth space. For example, an important area of research would be line clutter in frequency and azimuth, which is a common problem for high-resolution passive systems.

A final impression of many conference attendees was that the papers presented indicated that much of the work being done is state-of-the-art or beyond, although some is less well advanced. A forum such as this, which displays the work being done, tends to give a quantum jump to those who are not aware of current developments and allows cross-fertilization among those who are. It also allows participants to see where the research community has reached and how future research might be redirected to make a more meaningful contribution to the whole. Several individuals recommended that a similar conference be held in a year or two to see how far we have been able to advance and to establish another baseline in the future. There were even some who volunteered to organize it at their laboratory.

ROLE OF PROPAGATION IN AMBIENT NOISE

by

Donald Ross
DONANCO, INC.
San Diego, California, U.S.A.

ABSTRACT

To be useful for modern ASW systems design and analyses, descriptions of ambient noise fields must go beyond average omnidirectional spectra and include horizontal and vertical patterns, fluctuations with time, dependencies on depth, and variations with season as well as geographic location. This paper summarizes present understanding of ambient noise characteristics, stressing the role of propagation. To aid our basic understanding, the spectrum is divided into three distinct frequency regimes and observed results are then explained in terms of the different types of propagation that control each regime. The vertical-angle arrival structure is used as the framework for the discussion.

INTRODUCTION

The purpose of this paper is to summarize present understanding of the various characteristics of underwater ambient noise, stressing the role of propagation. The several surveys by Wenz and others (1-4) published over the past 20 years deal mainly with mean spectra as functions of such parameters as sea state, wind speed and shipping density. In addition to the surveys, the literature includes numerous reports from research on such subjects as horizontal directionality, vertical directionality, long-term and short-term fluctuations of ambient noise and the dependence of these on water and receiver depths as well as on locality and season of the year.

Several large computer models have been developed to calculate ambient noise (DANES, RANDI, FANM, SIAM, etc.). These models all recognize the importance of propagation, in that they assume a distribution of sources and use a propagation model to calculate the contribution from each source. The idea is good; the results often fall short. When the expected and measured characteristics disagree, there is no way of knowing whether the problem is with the source distribution, source spectrum or propagation calculation. The writer suspects that sometimes the problem is that some of the dominant sources were not included in the model, or an important propagation path may have been omitted (5).

The status of our knowledge of ambient noise can be described by the statement: While we cannot predict it reliably, we can usually understand what we measure. The object of this paper is to summarize that understanding and to illustrate its application.

1. SOURCES OF AMBIENT NOISE

The sources of ambient noise are well known. They include:

Biological (whales, certain fish, shrimp, etc.),
Meteorological (wind, waves, rain, ice), and
Commercial (ships, off-shore oil activities).

Of these, biological sources and noise from ice and rain are outside the scope of this paper. We will deal primarily with three sources: wind/waves, shipping, and off-shore oil exploration. These sources are described briefly in the following paragraphs.

Wind/Waves

Meteorological factors control the condition of the sea surface, including waves, swell and breakers. Noise is produced over the entire frequency range from under 1 Hz to over 100 kiloHz. At very low frequencies, the sources are probably pressures generated by large-scale wave motions and by turbulent pressure fluctuations of the winds on the sea surface (6-8). Above about 50 Hz, the dominant mechanism is usually splashes from breaking waves. Splashes produce noise by the impact of water drops on the ocean surface and by the oscillation and collapse of the numerous bubbles that are created by the breaking waves (9,10). Ambient spectra from splashes are relatively flat up to about 500 Hz, and decrease at higher frequencies at close to 6 dB per octave. The intensity is a function of the fraction of the sea surface covered by breakers and therefore of wind strength, fetch, and sometimes water depth.

In most ocean areas, meteorological sources are dominant below about 5 to 10 Hz and again above about 200 Hz, with shipping controlling between these frequencies. In some areas that are relatively remote from shipping, such as the Southwest Pacific, wind dominance is usually found over the entire frequency spectrum (11).

While local wind speed is the dominant factor controlling wind/wave noise for frequencies above about 500 Hz, this is not the case for lower frequencies, for which noise from distant areas may dominate when local winds are relatively calm. Thus, wind-dominated spectra are more variable at the lower frequencies, and information on both propagation and wide-ocean meteorological conditions is needed to calculate levels.

Figure 1 characterizes wind/wave noise in terms of sea conditions; however, this is an oversimplification. As discussed later in this paper, propagation affects ambient levels. It follows that there are predictable variations from the mean curves that correspond to different propagation conditions.

Surface Ships

The dominant sources of surface-ship radiated noise are propeller cavitation, propulsion machinery and propeller singing (12). It is estimated that 80 to 85% of the noise power radiated into the water by surface ships comes from propeller cavitation. There are two types of radiation from cavitating propellers: low-frequency tonals and a broad continuum (12,13). The tonals are radiated at up to the first ten harmonics of the blade frequency and are usually dominant for frequencies below about 40 to 50 Hz. The continuum controls the spectrum above about 50 Hz, generally peaking between 50 and 150 Hz. Above 150 Hz, the spectrum decreases with frequency at about 6 dB per octave. Both the tonals and the continuum are modulated at the shaft rotational frequency, and the continuum is even more strongly modulated at the blade frequency (12).

Three types of power plants are now commonly used in ocean-going merchant ships: geared steam turbines, direct-drive, slow-speed diesels, and geared medium-speed diesels. Of these, direct-drive, slow-speed diesels are the most common, about two-thirds of the ships at sea. Above 10 Hz the tonals generated by these engines are invariably swamped by those from propeller cavitation. Steam turbines account for about one-fourth of the ships at sea, and these often produce one or two strong tonals between 30 and 110 Hz that may stand out from the cavitation spectrum by as much as 20 dB. Tonals from geared, medium-speed diesels dominate the spectra of the ships employing them, particularly between about 30 and 300 Hz. However, less than 5% of ships at sea use this propulsion mode.

Mean surface ship spectra have been generated from surveys of merchant ship noise measurements (12). However, these surveys are mostly of data from older ship types and/or ships operating at below normal cruise speeds and are of only limited value. The several scaling formulas developed from the surveys, using ship speed, length, tonnage and horsepower as scaling factors, each give a somewhat different estimate of the noise from a modern, high-speed container ship, or from a supertanker. The formulas are useful only to predict gross trends.

While the nature of surface-ship radiated noise is well understood, insufficient information exists to predict the noise from a specific ship. Not only is noise a function of ship speed and propeller characteristics, it also depends on load and most probably on the state of the sea. In addition, the time lapse since the most recent hull scraping and the physical condition of the propeller are also important. It does not seem possible to know the noise characteristics of each of the more than 30,000 sea-going ships in any detail.

Since the noise radiated is a function primarily of ship size and speed, it follows that the ships with the highest propulsion powers are probably the noisiest. For the deep oceans, this means that the shipping contribution to ambient noise is probably controlled by the thousand or so largest and/or fastest ships. When lacking better information, the writer uses the formula:

$$L_S = 186 + 15 \log \frac{SHP}{10^4}$$

to estimate the total overall noise radiated by an individual surface ship. He finds that most measured surface-ship spectra are in fairly good agreement with this formula. Generally the total power radiated below 100 Hz exceeds that radiated above 100 Hz by about 6 dB. (SHP is the shaft horse power corresponding to the ship's speed.)

The importance of merchant shipping as a source of low-frequency ambient noise has increased significantly since the end of World War II. Not only has the number of ships at sea more than doubled, but, even more important, propulsion powers have increased dramatically. As shown in Fig. 2, typical noise levels have increased by the order of 10 dB in many parts of the world. This trend is not expected to continue, at least in the immediate future, since ocean trade is hampered by high oil prices and depressed economic conditions.

Off-Shore Oil Exploration

In recent years, a new, major low-frequency source has raised ambient levels below 100 Hz, occasionally by as much as 20 dB. The source is the explosion-like pulses used during seismic surveying. During seismic surveying, air guns or other pulse sources are fired once every 6 to 10 seconds. Each pulse produces a total energy source level of about 210 dBμPa-sec. At a repetition rate of one every 10 seconds, this corresponds to a mean source pressure level of about 200 dBμPa. This compares to 185 dBμPa for a typical modern merchant ship. In other words, one seismic profiler is equivalent to about 30 large merchant ships. The significance of off-shore oil exploration as a noise source is enhanced by the fact that locations for such activity are often optimum for propagation of the sound to distant receivers, as will be discussed later.

2. PROPAGATION CONSIDERATIONS

An important characteristic of the sources just described is that they are all located at or near the sea surface. This means that any discussion of the influence of propagation on ambient noise is concerned only with those paths originating in the vicinity of the surface.

Surface Decoupling Effect

The sea surface is a pressure-release surface. As a result, the basic pressure radiation pattern from near-surface sources is a sine function having its maximum straight down and a null in the horizontal (9,14). If the sea surface were flat and therefore a perfect pressure-release reflector, the null would be very deep due to perfect cancellation of the direct and surface-reflected paths. However, the sea is usually rough, and the sine pattern approaches a minimum rather than going to zero. One limitation on our ability to model ambient noise is incomplete knowledge of the surface decoupling effect for near-grazing angles for a rough surface.

For grazing angles greater than about 5°, the decoupling effect for sources close to the surface may be estimated from

$$\Delta TL = 20 - 16 \log (Fh\theta) \text{ dB}$$

where h is source depth in meters, F is frequency in kiloHertz and θ is the ray angle in degrees. Clearly the effect is more pronounced for low frequencies than for high ones.

Vertical Arrival Structure

It is instructive to use the vertical structure of the arrivals at the measurement location to explain the various characteristics of ambient noise. Instead of starting with a surface distribution of sources and integrating their contributions, we focus on the receiver and examine the contributions to the total noise power arriving in each vertical sector. The sources that contribute noise power to a vertical sector are those located where the outgoing ray bundle intersects the sea surface. It is important to realize that the same ray bundle may intersect the surface in several places. Figure 3 illustrates this point for shallow water. Noise received at each angle comes from distributed surface sources located in each of the zones where the ray paths intersect the surface. In deep water these may be RSR zones connected to each other by purely refractive paths.

Role of Attenuation

If the sources were uniformly distributed over the ocean surface, then the sound intensity received from each zone would be proportional to the zonal area and inversely proportional to the transmission ratio from that zone. Talham (15) considered bottom-bounce paths and concluded that the increase of the intercepted area with distance cancels the spreading loss. Williams (16) analyzed RSR propagation and found examples of distant zones contributing relatively more noise than close ones. It follows from these analyses that all zones must be considered out to distances for which the frequency-dependent absorption loss becomes dominant. In other words, were it not for the attenuation component of the propagation loss, sources over the entire ocean surface would contribute to the ambient noise. Attenuation limits this area.

Frequency Regimes

The frequency dependence of attenuation provides the framework for dividing the spectrum into two or three distinct frequency regimes. The high frequency regime is defined as that for which the attenuation is so great that only the closest intersection with the sea surface contributes significantly. In shallow waters, this regime occurs above about 10 kHz. However, in deep oceans, for which the distances between surface reflections of significant rays are usually at least 30 km, the high frequency regime applies down to about 1 kHz.

For all frequencies below these limits, more than one surface area will contribute significant noise power to at least some of the individual vertical arrival ray bundles. In fact, for a uniform distribution of noise sources, the power in each ray bundle will be related to the number of surface intersections for which the absorption loss is negligible.

For deep water, the low frequency regime divides into two parts. Below

about 150 Hz, the absorption loss may be so low that this factor no longer controls the ocean area contributing to the ambient. Sources located as far away as the edges of the ocean basin may make significant contributions (5). Thus, there are basically three frequency regimes to be considered in analyzing deep water ambient noise:

Below 150 Hz	Whole ocean basin
150 - 1000 Hz	Numerous surface zones may contribute
Above 1 kHz	Local surface dominates

Relationship of Vertical Structure to Depth Dependence

Recently Cavanagh and Renner (17) examined the relationship between the vertical distribution of ambient noise and the depth dependence of the total (omnidirectional) intensity. Through a relatively straightforward application of Snell's law they found that an isotropic vertical noise pattern implies levels independent of depth, while a highly structured vertical pattern is consistent with significant variations with depth. In fact, each depth function is related to a specific pattern of the vertical arrival structure. Since the vertical arrival structure is influenced by the velocity profiles and bathymetry at the source locations as well as at the receiver, it follows that these also play a role in the depth dependence of the ambient.

Regional and Seasonal Dependencies

It has long been recognized that the shipping-controlled ambient spectrum is dependent on location and, to some degree, on season. These dependencies have been attributed to such factors as proximity to heavy shipping lanes, and secondarily to propagation. The dependence on location and on season of the ambient for a given wind speed in the wind-dominated band from 200 to 500 Hz is more subtle, and it has been recognized only fairly recently (18). This dependence is due to the dependence of propagation from surface sources on place and season. We will demonstrate our understanding of these dependencies in the next section.

3. DEEP-OCEAN, WIND-GENERATED AMBIENT NOISE

The effects of propagation on ambient noise can be illustrated by considering the characteristics of wind/wave noise for various deep-ocean situations. With the current understanding one can now explain regional and seasonal dependencies of levels, as well as depth dependencies of both levels and directionality patterns, and one can predict when distant storms should dominate relative to local weather conditions.

Deep-Water Vertical Arrival Structure

We start our analysis by assuming a classical deep-water sound-speed profile exhibiting a deep sound channel and having its highest sound speed at a hard bottom (Fig. 4). Figure 5 shows the arrival structure for a hydrophone located in the channel at depth Z_o, for which the local sound speed is C_o. Four distinct angular arrival sectors are shown. Arrivals at

angles less than the surface-grazing angle do not intersect the sea surface at all. It follows that, unless mechanisms exist to transform ray angles, very little noise should be contributed at these angles. The limiting angle for the surface-grazing ray is given by:

$$\theta_{SG} = \cos^{-1}\left(\frac{C_o}{C_s}\right) \doteq \sqrt{2\left(\frac{C_s - C_o}{C_s}\right)} .$$

The extent of the RSR sector is controlled by the bottom-grazing ray angle, given by:

$$\theta_{BG} = \cos^{-1}\left(\frac{C_o}{C_B}\right) \doteq \sqrt{2\left(\frac{C_B - C_o}{C_B}\right)} .$$

Rays leaving, or arriving, in the sector between θ_{SG} and θ_{BG} intersect the sea surface numerous times and do not interact with the bottom. For frequencies for which the absorption loss is low, these RSR arrivals are a major source of the total noise because of the large number of zones that contribute.

For a hard bottom there is a critical angle below which bottom reflection losses are relatively small. Rays striking the bottom between grazing and the critical angle arrive at the receiver in the sector bounded by the bottom grazing angle and an angle given by:

$$\theta_{CB} = \cos^{-1}\left(\frac{C_o}{C_B}\cos\theta_{CR}\right) = \cos^{-1}\left(\frac{C_o}{C_{BB}}\right) ,$$

where C_{BB} is the sound speed in the hard bottom just below the water column and C_B is the speed in the water just above the bottom. This path is especially important for bottomed and near-bottom receivers (15,19).

While arrival paths more steep than θ_{CB} may intersect the surface many times, they intersect the bottom at angles for which the bottom loss is so high that noise from distant zones is severely attenuated. We may therefore treat the noise arriving at these angles as originating only at the sea surface in the immediate vicinity of the receiver. In the following discussion we will refer to this noise as being that from the local area, to distinguish it from noise originating in more remote areas arriving by paths involving at least one surface reflection.

The present description of ambient arrival paths is confirmed by data from the VLAM array in the Atlantic as analyzed by Kinnison and his coworkers (20). In the band from 250 to 500 Hz, their data taken with the array near the channel axis display two distinct peaks corresponding to the positive and negative RSR arrival angles, a deep null for smaller angles, and a broad maximum for the overhead direction. Below 250 Hz, there is a

tendency for the null to disappear. Fox (19) measured noise vertical directivity with an array just above the bottom, finding patterns as a function of frequency and sea state that also agree qualitatively with our analysis. Data from other experiments for frequencies above 1 kHz (21,22) show only the broad overhead maximum, as would be expected since absorption wipes out both the RSR and BB components.

Wind-Speed Dependencies

No matter what propagation paths are involved, one would expect that the rate of increase of ambient levels with wind speed would depend only on the rate of increase of the noise radiated by the surface. However, measurements made under different circumstances and/or at different locations reveal distinctly different slopes (18). In situations where the propagation is such that only close-by sources are important, the rate of increase is given approximately by 28 log WS. In other cases, where paths to more distant areas contribute significantly, the coefficient is close to 20. Apparently what happens is that increases of the surface roughness cause increased scattering losses at each reflection and thereby reduce the relative contributions of distant zones. This effect is illustrated in Fig. 6 which is based on Fox's data (19). While the distant contribution increases with sea state, its rate of increase is smaller than the local component.

It follows that measured rates of increase of noise with sea state are dependent on both the rate of increase of the source and the rate of decrease of the contributing surface area.

Depth Dependence

For frequencies above about 500 Hz for which the RSR contribution is not large and the vertical distribution is relatively smooth, ambient levels are virtually independent of depth. This result agrees with data for 500 and 800 Hz reported by Morris (23) for wind speeds of at least 10 knots. Of course, at very high frequencies absorption loss between the surface and the receiver will reduce levels measured at depths of several kilometers (24).

For the frequency band below about 500 Hz arrivals by RSR and/or bottom-grazing paths may contribute significantly. In this case, the depth dependence should show a small peak near the critical depth. With any further increase of receiver depth, the RSR contribution will be eliminated and the level will decrease to that produced by the direct surface radiation and bottom reflection paths. It follows that for depths between the critical depth and the bottom the reflectivity of the local bottom for near-grazing angles will be a critical factor. Figures 7 and 8 illustrate depth dependencies found in the Pacific as a function of frequency and sea state.

Regional and Seasonal Effects

From the above discussion we now understand why wind-generated ambient noise in the frequency band from 200 to 500 Hz varies both geographically and seasonally. The key is the dependence of the surface sound speed on

season and location. Returning to Fig. 5 we note that the lower the surface sound speed relative to that at the bottom, the larger the RSR contribution. It follows that the same sea state will produce higher levels in northern latitudes, and that levels in winter will be higher than those in summer. In areas and/or during seasons for which the surface sound speed exceeds the bottom sound speed, RSR paths will not exist and ambient levels will be relatively low, as found in the warm Parece Vela Basin west of Guam (18). In such areas the dependence of ambient levels on wind speed will be greater than normal.

Effect of Range-Dependent Environment

Our discussion thus far has assumed range-independent bathymetry and sound speed profiles. However, below about 250 Hz variations of these with distance from the receiver can be important. For the deep oceans for which bottom depths generally exceed the critical depth, the biggest effect is the dependence of surface temperature on geographical location, especially on latitude. It can readily be shown that near-grazing rays starting from the surface in cool water no longer interact with the surface as they proceed into regions having higher surface temperatures. Thus, some RSR paths in cool climates become RR paths in warmer areas. Since these paths avoid surface losses, they propagate with less loss. Noises from these cooler surface regions arrive at angles closer to grazing than θ_{SG}. As a result of this phenomenon, measurements with horizontal arrays in the deep sound channel invariably show higher levels in the direction of cooler surface temperatures.

In the Pacific, the surface isotherms are almost parallel with the latitude lines. Measurements made with horizontal arrays show a persistant bias toward the north. The bias is particularly strong in the winter since higher sea states are also found to the north at this time of year. The writer has examined ambient noise data from the Pacific Ocean and has concluded that whenever local winds are relatively calm during the winter season distant storms are likely to dominate for frequencies below about 250 Hz.

4. NOISE FROM DISTANT SHIPPING

The role of propagation in determining ambient noise characteristics is strongest in the shipping noise band, i.e., from 10 to 150 Hz. In this band, measurements of vertical arrival structure (19,20,25,26) invariably show a strong horizontal component. For receivers in the deep sound channel, the near-horizontal energy is the dominant component for frequencies below about 70 Hz and is an important contributor as high as 150 Hz. From our earlier discussion of vertical arrival structure it is apparent that some mechanism must exist whereby paths from surface sources are transformed from RSR and bottom-reflecting types into purely refractive ones having angles close to the horizontal in the deep sound channel

Coastal Enhancement Effect

A mechanism whereby sounds from surface or near-surface sources can be

propagated to a receiver by low-loss, deep-channel, near-horizontal refractive paths was originally postulated by the writer in the mid 1950's. He observed that long-range detection results and ambient noise horizontal directionality measurements implied exceptionally low transmission loss from sources near the edge of the continental shelf. The mechanism is angle transformation by reflections from the outwardly sloping bottom. One or two reflections from a moderate slope will change the vertical angles of rays leaving a surface source between 6^{o} and 18^{o} to rays propagating with effective angles under 6^{o}. This transformation is illustrated by Fig. 9, which is a typical ray trace for a source in shallow water propagating out into a deep basin. Figure 10 shows a typical transmission loss curve for a shallow source and a deep receiver, showing a greater than 10 dB peak when the source is located at the edge of the basin.

Originally the effect was called the "megaphone effect." Today it is usually referred to as the "coastal enhancement effect" (14,26) or sometimes as "SOFAR propagation" (5). A dramatic example of this effect was found by Northrop et al (27) who discovered that sounds from small explosives dropped in continental coastal waters could be picked up on deep-channel receivers at distances as great as 10,000 km, even though signals from shots in deep waters at closer distances were undetectable. Figure 11, which comes from their paper, illustrates this result.

The magnitude of the enhancement depends to a large extent on the distance to the shallow shelf. The mean transmission loss for the enhancement zone is usually close to that for pure refractive propagation and can be estimated from

$$TL = 63 + 10 \log R + \alpha R,$$

where R is distance in kilometers and the attenuation is that for pure volume absorption. The enhancement is the difference between this transmission loss and that for sources in deep water at close to the same distance.

The importance of the coastal enhancement effect for low-frequency ambient noise stems from the fact that there are places where shipping lanes converge over shallow sloping bottoms. Examples include the Straits of Gibraltar, the southwestern approaches to the English Channel, certain passages between islands, and the vicinity of numerous busy ports such as New York, Norfolk and San Francisco. Noises from these areas often dominate low-frequency ambient spectra for receivers located in the deep sound channel; yet, with the exception of Wagstaff's RANDI model, ambient noise models have ignored this effect. As noted by Wagstaff (5), models that ignore this important contribution are bound to produce erroneous results.

Horizontal Directionality

Not only does the coastal enhancement effect explain the vertical arrival structure measured with arrays in the Atlantic and Pacific Oceans (20,25, 26), but also it is required to explain persistent peaks that are found when using horizontal arrays in these areas. Figure 12 is a typical pattern measured in the Northwest Pacific. The figure shows a broad maximum

toward the north, due to the colder surface temperatures, and a narrow peak in the direction of San Francisco. Similar measurements with arrays in the North Atlantic have shown persistent peaks which in each case correspond to a location where shipping is concentrated in shallow water near an outwardly directed slope. The general northern bias is also observed.

In some places the bias toward sources to the north is so strong that it has been suggested that the differences between ambient spectra at two latitudes be used as a measure of transmission loss (28). Thus, comparing the spectra at two such locations 500 km apart, levels at the southern location were found to be lower at all frequencies. The difference between the two spectra is greater above 80 Hz due to the increased absorption loss and is a measure of this loss.

Depth Dependencies

Both magnitude and directivity patterns of low-frequency ambients from shipping vary with depth. As illustrated by the curves for 50 and 150 Hz in Fig. 7, levels are highest near the channel axis and decrease somewhat with depth. They drop significantly below the critical depth. As reported by Anderson (25), the corresponding vertical arrival structure shows a broad peak at the channel axis, encompassing both the RSR and refractive components. The peak becomes narrower and less intense with increase in depth.

The horizontal directionality pattern is also depth sensitive. The semipermanent horizontal directionality pattern previously described is most noticeable in the deep channel. As the critical depth is approached, this pattern disappears and is replaced by a more transient one representing the contributions of relatively nearby shipping. The bias toward colder waters also disappears at depths below the sound channel.

The writer is not aware of either horizontal or vertical directivity measurements for receivers in the surface sound channel. However, from our understanding of the role of propagation, we would expect the patterns to be similar to those found for receivers near the critical depth.

Geographic and Seasonal Dependencies

It is clear that geographic and seasonal dependencies of propagation can have as important effects on shipping-dominated ambient noise levels as do geographic and seasonal variations of shipping densities. For receivers in the sound channel, the RSR contribution for a fixed distribution of surface sources will increase markedly in the winter when the surface sound speed is lowest. In fact, the seasonal differences may be as much as 10 dB for some areas where RSR paths exist in the winter but are nonexistent in the summer.

There are some ocean areas for which the combination of warm surface temperatures and insufficient water depth eliminates the possibility of RSR paths throughout most of the year. In these situations, refracted paths from coastal enhancement zones account for almost the entire ambient noise from shipping.

Noise from Offshore Oil Exploration

The coastal enhancement effect also magnifies the importance of offshore oil exploratory activities. Seismic profiling in shallow waters near the edge of a continental shelf is in the optimum location to radiate sound into the deep sound channel. This sound can be received by hydrophones even thousands of kilometers distant. At the longer distances the discrete pulse nature of the sound disppears because of the span of travel times for the various contributory paths.

5. SUMMARY

The idea that ambient noise is primarily a function of the distribution and characteristics of its sources has been replaced by recognition that propagation plays an equal role. Dependencies of ambient spectra and directional patterns on depth, location and season are now understood in terms of changes of propagation as well as of source distributions. The role of propagation is most important for the low frequencies, for which distant sources are often the dominant contributors. RSR paths are important for frequencies below about 1 kHz, and coastal-enhancement refractive paths below 150 Hz.

REFERENCES

1. Wenz, G.M., Acoustic ambient noise in the ocean: spectra and sources, J.A.S.A. 34, 1962: 1936-1956.

2. Wenz, G.M., Review of underwater acoustic research: noise, J.A.S.A. 51, 1972: 1010-1024.

3. Perrone, A.J., Deep ocean ambient noise spectra in the Northwest Atlantic, J.A.S.A. 46, 1969: 762-770.

4. Urick, R.J., "Principles of Underwater Sound," Second Edition, McGraw-Hill, 1975: Chapter 7.

5. Wagstaff, R.A., Low-frequency ambient noise in the deep sound channel - the missing component, J.A.S.A. 69, 1981: 1009-1014.

6. Nichols, R.H., Infrasonic ambient ocean noise measurements, J.A.S.A. 69, 1981: 974-981 (has extensive list of references).

7. Wilson, J.H., Very low-frequency wind-generated noise produced by turbulent fluctuations in the atmosphere, J.A.S.A. 66, 1979: 1499-1507; 69, 1981: 1517-1518; 70, 1981: 1783-1786.

8. Liu, A.K. and Larry, T.L., Mechanisms and modeling of wind-generated ambient noise in the ocean, Paper PP5, 103rd Mtg A.S.A. Chicago, April, 1982.

9. Ross, D., "Mechanics of Underwater Noise," Pergamon Press, 1976: Chapter 4.

10. Wilson, J.H., Low-frequency wind-generated noise produced by the impact of spray with the ocean's surface, J.A.S.A. 68, 1980: 952-956.

11. Bannister, R.W., et al, Ambient sea noise measurements near New Zealand, Paper P4, A.S.A. Mtg, Austin, Texas, April 1975 (Abstract, J.A.S.A.55, 1974: 418).

12. Ross, D., "Mechanics of Underwater Noise," Pergamon Press, 1976; Chapters 8, 9 and 10.

13. Gray, L.M. and Greeley, D.S., Source level model for propeller blade-rate radiation, J.A.S.A. 67, 1980: 516-522.

14. Bannister, R.W. and Pedersen, M.A., Low-frequency surface interference effects in long-range sound propagation, J.A.S.A. 69, 1981: 76-83.

15. Talham, R.J., Ambient sea noise model, J.A.S.A. 36, 1964: 1541-1544.

16. Williams, R.B., Vertical noise distributions in the ocean: models and measurements, Paper EE10, 102nd Mtg A.S.A., Miami Beach, December 1981.

17. Cavanagh, R.C. and Renner, W.W., Vertical directionality and depth dependence of averaged acoustic signals and noise, J.A.S.A. 68, 1980: 1467-1474.

18. Shooter, J.A. and Gentry, M.L., Wind-generated noise in the Parece Vela Basin, J.A.S.A. 70, 1981: 1757-1761.

19. Fox, G.R., Ambient noise directivity measurements, J.A.S.A. 36, 1964: 1537-1540.

20. Kinnison, G.L. et al, NUC unpublished Technical Note, 1972.

21. Axelrod, E.H., Schoomer, B.A. and Von Winkle, W.A., Vertical directionality of ambient noise in the deep ocean near Bermuda, J.A.S.A. 37, 1965: 77-83.

22. Anderson, V.C., Non-stationary and non-uniform oceanic background in a high-gain acoustic array, J.A.S.A. 67, 1980: 1170-1179.

23. Morris, G.B., Depth dependence of ambient noise in the northeastern Pacific Ocean, J.A.S.A. 64, 1978: 581-590.

24. Bradner, H. and Howard, R.S., Attenuation of surface-generated noise received deep in the ocean, J.A.S.A. 64, 1978: 322-324.

25. Anderson, V.C., Variation of the vertical directionality of noise with depth in the North Pacific, J.A.S.A. 66, 1979: 1446-1452.

26. Wales, S.C. and Diachok, O.I., Ambient noise vertical directionality in the Northwest Atlantic, J.A.S.A., 70, 1981: 577-582.

27. Northrop, J., Loughridge, M.S. and Warner, E.W., Effect of near-source bottom conditions on long-range sound propagation in the ocean, J. Geophysical Res. 73, 1968: 3905-8.

28. Kibblewhite, A.C., Shooter, J.A. and Watkins, S.L., Examination of attenuation at very low frequencies using the deep-water ambient noise field, J.A.S.A. 60, 1976: 1040-1047.

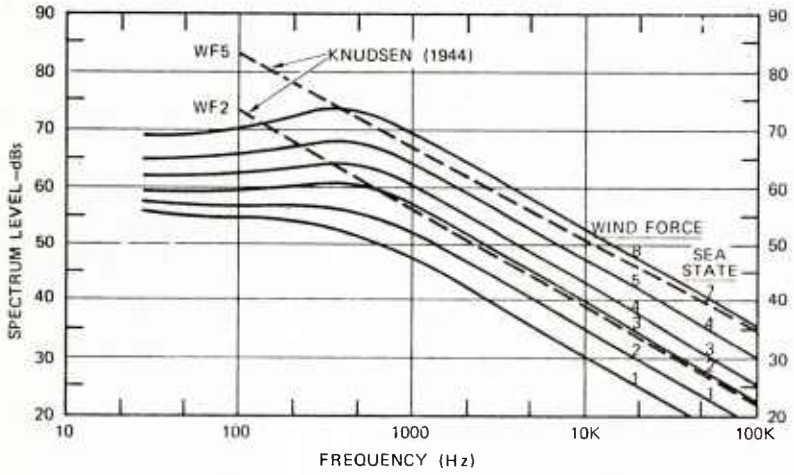

FIG. 1

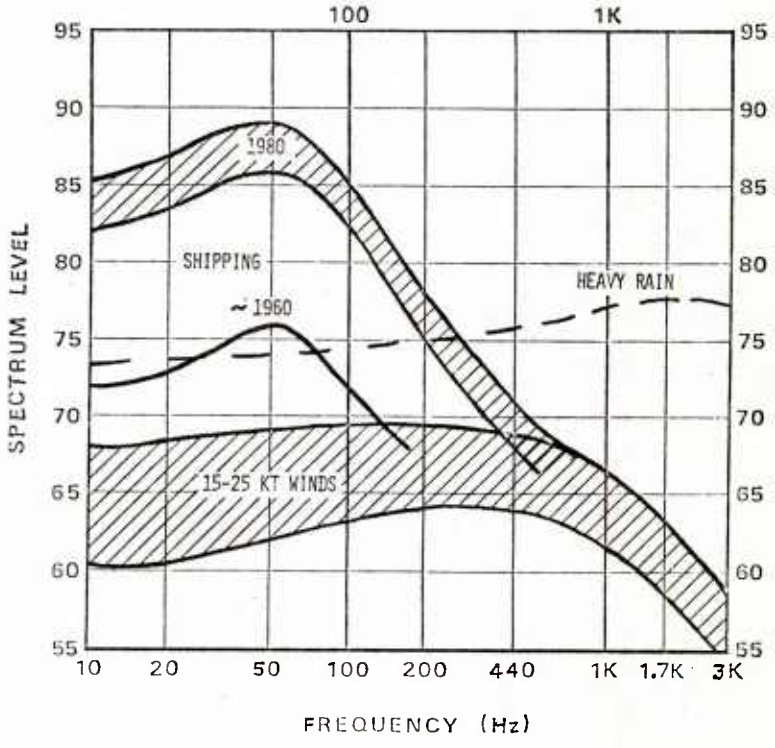

FIG. 2

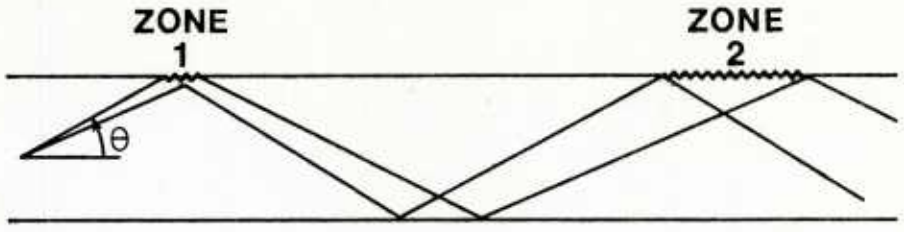

FIG. 3

TYPICAL S.V.P.

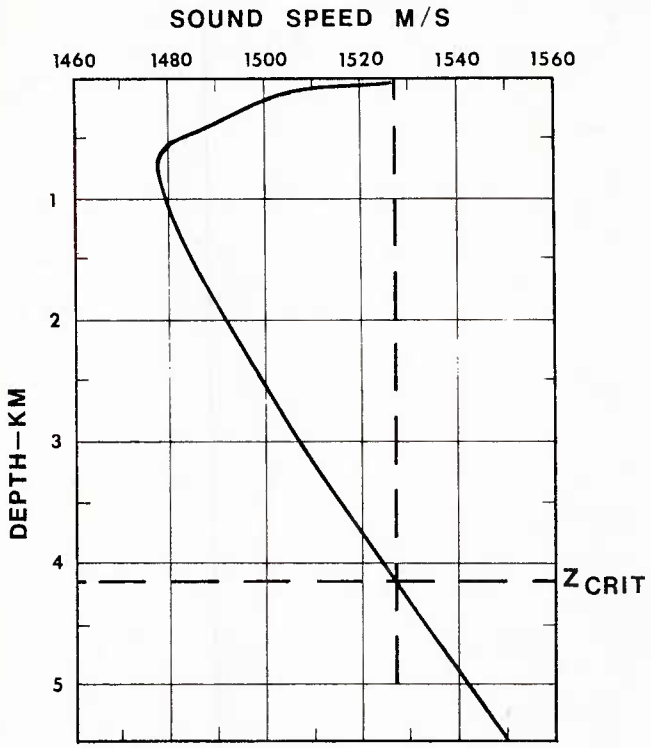

FIG. 4

DEEP-WATER
VERTICAL ARRIVALS

$C_O < C_S < C_B$

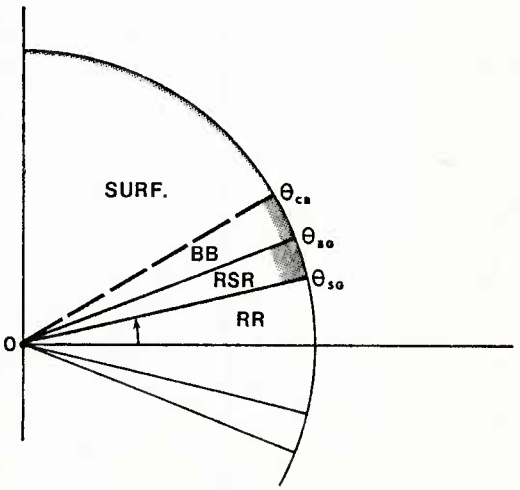

FIG. 5

VERTICAL ARRIVALS
OF
AMBIENT NOISE
250 Hz NEAR BOTTOM

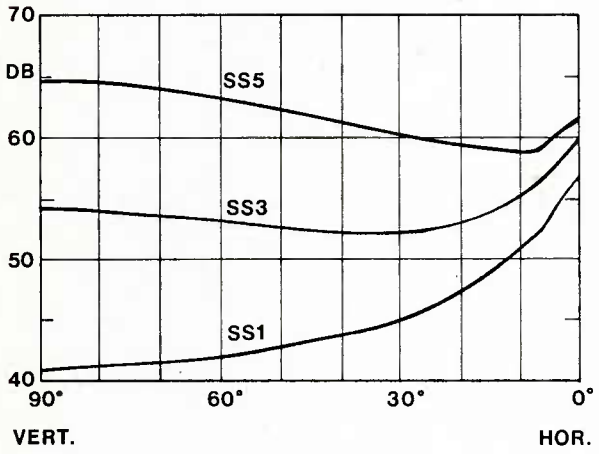

FIG. 6

AMBIENT VS. DEPTH
(<10 KT)

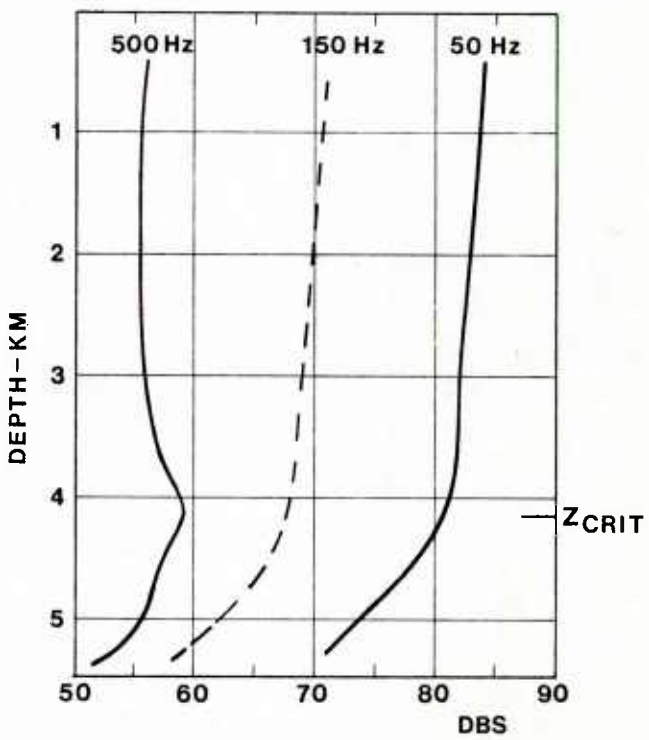

FIG. 7

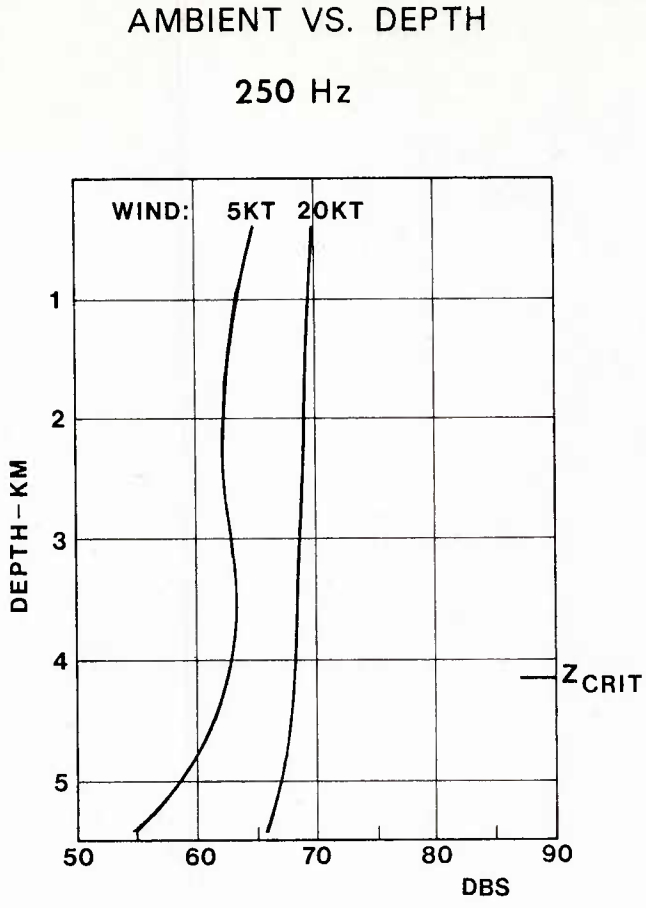

FIG. 8

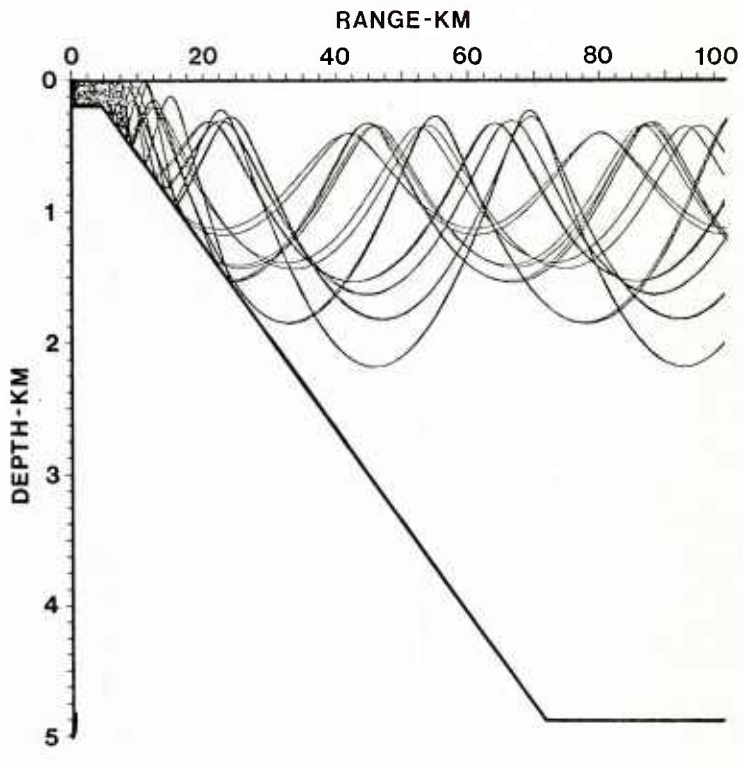

FIG. 9

RAY TRACE FOR A 10 m SOURCE
5 km FROM EDGE OF 4° SLOPE.

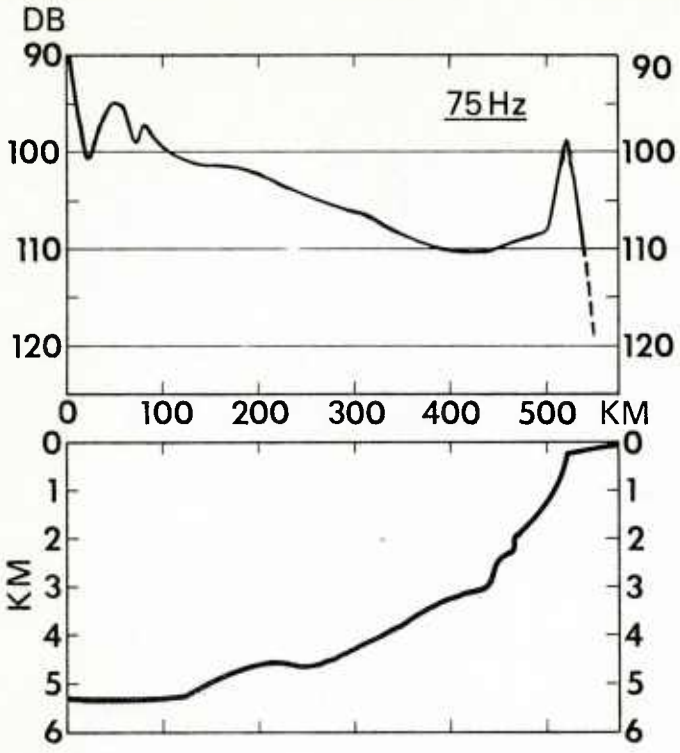

FIG. 10

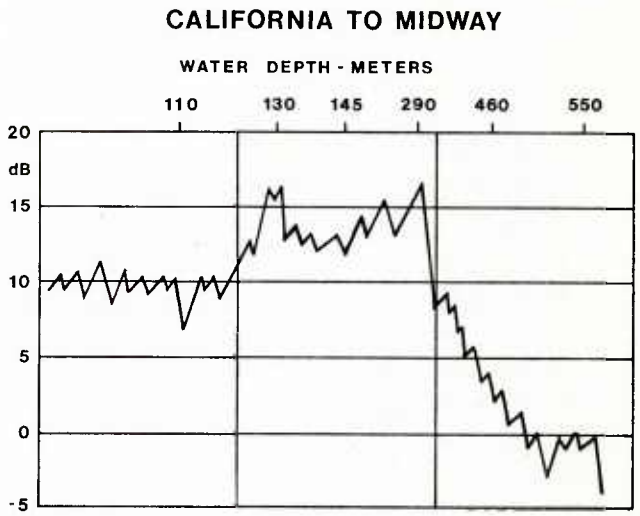

FIG. 11

HORIZONTAL DIRECTIONALITY OF AMBIENT NOISE

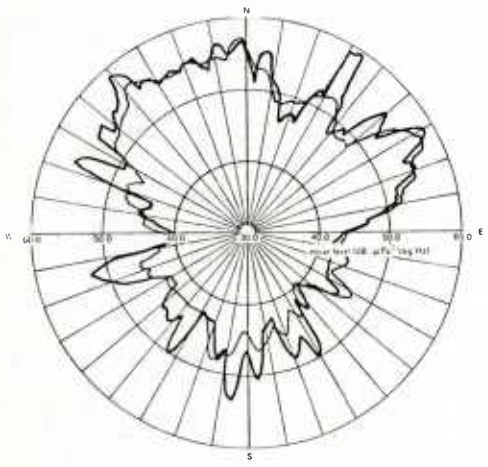

FIG. 12

ACOUSTIC SOURCE CHARACTERISTICS OF MERCHANT SHIPS

by

John C. Heine
Bolt Beranek and Newman Inc.
Cambridge, Ma., USA

ABSTRACT

Merchant ships are sources of broadband acoustic noise which can interfere with and confuse ocean surveillance. The purpose of this discussion is to review: the status of research on and measurements of merchant ship acoustic characteristics; and known and conjectured properties of merchant ship acoustic signatures. Sources of continuous and discrete, or tonal, radiation are discussed, including ship propellers and internal machinery. Mechanisms which can cause tonal bandwidth are identified. These concepts are illustrated through a discussion of some results obtained from a detailed measurement of a bulk carrier.

INTRODUCTION

Low frequency ambient noise, that in the 20-200 Hz region, is dominated in most deep water locations by acoustic radiation from merchant shipping. Noise from merchant ships has both continuous and discrete components, and each of these components has a different impact on the performance of undersea surveillance systems. The continuous components provide the background against which these systems must make detections. The tonal components provide clutter and limit classification decisions and the capability for providing localization and tracking information.

Clearly, therefore, any attempt at modeling or predicting performance of acoustic surveillance systems must include descriptions of merchant ship noise radiation. The objectives of this discussion are to first briefly report on the status of merchant ship noise signature descriptions and modeling; secondly to describe the mechanisms which cause these observed characteristics; and finally to illustrate the parameters of importance and the status of our ability to predict these parameters by considering, for a specific ship, narrowband, broadband and directional characteristics.

The underlying rationale for studying merchant ship acoustic radiation is to develop enough understanding to enable predictions of noise characteristics for system performance studies. Historically, measurements of merchant ships' characteristics predate 1948 and have continued to the present. [1-10]* The largest data base consists of a set of measurements on over one hundred ships at the Fort Story range reported on by BBN in 1966. [1] The most recent measurements this author has observed are those of icebreakers, [8-10] where the need to describe source characteristics was motivated by a requirement to predict the impact of icebreaker acoustic radiation on arctic mammals, a major issue in the process of approval of "Mega" projects.

Two approaches have been used for the genaralization of measurement experience to the description of source characteristics for the merchant fleet. The first [1] provides only a frequency averaged description of source level. No information is provided about narrowband components. Variations of peak spectrum levels for ships of different designs are estimated on the basis of gross ship parameters such as length, speed and horsepower. The second approach [11, 12] provides a statistical description of both tonal and continuous radiation. Predictions of fleet characteristics are based on probability distributions of somewhat more detailed ship properties such as peak cavitation volume, propeller diameter and cavitation inception speed.

As of this time, only the first of these approaches has had any widespread application. Current noise models (e.g., ASEPS and DANES) in fact include only ensemble averages, over the merchant fleet, of frequency smoothed characteristics. Techniques are available for describing higher order statistics [13-15], however these techniques have not been implemented in any model used for fleet applications. Should there be a need for higher order descriptions of noise (e.g., variance of beamformer noise output), these more detailed descriptions of source characteristic will have to be considered as input.

Improved understanding of merchant ship radiation requires a substantial commitment. Our experience with such an effort is based on a program, initiated in 1976, by NAVELEX 320 to study merchant ship source characteristics. This program focussed on describing radiation due to cavitation and to the low frequency main propulsion diesels employed by a large fraction of the merchant fleet. Subsequently, the NORDA/SEAS program also recognized the need for a description of merchant ship source characteristics [16] and joined the NAVELEX 320 effort (then managed by the Naval Research Laboratory) in an effort which culminated in the most detailed measurement of a merchant ship to date. This measurement, performed in deep water under carefully controlled conditions by a team of investigators including NRL, DTNSRDC, NORDA, and BBN, include a large number of coordinated acoustic radiation measure-

* Numbers in brackets represent references presented at the end of the paper.

ments, at a variety of ranges and depression and aspect angles, coordinated with on-board measurements of the vibration of major ship panels and of machinery characteristics.

In general the merchant ship noise program may be characterized as having led to advances in the description of machinery and cavitation related noise levels and directivity and, as an ancillary benefit, to the development of improved measurement techniques for characterization of merchant ship acoustic radiation, where improved in this sense is equated with substantially reduced costs over chartering a ship and making measurements at a calibrated acoustic range.

The potential for improvements in understanding the physics of the underlying processes leading to acoustic radiation unfortunately has not been achieved in this program, however, because reduced interest on the part of the Navy has led to the program being essentially unfunded for the last two years. As implied above, other measurements of surface vessels are continuing (I have not even mentioned to this point the continuing measurements of U.S. Naval surface vessels at AUTEC) but no systematic effort is currently being made to consolidate, evaluate and employ the resulting information. Thus, source model development should be described as being "on hold" until sufficient motivation can be established within the U.S. Navy.

MERCHANT SHIP ACOUSTIC SOURCE CHARACTERISTICS

Overview of Characteristics and Mechanisms

Let us consider separately the acoustic radiation characteristics and the mechanisms which cause them. Measurements of merchant ship radiation (e.g., Fig. 4) show that the acoustic source spectrum of typical merchant ship has both tonal or narrowband, and continuous (in frequency) radiation components. Continuous noise is dominatated by cavitation [17] and narrowband noise can be due to either cavitation or to internal machinery.

The basic characteristics of interest in describing this radiation are:

- The spectral shape of the broadband cavitation noise
- The levels of line components
- The directivity of the acoustic radiation in both depression and aspect angles
- The bandwidth of narrowband components.

Cavitation occurs when the pressure on the suction side of a propeller is reduced below the vapor pressure. In fact cavitation is a penalty paid to generate the lifting forces needed to propel the ship, and merchant ship propellers are designed to withstand it during normal operating conditions. To see why cavitation occurs consider Fig. 1. Water flows around the ship and into the plane of the propeller plane. This field is not uniform. As a propeller blade passes through the in-flow field, it generates lift which varies with shaft angle. Lift variations (Fig. 2) occur because the resultant in-flow velocity changes the effective angle of attack of the blade and the varying angle of attack changes the pressure field on the blade. At some shaft angle this pressure falls below the vapor pressure and a cavitation bubble spontaneously forms. As the blade continues to rotate over a cycle (Fig. 3), the volume of cavitation changes with the blade shaft angle. This modulation of the bubble volume creates narrowband components at the blade passage rate (the number of blades times shaft rotation rate) and harmonics. When the cavity bubble collapses, broadband noise is created.

Other sources of narrowband radiation are machinery. In order of likelihood of observation, lines can be associated with main propulsion diesel engines (harmonics of shaft rate*), auxillary diesels, and other on-board rotating machinery (e.g., pumps). A detailed examination of representative merchant ship spectra has shown that the observability of machinery induced lines is unpredictable, almost certainly because the presence of a line is highly dependent on the details of operation of the machine and on the structure on which a given machine is fastened. The author's experience is that the number of lines observed in typical spectra which are machinery related is sufficiently small as to suggest that attempts to predict fleet characteristics be postponed until the more dominant, cavitation related mechanisms are better understood.

Cavitation lines have two basic properties: level and bandwidth. Generally, the level of cavitation lines depends on the cavitation volume time history as shown in Fig. 3, and on the number of propeller blades. (The total radiation is an incoherent sum of the radiation from all blades.) A description of bandwidth must account for two "bandwidth producing" mechanisms: Frequency stability and amplitude modulation. Frequency stability depends on propeller loading fluctuations caused by the motion of the ship in the seaway as controlled by the on-board main propulsion governor. Bandwidth depends on variations in the cyclical cavitation volume versus time history [18] which in turn depends on temporal variations in the spatial in-flow field at propeller plane.

* Another source of radiation at shaft rotation rate is a single propeller blade with anomolous lift and hence cavitation characteristics. The relative importance of diesel engine induced radiation to that from a single blade, has not been investigated.

Finally, the directivity of the acoustic radiation of merchant ships due to the cavitation process is influenced in the vertical plane by the free-surface and exhibits the Lloyd-Mirror induced dipole directivity expected for any point source beneath a pressure release surface. Aspect related directivity, except in fore and aft directions which may be influenced by sound grazing the hull (forward) and by intrained air in the propeller wake (aft) can be expected, for the low frequencies of concern here to be negligible, simply because the wavelength of sound is large compared to the size of the propeller cavitation bubble.

Let us consider properties of cavitation in more detail.

Cavitation Properties

Cavitation properties will be illustrated by measurements obtained from a 600 foot long bulk carrier with a design speed of 16 kts. These measurements were taken at a number of depression and aspect angles under conditions where propagation from the ship to the measurement hydrophones was dominated by the direct path. An example of the source level spectrum (spherical spreading has been removed) is shown in Fig. 4 for frequencies less than 200 Hz [19]. This spectrum was developed from a measurement at a depression angle of 29 degrees. For the purposes of this discussion we will simplify this spectrum to show only a continuous portion (Fig. 5) and the narrowband components due to cavitation (Fig. 6).

In both of these spectra the Lloyd-Mirror effect is a key factor and is observable in both spectra as a 6 dB per octave reduction in level with decreasing frequency. To see why this occurs recall that for a source depth of d, and a vertical trace wave number k sin ϕ, where k is the acoustic wave number, and ϕ is the depression angle measured at the surface, the directivity induced in a monopole source by the free surface can be given by the equation.

$$I(\phi) = 4I_o \sin^2[kd \sin\phi] \qquad (1)$$

For low frequencies, the argument kd sinϕ < 1. Then (1) can be approximated by

$$I \cong 4I_o (kd \sin\phi)^2$$

and, since k ~ f.

$$I \sim I_o f^2 d^2 \sin\phi^2.$$

Thus, for a fixed measurement geometry, we expect the received intensity at low frequencies to increase with f^2 (6 dB per octave). Further, for fixed frequency, the intensity increases as the square of the depression angle (6 dB per doubling of the depression angle) for small depression angles ($\phi < 1$ radian).

Typical directivity measurements, made in depression angle and aspect for blade rate lines at 9.3 and 37 Hz, are shown in Fig. 7. These results confirm that vertical directivity is indeed dominated by Lloyd-Mirror at low depression angles (Fig. 7a) and can be adequately described as an acoustic dipole. A more complete examination of these results [19] has shown that the vertical directivity is consistent with a source depth of 16 feet. Horizontal directivity does show some bow and stern aspect dependence. It is, however, reasonably horizontally isotropic at angles between $\pm$ 65° re broadside.

Now let us consider how these data match predictions.

Broadband Cavitation Level Properties

In reference 11, the broadband cavitation spectrum was defined in terms of the frequency of the cavitation peak; the source level at that frequency and of a spectrum shape which decreased at frequencies greater that the peak frequency at a rate of 6 dB per octave. These parameters correspond in Fig. 5, to the break point observable at 120 Hz, to the level of 167 dB observed at that point and to the fall-off in frequency with level observed and noted on Fig. 5 to be at a rate of 15 dB per octave. The level and frequency can be predicted from:

$$f_p = 120\,[U_s/V_c]^{-0.7},\quad 1.7 < \frac{U_s}{V_c} < 4 \qquad (2)$$

where U_s = ship speed (16 kts)

V_c = the cavitation inception speed (6 kts)*

and from

$$L_{p,BB} = 91 + 10 \log [D \cdot B(U_s/V_c)(\frac{U_s}{V_c} - 1)^2] + 25 \log [TPK \cdot V_c \cdot D] - 17 \log f_p \qquad (3)$$

* Numbers in () are values specific to the bulk carrier (19) measurement outline above.

where D = the propeller diamter (17 ft)
B = the number of blades (4) and
TPK = turns per knot (8.75).

Equations 2 and 3 yield values for f_p and $L_{p,BB}$ of 60 Hz and 164 dB// 1μPa/1Hz. Note that the location of the peak frequency is one octave away from the measured frequency, and that the level predicted for the observed peak is three dB lower than the observed level. These results have the right magnitudes. The major deviation of the observed properties from predicted properties is that the high frequency fall-off of the broadband spectrum is larger by a substantial amount (9dB per octave). This deviation is unexplained, but is not an isolated observation [6] for merchant ships.

Narrowband Cavitation Level Properties

Using methods outlined in reference 12, the level and envelope of blade rate related lines can be predicted for a measurement taken at a specified depression angle.

Specifically:

$$I \simeq 140 + 20 \log [f^3 H V_{max} \sin \phi] \quad (4)$$

where f = frequency of the blade rate fundamental (9.3 Hz at 16 kts)
H = the depth of the cavitation bubble (4.9 meters, or 16 feet)
ϕ = the depression angle (e.g., 30°)
V_{max} = the maximum volume of the cavitation, which may be estimated from the relation.

$$V_{max} = .00012\ D^3$$

where D = the propeller diameter in meters (5.25 meters).

Equations 4 and 5 lead to a prediction that the blade rate fundamental level at 30° is 170 dB. From Fig. 6 the actual measured level was 164 dB// μPa. Again, this prediction appears to be in the correct range.

Further consideration of the envelope of line levels in a free field from a monopole source with a periodic amplitude modulation suggests that to first order we can anticipate an envelope spectrum which is approximately flat. The argument for this property is as follows: The power radiated from a monopole source with a constant volume amplitude increases as frequency to the fourth power. We anticipate that the volume vs time history of a cavitation bubble is (excluding time varying effects in the velocity in-flow field) periodic, where the rate of repetition for each blade is the shaft rotation rate. For many pulse shapes, the amplitude of the Fourier components of the repeated pulse falls off as frequency squared. The intensities

of the harmonics should therefore fall off as frequency to the fourth, just balancing the increasing level associated with the increased efficiency of the monopole source. The resulting flat spectrum is however modified at low frequencies by the Lloyd-Mirror effect discussed earlier and at high frequencies by deviations of the actual volume vs time history from a simple shape. Including the former effect, at low frequencies the observed blade rate related levels should increase at 6 dB per octave until the argument $kd \sin\phi$ in (1) is equal to $\pi/2$. For a source depth of 16 feet (4.9 meters) this frequency is 75 Hz. Reference to Fig. 6 shows that the characteristics of the cavitation line envelope follow the Lloyd-Mirror envelope (dashed line) and thus have roughly uniform free field levels over the first 10 harmonics, as predicted.

Narrowband Cavitation Bandwidth Properties

Considering that typical processing systems employed in undersea surveillance applications are based on narrowband analysis which includes significant coherent and incoherent averaging times, bandwidth observed at the output of these systems can be due to either amplitude modulation, the traditional concept, or to frequency modulation--frequency instability at the source. Mechanisms causing amplitude or frequency modulation may be summarized as follows:

Variation in Turbulent In-Flow Field: Turbulence causes changes in lift which modulate the cavitation volume vs time process. This is constant bandwidth effect over the observed set of harmonics (the modulation spectrum is effectively convolved with the line spectrum of the source).

Gross Ship Motion: Ship motion introduces amplitude modulation through varying the depth of the cavitation bubble, and hence through a time varying Lloyd-Mirror effect. It also introduces frequency modulation through

a. Doppler variations due to changes in vertical and horizontal ship speed in the seaway, and

b. Variations in propeller loading which, with governor response change the shaft speed and hence the blade rotation rate.

Propagation Effects: Interaction of sound with the moving sea surface introduces a doppler smear in propagating energy.

The concept that frequency modulation effects, introduced by thrust variations due to gross ship motion in a seaway, may be an important factor in determining observed bandwidth was quantitatively evaluated by measurements made on bulk carriers. In the remainder of this paper I want to present some results obtained from those measurements.

Shaft frequency stability measurements were obtained for the bulk carrier by placing a magnetic pickup in close proximity to the main propulsion diesel engine starting gear. At normal cruising speed (16 kts, 140 rpm) the gear tooth passage frequency was 117 Hz. Slow variations in this frequency were observed using a frequency discriminator. The deviation voltage was then plotted as a function of time and recorded for further analysis. Simultaneous measurements of ship heave, made using a low frequency accelerometer were also plotted. Fig. 8 shows typical rpm and heave time series for a sea state 0-1, the only sea state experience during the measurement sequence. An examination of these two time series suggests an apparent correlation.

Detailed analysis of these waveforms was carried out to assess: the probability of observing a give frequency deviation (defined as the difference between the observed instantaneous frequency and the average frequency) (Fig. 9); the spectra of frequency modulation (Fig 10A) and of ship heave (Fig. 10B); and the coherence between rpm fluctuations and observed heave acceleration (Fig. 10C). For this low sea state, we observe from Fig. 9 that the frequency modulation had a 68% probability of lying within a .54% bandwidth. It is not clear whether this level of frequency deviation indicates a reaction to hydrodynamic acting on the propeller forces or is a basic property of the governor controlling engine rpm. However, it would certainly appear reasonable that this range of frequency deviation is the minimum that this ship would experience, particularly since hydrodynamic forces acting on the propeller should increase dramatically as the sea state increases. Note from Figs. 10A and 10B the spectra of both the ship heave and the rpm frequency deviation have their major energy at 0.16 Hz, indicating a basic fluctuation period of about 7 seconds. This is consistent with typical periods observed in Fig. 8. Finally, the apparent correlation of rpm and heave noted earlier is confirmed by a measured .68 coherence of their time series. This coherence is significant in a statistical sense because the signal to noise ratio of both signals exceeded 15 dB and the number of degrees of freedom in the determination of coherence exceeded 100.

A key issue is whether or not the bandwidth of cavitation line radiation was dominated by this frequency modulation. The bandwidth of several blade rate harmonics was measured during these experiments using a hull mounted accelerometer in close proximity to the propeller. Bandwidths (approximate 3 dB down points) were on the order of .5 to 1% of center frequency. This is consistent with the bandwidth of frequency deviation, and suggests though does not prove, that the frequency modulation effect may dominate observed bandwidth at low sea states. Since frequency modulation is correlated with ship response in the seaway, this results also suggests that if sea state increases, the observed bandwidth may also increase. It further suggests that amplitude modulation may be essentially insignificant under most real ship operating conditions. The form of these results is presented for clarity in Fig. 11 under the assumption that the contributions to observed bandwidths are equal at one Hertz under operating conditions

at sea state zero.

SUMMARY AND CONCLUSIONS

Significant progress has been made in describing the radiated acoustic properties of merchant ships. Estimates can now be made for a number of significant characteristics of source spectra, including:

1. Peak broadband cavitation level
2. Frequency at which the peak level occurs
3. The envelope characteristics of cavitation modulation induced narrowband spectra.

Frequency modulation caused by the response of the ship to the seaway has been shown to be a major source of bandwidth for undersea surveillance systems.

Prediction methodologies, if used in conjunction with distributions of engineering properties of merchant ships can yield descriptions of merchants ship source level characteristics with significantly more detail than the ensemble averaged, frequency smoothed spectra currently in use in noise prediction models.

Further advances in characterization of noise spectra, which can only be made under the auspices of the program dedicated to such development, must await a rekindling of interest within the U.S. Navy in the development of advanced noise prediction models.

REFERENCES

1. Gogos, C.M. *et al.*, "A Summary of Underwater Radiated Noise Data (U)", Bolt Beranek and Newman Inc. Report 1148 (March 1966), SECRET This report contains an extensive bibliography of ship noise measurements dating back to 1948. Some of this material was reported in Ross, D. and Alverez, F.F., "Radiated Underwater Noise of Surface Ships (U)", JUA, Vol. 14, (April 1964) CONFIDENTIAL.

2. Delco Electronics, "Deep Water Narrowband Radiated Noise Measurements of Merchant Ships", Technical Report TR72-28, (September 1972).

3. Naval Oceanographic Office, "A Pilot Study for Underwater Radiated Noise Measurements of Merchant Ships for Aircraft", Technical Note TN 6130-2-76, (December 1975).

4. Cybulski, J., "Probable Origin of Measured Supertanker Radiated Noise Spectra", IN: Oceans '77 Conference Record, 3rd Annual Conference sponsored by the Marine Technology Society of I.E.E.E., New York, Vol. I (1977).

5. Naval Ship Research and Development Center, "Merchant Ship Measurements", Memorandum From D.J. Vendittis, (January 1975).

6. Shooter, J.A., K. Russell Peterman, "Merchant Ship Signature", ARL Tech Report TR-77-47, (18 August 1977).

7. Naval Research Laboratory, "Sonobuoy Evaluation, Acoustics and Vibration Measurements on M/V Overseas Harriette (U)", Report 4529, (July 1981) CONFIDENTIAL.

8. Leggat, J.M., "Analysis of Underwater Radiated Noise of the Ice Breaker CCGS Louis St. Laurant," DREA Technical Memorandum in preparation.

9. Caulfield, D., "Development of the Practical System for Measuring Arctic Ships Radiated Noise Characteristics and a Discussion of Typical Results", Proceedings of a Workshop on the Question of Sound from Icebreaker Operations", sponsored by the Arctic Pilot Project, Petro Canada, (February 1981).

10. Thiele, Lars, "Underwater Noise from the Icebreaker M/S Voima", Odegaard and Danneskiold-Samsoe K/S", Report No. 81.42 (October 1981).

11. Heine, J.C. and L.M. Gray, "A Narrowband Source Model for Merchant Ships", J. Underwater Acoust. Vol. 28, No. 1, January 1978 CONFIDENTIAL, Also presented at the 31st Navy Symposium on Underwater Acoustics, San Diego, Ca., November 1976.

12. Gray, L.M., "Source Level Model for Propeller Blade Rate Radiation for the World's Merchant Fleet", J. Acoust. Soc. Amer. 67(2), (February 1980).

13. Heine, John C., "Estimates of Ambient Noise Properties at the OMAT Site", Bolt Beranek and Newman Inc. Technical Memorandum No. 391 (May 1978) CONFIDENTIAL

14. Moll, M., R.M. Zeskind, F.J.M. Sullivan, "Statistical Measures of Ambient Noise: Algorithms, Program, and Predictions", Bolt Beranek and Newman Inc. Report No. 3390 (June 1977).

15. Goldman, J., "OSTP-31JG: A Model of Broadband Ambient Noise Fluctuations Due to Shipping (U)", Bell Laboratories Report (September 1974) CONFIDENTIAL.

16. Moritz, Steven H. "The Generation of Noise by Surface Ships: A Description of the Principal Sources (Final Report)", TRW Report (15 March 1980).

17. Ross, Donald, *"Mechanics of Underwater Noise"*, Pergamon Press, New York, 1976.

18. Mark, William D., "Theoretical Prediction of Power Spectral Density of Merchant Ship Propeller Cavitation Volume Time Histories (Interim Report)", Bolt Beranek and Newman Inc. Technical Memorandum No. 477 (November 1977).

19. Personal communication from Dr. Paul Arveson, DTNSRDC Carderock. Dr. Arveson was responsible for the detailed planning for acoustic data acquisition and for the analysis of that data.

FIG 1: PROPELLER BEHIND STERN OF SHIP
VIEW LOOKING FORWARD

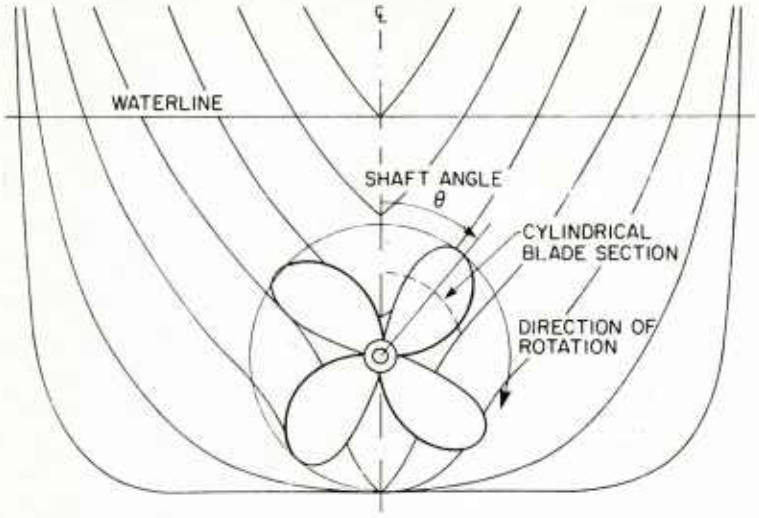

FIG 2: PROPELLER BLADE SECTION
INFLOW GEOMETRY

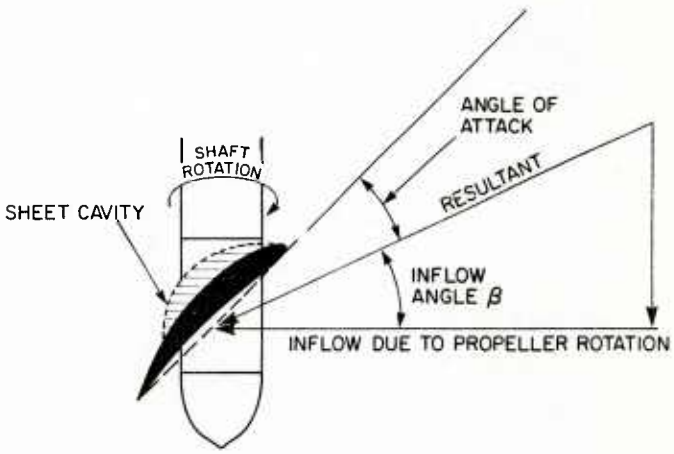

FIG 3: CAVITATION PATTERN FOR
TYPICAL PROPELLER

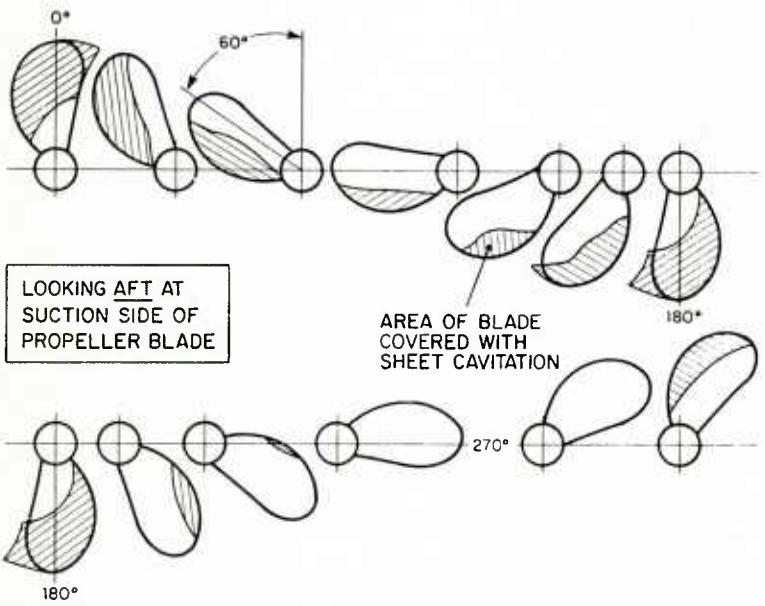

FIG. 4: SOURCE POWER SPECTRUM LEVEL OF A 600 ft BULK CARRIER MEASURED AT A DEPRESSION ANGLE OF 29°

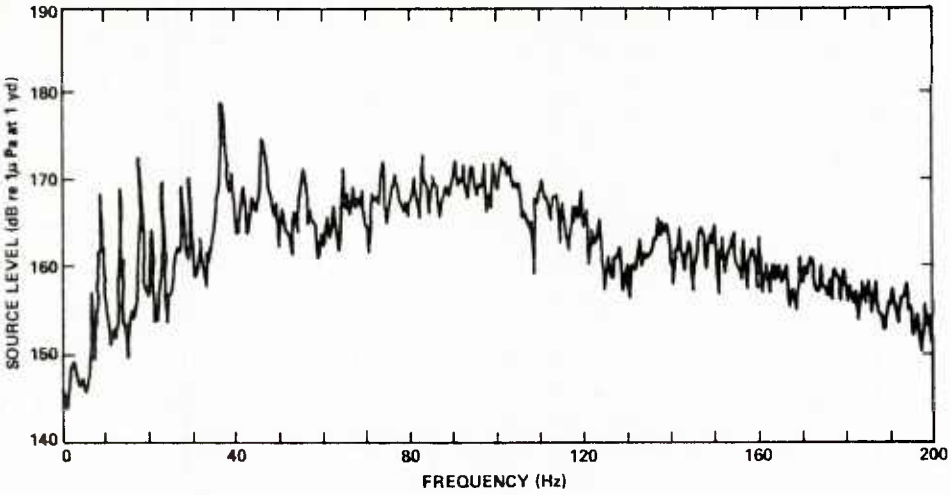

FIG 5: ENVELOPE OF CONTINUOUS RADIATION FROM A BULK CARRIER OBSERVED AT A 29° DEPRESSION ANGLE

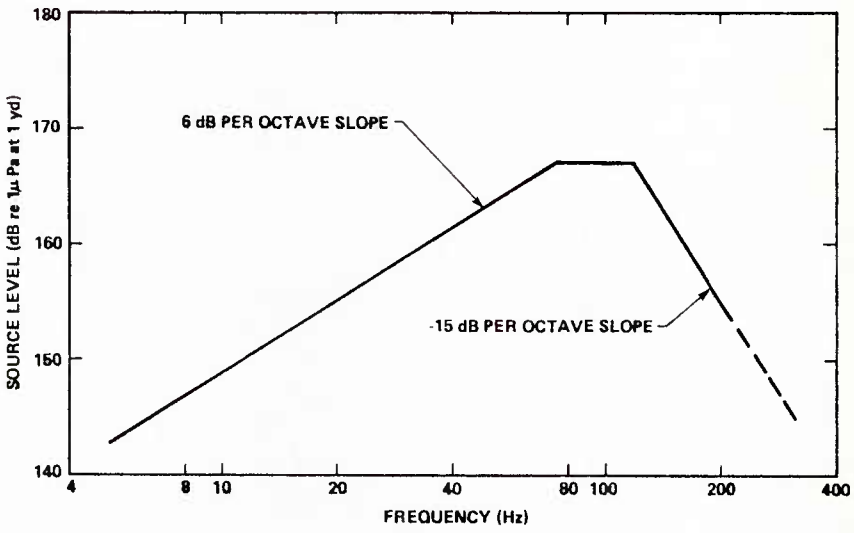

FIG 6: BLADE RATE HARMONIC LINE LEVELS OF A BULK CARRIER OBSERVED AT A DEPRESSION ANGLE OF 29°

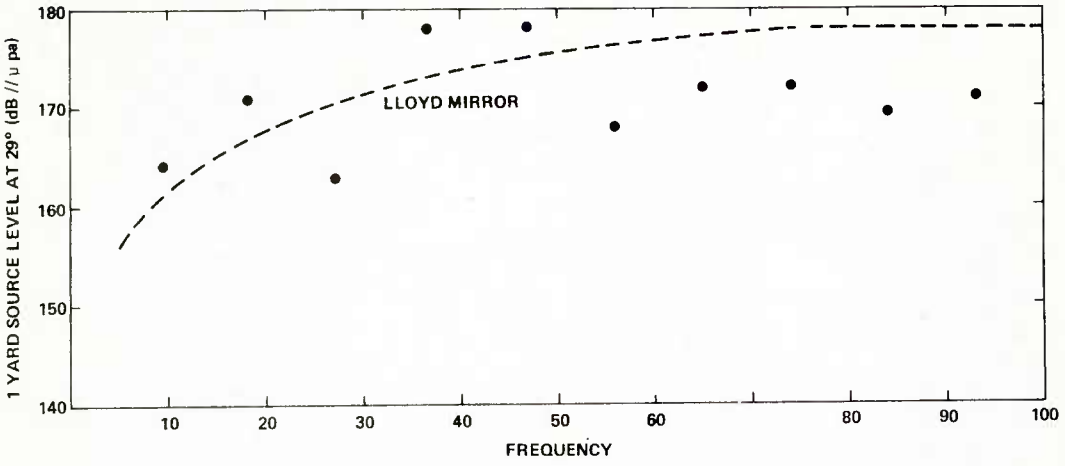

FIG 7: DIRECTIVITY OF 600 ft MERCHANT VESSEL AT 9.3 AND 37 Hz VERSUS (a) DEPRESSION ANGLE AT 90° ASPECT AND VERSUS (b) ASPECT AT A 15° DEPRESSION ANGLE

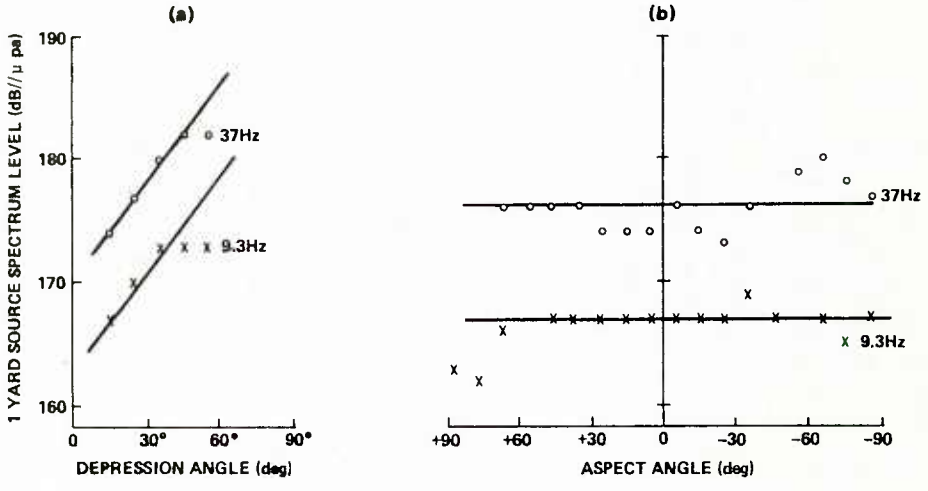

FIG 8: OBSERVED FLUCTUATIONS IN SHAFT ROTATION RATE AND SHIP HEAVE

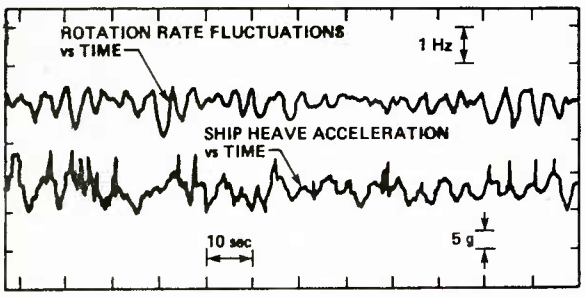

FIG 9: PROBABILITY DENSITY FUNCTION FOR
PERCENT SHAFT ROTATION RATE DEVIATION

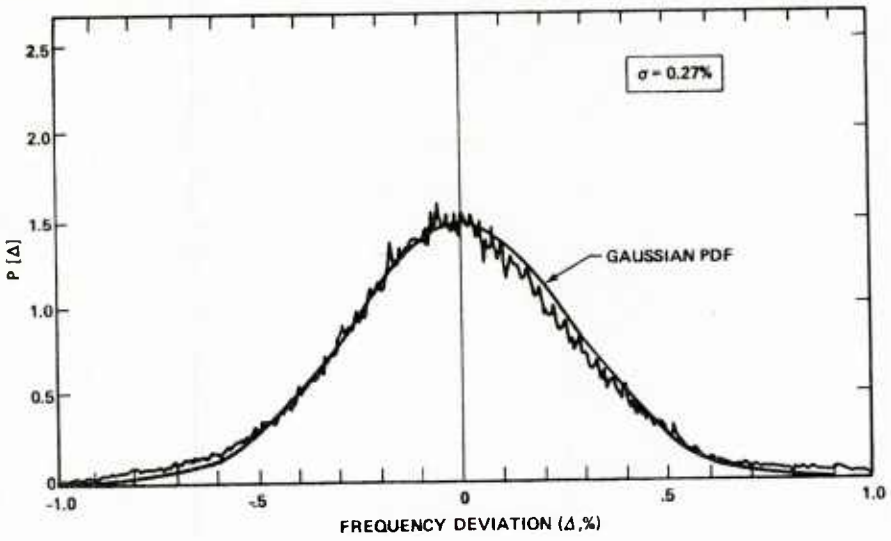

FIG.10: PROPERTIES OF RPM MODULATION
(a) AUTO SPECTRUM OF RPM TIME SERIES
(b) AUTO SPECTRUM OF SHIP HEAVE ACCELERATION
(c) CROSS COHERENCE OF RPM AND SHIP HEAVE

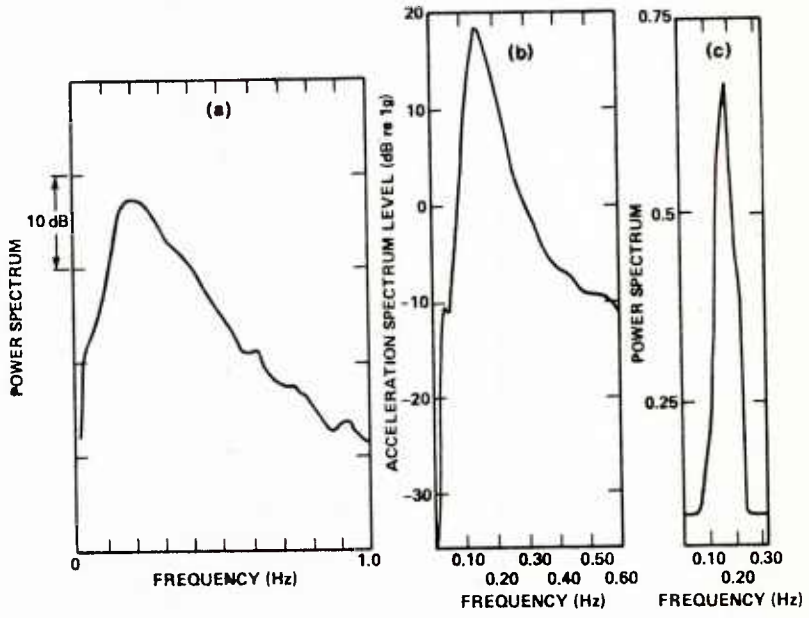

FIG 11: POSSIBLE MERCHANT SHIP LINE BANDWIDTH CHARACTERISTICS

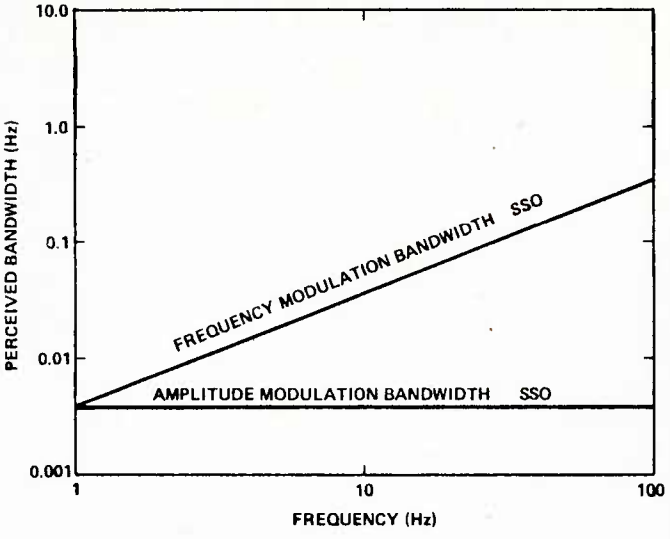

FLOW NOISE INTERFERENCE IN MEASUREMENTS OF INFRASONIC AMBIENT NOISE

by

M. Strasberg
David Taylor Naval Ship R&D Center
Bethesda, MD 20084, USA

ABSTRACT

Estimates are presented of the local noise generated at infrasonic frequencies by turbulent water flowing in the vicinity of hydrophones used for measurements of ambient noise in the sea. Three situations are discussed: a hydrophone held between the surface and the bottom with water streaming past it; a hydrophone resting on the bottom with a turbulent boundary-layer flow above it; and a neutrally buoyant hydrophone floating with the mean speed of the current. The estimates are compared with published data on infrasonic ambient noise, and it is shown that some of the data may be contaminated by flow-noise interference.

INTRODUCTION

Measurements of ambient noise in the sea can be disturbed by local non-acoustic pressure fluctuations developed by turbulent water flowing in the vicinity of the measurement hydrophones, especially at infrasonic frequencies. The possibility that local turbulent flow may generate noise which interferes with the true ambient noise arriving from distant sources has been recognized for some time; e.g., by Bardyshev et al [1], among others. The purpose of the present paper is to describe quantitative estimates of the flow noise level for the frequency range 0.1 to 10 Hz, and to compare these estimates with reported ambient noise levels so as to indicate the extent of the interference problem.

Four hydrophone arrangements will be discussed which are shown schematically in Fig. 1. A common arrangement is to suspend a negatively-buoyant hydrophone at some depth below the surface from a cable attached to a surface float. An alternate arrangement uses a submerged, positively-buoyant hydrophone floating at a predetermined depth while tethered to a bottom anchor. In both cases, some relative motion between the hydrophone and the water around it is almost always present. In the former case, relative motion results from the difference between the drift of the surface float and the naturally occurring current in the water at the hydrophone depth. In the latter case, the current is the only source of relative motion. A third arrangement uses a hydrophone resting on the bottom, and a fourth uses a neutrally buoyant hydrophone floating freely at a predetermined

depth and moving with the local current. In the latter two configurations, there is substantially no mean flow around the hydrophone, but naturally occurring turbulence in the water results in pressure fluctuations which are transmitted to the hydrophone.

The noise associated with each of these configurations is discussed in the sections which follow. The estimates of absolute noise level are only rough approximations, unfortunately, for several reasons. Firstly, the theoretical analyses involve simplifying assumptions and approximations. Secondly, values of some of the physical quantities required for the estimates are not generally available with any degree of certainty. Indeed, the lack of precise data on the physical quantities makes improvements to the theory of little consequence at this time. The most that can be accomplished with existing data is to indicate those circumstances where there is a significant possibility that reported levels of ambient noise are contamined by flow-induced noise interference.

1. HYDROPHONE IN THE FLOW

The first two configurations, where water flows directly around the hydrophone surface, have been discussed in detail in an earlier paper [2]. Only a brief summary of the results of that paper will be given here, with the level estimates extended down to 0.1 Hz.

Flow around the hydrophone can generate pressure fluctuations in two ways. Firstly, the flow develops local turbulence in the boundary layer directly on the hydrophone and in the wake behind it, and this turbulence generates local pressure fluctuations sensed by the hydrophone. Secondly, any pre-existing turbulence in the water flowing past the hydrophone results in additional pressure fluctuations.

In the earlier paper, it was shown how the pressure fluctuations generated on a hydrophone by locally developed turbulence can be estimated from measurements in air of the wind noise sensed by a microphone inside a wind screen having the same shape as the hydrophone. Although air and water have very different compressibilities, both fluids behave in an essentially incompressible manner at the low subsonic flow speeds and low frequencies of interest here (the frequencies of interest correspond to acoustic wavelengths much larger than the dimensions of the wind screen and hydrophone). The difference in the density of air and water, and differences in physical dimensions, are accounted for by expressing the data in non-dimensional form, as is commonplace in hydrodynamics.

Some old data on wind noise inside a cylindrical wind screen [3] leads to the following approximate relation for the spectrum of the wind-generated noise, expressed in dimensionless form:

$$\frac{f\, S_p(f)}{\rho^2 U^4} \simeq 3\times10^{-8}\left[\frac{U}{fD}\right]^3 \qquad (1)$$

where $S_p(f)$ is the spectral density of the fluctuating pressure at cyclic frequency f, ρ is the fluid density, U the relative velocity of water flowing past the cylinder, and D the cylinder diameter. Spectral density is defined in this paper so that its integral on positive cyclic frequency equals the total mean square, e.g.,

$$\overline{p^2} = \int_0^\infty S_p(f)\, df$$

Equation (1) is based on data covering only a limited range of the variable, viz. $0.1 < (fD/U) < 5$, but this range includes most of the present range of interest. For example, if f = 5 Hz, D = 2 inches (5 cm), and U = 1/2 knot (25 cm/sec), then (fD/U) = 1.

Equation (1) applies to any fluid, air or water, provided the appropriate density is used and provided the variables are limited to the range just discussed. The equation can be converted into the following numerical formula relating the spectrum level of the pressure fluctuations to the other variables expressed in commonly used units:

$$\underline{L}_p = 144 + 20 \log \underline{\rho} + 70 \log \underline{U} - 30 \log \underline{D} - 40 \log \underline{f} \ , \qquad (2)$$

where $\underline{L}_p$ is the pressure spectrum level in dB re 1 μPa for a 1-Hz band, $\underline{U}$ velocity in knots, $\underline{D}$ cylinder diameter in cm, $\underline{f}$ frequency in Hz, and $\underline{\rho}$ is fluid density in gm/cm (log $\underline{\rho}$ = 0 for water). In this formula, and those which follow, underlined symbols are used for quantities requiring the specified units in equations which are not dimensionally homogeneous. The formula was derived in the earlier paper and displayed there as Eq. (10), with $\underline{D}$ in different units.

Equation (2) indicates that this type of flow noise is very dependent on speed; the spectrum level increases 21 dB for each doubling of speed at a fixed frequency. The level decreases 12 dB per frequency double and 9 dB per diameter double.

Another component of fluctuating pressure will be generated by interaction of the hydrophone with any turbulence already present in the water. As discussed in the earlier paper [2], turbulent currents ordinarily occur in the sea with rms velocity fluctuations typically ranging from 0.05 to 1 cm/sec superimposed on mean flow velocities from 5 to 50 cm/sec (0.1 to 1 knot). When a turbulent current flows past a hydrophone, the small variations in flow velocity result in fluctuations in the hydrodynamic pressure on the hydrophone surface which are sensed by the hydrophone as noise.

A simple, approximate analysis of this noise-generating mechanism indicates that the spectra of the pressure and velocity fluctuations are approximately related by

$$S_p(f) \simeq \rho^2 C^2 U^2 \, S_u(f) \ , \qquad (3)$$

where $S_p(f)$ is the spectral density of the fluctuating pressure, $S_u(f)$ the one-dimensional spectral density of the turbulent velocity component in the direction of the mean flow, U the mean flow velocity, and C is a constant whose value depends on the size and shape of the hydrophone and also, in general, on the frequency. Equation (3) was derived in the earlier paper for a cylindrical housing (for which C = 1) and displayed there as Eq. (5).

Equation (3) can be converted in a numerical formula

$$\underline{L}_p(f) = 125 + 20 \log C + 20 \log \underline{\rho} + 10 \log U + \underline{L}_u(k_1) \quad , \tag{4}$$

where, as before, $\underline{L}_p$ is the spectrum level of the pressure flucuations in dB re 1 μPa for a 1-Hz band, $\underline{\rho}$ fluid density in gm/cm^3, U mean flow velocity in knots, $\underline{L}_u(k_1)$ is the spectrum level of the turbulent velocity component in the direction of the mean flow, re 1 cm/sec for a 1 rad/cm band of wave number, and wave number is related to frequency by $k_1 = 2\pi f/U$.

The constant C in the above equations will be independent of frequency or hydrophone dimensions if both quantities are small enough. For high frequencies, or large hydrophones, the turbulence-induced pressure fluctuations tend to have opposing phases and partially cancel on different portions of the hydrophone surface, and thus the excitation of the hydrophone is attenuated. The small-attenuation condition is limited to values of the variables defined approximately by

$$(fL/U) < 1/2 \quad , \tag{5}$$

where L is the largest dimension of the sensitive region of the hydrophone. For lower frequencies, or smaller dimensions, the constant C depends only on the shape of the hydrophone; C = 1 for a cylindrical hydrophone and 1/2 for a spherical one.

To use Eq. (4) for quantitative estimates of the turbulence-hydrophone interaction noise, the spectrum of the naturally occurring turbulence in the sea must be known. Unfortunately, there is a paucity of data on turbulence spectra for the small wave numbers of interest here (0.01 to 10 rad/cm). To obtain an order of magnitude estimate, a spectrum reported by Grant et al [4] was used. This spectrum was measured off the Canadian Pacific Coast at a depth of 89 m. Two intersecting straight lines were used to represent the data points of Grant's Fig. 11, one for wave numbers below 0.2 rad/cm and the other for higher wave numbers. With the values given by the lower-wave number line substituted for $S_u(k_1)$ in Eq. (4), the estimate for pressure spectrum level becomes

$$L_p(f) \simeq 117 + 27 \text{ Log } U - 17 \log f \tag{6a}$$

For higher wave numbers, corresponding to (f/U) > 1.6 Hz/knot, the estimated spectrum level becomes

$$\underline{L}_p(f) \simeq 119 + 37\ \underline{U} - 27 \log \underline{f} \quad , \tag{6b}$$

Both numerical formulas require the same units as Eq. (4). They are also both limited to frequencies and dimensions given by Eq. (5), viz., $fL < \frac{1}{2} U$.

No other data has been found for turbulence levels in the wave-number range of interest, so it is not possible to determine whether Grant's turbulence levels, or the estimates made using them, have any universal applicability. Nevertheless, whenever the speeds and frequencies are such that the estimates given by Eq. (6) are higher than those of Eq. (2), there should be concern with the possibility of noise due to hydrophone-turbulence interaction.

2. HYDROPHONE ON THE BOTTOM

No matter how large the current in the ocean, the flow velocity decreases to zero at the bottom, because of the finite viscosity of the water. Accordingly, there will never be any substantial flow directly around a small or flat hydrophone resting on the bottom. Nevertheless, water flowing above the bottom will develop a turbulent boundary layer which will generate fluctuating pressures sensed by a bottom hydrophone.

The pressure fluctuations at the boundary of turbulent boundary layers have been studied extensively for the past 20 years. The experimental data fall into two categories: measurements made in laboratory facilities, mainly wind tunnels, and measurements made outdoors in the naturally occurring boundary layer developed by winds over open spaces. Although these measurements have been made in air, the data should be applicable to water if the data are expressed in non-dimensional form, as discussed in the previous section.

For the present, the estimate will be based on measurements reported by Elliot [5] of pressure fluctuations above the water surface of a tidal flat. The straight line through the data points on Elliot's Fig. 5(a) leads to the following numerical formula for the spectrum level of the boundary-layer pressure fluctuations on the sea bottom:

$$\underline{L}_p = 100 + 57 \log \underline{U}_\infty - 17 \log \underline{f} \quad , \tag{7}$$

where $\underline{U}_\infty$ is the so-called free stream velocity, i.e., the velocity at a large distance above the bottom. All quantities have the units previously specified for Eq. (4). The formula is based on data covering the range $5 \times 10^{-4}\ \text{cm}^{-1} < (f/U_\infty) < 2 \times 10^{-2}\ \text{cm}^{-1}$.

Equation (7) implies a spectrum level independent of the size of the hydrophone. This is indeed the case for a very small hydrophone at sufficiently low frequencies. When the hydrophone is large and the frequencies high enough, however, the pressure fluctuations have opposing phases on different portions of the hydrophone surface and tend to partially cancel. The attenuation of the pressure fluctuations due to this cancellation has been discussed in several papers. The calculations of White [6], for example, indicate that the attenuation of a hydrophone having uniform sensitivity over a circular region of diameter D will be 3 dB when $(fD/U_\infty) = 1/4$, and 10 dB when $(fD/U_\infty) = 0.6$. For a flow speed of 1 knot and a frequency of 1 Hz, for example, the attenuation will be 3 dB if the diameter is 12 cm, and 10 dB if 30 cm.

3. HYDROPHONE MOVING WITH THE CURRENT

When a submerged, neutrally buoyant hydrophone is allowed to float freely along with the local current, the mean velocity between the hydrophone and the water is substantially zero. Under these circumstances, the noise generating mechanisms described in the previous sections are absent, and the only pressure fluctuations sensed by the hydrophone are those that occur naturally in the sea, in the absence of the hydrophone. Wenz [7] discusses naturally occurring pressure fluctuations, but his estimates are not entirely relevant to the freely-floating hydrophone, for reasons to become apparent in the discussion which follows.

No experimental data on the pressure fluctuations in a turbulent region have been found for circumstances like those existing in the open sea. Theoretical relations between fluctuating pressure and velocity have been derived by Batchelor [8], and by others, for turbulence which is at least locally homogeneous and isotropic. These conditions are approximately satisfied in the open sea. It is thus possible, in principle, to calculate the spectrum of the pressure fluctuations by numerical integration of an integral such as Batchelor's Eq. (5.13), using experimentally determined turbulent velocity spectra in the integrand. Such a detailed calculation does not seem to be worthwhile, however, because of the uncertainty in the universal applicability of the available velocity spectra. Instead of a detailed calculation, an approximate relation between turbulent velocity and pressure spectra seems more appropriate for the order of magnitude estimates being attempted here.

An approximate relation between the two spectra can be derived for isotropic and homogeneous turbulence by noting that if the correlation function $R_u(r)$ of the turbulent velocities at two points separated by distance r varies with r in accordance with the Gaussian function

$$R_u(r) = \tilde{u}_r^2 \exp(-a^2 r^2) \quad ,$$

then, as a consequence of Batchelor's Eq. (5.5), the correlation of the fluctuating pressure at two points has the same Gaussian dependence on r, viz.,

$$R_p(r) = \rho^2 \tilde{u}_r^4 \exp(-2a^2 r^2) \quad ;$$

but with the exponent increased by the factor 2. In these relations, the correlations are for the velocity component u_r which is directed along the line between the two points, and the circumflex (~) indicates an rms value. Since the turbulence is assumed to be isotropic, u_r and the correlations are independent of direction.

The spectral densities of the fluctuating pressure and velocity are equal to the Fourier transforms of their correlation functions. Since Gaussian functions are their own Fourier transforms, the spectral densities are also Gaussian functions. Accordingly, the velocity and pressure spectral densities are, respectively,

$$S_u(k_r) = (\sqrt{\pi}/a)\, \tilde{u}_r^2 \exp[-(k_r/2a)^2] \quad ,$$

and

$$S_p(k_r) = (1/\sqrt{2})\, \rho^2 \tilde{u}_r^2\, S_u(k_r/\sqrt{2}) \quad , \qquad (8)$$

where k_r is the magnitude of the three components of the wavenumber. Both spectral densities have the same functional dependence on wave number k_r except that values of pressure spectrum are shifted to a wave number lower by a factor $\sqrt{2}$. Note that Eq. (8) relates pressure and velocity spectra.

To use this relation for estimates, the bold generalization is now made that it is approximately valid for all forms of correlation function. Somewhat as an aside, it is noted that Eq. (8) appeared in my earlier paper [2], without the factor $\sqrt{2}$. In that paper, I stated that the equation "had no theoretical foundation." There does, indeed, seem to be a basis for the equation, although some may consider the basis to be tenuous.

Equation (8) expresses the spectra in terms of wave-number components, i.e., in terms of the spatial fluctuations of the pressure and velocity. However, a hydrophone moving with the mean flow will not sense these spatial fluctuations at all. The hydrophone only senses temporal functions. Accordingly, what is required is a relation between spatial and temporal fluctuations in a coordinate system moving with the mean flow.

To obtain such a relation, an ergotic-like hypothesis is made, that the spatial statistics of the isotropic turbulence have the same functional form as the temporal statistics. With such an hypothesis, spatial wave number and temporal frequency are related to each other by a scale factor, and the spectral density $S_p'(f)$ of the pressure fluctuations, on frequency, is related to the spectral density on wave number, by

$$S_p'(f) = (2\pi/U_s)\, S_p(k_r)$$

where U_s is the as yet unknown space-time scale factor, with dimensions of a velocity, such that $k_r = (2\pi f/U_s)$. Equation (8) then becomes

$$S'_p(f) = (\pi\sqrt{2})\, \rho^2 \tilde{u}_r^2\, U_s^{-1}\, S_u(k_r/\sqrt{2}) \quad , \tag{9}$$

The unknown space-time scaling factor U_s may be expressed as an unknown fraction s of the mean velocity U of the current, viz., $U_s = sU$. With this substitution, Eq. (9) may be converted into the following numerical formula for the spectrum level of the pressure fluctuations at frequency f:

$$\underline{L}_p(f) = 90 + 20 \log \underline{\rho} + 20 \log \underline{\tilde{u}}_r - 10 \log s - 10 \log \underline{U} + \underline{L}_u(k_r/\sqrt{2}) \tag{10}$$

Here L_p is in dB re 1 μPa in a 1-Hz band; $\underline{\rho}$ fluid density in gm/cm^3; $\underline{\tilde{u}}_r$ the rms velocity of one component of the turbulence in cm/sec; U the current velocity, in knots; $\underline{L}_u(k_r)$ the spectrum level of one component of the turbulent velocity, in dB re 1 cm/sec in a 1-rad/cm band of wave number; and wave number and frequency are related by $k_r = (2\pi f/sU)$.

To obtain an estimate of the spectrum level, values must be assigned to the rms velocity $\tilde{u}_r$, the spectrum of the turbulence L_u, and the scale factor s. For the turbulence spectrum, the data in Fig. 11 of Grant et al [4] is used again. The rms velocity u_r is also obtained from Grant's Fig. 11 by integrating the spectrum over frequency to give $\tilde{u}_r \simeq 0.7$ cm/sec.

The space-time factor s is entirely unknown. The only available information on this quantity comes from measurements made in wind-tunnel boundary layers of a type of fluctuating-pressure correlation called a "moving-frame correlation" by Fisher and Davies [9] or a "space-time correlation" by Willmarth and Woodridge [10]. These wind-tunnel data can be interpreted to indicate that the scale factor is equal to about 0.1. Whether this result applies to ocean turbulence is not known; but in the absence of anything better, it is assumed that s = 0.1 in Eq. (10). With this value for s, and Grant's values for the turbulence, Eq. (10) becomes

$$L_p = 67 + 17 \log \underline{U} - 27 \log \underline{f} \quad , \tag{11}$$

where the same units are used as before.

It should be noted that the levels estimated by Eq. (11) are much lower than Wenz's estimates [7] of turbulent pressure fluctuations, shown in his Fig. 11. One reason for the difference is that Eq. (11) applies to a hydrophone moving with the current and sensing only temporal fluctuations. Wenz presumably assumed that the current was moving relative to the hydrophone, so the hydrophone was scanning through the spatial pattern of fluctuations. If a hydrophone scans through a spatial pattern at speed U, it will sense fluctuations at a frequency f related to the spatial wave number k by $k = (2\pi f/U)$. In contrast, if only temporal fluctuations are sensed, the wavenumber will depend on the space-time scaling velocity U_s instead of U, so $k = 2\pi f/U_s$. If $U_s = 0.1\ U$, as was assumed to obtain

Eq. (11), the latter wave number will be 10 times higher than the former one, for the same temporal frequency. If the spectrum level of the turbulence has a negative slope of 27 dB/decade, as in Eq. (11), then the spectrum level will be 27 dB lower at the latter wave number. Wenz also assumed higher values for the turbulent velocity; the smallest rms value in his Fig. 11 is 2 cm/sec, compared with 0.7 cm/sec assumed here.

4. DISCUSSION

Estimated spectrum levels for the four types of flow-generated noise are compared in Fig. 2, all for a current of 1/2 knot. It is apparent that the noise level is highest when the current flows directly around the hydrophone, lowest when the hydrophone is free and allowed to move with the current, and between these extremes when the hydrophone is resting on the bottom. An intuitive guess might, perhaps, have led to the same conclusion.

To indicate how much interference these flow-induced pressure fluctuations can cause, the estimated spectrum level of the noise generated by flow directly around a cylindrical hydrophone is compared in Fig. 3 with several measured spectra of ambient noise in the sea. This figure is taken from the earlier paper [2]. The flow-noise estimates are indicated in the figure by broad straight-line stripes, for flow speeds of 1/4, 1/2, and 1 knot. The zig-zag stripes correspond to the level estimate of Eq. (2), for non-turbulent water passing a hydrophone whose diameter is 5 cm. The level decreases 9 dB with each double of diameter. The stippled stripes, with smaller slopes but higher levels, show the estimate of pressure fluctuations due to interaction between the hydrophone and pre-existing turbulence, as given by Eq. (6b). These levels are independent of cylinder diameter provided it is small enough to satisfy Eq. (5); the stripes in the figure end at the highest frequency satisfying this inequality when L = 5 cm.

The measured ambient noise spectra shown in the figure come from various sources. The "Wenz" curve is a deep-water average shown in Fig. 14 of his survey [7]. Citations for the other curves are given in the earlier paper [2]. All these measured ambient noise spectrum levels are within the range of the estimated interference levels for currents above 1/2 knot. Whether or not such currents existed during the measurement periods is not known.

Figure 4 shows estimated spectrum levels of the boundary-layer pressure fluctuations sensed by a hydrophone resting on the bottom, and compares these estimates with levels reported by Nichols [11] of ambient noise measured with a hydrophone on the bottom. The data points are Nichols' levels, taken from his Fig. (4) and averaged for two bottom depths of 300 m and 1200 m. His hydrophone was placed inside a large, flat housing perforated with holes over a circular area about 70 cm in diameter. The three straight lines in the figure indicate the estimated flow-noise levels given by Eq. (7), for currents of 1/4, 1/2, and 1 knot (50 cm/sec). The dashed curves peeling off these straight lines indicate the estimated attentuation due to Nichols' housing, calculated from Fig. (1) of White [6], assuming that the perforations in Nichols' housing provide a circular area of uniform sensitivity.

Nichols' measured levels are somewhat higher than the estimated boundary-layer noise. Accordingly, it is not likely that flow noise interference occurred, unless the current exceeded 1 knot.

The pressure fluctuations sensed by a hydrophone moving with the current, as estimated by Eq. (10), are too small to be of concern. These levels set a lower limit for the flow-noise level during ambient noise measurements in the sea.

These estimates of flow-induced noise are based on what are admittedly oversimplified theoretical analyses of the phenomena, combined with data on turbulence levels whose universal applicability is not verified. Nevertheless, the estimates are presented despite these uncertainties to indicate that the existence of flow-noise interference in infrasonic ambient noise measurements cannot be dismissed without further consideration.

REFERENCES

[1] V.I. Bardyshev, A.M. Velikanov, and S.G. Gershman, "Experimental Studies of underwater noise in the ocean," Sov. Phys. Acoust. 16, 512-513 (1971).

[2] M. Strasberg, "Nonacoustic noise interference in measurements of infrasonic ambient noise," J. Acoust. Soc. Am. 66, 1487-1493 (1979).

[3] "Self noise of cylindrical windscreens," Bolt Beranek and Newman Report 225, Job 637 (August 1954) (author's name not listed, but known to be I. Dyer).

[4] H.L. Grant, B.A. Hughes, V.M. Vogel, and A. Moilliet, "The spectrum of temperature fluctuations in turbulent flow," J. Fluid Mech. 34, 423-442 (1968), Fig. 11.

[5] J.A. Elliot, "Microscale pressure fluctuations measured within the lower atmosphere boundary layer," J. Fluid Mech. 52(2), 351-383 (1972).

[6] Pritchard H. White, "Effect of transducer size, shape and surface sensitivity on the measurement of boundary-layer pressures," J. Acoust. Soc. Am. 41, 1358-1363 (1966).

[7] M. Wenz, "Acoustic ambient noise in the ocean," J. Acoust. Soc. Am. 34, 1936-1956 (1962).

[8] G.K. Batchelor, "Pressure fluctuations in isotropic turbulence," Proc. Camb. Phil. Soc. 47, 359-374 (1951).

[9] M.J. Fisher and P.O.A.L. Davies, "Correlation measurements in a non-frozen pattern of turbulence," J. Fluid Mech. 18(1), 97-116 (1964).

[11] R.H. Nichols, "Infrasonic ambient ocean noise measurements: Eleuthera," J. Acoust. Soc. Am. 69, 974-981 (1981).

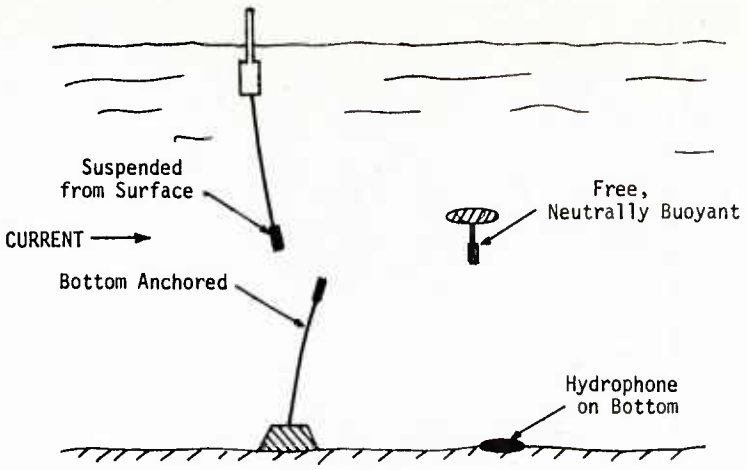

FIG. 1 FOUR HYDROPHONE ARRANGEMENTS SUBJECT TO FLOW-INDUCED NOISE

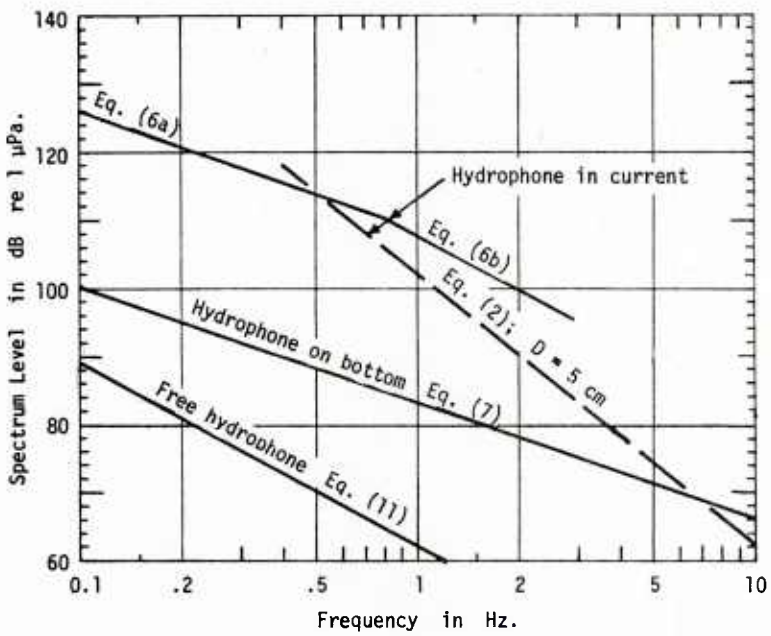

FIG. 2 ESTIMATES OF FLOW-INDUCED NOISE FOR VARIOUS HYDROPHONE ARRANGEMENTS, ALL FOR A CURRENT OF 1/2 knot (25 cm/sec). The upper set of lines, labelled "hydrophone in current". are for the two arrangements shown in Fig. 1 on the left. The lower two lines are for the two arrangements on the right of Fig. 1

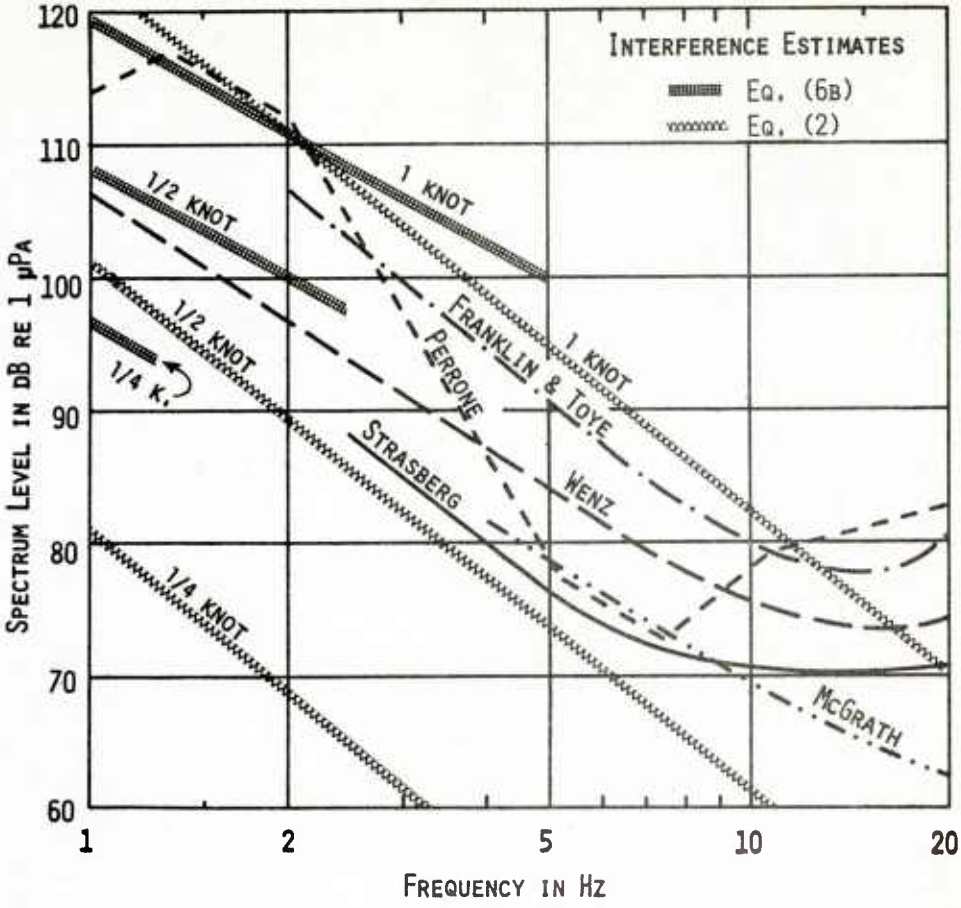

FIG. 3 COMPARISON OF VARIOUS MEASURED SPECTRA OF AMBIENT NOISE WITH ESTIMATES OF FLOW NOISE WHEN THE CURRENT FLOWS DIRECTLY AROUND THE HYDROPHONE. The zig-zag stripes are estimates at three speeds for a hydrophone 5 cm in diameter, based on Eq.(2). The shorter stippled stripes are based on Eq.(6b); these are independent of hydrophone size if smaller than 5 cm.

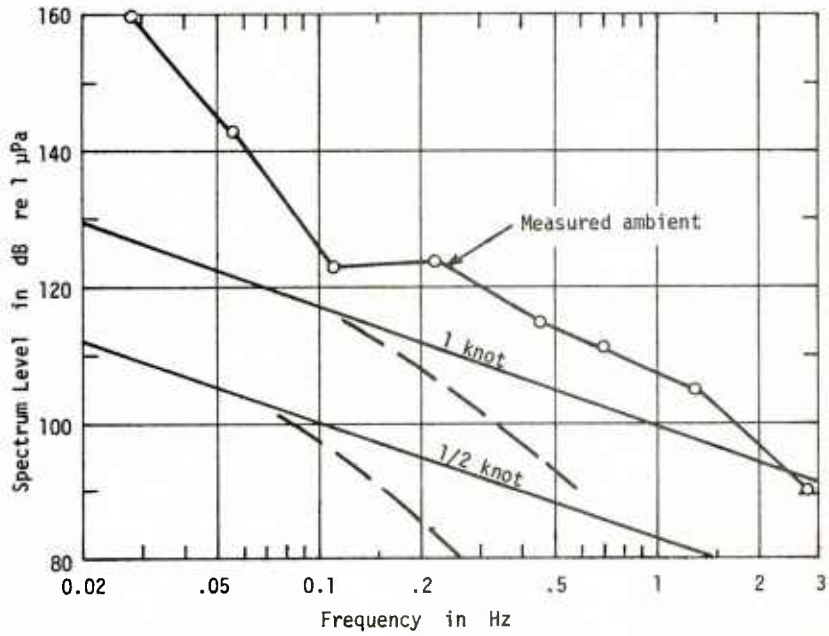

FIG. 4 VERY LOW-FREQUENCY SPECTRA OF AMBIENT NOISE MEASURED BY NICHOLS [11] WITH A HYDROPHONE RESTING ON THE BOTTOM, COMPARED WITH ESTIMATES OF THE FLOW NOISE INDUCED BY THE TURBULENT BOUNDARY LAYER, BASED ON EQ.(7)

LOW FREQUENCY SEISMIC AND HYDROACOUSTIC NOISE MEASUREMENTS IN A FJORD

by

Erik Sevaldsen
Norwegian Defence Research Establishment
Div U, Horten, Norway

ABSTRACT

Low frequency ambient noise signals from an ocean bottom seismometer (OBS) put on the sea floor of a Norwegian fjord have been studied. The instrument contains 3 seismometers and one hydrophone, and signals from all 4 sensors are analyzed. Measurements have been done over several local areas which have been found to be reasonably well stratified. Depth and bottom parameters like sediment type and -thickness and subbottom type vary from place to place. Noise characteristics in terms of power spectral densities, amplitude statistics and directionality are treated with emphasis on variations with time and changes in environmental parameters. The statistical processes involved are highly variable and may not in general be considered stationary. Noise spectrum levels have been found to be higher than reported from open waters. Human activity in and around the closed fjord area must be the main cause of this increased noise.

INTRODUCTION

Under the NDRE marine seismic program characteristics of low frequency ambient seismic noise should be studied among other aspects of underwater seismic propagation. Limitations to the study are largely determined by our equipment - one Ocean Bottom Seismometer (OBS) station of the Saclantcen type (ref 1). Thus spatial coherence of the noise field has been excluded, and the range of frequency is limited to (1 - 100) Hz.

We think that the most important factors to influence seismic background noise at sea are

- seismicity (microseisms, small earth quakes)
- nearby ship traffic
- distante shipping
- environmental factors (water depth, wind, waves ice)

- open or closed area

  in closed areas

  - land traffic
  - nearby factories (ship yards, other)
- bottom parameters (hard or soft bottom)

Most of the factors listed represent sources of noise. Only bottom parameters and type of area (open or closed) have to do with the seismic propagation properties of the sea floor.

Our seismic program covers studies of seismic propagation in several areas of various bottom composition in open and closed waters.

This paper presents data from one particular area only, a fjord near the lab. The emphasis of the study has been on the effects of environmental factors, on bottom properties, and on human activity in the area (on sea and land).

1 MODELS AND SIMULATIONS

Our test area is located in the Oslo fjord near Horten, Norway (Fig 1). Data have been collected at 5 different locations for short periods of time during a cruise in November/December 1981. Measurements have also been done over longer time periods at one particular location (inside area no 2, see Fig 1), where the OBS was put down for the winter.

To be able to model seismic propagation in an area it is necessary that the subbottom be reasonably well stratified. Obviously the fjord is not really stratified. There are, however, local areas numbered 1 to 5 which can be considered stratified. The extent of these areas is small, around 5 km at most.

What characterizes the sea floor of the fjord is a very hard subbottom. The areas 1 to 5 are not at all equal as can be seen from Table 1, but all of them exhibit this hard acoustic basement with shear speeds much higher than sound speed in water. The geoacoustic models shown in Table 1 represent in an approximate way the subbottom layering of area 1 to 5. Only layer thickness and bulk velocities are shown. Damping constants and densities are not included in the table. These model parameters have been used for simulations of propagation conditions on our Fast Field Program (FFP) model. Results from area 2 are presented in Fig 2.

Simulation results from all 5 areas are quite similar in that they are all dominated by the very hard subbottom. The phase velocity of mode ϕ, the Scholte or Stonley wave at the basement interface is higher than the speed of sound in water. Mode ϕ dominates the propagation at the lowest end of the spectrum and also at intermediate frequencies.

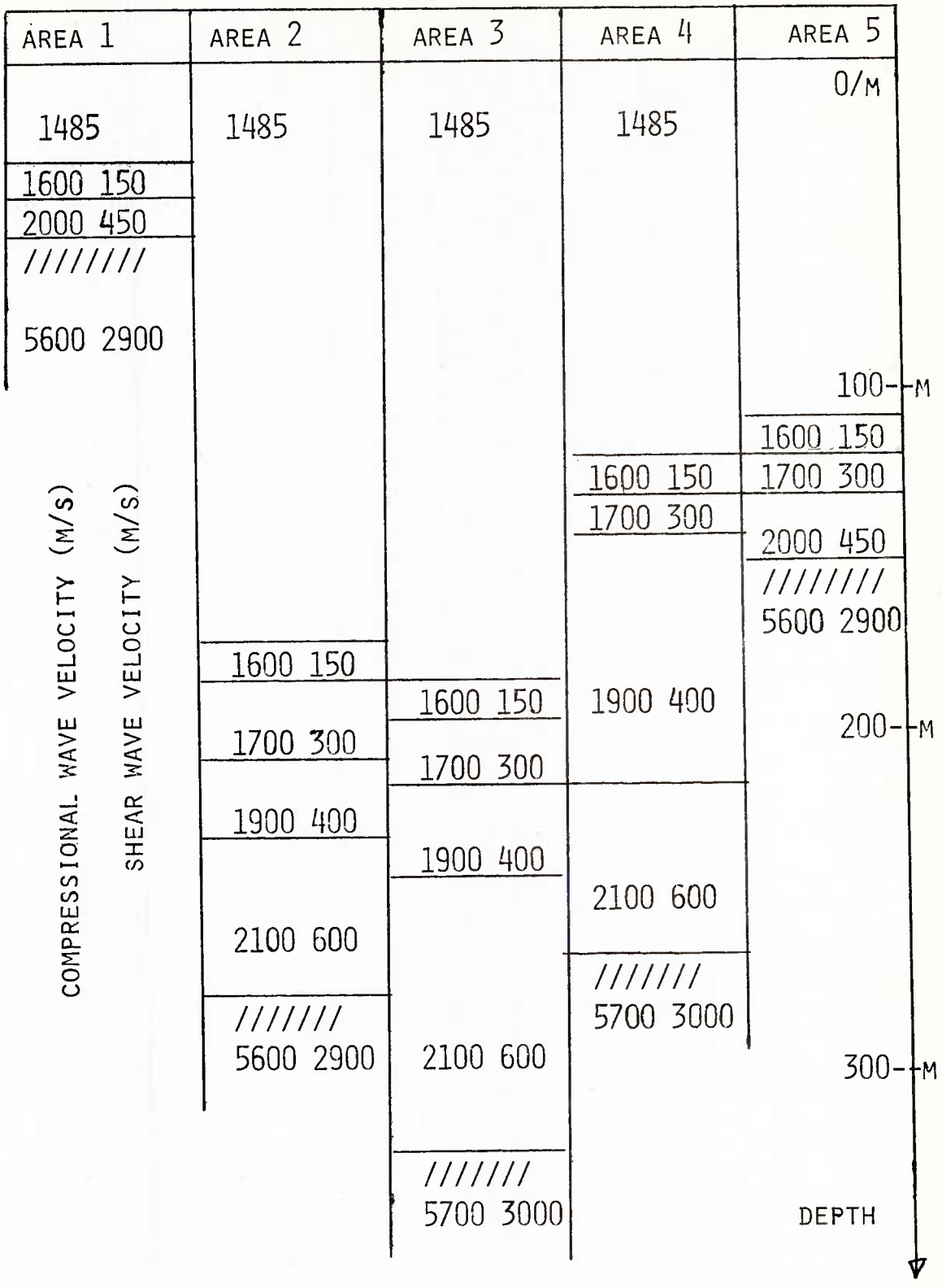

TABLE 1 GEOACOUSTIC MODELS FROM THE OSLO FJORD AREA

Areas no 2, 3 and 4 show a low speed seismic wave propagating in the unconsolidated sediment layer. It is not of much importance but contributes to the propagation in the frequency range 2 - 3 Hz (area 2 and 3). Depending on water depth and thickness of sediments the number of water modes inside the frequency band of interest will vary.

2 MEASUREMENTS

The OBS equipment used for data collection has been develloped at Saclantcen, La Spezia, Italy, and has been thoroughly described elsewhere (ref 1). Here we only mention that the OBS incorporates 4 sensors, 3 seismometers and one hydrophone. The system is devided in 3 parts as shown in Fig 3, a sensor unit connected to a surface radio buoy by coaxial cable and a receiving unit which delivers digital data to the computer and to the monitoring and recording equipment.

The seismometers limit the useful frequency band to 1 - 100 Hz. A 200 Hz LP-filter limits the hydrophone signal frequency band. Sampling frequency of the system is 600 Hz pr channel, i e 2400 Hz in total. Dynamic signal range is 120 dB.

Data collection was done in the following way: In each of the five local areas involved a particular position for the OBS was selected. The OBS was then lowered to the sea floor and we were ready for the measurements. The purpose of the experiments was twofold, propagation and noise studies. Propagation sound sources were explosives fired on the bottom or at mid-water depth at various distances from the OBS. Our research vessel, "H U Sverdrup", was used both as source- and receiving platform. Each shot was recorded on digital tape, and the records were made long ($1\frac{1}{2}$ minute) to include ambient noise. Also longer (10 minute or more) noise samples were taken at various times during the experiments. At the end of this series of measurements the OBS was put down for the winter on the bottom at a location near the lab. The location is shown on the map (Fig 1). The surface end of the cable was taken on shore and the receiving unit was placed in the lab and connected to a computer. During the winter 1982 we have recorded ambient and ship noise several times. Collection of data will be continued this summer and fall in other areas with different types of bottom. We will be making measurements both in the North Sea, in the Barent Sea and on the Continental Shelf outside North Norway.

3 ANALYSIS

Before the analysis starts the data is inspected visually to detect and remove bad data records. Bad data can arise from movements of the OBS due to cable drag or drag in the recovery line caused by strong winds or currents. Also bad coupling to the bottom may cause visible OBS signal distortion.

The factors mentioned, however, have turned out to be of minor importance

compared to loss of syncronization in the digital data link from the OBS to the receiving unit. Short duration syncronization losses are likely to occur when the radio distance becomes large.

The preprocessing includes low pass filtering to 50 Hz and decimation to 100 Hz to reduce the amount of data. A notch filter removes the DC-components from the signals. We also rotate the coordinate system of the OBS into radial and transverse horizontal signal components relative to the direction of the explosions.

The analysis itself is divided in 2 parts

a) Assessment of data quality

b) Analysis and characterization of the noise process

However, for convenience we present the results of the analysis in terms of statistics and spectrum analysis products.

Assessment of data quality involves checking the character of the noise process at the time of measurements. We check the stationarity of the noise signal (amplitude distribution) by a Kolmogorov-Smirnov two-sample stationarity test (Ref 2). Linear trends we look for by Kendalls rank correlation test, short transients by the Mean Square Successive Difference test and Spearmans rank correlation coefficient is used to check crosstalk between the sensors (Ref 3). Crosstalk can be a measure of bad OBS coupling to the bottom.

The way we characterize the noise process is by

- statistical moments
- frequency distribution (histogram) and distribution functions
- test on normality
- power spectra and cross spectra
- directionality in terms of azimuthal power distribution

4 RESULTS

First we show an example of an explosive charge signal (Fig 4). We observe the response of the shot and also the background noise when the effect of the explosion has died out. As can be seen slow, low frequency interface waves (Scholte waves) are not exited on any of the 4 channels. This confirms the simulation results discussed in part 2. We also observe that the dominant shot signal frequencies are considerably higher than those of the noise.

4.1 Two noise examples compared

We compare two particular cases, a low noise situation from 4 o'clock in the night and a busy morning hour (at 9) with ships passing through the area. The data are from area 2, OBS winter position, and the examples serve to illustrate the processing used and some of the characteristics of the noise processes we are studying. Each signal consists of 2 records of size 1024 samples. Sampling frequency is 100 Hz. The noise signals are shown in Fig 5. As can be seen, the character of the signals from the two cases are quite different. Of course the signal amplitudes are quite different too. The results are presented in terms of statistics and spectrum analysis products. Both types of analysis have been applied to the data.

The emphasis of the statistical analysis has been on stationarity of the processes involved. A general impression is that the noise processes cannot be considered stationary. However, the picture is rather confused because there is a lot of variability. Sometimes the statistical distribution change a lot from one record to the next, but it also happens that the changes are negligible. In the low noise case shown in Fig 6, the process could be considered stationary at a 5 % significance level for the vertical geophone component. The X and Y components are more doubtful, but the changes from one record to the next are fairly small. On the contrary, the hydrophone signal is definitely not stationary.

Any ship traffic in the area seem to cause increased unstationarity. This can be seen from Fig 7 which displays processed high noise level signals from the case with ship traffic in the area. The important difference between the processes involved (Fig 6 and 7) is the higher degree of variability from record to record in the ship noise case.

Frequency distributions have been estimated and are also shown in Fig 6 and 7. The histograms are used as basis for the Kolmogorov-Smirnov two-sample stationarity test.

It has been checked how well our experimental data can be fitted to a normal distribution. We observe that some of the histograms seem to have a gaussian shape. But the curve fitting quite often reveals that the frequency distributions are not gaussian. The variability of the processes is reflected in the fact that in a sequency of records some records can be considered gaussian and others definitely not. There are differences between low noise and high noise cases, but no clear trend is found. For instance, in Fig 6 the second X-record is the only one clearly gaussian (96 % probability). The remaining 7 are all below 50 %. Comparing now with Fig 7 we find that both Y- records and the second X-record are gaussian with a probability from 70 % to 83 %. The rest of the records are clearly outside.

Several statistical tests on the data have been performed. Results are shown in table 2 and 3.

Skewness is a measure of asymmetry of the frequency distribution functions, Kurtosis tells something about how narrow (positive Kurtosis) or flat/wide

1. RECORD:		X	Y	Z	H
MAX		0.012	0.012	0.018	0.012
STANDARD DEV		0.003	0.004	0.009	0.005
SKEWNESS		0.266	0.100	-0.347	-0.165
KURTOSIS		-0.051	-0.117	-0.639	-0.407
	X		-0.009	-0.042	0.017
SPEARMAN	Y			0.005	-0.052
	Z				0.499
KENDALL		-0.051	0.016	0.009	-0.297
MSSD		0.067	0.061	0.272	0.374

2. RECORD:		X	Y	Z	H
MAX		0.011	0.008	0.020	0.020
STANDARD DEV		0.004	0.003	0.009	0.009
SKEWNESS		-0.040	-0.504	-0.320	-0.110
KURTOSIS		-0.201	1.273	-0.614	-0.780
	X		0.037	-0.056	0.003
SPEARMAN	Y			-0.055	-0.091
	Z				0.219
KENDALL		-0.003	-0.054	-0.005	0.075
MSSD		0.042	0.092	0.252	0.115

TABLE 2 STATISTICAL TESTS

RUN 19: REC 1 & 2
AREA : 2
TIME : 4.15 AM 3 MARCH 82

1. RECORD:		X	Y	Z	H
MAX		0.060	0.065	0.060	0.045
STANDARD DEV		0.022	0.022	0.023	0.023
SKEWNESS		0.071	-0.004	-0.220	0.206
KURTOSIS		-0.567	-0.271	-0.251	-1.088
SPEARMAN	X		-0.101	0.176	-0.024
	Y			-0.014	-0.230
	Z				-0.084
KENDALL		-0.002	0.006	0.028	-0.034
MSSD		0.708	0.755	0.195	0.025

2. RECORD:		X	Y	Z	H
MAX		0.055	0.050	0.092	0.047
STANDARD DEV		0.018	0.016	0.026	0.032
SKEWNESS		0.050	0.024	0.091	-0.139
KORTOSIS		-0.335	-0.264	0.374	-1.518
SPEARMAN	X		0.291	0.065	-0.001
	Y			-0.002	-0.022
	Z				-0.046
KENDALL		-0.001	0.005	0.090	-0.712
MSSD		0.596	0.742	0.147	0.012

TABLE 3 STATISTICAL TESTS

RUN 3: REC 1 & 2
AREA : 2
TIME : 9.45 AM 2 MARCH 82

(negative Kurtosis) a given distribution is relative to a normal distribution.

More important than these statistical moments are the mean square successive difference test (MSSD), Kendall's rank correlation coefficient (RCC) and Spearman's rank correlation matrix (RCM). MSSD detects certain short duration transients. Kendall's RCC is used to look for linear trends while Spearman's RCM is used to measure the association or correlation between the sensors.

Looking now at tables 2 and 3 we find that

- in the low noise case transients may have been present in both Z records and in the first H record which also show a small negative linear trend in the data. There also is nearly 50 % correlation between the first Z and H records.

- In the high noise case there seem to have been present strong transients in both X and Y signals, both records. A strong negative linear trend is found in the second H record, and there is some association between X and Y, second record, and Y and H, first record.

Looking at the signals (Fig 5), we find that at least some of the test results from the tables are verified visually. It is clear that the observed associations between sensor signals reflect characteristics of the signals rather than cross-coupling between the sensors or bad coupling of the OBS to the sea floor. This is because the correlation changes so much from one record to the next.

We now turn to the frequency analysis part of the processing. For each sequence of signal records we produce

- power spectra for all channels

- cross spectra (module and phase) between sensors

- magnitude squared coherence functions

- azimuthal power distribution

In the context of noise analysis the cross spectra and coherence between channels turn out to be of little interest and are not shown here. Power spectra of the horizontal signal components are compared in Fig 8. Also shown are the azimuthal power distribution for the two cases. In Fig 9 we compare the vertical geophone signals and the hydrophone signals. Horizontal power spectral densities differ considerably in the two cases. The low noise spectra show a small fall-off with increasing frequency while the ship noise spectra have their power maximum in the 20 - 30 Hz range. In this frequency band the average ship noise power levels are some 20 dB above the low noise spectrum levels.

It should be noted that the fall-off with frequency which we observe for the low noise case is much less in terms of dB pr decade than reported by other workers in the field (Ref 4). The azimuthal power distribution is computed for all frequencies 0 - 40 Hz. It tells us from where in the horizontal plane the major part of the energy comes in. As can be seen neither the low noise signals nor those from the case with ship traffic in the area seem to have any preferred direction. One would expect, however, that ship signals from one source would be directional. The lack of directionality may be caused by too long averaging time, too wide frequency band, or the signals may come from several sources in the area.

Signal spectra from the vertical geophones and the hydrophones differ much less than the horizontal spectral densities. Still the ship noise spectra are higher than the low noise ones. More impressiv, however, are the strong frequency lines present in both cases. We will come back to these line components when we study noise characteristics from the fall measurements (all areas 1 - 5, Fig 1).

4.2 Noise from 5 different areas

Geoacoustic models of the five areas (Fig 1) are shown in Table 1. Environmental conditions at the time of measurements (late fall 81) were for

Area 1: Calm weather

Area 2: Some wind, no swell

Area 2 (winter): Calm weather, part of the area covered with drifting ice

Area 3: Calm weather

Area 4: Wind, some swell

Area 5: Strong wind, swell

Nearby ship traffic has been plotted during the measurements and is excluded from this part of the analysis.

Spectra are calculated on records of size 1024 samples, sampling frequency 100 Hz, with averaging over 6 records with 50 % overlap. Due to the general unstationarity of the noise generating processes the power spectral density curves vary with time during any particular series of measurements. From each area we have chosen to display spectra which we have found to be typical for that measurement series and situation. One particular run is selected and power spectra for all 4 sensors are displayed. We also show azimuthal power distribution (APD) from the run being analyzed plus 1 or 2 other runs.

Area 1 is treated in Fig 10. The spectra do not fall off smoothly with frequency as one might expect if distant sources only contributed to the

(ambient)noise process. A steep slope (-27 dB/oct) from 1 to 4 Hz is reported to be a common feature of marine seismic background noise in open waters (Ref 4). The noise spectra from Area 1 have broad local maxima around 6, 12 and 24 Hz.

Spectra from Area 2 are much smoother than those from the previous area (Fig 11). Still we observe in the X and Y signals an increased spectral level in the frequency range from 4 to 8 Hz relative to the smooth curves from Area 3 (Fig 12). Disregarding for the moment the line components observed in the Z and H signals the observed noise from Area 3 seems to represent the minimum or true background level relative to the other fall measurements. The increased noise level in the range 4 - 8 Hz observed in the data from Area 2, 4 and in particular from Area 5 (Figs 11, 13 and 14) most likely is caused by wind and waves.

So to the line components in the spectra of (mainly) the Z and H sensor signals. The same spectral components seem to be present in data from all areas except probably Area 4. It is not likely that they belong to the background noise. We believe that they are artifacts generated or picked up inside the OBS sensor unit. It is not clear why the spectra from Area 4 are different. Because the OBS sensor unit is still on the sea floor of Area 2 it has not been possible to check the assumption of artifacts being generated in the OBS. In some cases spectrum lines from other sources (ships, land activity) may be confused and masked by these artificial lines (Areas 1 and 5).

Having excluded what we believe is artifacts we return to the ambient noise.

We have observed that signals from all 5 areas seem to have the same basic background noise spectra. In some areas the noise spectrum levels are considerably higher over parts of the frequency band covered. This increase in noise level must be caused by some local sources.

The spectra differing most from the background curves are from Area 1 (Fig 10). This area is quite different from the other test areas in terms of bottom composition (see Table 1). An oil refinery is situated on land near our test area. Such a refinery with all the various types of activity associtated with it can be a considerable source of seismic noise. We believe that the activity at the refinery combined with the special bottom characteristics of Area 1 can account for the increased spectrum levels around 6, 12 and 24 Hz and also for a wider frequency band than in most of the other areas.

The azimuthal power distribution (APD) indicates weekly a preferred direction of noise propagation from the location of the refinery (Run 8). At a later point of time the preferred direction seems to have shifted away from land towards the opening of the fjord (Run 18).

Area 5 (Fig 14) also have noise spectra quite different from the background found in Area 3 (Fig 12). The roughest weather conditions we encountered there, and this has caused increased noise levels particularly near 5 Hz but also at 10 Hz (hydrophone) and 22 Hz. It seems that the rough sea can account for the increased noise spectrum levels in Area 5.

The higher noise level in the frequency range 4 - 8 Hz observed in signals from Area 2 and 4 (Fig 11 and 13) relative to Area 3 (Fig 12) are also believed to be caused by wind and waves. Note that the spectrum peak caused by sea roughness is shifted down in frequency in the Area 5 Case. This must be due to the lower frequency surface wave spectrum generated during the rougher weather.

4.3 Shape and level of noise spectra

The shape of the background spectra (Fig 12) is characterized by a maximum at 1 - 2 Hz, a slope of maximum 24 dB/octave on the high side and also a steep slope below 1 - 2 Hz. This low-end slope is partly due to the seismometer response curves, partly due to a real decrease in spectrum level. This can be seen from most of the hydrophone spectra.

Maximum noise spectrum levels from open waters are generally below 0 dB re $(1(\frac{\mu m}{s})^2/Hz)$ (Rauch and Schmalfeld, Ref 4). The peak levels at 1 - 2 Hz observed by us (Area 1 - 5) are (10 - 15) dB re $(1(\frac{\mu m}{s})^2/Hz)$ for geophone signals and (0 - 10) dB re $(1(Pa)^2/Hz)$ for hydrophone signals. The higher levels found in the Oslo fjord compared with open waters must be due to the proximity of the shore. Differences in propagation conditions between open and closed waters are thought to be an important factor. Also human activity on land and sea and wind/wave action contribute to the increased noise.

Going back to the winter measurements (Fig 8 and 9) with the OBS close to shore, we find a peak noise level at 1 - 2 Hz close to 40 dB below the levels from Area 1 - 5. This applies both to the low noise and ship noise cases. Ship noise causes increased levels at higher frequencies as pointed out in section 4.1. Spectra from Area 1 - 5 fall off much more rapidly with increasing frequency than do the winter spectra. Noise from drifting ice covering part of the fjord during the winter measurements may account for this difference at the high end of the frequency band. The big differences between peak noise levels from fall and winter could have as one cause changes in propagation conditions with snow, frozen earth and drifting ice. However, it is more likely that the propagation conditions associated with the particular measurement site are causing the observed differences in noise levels. The OBS winter location close to shore is definitely outside the (presumably stratified) Area 2. Propagation condiditons cannot be expected to be the same as in Area 2. Results from this location are not considered typical for the fjord area.

4.4 Noise directionality

Noise directionality is presented in terms of Azimuthal Power Distribution (APD).

First we should point out that the directionality found from the APD plots are rather weak. Generally there is only a slight increase in power level in the preferred direction relative to the normal (transverse) direction. The variability of the processes is reflected also in the APD plots. Quite often we find changes in preferred directions from one record to another.

We have already observed in section 4.1 rather surprisingly that there was no significant difference between the low noise and high noise case.

From Area 1 we have observed a weak preferred direction from the oil refinery site (Run 8), but later (Run 18) a change towards the opening of the fjord has taken place: This should reflect changes in the noise generating process.

Area 2 Run 13 and 27 both give the same preferred direction - i e along the fjord. The only change in the noise processes visible in the APD is a small increase in directionality.

From Area 3 we observe a change in preferred direction from Run 4 to Run 19 of approximately 60°. The first and weakest points towards land where there is a big wood products factory. The second and stronger preferred direction points towards the fjord entrance. In a majority of the cases reported distant shipping in some part of the fjord may have caused an increase in noise which is observable in APD plots.

Area 5 is different. Here the APD plots point towards the nearest shore (Run 5 and 14). We recall that the sea was rough during these measurements. Waves hitting the nearby shore must be the noise sources. In the time period between Run 5 and Run 14 the wind increased and its direction also changed to become more along the fjord. Run 18 is from the next day when wind and sea had calmed down considerably.

4.5 Statistics of the fall measurements

The general impression of great variability with time is valid also for the fall measurements. The quiet situation (Area 3) in terms of unstationarity is not significantly different from the rough sea situation from Area 5. The processes during measurements in Area 4 seem to have been closer to stationarity than in other areas. Variability from record to record is clearly less than observed in other cases. We don't know why this is so.

5 CONCLUSION

We have found that the noise generating processes are highly variable and in general cannot be considered stationary. A test on the observed amplitude distribution has shown that the distribution generally is not normal. The noise quite often is dominated by local sources the most important of which is ship traffic in the area. Unstationarity seem to increase with ship traffic. Also factories, land traffic and rough seas will influence the seismic and hydroacoustic noise in the area. A certain directionality in the noise propagation is found. Following the sources of noise it is also variable, but seem to be of minor importance. Behind the noise generated by local sources we find a background noise spectrum with maximum at 1 - 2 Hz, a steep slope of up to 24 dB/octave towards high frequencies and a maximum level of near 15 dB above reference level (daytime, fall).

Our background noise spectra exhibit some differences compared with spectra from open waters (Ref 4). The peak levels are (10 - 20) dB higher and the sloping towards higher frequencies are more gradual than reported by others. We believe that the differences in spectral level and shape are caused partly by human activity and wind/waves, partly by the special propagation conditions of this closed fjord area. It is not likely that background noise spectra should be the same in open and closed waters. Winter measurements from a location close to shore give rise to spectra which are rather different from those presented above. Some of the observed differences can be accounted for by noise from drifting ice in the area. However, the most important cause is believed to be differences in propagation conditions between this particular location and the Areas 1 - 5 which have been found to be reasonably well stratified. The differences in bottom characteristics found among the Areas 1 - 5 do not seem to be important in the context of noise generation and propagation.

REFERENCES

1) RAUCH, Dieter: Experimental and Theoretical Studies of Seismic Interface Waves in Coastal Waters, in Bottom-Interacting Ocean Acoustics, Plenum Press, N.Y. 1981, Proceedings from a conference held in La Spezia, Italy, June 1980. Edited by W. A. Kuperman and F. B. Jensen

2) Fisz, M: Probability Theory and Mathematical Statistics, 3rd edition. New York, Wiley 1963

3) Wagstaff, R. A: Onboard acoustic data-processing for the statistical analysis of array beam-noise, Saclantcen Memorandum SM-114, 15 Dec 1980

4) Schmalfeld, Bernd and Rauch, Dieter: Ambient and ship-induced low-frequency noise in shallow waters. Bottom-Interacting Ocean Acoustics, Plenum Press, N.Y. 1981. Proceedings from a conference held in La Spezia, Italy, June 1980. Edited by W. A. Kuperman and F. B. Jensen

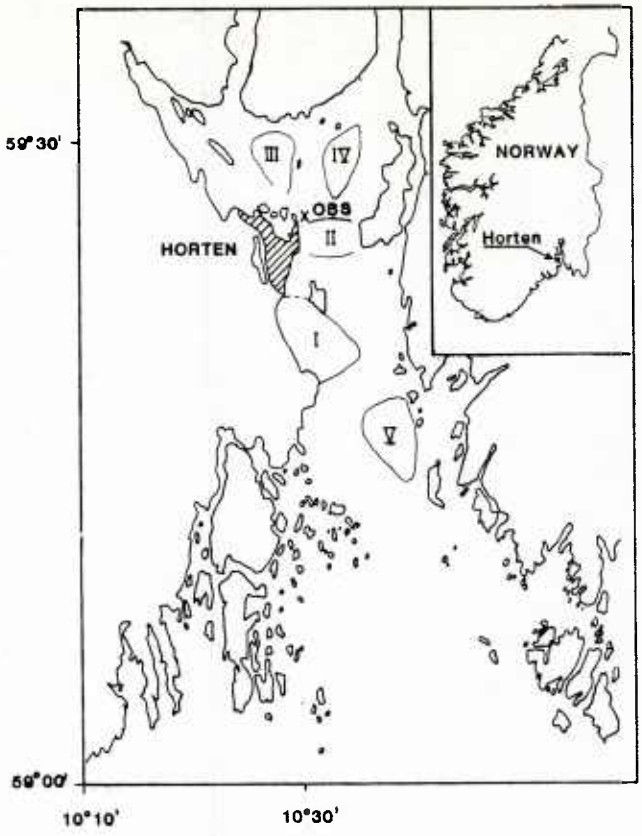

FIG. 1 TEST AREA

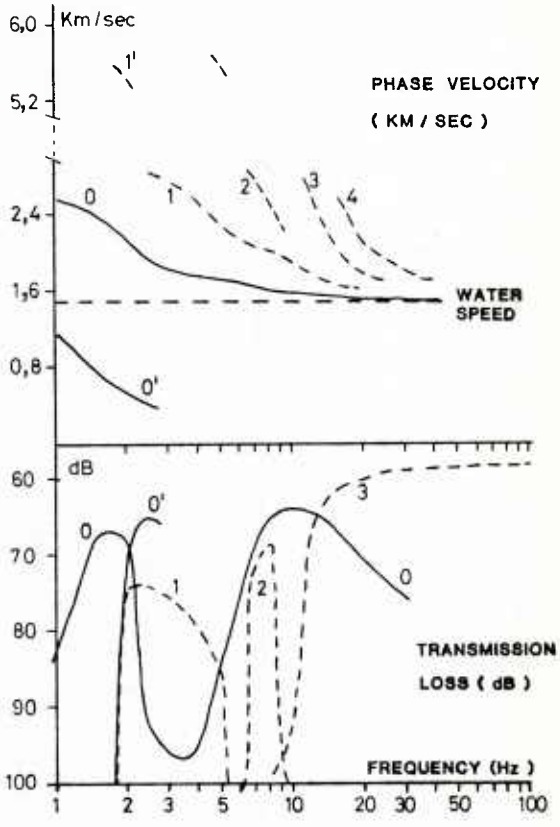

FIG. 2 SIMULATION ON FFP - AREA 2

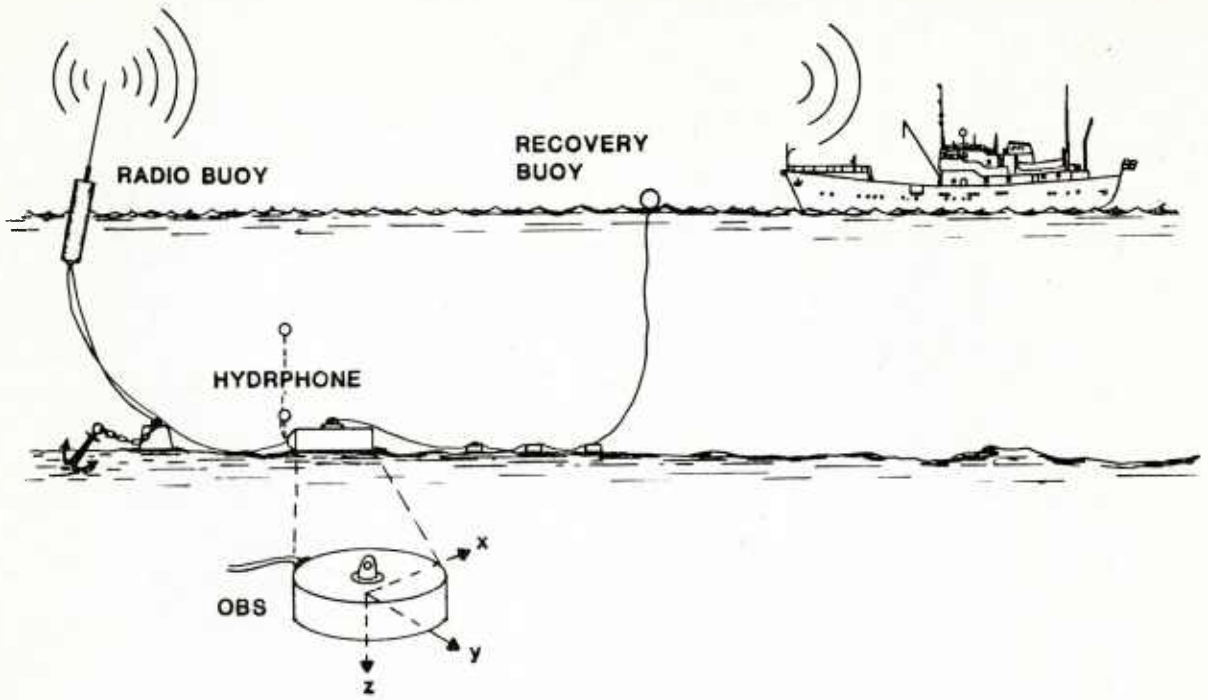

FIG. 3 OBS SYSTEM

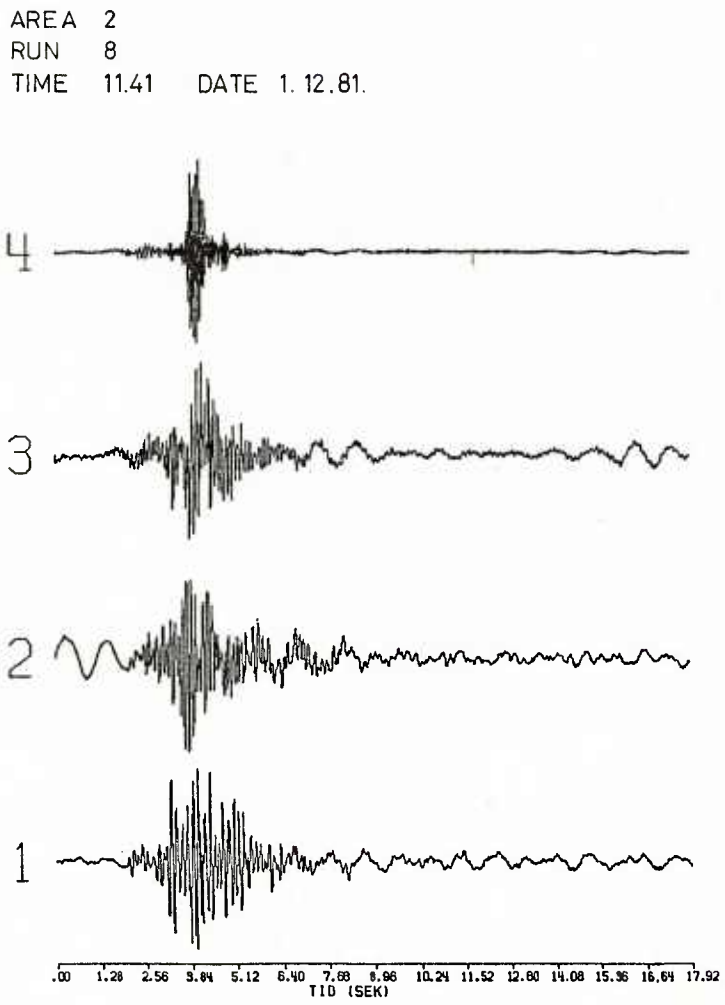

FIG. 4 SIGNAL AND NOISE EXAMPLE

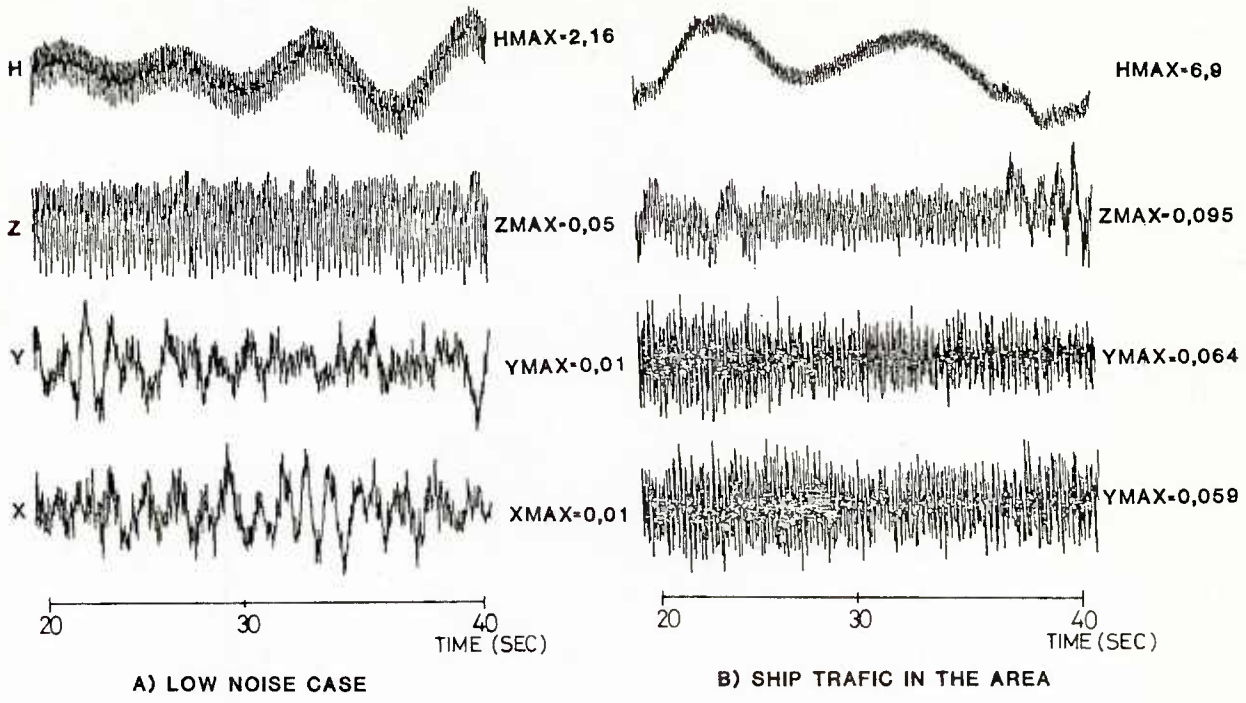

FIG. 5 NOISE SIGNALS, TWO EXAMPLES

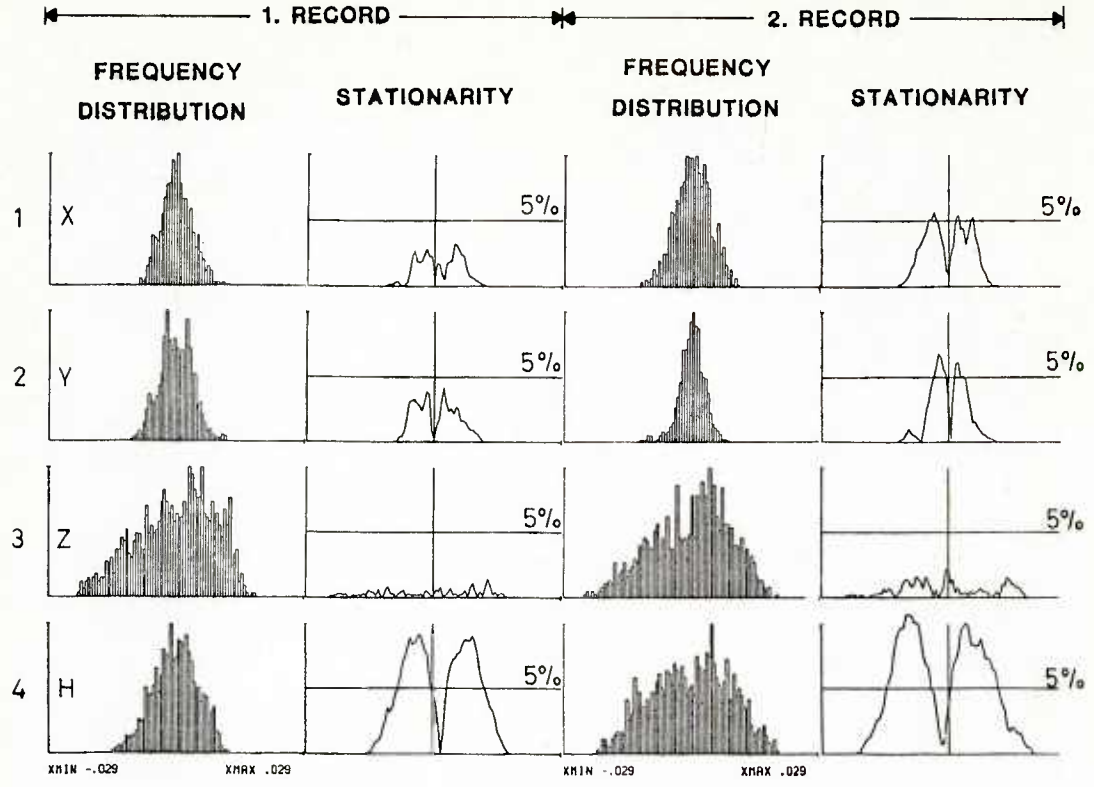

FIG. 6 STATIONARITY (LOW NOISE CASE)

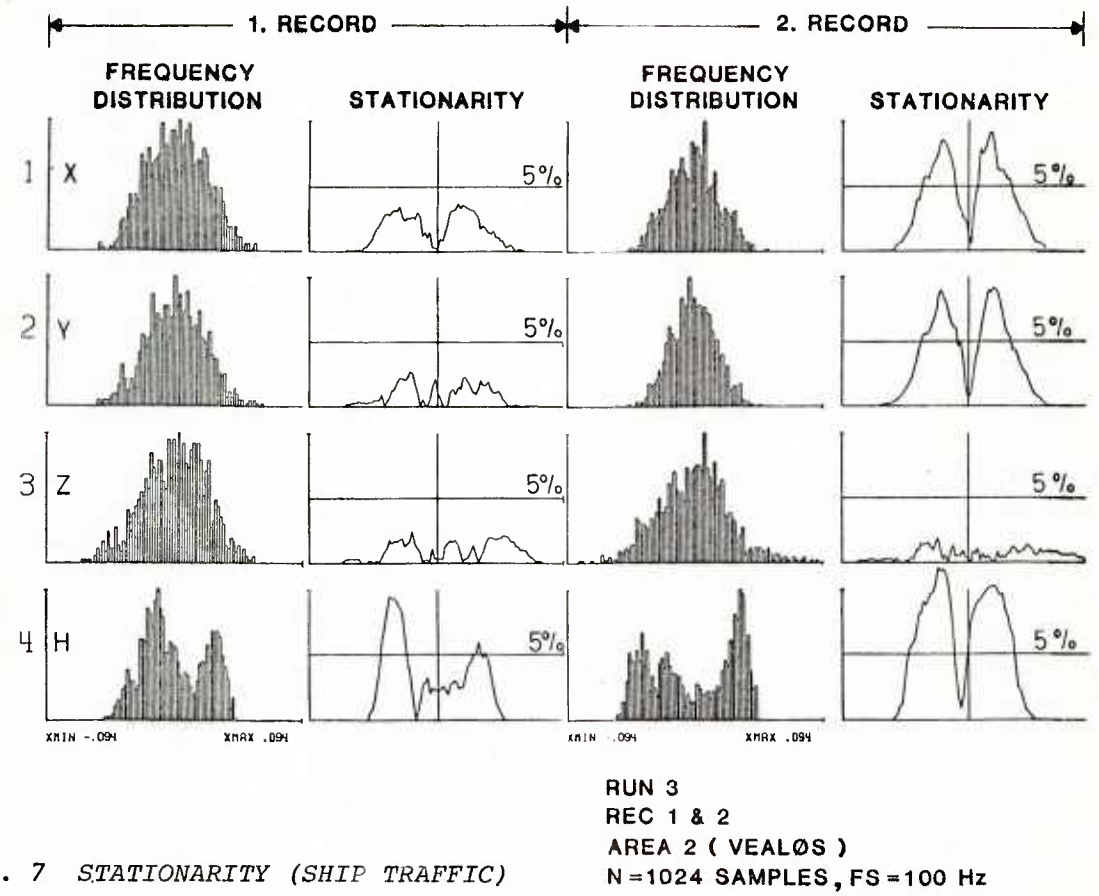

FIG. 7 STATIONARITY (SHIP TRAFFIC)

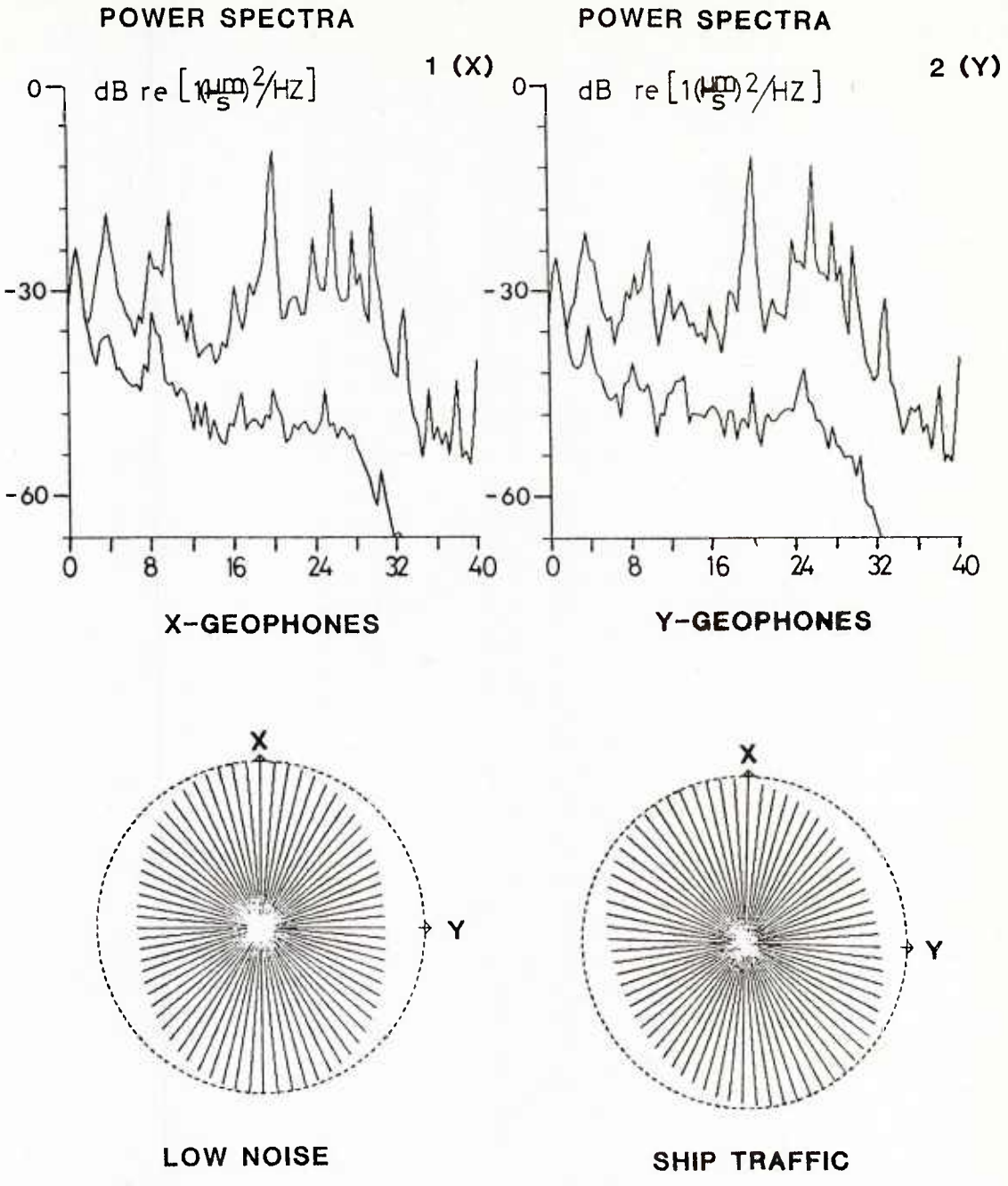

FIG. 8 COMPARISON OF POWER SPECTRA AND AZIMUTHAL POWER DISTRIBUTION

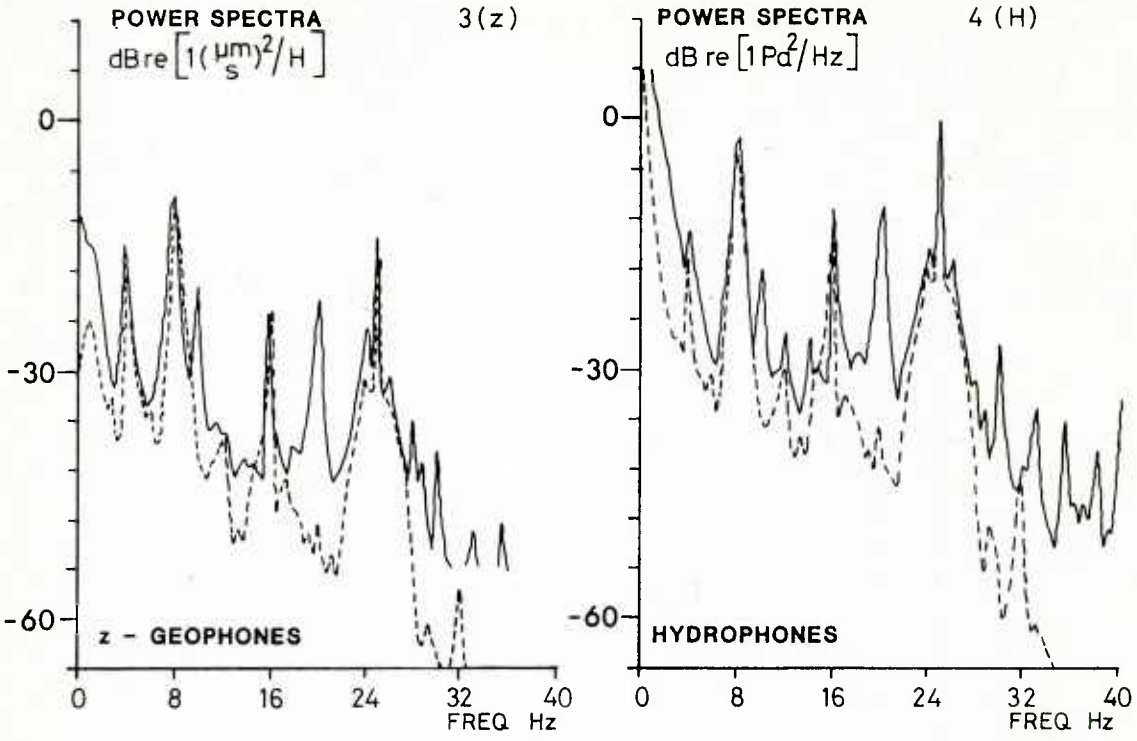

FIG. 9 COMPARISON OF POWER SPECTRA — VERTICAL GEOPHONE AND HYDROPHONE

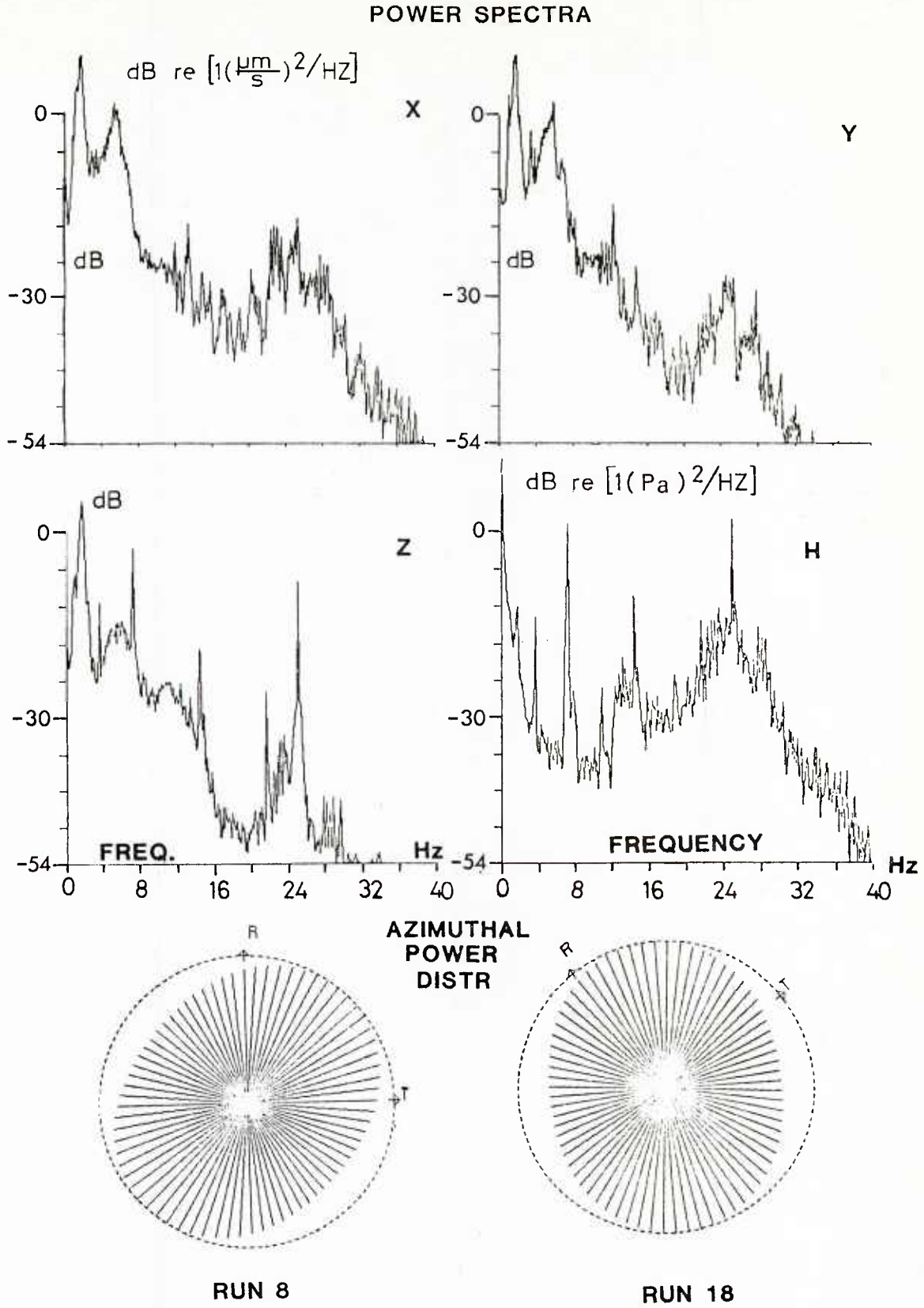

FIG. 10 POWER SPECTRA AND AZIMUTHAL POWER DISTRIBUTION, AREA 1 RUN 8

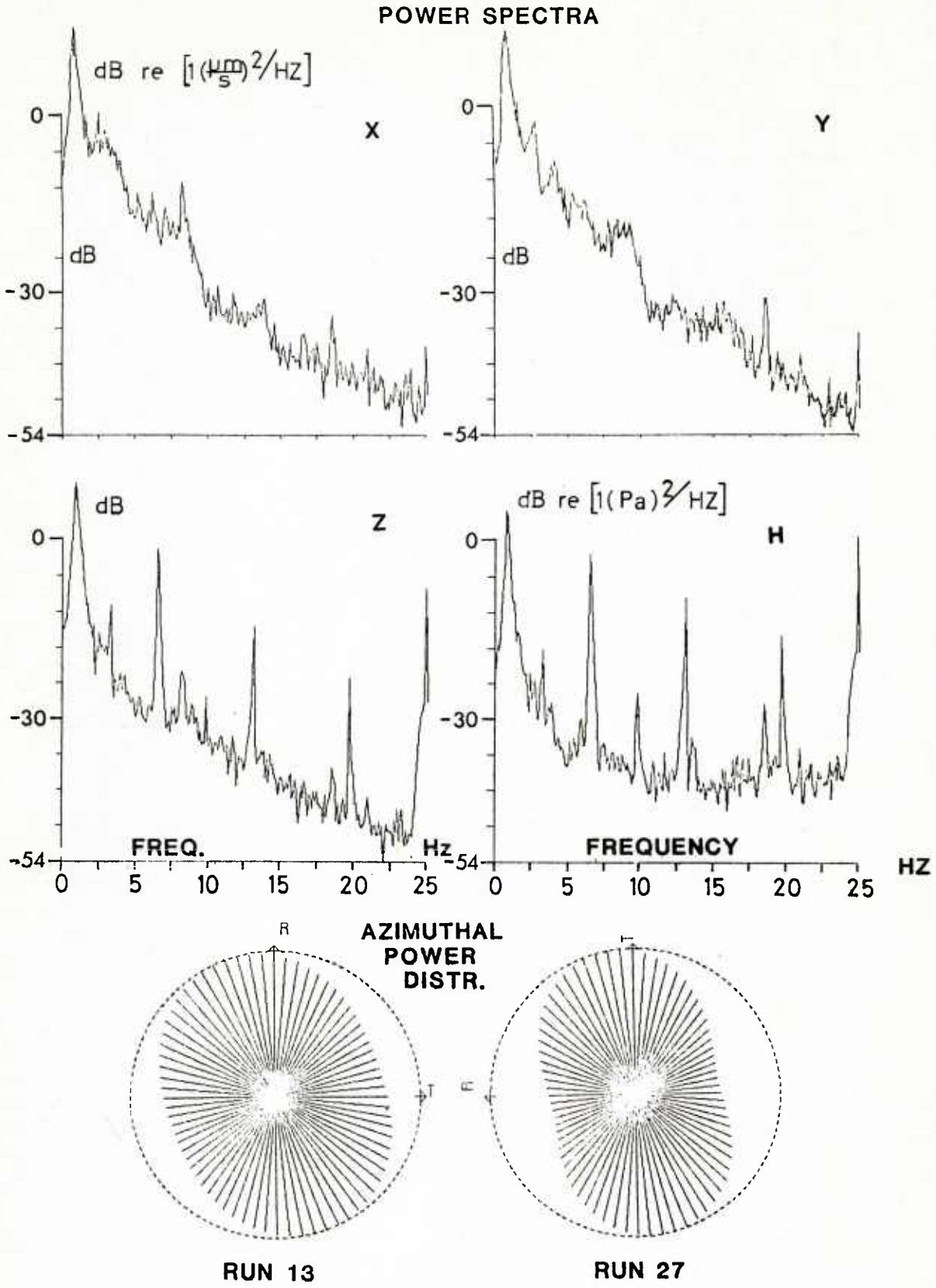

FIG. 11 POWER SPECTRA AND AZIMUTHAL POWER DISTRIBUTION, AREA 2 RUN 13

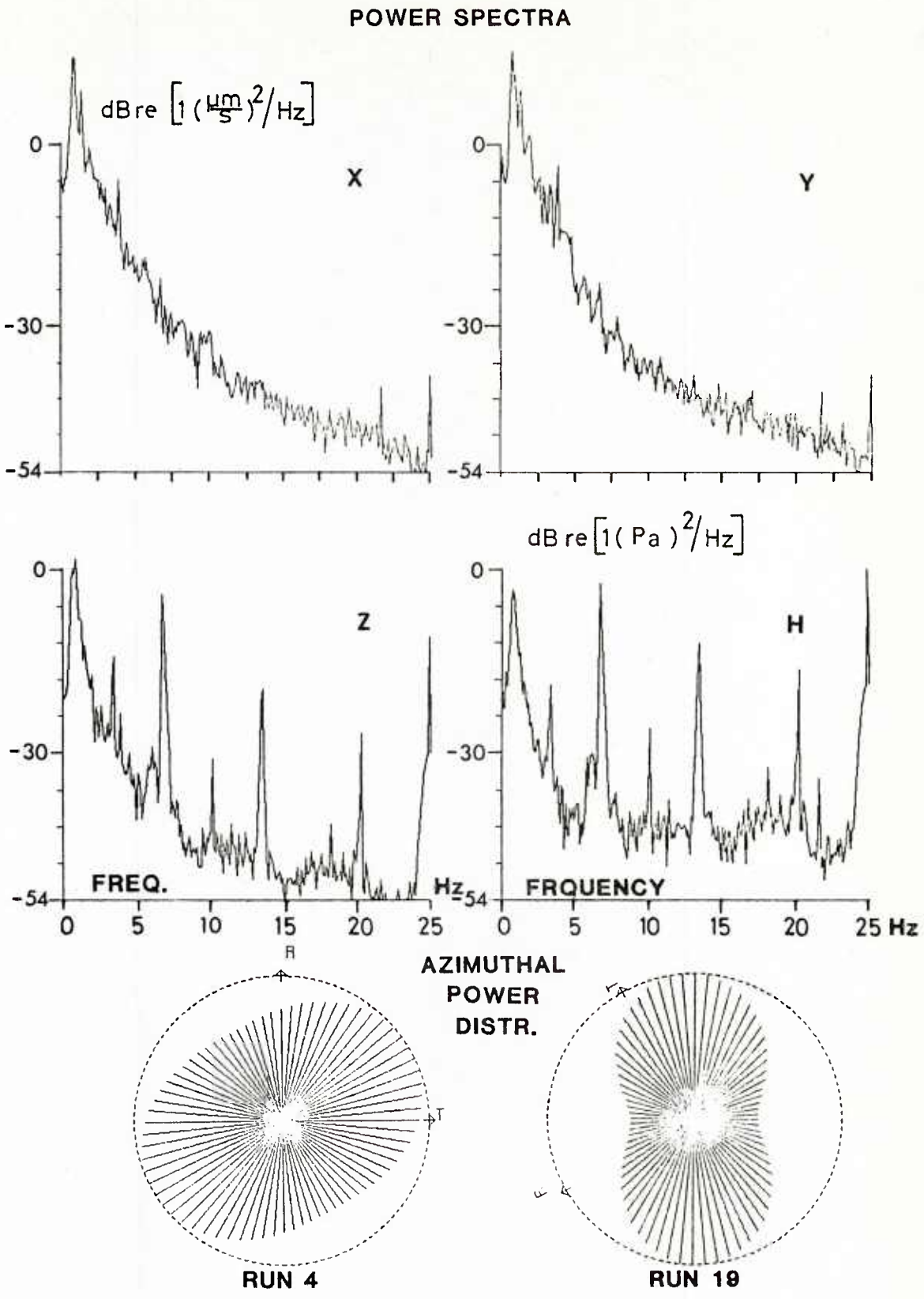

FIG. 12 POWER SPECTRA AND AZIMUTHAL POWER DISTRIBUTION, AREA 3 RUN 4

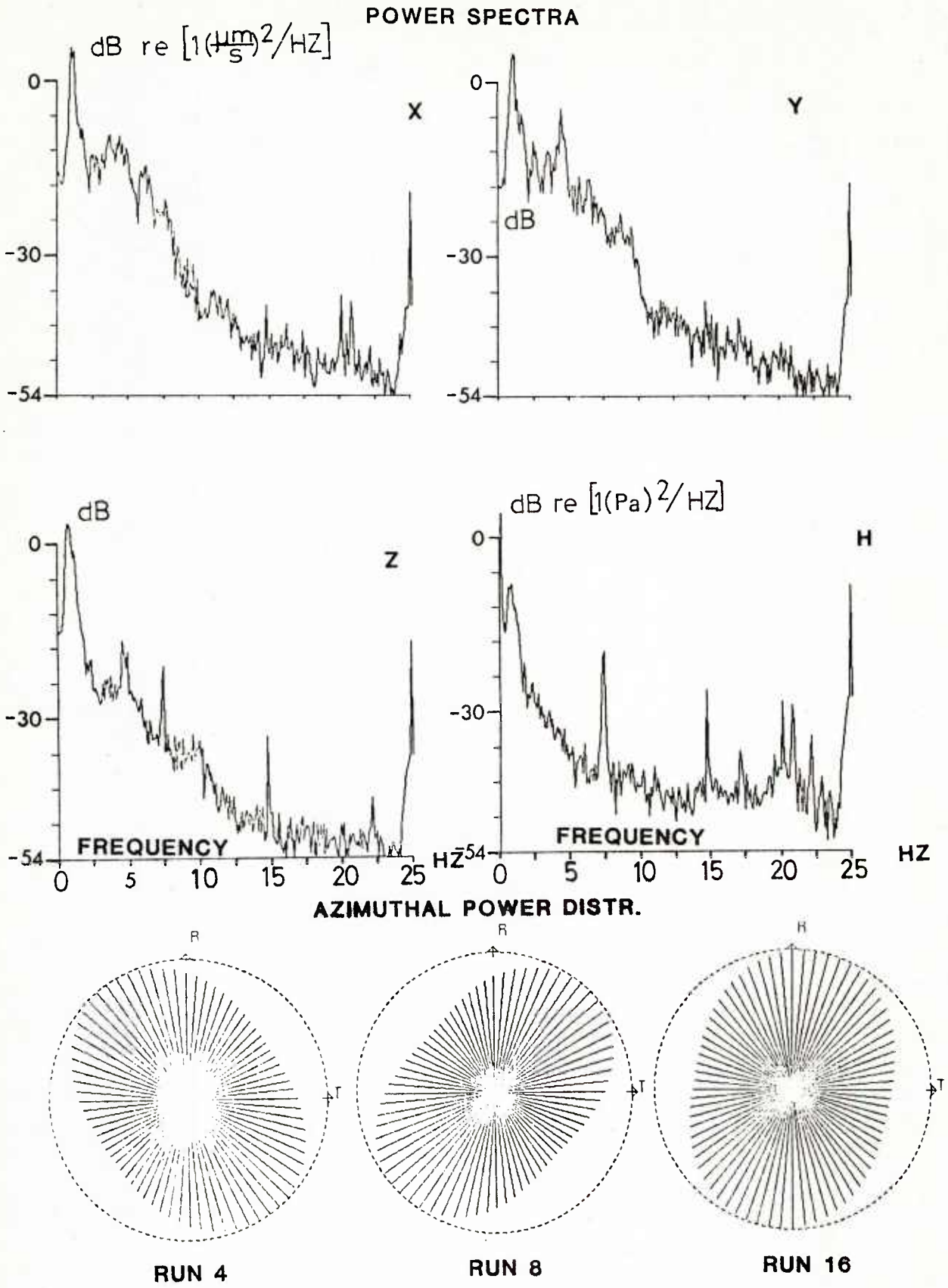

FIG. 13 POWER SPECTRA AND AZIMUTHAL POWER DISTRIBUTION, AREA 4 RUN 8

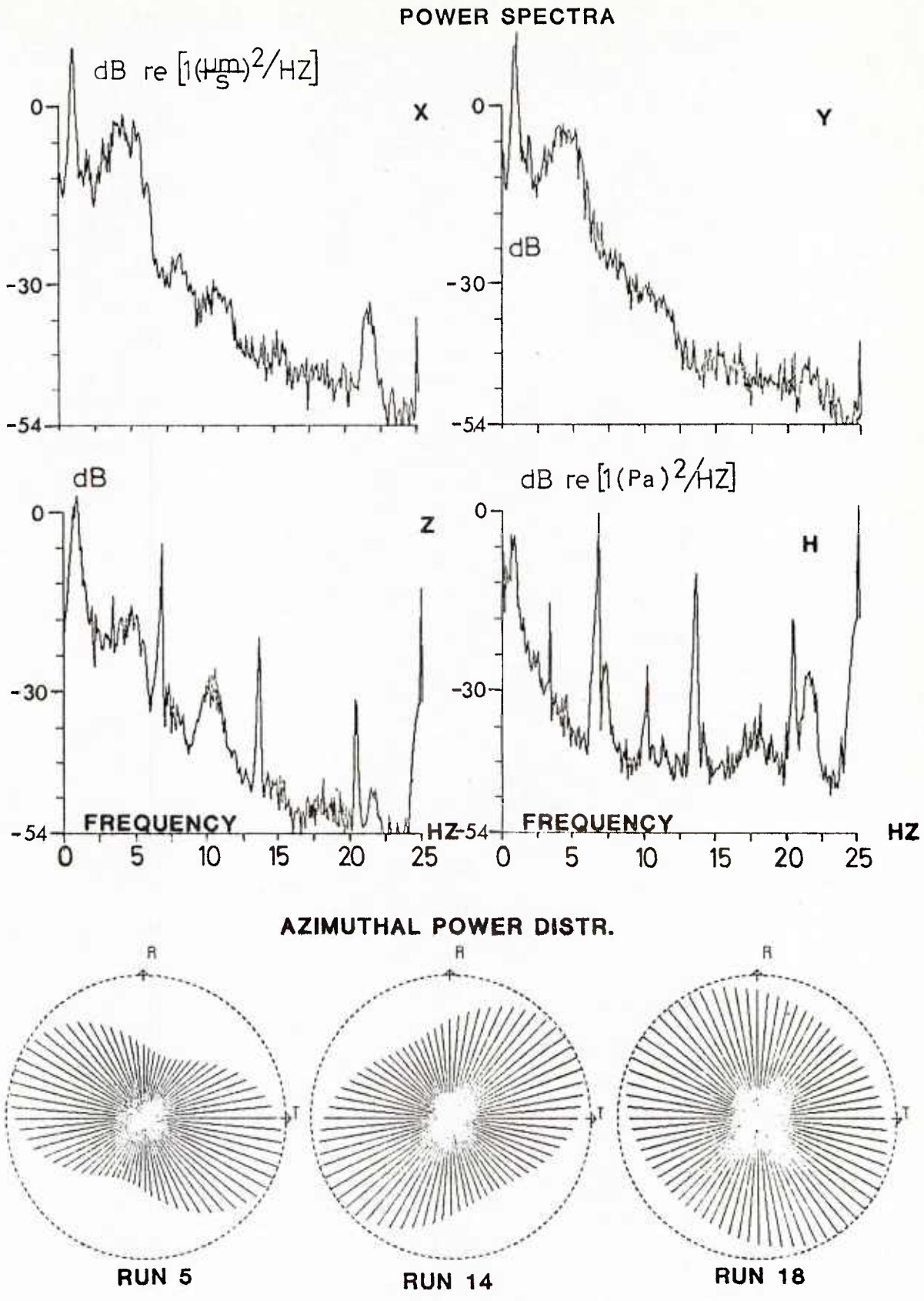

FIG. 14 POWER SPECTRA AND AZIMUTHAL POWER DISTRIBUTION, AREA 5 RUN 14

SEISMIC AND HYDROACOUSTIC SENSING OF INFRASONIC NOISE IN COASTAL WATERS

by

Bernd Schmalfeldt and Dieter Rauch
SACLANT ASW Research Centre
La Spezia, Italy

ABSTRACT

Three-component ocean-bottom seismometers with radio links have been deployed in coastal waters to investigate natural and man-made noise at extremely low frequencies. Seismograms from one or up to three sensor stations are analyzed in terms of amplitude and cross-spectra at frequencies between 1 and 18 Hz. Examples of area dependence and wind dependence are given, and the underlying propagation mechanism is investigated. Finally ship-radiated noise is used to demonstrate the directional selectivity of those sensor units.

INTRODUCTION

Seismic and hydroacoustic noise-measurements in the frequency range from 1 to 18 Hz have been performed in shallow-water areas. Because it is at the high-frequency end of microseismic field work and the low-frequency end of underwater acoustic noise measurements, this transition range is characterized by a lack of field data and by some uncertainties concerning the underlying propagation phenomena. The dominating source phenomena may be considered to be movements of the earth's crust and the superimposed man-made activities (industry and traffic). For the underwater acoustician this infrasonic regime is highly interesting in that it covers a band that may be to some extent below the acoustic cut-off frequency of many shallow-water areas.

Spectra from the few published geophone or hydrophone records on the sea floor in deep <1,2,3> and shallow water <4> reveal a relatively high variability in intensity but have also in common two pronounced features: towards the lower limit of the frequency band the noise level increases drastically with decreasing frequency while the rest of the band shows a relatively uniform distribution with almost no frequency dependence.

1 FIELD WORK

To make these ambient-noise measurements and to perform particular propagation studies, a (digital) ocean-bottom seismometer (OBS) was developed at SACLANTCEN using a new type of active and lightweight 1 Hz geophone (velocity sensor). The triaxial seismic sensor set is completed by a variable-depth hydrophone mounted outside the OBS or floating above it. The technical features of this sensor package – its radio-link and the on-board preprocessing facilities – are described in detail in <5,6>. It

is believed that the OBS is one of the most advanced tools in seismic research at present <7>. Figure 1 demonstrates how the complete system is deployed in shallow-water areas.

Figure 2 shows the nine positions off the Italian coast where up to three OBS stations have been installed on the continental shelf at depths from 15 to 45 m. Seven of these positions are situated within a few miles of the shore line and the other two are located close to small islands far from the coast. At six of these positions (1, 5-9) the upper seafloor is characterized by relatively soft sediment layers (clay and silt) at the other three (2,3,4) by harder layers consisting of consolidated sediments.

Propagation measurements were made at each position for several days. The noise samples presented in this paper were recorded between those measurements at intervals of 3 to 24 hours. Almost all noise records were taken under very good weather conditions (sea-state 0 to 1).

Before presenting the results the applied analysis method is described.

2 ANALYSIS TECHNIQUE

This paper presents amplitude spectra, coherence, and phase spectra. The underlying mathematics for these spectral estimates is well reported in the literature (direct method of overlapping FFT technique <8,9>). We therefore restrict ourselves to a broad sketch of the main features.

Two digitized time series $x(n\Delta t)$, $y(n\Delta t)$ are segmented into N adjacent (or overlapping) sections of length T. After subtracting the mean value and weighting each section by cos-window, a discrete Fourier transformation is applied, yielding the Fourier coefficients:

$$X_i,\ Y_i \quad (i = 1, \ldots, N)$$

A stable estimate for the linear (or amplitude spectrum $\hat{A}_x$ is obtained by accumulating the magnitudes $|X_i(w)\ X_i^*(w)|$ for all segments

$$\hat{A}_x(w) = 1/N \sum_{i=1}^{N} \left| X_i(w)\ X_i^*(w) \right|$$

(Amplitude spectra rather than power spectra have been chosen to cope with the limited dynamic range of the computer).

Estimates for the magnitude squared coherence, ρ^2, and phase, ϕ, between the series x and y are derived from the smoothed cross-spectrum $\hat{C}_{xy}$

$$\hat{C}_{x,y}(w) = \frac{1}{N} \sum_{L=1}^{N} X_i(w)\ Y_i^*(w) = \hat{L}_{xy} - i\ \hat{Q}_{xy}$$

as follows:

coherence

$$\rho^2_{xy} = \frac{\hat{C}^2_{xy}}{\hat{P}_x \hat{P}_y} \qquad 0 < \rho^2_{xy} < 1$$

$\hat{P}_x$, $\hat{P}_y$ smoothed power spectra

phase

$$\phi_{xy} = \arctan - \frac{\hat{Q}_{xy}}{\hat{L}_{xy}} \qquad -\pi < \phi < \pi$$

The parameters have been chosen to suit our special case. The length of one segment (T) was set at 6.8 s, which is long enough to allow spectral reliability down to 1 Hz or even below (important for the hydrophone). If possible a complete set of N = 8 to 11 adjacent segments (with additional 50% overlap) has been analysed; however, occasionally some sections had to be skipped due to signal contaminations of mechanical or electronical origin.

According to the number of independent segments (8 to 11) the total analysis interval has a length of 55 s to 75 s and the variance of the spectra corresponds to 22 to 31 degrees of freedom <10>. The pertinent 80% confidence interval is indicated in the spectra as a vertical bar.

The total analysis interval (about 1 min) seems to be sufficient, as we experienced a remarkable stationarity of the spectra. The differences between a spectrum analysed for a 4-minute interval and that for a 1-minute interval stemming from the same record are less than to be expected by the variance of the spectra itself.

In all seismic spectra, values below 1 Hz have been suppressed because the response curve of the geophones drops off by -18 dB/oct below that frequency.

3 RESULTS

3.1 Area Dependence

Figure 3 compares two amplitude spectra from a position with a relatively soft sea floor with a third one from a harder bottom. In the range from 1 to 5 Hz the data from a sea floor with unconsolidated sediment layering on top show a steep decay of the levels of the order of -30 to -35 dB/oct, while those from a consolidated bottom are subject to a more moderate decay of about -20 dB/oct. Between 5 and 18 Hz we notice different, but almost constant, noise levels for both bottom-types.

Previous propagation measurements and modelling studies concerning the transmission of infrasound have already demonstrated that a soft sea-floor usually acts as a relative sharp filter in favouring low frequencies. This is due to the more regular layering (dispersion) and the higher absorption coefficients (attenuation). For frequencies above 4 to 5 Hz the bottom-type seems to influence merely the magnitude of the noise-level but not the frequency characteristic.

3.2 Wind Dependence

Having treated the influence of the bottom-type we now discuss a typical phenomenon that affects the sea surface.

Figure 4 presents examples of the influence of local wind conditions on the noise-levels sensed by the bottom-mounted hydrophone and the vertical geophone. It shows spectra both with no wind (T_1 and T_3) and with moderate wind of 15 kn in between (T_2). The hydrophone spectrum (Fig. 4a) from sample T_2 reveals an irregular level increase of up to 10 dB in the range from 5 to 14 Hz and a more or less constant increase of about 10 dB for all higher frequencies. This latter trend was crosschecked up to 75 Hz. On the other hand, the corresponding spectrum from the vertical geophone (Fig. 4b) is almost identical with those of the no-wind cases (T_1 and T_3) for all frequencies above 5 Hz.

Below 5 Hz this surface-generated noise does not systematically affect the recorded levels: both sensors seem to follow consistently the rise of the wind (T_2) but only to a small extent do they follow its decay (T_3). The fact that the noise levels at extremely low frequencies remain high even after the wind has dropped, which is most evident on the hydrophone channel, indicates that this regime is much less influenced by the local wind. Therefore more remote effects, together with propagation phenomena, have to be taken into account. The transmission aspects are investigated in the following section.

3.3 Propagation Features

Using our experience in shallow-water infrasonics we have compared ambient-noise records with explosion-generated signals from the same soft-bottom area. For this purpose charges of 360 g TNT were fired on the sea floor at a depth of 16 m and a distance of about 1.2 n.mi.

Figure 5, which is a plot of two amplitude spectra sensed by the vertical geophone, reveals that only in the range from 1.5 to 5 Hz is there a systematic level-increase of about 10 to 15 dB as a consequence of the shot. This surprisingly small change in the spectrum is due to two facts: the relatively low energy of such a small charge at very low frequencies and the very pronounced selectivity of a soft bottom, as explained before. The geoacoustic energy in that frequency regime is transmitted in the form of seismic interface waves propagating along the sea-floor, as a careful study of the shot-generated wave field <6> has proved. These waves are always trapped by the acoustically most significant interface separating the water layer (including liquid-like sediments) from the solid bottom and characterized by some very particular features:

a) There is a well-defined correlation between the vertical particle velocity at the water/bottom interface and the accompanying pressure variation immediately above it <11,12>.

b) The particle orbits or hodographs are always prograde or retrograde circumscribed ellipses in the radial/vertical plane (with respect to propagation direction and guiding interface).

We therefore cross-check these features by comparing ambient-noise data with signals from explosions. Figure 6a reproduces the coherence-spectrum and the phase-spectrum between vertical geophone and hydrophone channels for an ambient-noise record. We notice a very high coherence in the interval from 1.5 to 3 Hz and a stable phase-shift of about 80° from 1.5 to 4 Hz. Figure 6b shows the corresponding results for an explosion. In this case a coherence of exactly 1 extends up to 4 Hz and the stable phase-shift of about 80° up to 5 Hz. Thus the underlying transmission characteristics for both phenomena are indeed the same.

Due to the above-mentioned regular particle motion, the radial deflection indicates the propagation direction; moreover, the phase-shift between radial and vertical component is stable. Figure 7 plots the azimuthal power distribution, coherence, and phase between these velocity components for the same shot. The power pattern shown in Fig. 7a has been calculated for the interval between 1.2 and 4.5 Hz and is almost identical with the ideal dipole characteristics of a unidirectional geophone. This proves that only a small fraction of the total seismic energy is being carried by the so-called Love-waves, with purely transverse particle deflections. The pertinent coherence and phase-shift in Fig. 7b confirm the described regular particle motion.

Figure 8 plots the corresponding results for the underlying background noise. The omnidirectional power distribution of Fig. 8a demonstrates that the noise is generated by waves coming in from all directions. Accordingly, there should no longer be any significant coherence or stable phase shifts between all possible horizontal and vertical velocity components, as Fig. 8b indicates. This conclusion can also be confirmed by processing small time-windows (some seconds instead of one minute) wherein the energy flux in a certain propagation direction strongly dominates the underlying interference pattern and thus the particle motion is a well-defined ellipse in the radial vertical plane <7>.

Thus we can state that the infrasonic noise in the frequency range up to about 5 Hz is chiefly transmitted in shallow-water areas in the form of seismic interface waves propagating along the sea floor in many different directions.

3.4 Level-variations

Figure 9 presents a set of seismic amplitude spectra comprising typical examples from all the positions plotted in Fig. 2. The curves of Fig. 9a are derived from the records of one of the horizontal geophones while Fig. 9b reproduces the corresponding results for the vertical sensor of the same OBS. We notice that both groups of curves are very similar with regard to the strong increase in noise level below 5 Hz and in the much

more moderate variation or almost constant level above this frequency. In Fig. 9b we have superimposed the standard deviations of these curves at 2, 5, 10 and 15 Hz to indicate more clearly the trends and variations of the collected data.

3.5 Ship Source

As another example of man-made noise, Fig. 10 shows a typical infrasonic line spectrum and the resulting directivity pattern for a passing merchant ship. In this case the OBS was deployed at a depth of 30 m on a sedimentary sea-floor. The ship was passing at a distance of about 0.6 n.mi; it had a constant shaft-rotation of 180 rev/min and was thus radiating at 3.0 Hz. This pronounced line occurs clearly below the acoustic cut-off frequency of the shallow-water duct. The ambiguity of the directivity pattern can be removed by exploiting the additional phase informations carried by the seismic interface wave as shown by the lobe with broken lines <13>. Thus we are able not only to detect extremely low-frequency noise radiated by ships, but also, with merely a single OBS, to determine the ship's bearing and, with an array of OBS sensors, its exact position.

CONCLUSIONS

The results are summarized as follows:

1) At all sites the noise level is characterized by a steep negative gradient (-20 to -35 dB/oct) between 1 Hz (or below) and about 4 to 5 Hz, and a more or less constant level up to 18 Hz (and above).

2) For all experiments the measured ambient noise values varied only within a band of ± 6 dB, depending on location.

3) The transmission of infrasonic energy below 4 to 5 Hz is strongly governed by a particular wave-type: the seismic interface wave or Scholte wave.

4) Based on this special propagation mechanism, ocean-bottom seismometers can be used to detect and track sources radiating below the acoustic cut-off frequency of the shallow-water duct.

REFERENCES

1. BRADNER, H., DOODS, J.G. and FOULKS, R.E. Investigation of microseism sources with ocean-bottom seismometers. Geophysics, 30, 1965: 511-526.

2. PERRONE, A.J. Infrasonic and low-frequency ambient noise measurements on the Grand Banks. Journal of the Acoustical Society of America, 55, 1974: 754-758.

3. RYKUNOV, L.N. and SEDOV, V.V. Seismic noise in the 2- to 15- cps frequency range on the bottom of the Black Sea. Physics of the Solid Earth, 7, 1965: 443-448.

4. NORTHROP, J. Some underwater sound propagation studies in the vicinity of the NOSC oceanographic tower: Final Report, NOSC TR-424. San Diego, CA, U.S. Naval Ocean Systems Center, 1979.

5. BARBAGELATA, A., MICHELOZZI, E., RAUCH, D., and SCHMALFELDT, B. Seismic sensing of extremely-low-frequency sounds in coastal waters. In: ICASSP 82, Proceedings of IEEE International Conference on Acoustics Speech and Signal Processing in Paris, France, 3-5 May 1982. Piscataway N.J., IEEE Service Center, 1982: 1878-81.

6. RAUCH, D. Experimental and theoretical studies of seismic interface waves in coastal waters. In: KUPERMAN, W.A. and JENSEN, F.B., eds. Bottom-Interacting Ocean Acoustics, Proceedings of a conference held on 9-12 June 1980 at SACLANT ASW Research Centre, La Spezia, Italy. NATO Conf. Series IV, Marine Sciences 5. New York, NY, Plenum, 1980: 307-328.

7. SUTTON, G.H., LEWIS, B.T.R., EWING, J., DUENNEBIER, F.K., IWATAKE, B., TUTHILL, J.D. Lopez Island ocean bottom seismometer intercomparison experiment. Final Report, HIG-80-4. Honolulu, HI, Hawai Institute of Geophysics, 1981.

8. HAUBRICH, R.A. Earth noise 5 to 500 millicycles per second. 1. Spectral stationarity normality, and nonlinearity. Journal Geophysical Research, 70, 1965: 1415-1427.

9. NUTTALL, A.H. Spectral estimation by means of overlapped FFT processing of windowed data. NUSC Report 4169 (and supplement TR-4169S). New London, CT, U.S. Naval Underwater Systems Center, 1971.

10. JENKINS, G.M., and WATTS, D.G. Spectral Analysis and its Applications. San Francisco, CA, Holden-Day, 1968: p.255.

11. BRADNER, H. Probing sea-bottom sediments with microseismic noise. Journal Geophysical Research, 68, 1963: 1788-1791.

12. LATHAM, G.V. and SUTTON, G.H. Seismic measurements on the ocean floor. Journal Geophysical Research, 71, 1966: 2545-2573.

13. SCHMALFELDT, B. and RAUCH, D. Ambient and ship-induced noise in shallow water. In: KUPERMAN, W.A. and JENSEN, F.B., eds. Bottom-Interacting Ocean Acoustics, Proceedings of a conference held on 9-12 June 1980 at SACLANT ASW Research Centre, La Spezia, Italy. NATO Conf. Series IV, Marine Sciences 5. New York, NY, Plenum, 1980: 329-344.

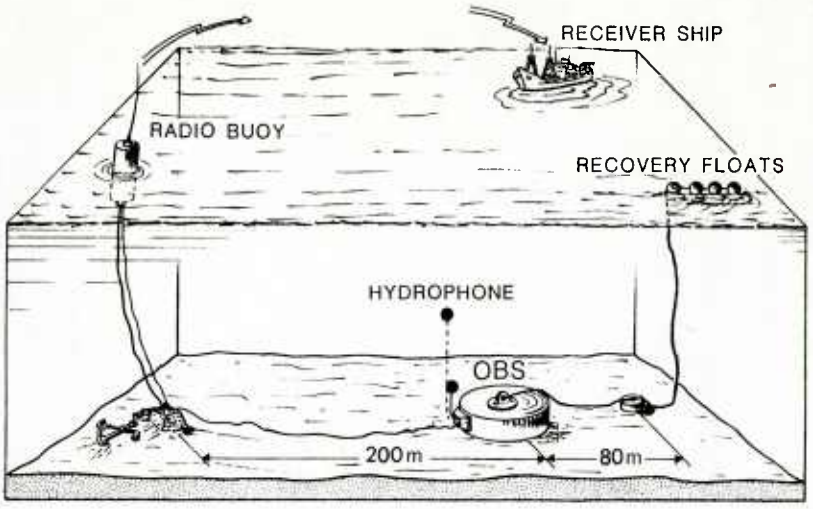
RECEIVER SHIP
RADIO BUOY
RECOVERY FLOATS
HYDROPHONE
OBS
200m
80m

FIG. 1

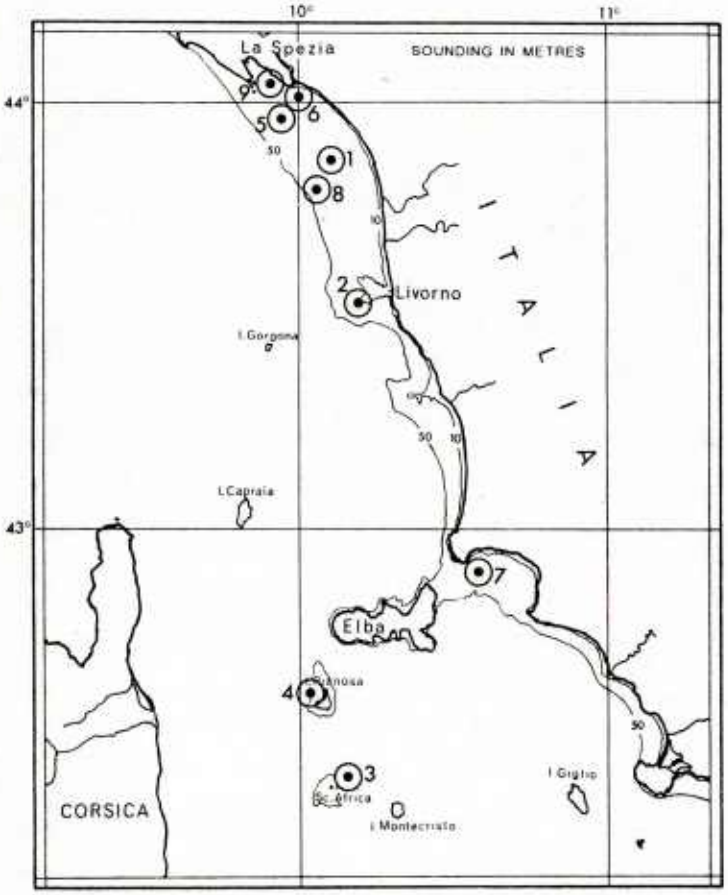
10°
11°
La Spezia
SOUNDING IN METRES
44°
43°
Livorno
I. Gorgona
I. Capraia
Elba
CORSICA
I. Giglio
I. Montecristo

FIG. 2

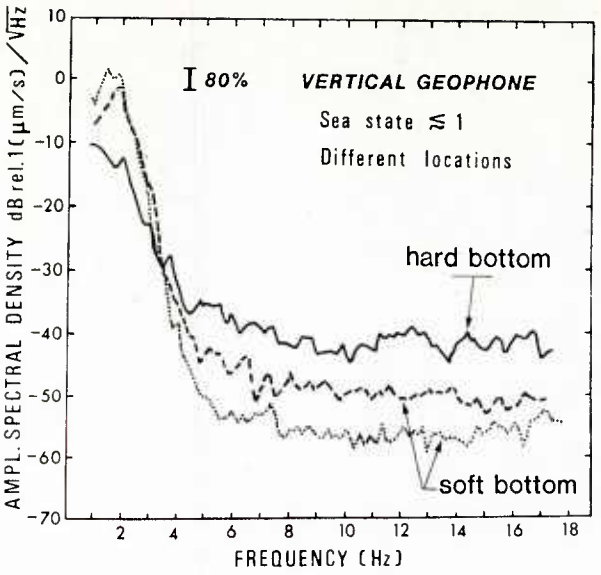

FIG. 3

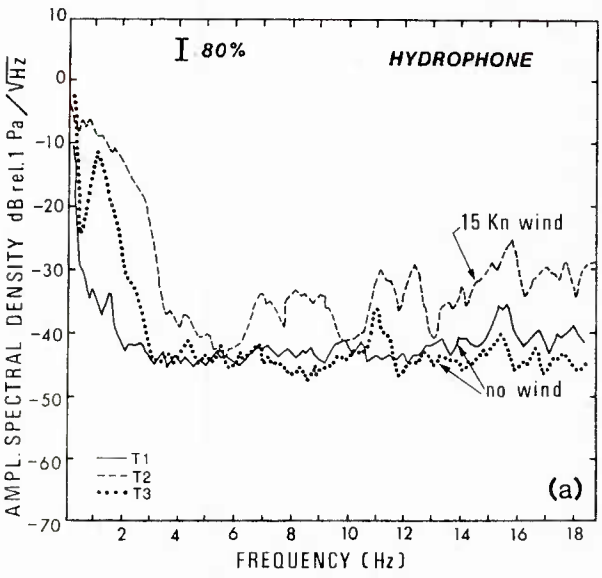

FIG. 4a

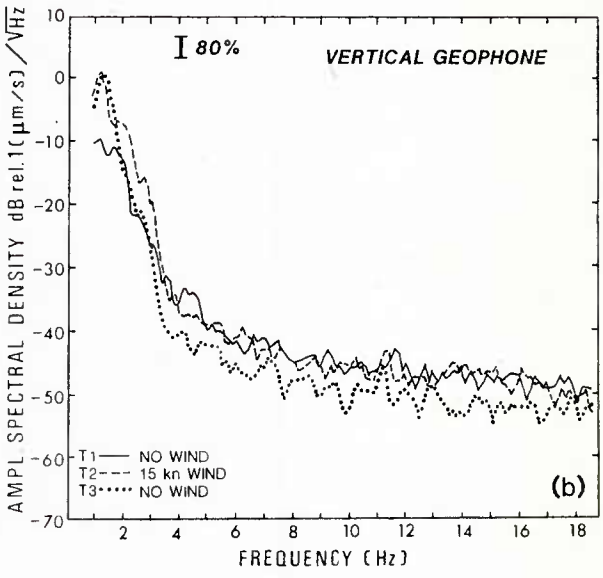

FIG. 4b

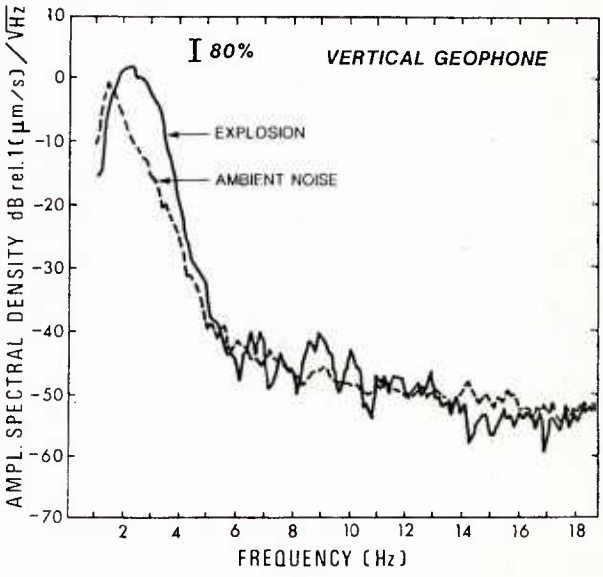

FIG. 5

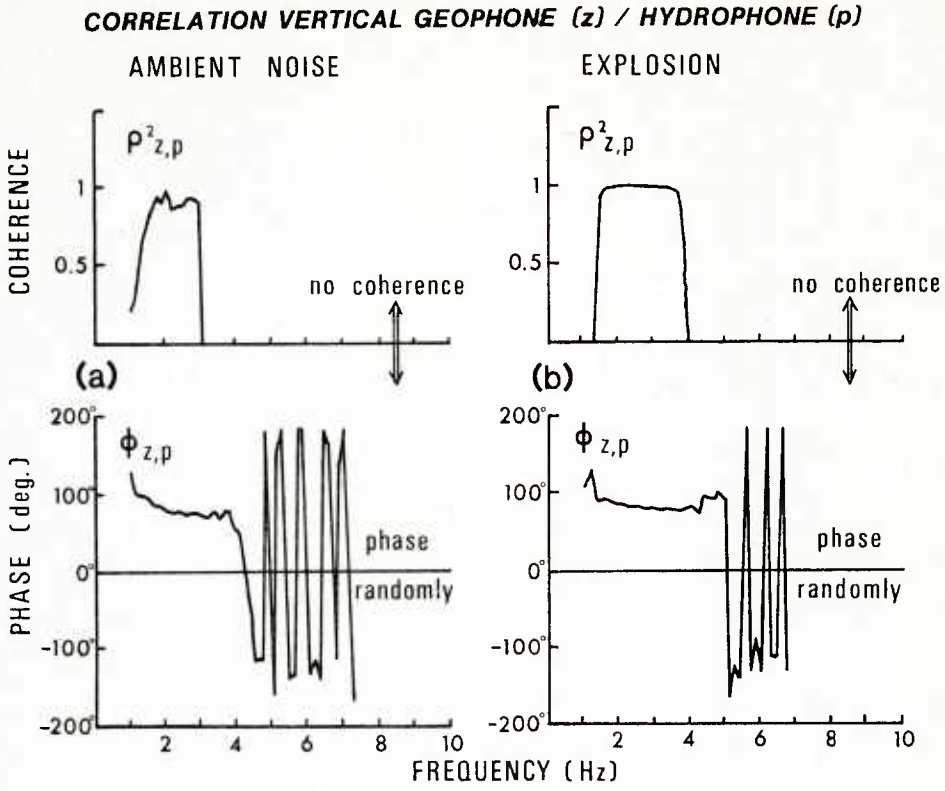

FIG. 6a/b

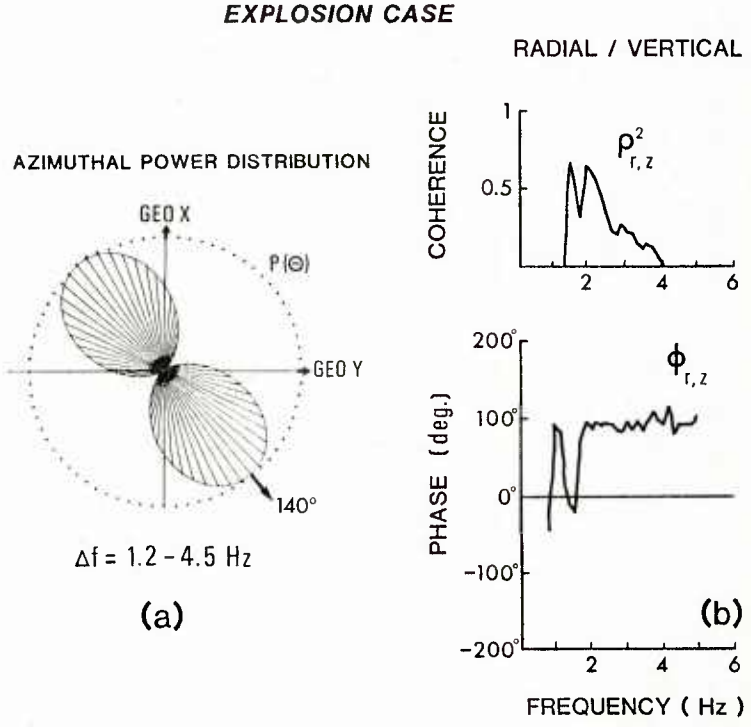

FIG. 7a/b

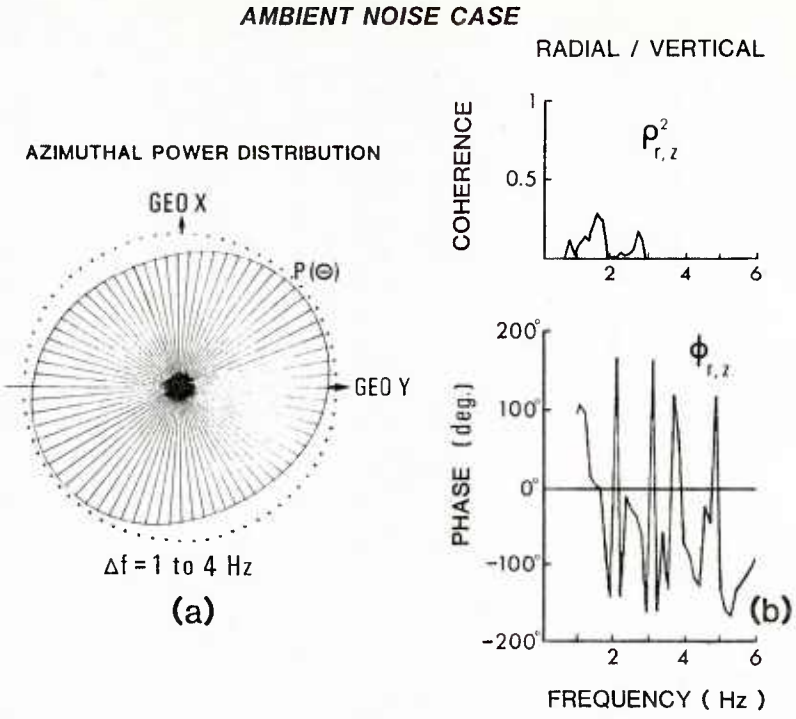

FIG. 8a/b

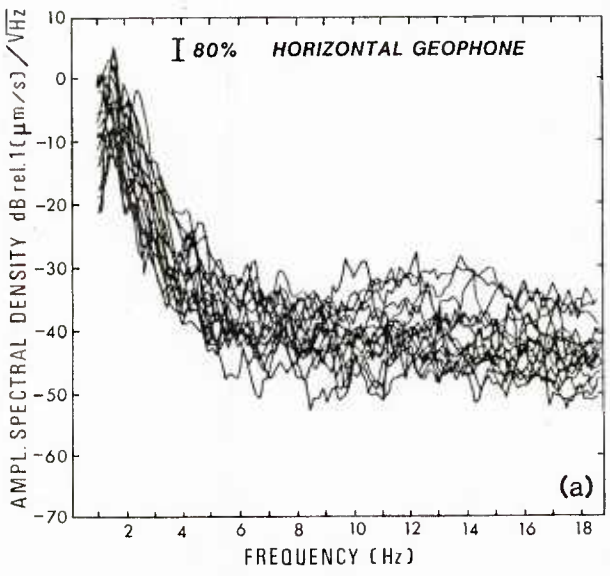

FIG. 9a

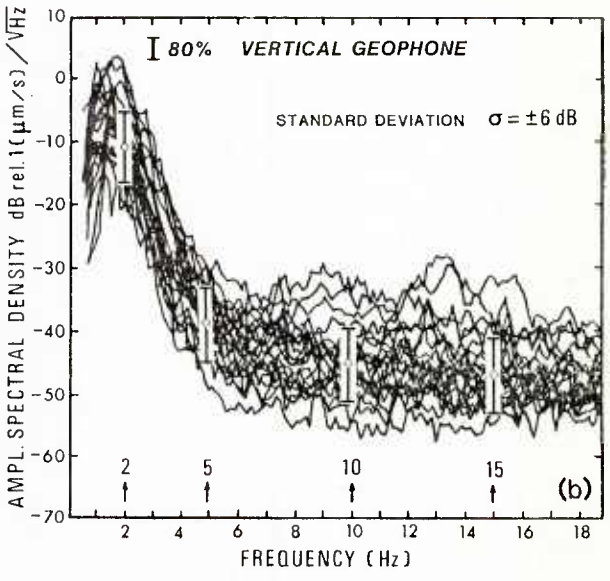

FIG. 9b

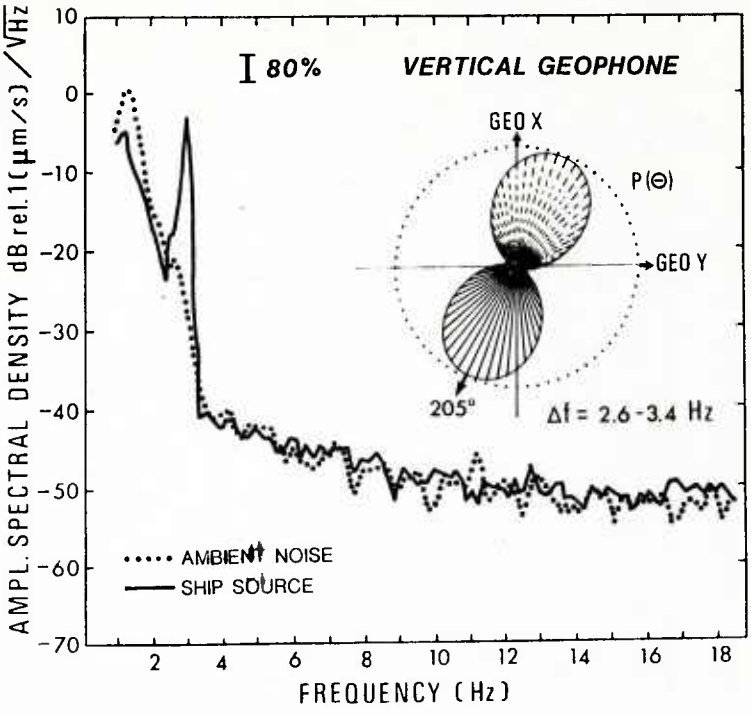
I 80%
VERTICAL GEOPHONE
GEO X
P(Θ)
GEO Y
205°
Δf = 2.6-3.4 Hz
AMBIENT NOISE
SHIP SOURCE
AMPL. SPECTRAL DENSITY dB rel.1(μm/s)/√Hz
FREQUENCY (Hz)
10
0
-10
-20
-30
-40
-50
-60
-70
2
4
6
8
10
12
14
16
18

FIG. 10

"LE PROGRAMME ULYSSE"

(Réseau de bouées dérivantes pour l'étude statistique du bruit ambiant sous-marin)

par

Jean-Alain ROY
GERDSM - Le Brusc
DCAN de TOULON
(France)

1 OBJECTIF

L'étude du bruit ambiant, comme toute étude d'un phénomène physique peut suivre deux approches :

- l'une tend vers l'objectif final, qui est la modélisation mathématique précise du phénomène
- l'autre, d'ambition plus modeste mais permettant de disposer d'informations plus rapidement, se limite à une formulation empirique basée sur des données expérimentales.

Le but du programme Ulysse rentre dans la seconde catégorie.

2 CHOIX DE LA METHODE

L'objectif étant posé, il faut alors sélectionner une méthode de travail.

Un premier élément fondamental pour ce choix est donné par l'objectif lui-même. Une formule empirique, basée sur des données expérimentales, est presque inévitablement associée à une approche statistique. Le résultat obtenu sera alors d'autant plus crédible que le nombre de mesures et le nombre de cas de mesures seront élevés.

Le second élément très important pour définir une méthode de travail est lié au paramètre physique. La mesure du bruit ambiant ne sera acceptable que si rien ne vient perturber celui-ci : le support devra donc être totalement discret.

Ces bases étant posées, il est apparu que le meilleur outil était la bouée autonome, pour la discrétion, dérivante et à longue durée de vie, pour un plus grand nombre d'environnements.

Il restait à choisir un mode de récupération des mesures ; le satellite a été préféré à l'avion car beaucoup plus économique bien que limitant le débit des informations. Parmi les divers types de satellites, on a retenu le géostationnaire car il donne une localisation précise de la bouée, importante pour 2 raisons : d'une part car l'un des objectifs finaux est de coupler des valeurs statistiques de bruit ambiant à des zones d'autre part car la position permet d'atteindre la connaissance de l'environnement sur des atlas (hauteur d'eau, nature du fond, existence de courant, ...).

3 SELECTION DES MESURES

3.1. Le bruit

Le choix dans la mesure se porte à deux niveaux :
- à l'acquisition où l'on peut utiliser soit de simples hydrophones omnidirectionnels soit une antenne (verticale ou horizontale). A la sortie, cela revient à choisir entre n hydrophones situés à des immersions différentes et une antenne qui écoute dans n directions différentes.
- à l'analyse où il faut définir une gamme de fréquences et choisir entre une transmission de données non traitées et une analyse faite dans la bouée. Dans ce dernier cas il faut définir des bandes d'analyse.

En fait le choix est très largement orienté par les limites de transmission du satellite. Dans le programme Ulysse, le satellite retenu imposait un traitement à bord de la bouée. Pour le reste, ayant retenu une gamme de fréquences relativement étendue (20 Hz - 20 kHz) et des filtres tiers d'octave, le nombre de mesures de bruit était limité à trois. On a préféré étudier l'influence de l'immersion avec des hydrophones omnidirectionnels plutôt que l'effet de direction avec des formations de voies sur antennes.

3.2. L'environnement

Nombreux sont les facteurs qui influencent le niveau du bruit de mer et il est donc indispensable de se limiter.

Certaines remarques préliminaires s'avèrent très utiles pour la sélection des paramètres d'environnement :
- il est bien connu que deux facteurs sont fondamentaux : le trafic maritime en dessous de quelques centaines de Hertz et les vagues (donc le vent) au dessus de cette limite

- certaines données peuvent être déduites de la position et de la date de la mesure. Par exemples la hauteur d'eau (ne serait-ce que grossièrement l'étiquette "petits fonds" ou "grands fonds"), la proximité de côtes ou d'un rail de trafic maritime, l'existence d'une plate forme de forage, la présence d'une activité biologique particulière, ...
- deux paramètres particuliers sont très importants : la pluie qui peut être la source de bruit dominante, et le profil bathycélérimétrique qui conditionne la transmission du bruit de trafic et doit être associé à toute étude de l'influence de l'immersion du capteur.

A partir de ces considérations, il a été décidé que les bouées Ulysse soient capables de mesurer, en plus du bruit et de leur position :
- la vitesse du vent (la direction n'a pas été retenue car les hydrophones sont omnidirectionnels)
- le profil bathythermique dans la couche la plus instable (les 100 mètres supérieurs sous la surface)
- les caractéristiques de la pluie (densité et taille des gouttes par exemple).

Un problème difficile s'est posé pour le trafic maritime. L'idéal est de connaître le nombre, la taille, la position et la vitesse des bateaux présents dans le secteur. Un minimum serait la reproduction d'un scope radar donnant le nombre et les positions des bruiteurs. Rien d'embarquable sur une bouée de la taille prévue pour Ulysse n'ayant été trouvé, on s'est contenté d'un intercepteur radar. Une fnformation plus précise sur le trafic maritime devant être obtenue par envoi d'un avion sur le site, à l'instant de la mesure.

4 CONSTITUTION DU MESSAGE TRANSMIS PAR SATELLITE

4.1. Programme Argos - Taille limite du message

Le choix des satellites s'est assez rapidement orienté vers ceux du système Argos car tout en répondant au besoin de la localisation des bouées, ils présentaient l'avantage d'être liés à un organisme français, le CNES (Centre National d'Etudes Spatiales de Toulouse). La taille des messages en principe limitée à 256 bits peut être quadruplée si on accepte de réduire le nombre de répétitions par le même facteur, et le millier de bits alors atteint convient au besoin.

Sans s'étendre sur la description du système Argos, on peut rappeler qu'il a été mis en place pour répondre aux besoins des sciences de la terre, de la mer et de l'atmosphère, qu'il utilise simultanément deux satellites héliosynchrones volant à environ 850 km d'altitude et permettant d'atteindre environ 3 km de précision pour la localisation des plateformes, et enfin que le nombre de visibilités journalières est pratiquement toujours supérieur à 6.

4.2. Message relatif au bruit ambiant

L'enveloppe globale étant donc de 4 fois 256 bits, il était tentant d'en réserver le quart pour l'environnement et remplir les 3 morceaux restants avec 3 mesures de bruit. C'est ce qui a été fait.

Avec 256 bits, il était hors de question de transmettre le bruit en bande large, aussi a-t'on installé dans la bouée un analyseur spectral câblé analysant en bandes tiers d'octave à partir de FFT.

Pour rester inférieur à 256 tout en gardant de l'ordre de 60 dB en dynamique sur un spectre, on a pu retenir 24 bandes d'analyse en écrivant le niveau dans chaque bande avec 10 bits et en ajoutant 3 bits au message pour un exposant commun aux 24 bandes.

4.3. Message relatif à l'environnement

On a vu précédemment (paragraphe 3) la liste des paramètres retenus pour accompagner chaque mesure de bruit de mer. Au sein des messages, ils se répartissent ainsi :

- la température occupe 210 bits : 10 par capteur, à raison d'un capteur tous les 5 mètres entre 0 à 100 mètres d'immersion (plus une référence)
- la vitesse du vent est codée sur 10 bits
- la pluie occupe 8 bits pour la densité (nombre de gouttes) et 10 bits pour l'intensité (énergie)
- l'intercepteur radar prend 1 bit.

4.4. Message relatif aux servitudes

La place restant disponible dans chacun des 4 messages précédents est utilisée pour les informations complémentaires indispensables :

- numéro d'ordre de chacun des 4 messages (4x2 bits)
- date (nombre de jours écoulés), sur 10 bits
- tension de l'alimentation principale, sur 8 bits
- tension d'alimentation du système de repérage radio-goniométrique, sur 4 bits
- immersion des 2 hydrophones profonds (mesure de pression), sur 8 bits chacun
- allure de la bouée (horizontale ou verticale), par 1 bit répété dans chacune des 4.

5 CONSTITUTION DE LA BOUEE

5.1. Corps de bouée (fig. 1)

Les batteries au lithium et l'ensemble de l'électronique (analyse et transmission) sont contenus dans un caisson flottant, de forme cylindrique (4 m de long, 25 cm de diamètre), en fibre de verre et résine synthétique.

Il supporte dans sa partie inférieure un lest ajustable (disques en fonte), et dans sa partie supérieure une surépaisseur de flottaison et un mât de 2,40 m de long. Ce mât porte un réflecteur radar, la balise d'émission Argos, celle pour le repérage radio-goniométrique et les 3 capteurs d'environnement pour la pluie, le vent, l'interception radar (fig.2).

5.2. Ligne sous-marine (fig.3)

Les trois hydrophones et le réseau de thermistances sont portés par une ligne sous-marine constituée de 3 tronçons :

- la partie supérieure, elle-même divisée en deux morceaux : un câble électrique de 40 conducteurs (32 simples et 4 paires blindées) doublé par une corde de nylon. Le câble électrique, qui forme une boucle plongeante jusqu'au raccordement au second tronçon, porte la première thermistance à 5 mètres d'immersion. Il mesure 18 mètres, pèse 50 kg dans l'air et 25 kg dans l'eau. La corde de nylon porte une chaine de flotteurs afin d'amortir les mouvements de surface. Elle mesure 15 mètres, pèse 80 kg dans l'air et vaut 280 kg de flottabilité.
- la partie intermédiaire, un câble électroporteur (même nombre de conducteurs et armature en kevlar), mesurant 94 mètres, pesant 196 kg dans l'air et 90 kg dans l'eau. Il porte les 19 thermistances restantes et l'hydrophone supérieur (40 m d'immersion).
- la partie inférieure, constituée d'un câble électro-porteur de 13 conducteurs (7 simples et 3 paires blindées), longue de 400 mètres, pesant 380 kg dans l'air et 150 kg dans l'eau, porte les 2 hydrophones inférieurs (immersions 120 m et 500 m) et un lest-amortisseur (plaque métallique circulaire).

6 ORGANISATION DES MESURES

L'équipement a été conçu pour fonctionner de façon autonome pendant 12 mois, effectuant 2 mesures par 24 h (l'une de jour, l'autre de nuit).

A chacune de ces mesures, la séquence des prises de données est la suivante :

- mesure de bruit sur les 3 hydrophones pendant 1 seconde entre To et To + 1 s
- mesures de pressions, températures, et relevé des informations de servitudes (tensions batterie, horizontalité, date, ...) dans le même créneau

- écoute radar, vitesse du vent, pluie, pendant 30 secondes entre To - 15 s et To + 15 s.

L'analyseur spectral est alimenté entre To - 1 s et To + 2 s.

7 EXPLOITATION DES DONNEES

Le système de transmission Argos permet de récupérer les messages de 2 façons :
- en interrogeant un centre de distribution (CNES de Toulouse) par téléphone ou télex
- en recevant régulièrement des bandes magnétiques sur lesquelles sont enregistrées les mesures sous forme numérique.

Les deux méthodes sont utilisées :
- l'interrogation par téléphone, exploitée sur mini-calculateur HP 9845, permet de suivre régulièrement le bon fonctionnement de la bouée, ainsi que la route suivie.
- la bande numérique sert de support à l'exploitation statistique qui fait l'objet du programme.

La présentation des résultats est délivrée sous de nombreuses formes. Les principales sont :
- tableau général des mesures faites lors d'une prise de données (fig.6)
- spectre de bruit relatif à chacun des hydrophones et profil bathythermique pour une prise de données (fig.7)
- niveau moyen sur un hydrophone pour une période donnée (fig.8)
- évolution du niveau de bruit en fonction de la date à différentes fréquences, corrélativement au vent, à la pluie, et aux interceptions radar (fig.9)
- profils de température et de célérité pour une prise de données (fig.10)
- courbes isothermes pour une période donnée (fig.11).

De plus, il est possible d'afficher :
- la liste des prises de données relatives à une mesure, pour l'ensemble des bouées
- le trajet suivi par une bouée en dérive (fig.12).

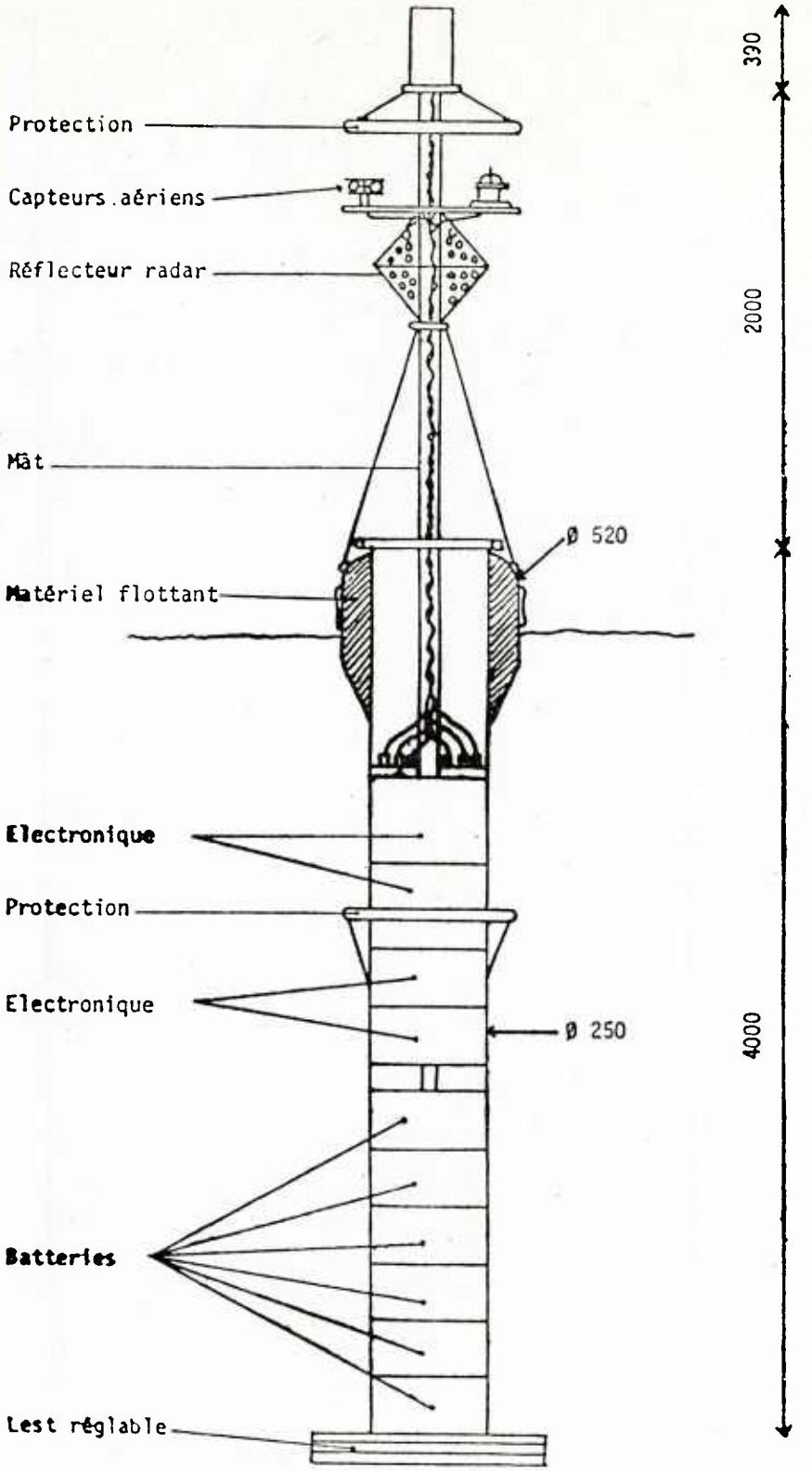
Protection
Capteurs aériens
Réflecteur radar
Mât
Matériel flottant
Ø 520
Electronique
Protection
Electronique
Ø 250
Batteries
Lest réglable
390
2000
4000

FIG. 1

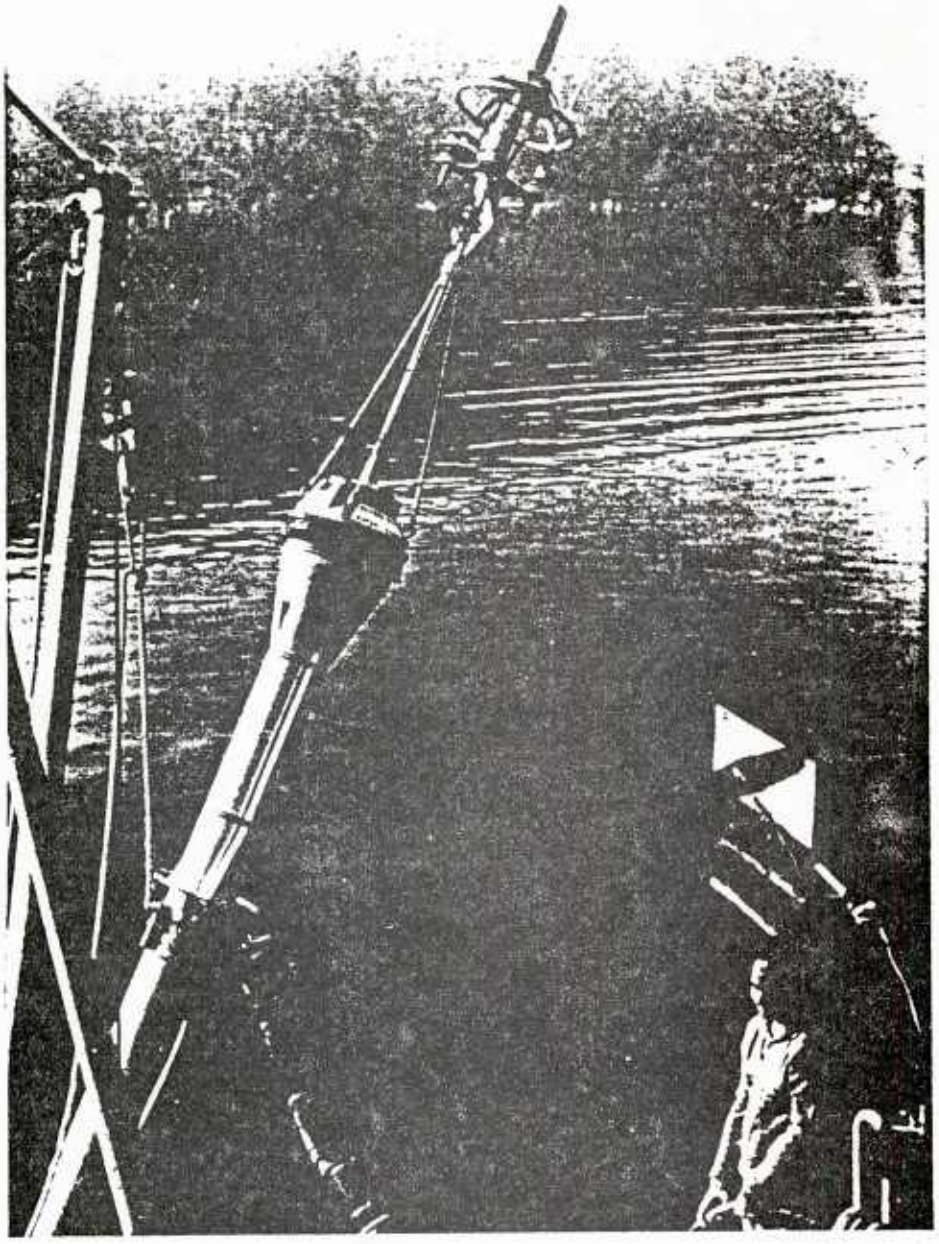

FIG. 2

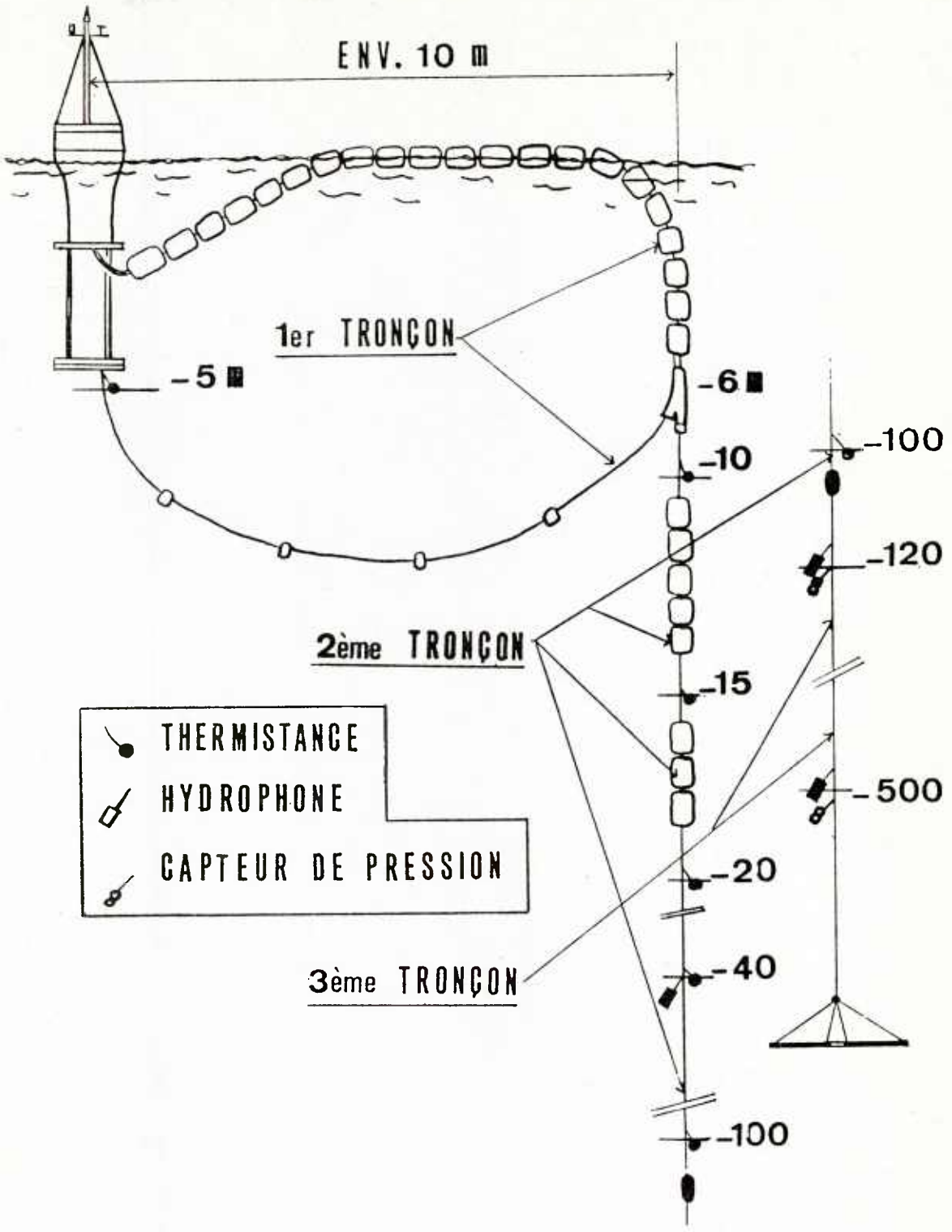
ENV. 10 m
1er TRONÇON
-5
-6
-10
-100
-120
2ème TRONÇON
-15
-500
THERMISTANCE
HYDROPHONE
CAPTEUR DE PRESSION
-20
-40
3ème TRONÇON
-100

FIG. 3

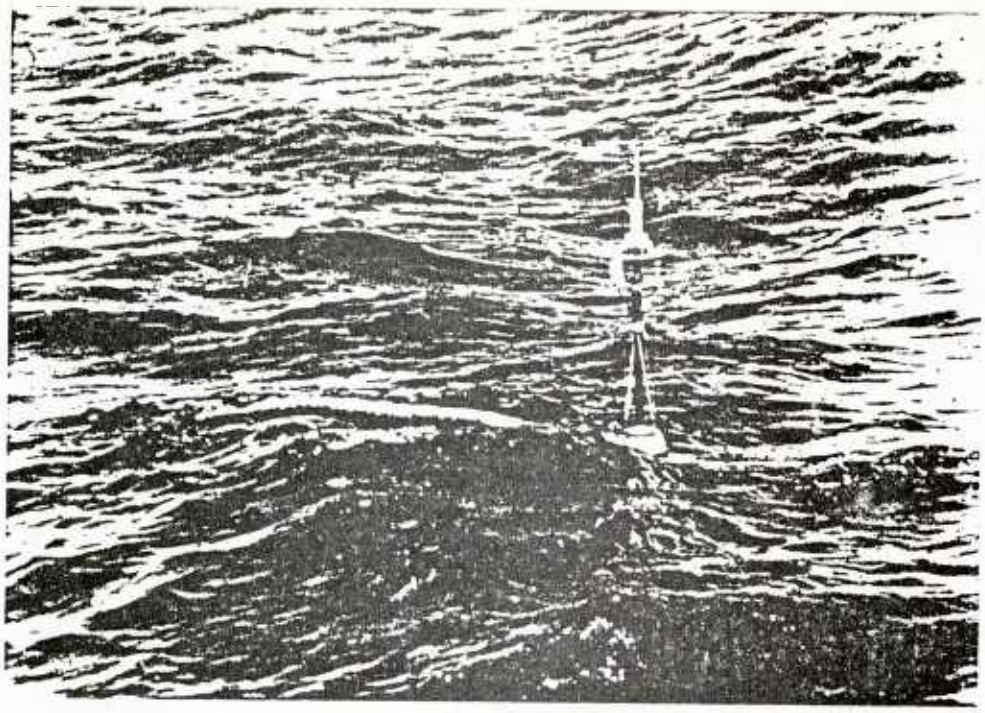

FIG. 4

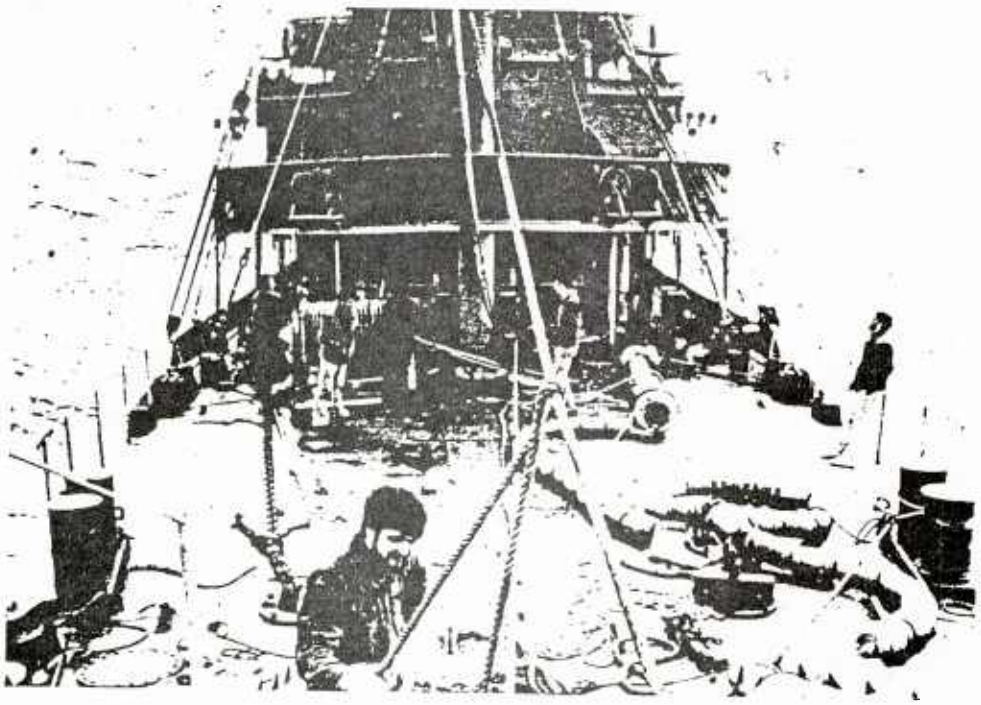

FIG. 5

PROGRAMME ULYSSE (25/ 4/1981)

N- EXPERIENCE	: 69	FREQUENCE EMISSION	:401.649799 (MHz)
N- JOUR DANS L ANNEE	: 115	LATITUDE	:41.146
JOUR JULIEN	:11437	LONGITUDE	: 7.443
MOIS	: 4	VITESSE EN LATITUDE	:-0.017
ANNEE	: 1981	VITESSE EN LONGITUDE	:-0.288
HEURE PASSAGE MESSAGE (HEURE-MINUTE-SECONDE)	: 6-59-48		
HORLOGE	: 24		
NOMBRE DE JOURS ECOULES	: 3	N- BOUEE : 4	ALTITUDE BOUEE : 0

TENSION GONIO : 10.4 (Volts) TENSION BATTERIE : 19.7 (Volts) TRAFIC : 0 HORIZONTALITE BOUEE : 1

PLUIE — DENSITE DE PLUIE : 72 (DEPASSEMENT : 0) ENERGIE DE PLUIE : 0 (DEPASSEMENT : 1)

VENT — VITESSE DU VENT : 14.40 (m/s)

PRESSION — PRESSION HYDRO 120 M : 12.25 (bars) PRESSION HYDRO 500 M : 50.25 (bars)

TEMPERATURE (DEGRES CENTIGRADES)

IMMERSION (M)	TEMPERATURE
5	14.80
10	40.75
15	14.49
20	13.59
25	14.14
30	5.46
35	4.66
40	13.51
45	13.06
50	12.76
55	12.56
60	12.50
65	12.39
70	12.36
75	15.71
80	8.63
85	8.94
90	8.98
95	9.31
100	11.45
Reference :	10.00

BRUIT (REF:MICRO PASCAL)

HYDRO 40 M FREQ	- NIVEAU	HYDRO 120 M FREQ	- NIVEAU	HYDRO 500 M FREQ	- NIVEAU
20.	94.5	20.	89.3	20.	91.7
25.	88.8	25.	86.6	25.	91.4
31.	89.1	31.	84.7	31.	88.2
40.	86.8	40.	80.3	40.	84.4
50.	88.2	50.	77.6	50.	80.0
63.	85.4	63.	73.7	63.	76.5
80.	79.9	80.	70.4	80.	77.7
100.	80.8	100.	66.9	100.	73.6
125.	79.9	125.	66.8	125.	76.4
160.	77.0	160.	63.5	160.	71.4
200.	75.8	200.	59.9	200.	70.6
250.	73.6	250.	58.1	250.	69.0
315.	72.3	315.	58.1	315.	69.0
400.	70.0	400.	53.4	400.	66.0
500.	67.8	500.	52.6	500.	67.7
630.	65.7	630.	50.0	630.	66.0
800.	65.7	800.	49.1	800.	64.6
1000.	63.0	1000.	46.8	1000.	62.4
1250.	60.5	1250.	44.8	1250.	62.0
1600.	59.1	1600.	43.6	1600.	61.4
2000.	56.5	2000.	43.2	2000.	61.3
2500.	55.3	2500.	40.4	2500.	59.8
3150.	53.1	3150.	39.5	3150.	57.8
4000.	52.1	4000.	40.9	4000.	57.6

FIG. 6

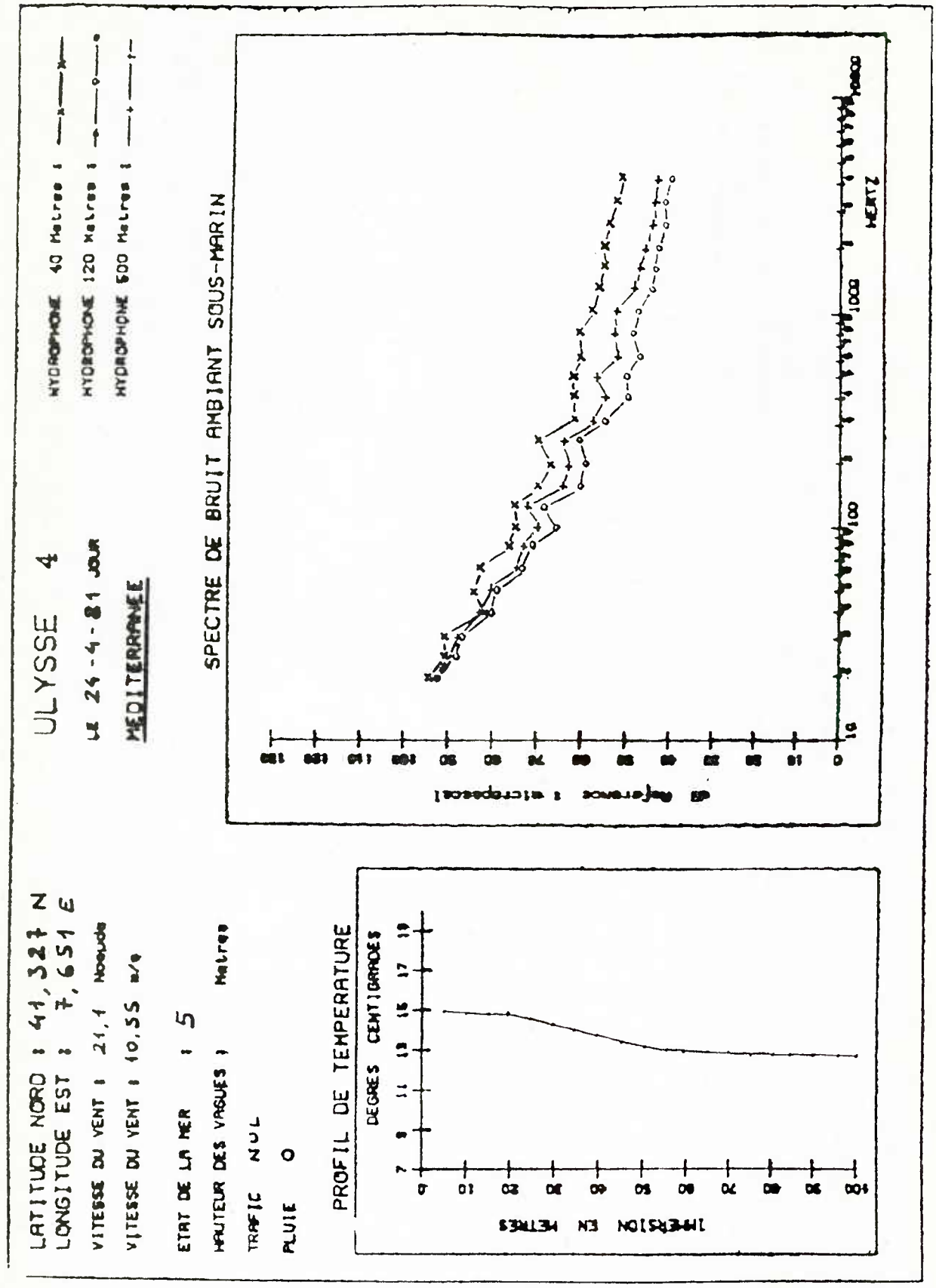
ULYSSE 4
LE 24-4-81 JOUR
MEDITERRANNEE
LATITUDE NORD : 41,323 N
LONGITUDE EST : 7,651 E
VITESSE DU VENT : 21,1 Noeuds
VITESSE DU VENT : 10,55 m/s
ETAT DE LA MER : 5
HAUTEUR DES VAGUES : Metres
TRAFIC NUL
PLUIE 0
HYDROPHONE 40 Metres
HYDROPHONE 120 Metres
HYDROPHONE 600 Metres
SPECTRE DE BRUIT AMBIANT SOUS-MARIN
HERTZ
PROFIL DE TEMPERATURE
DEGRES CENTIGRADES
IMMERSION EN METRES

FIG. 7

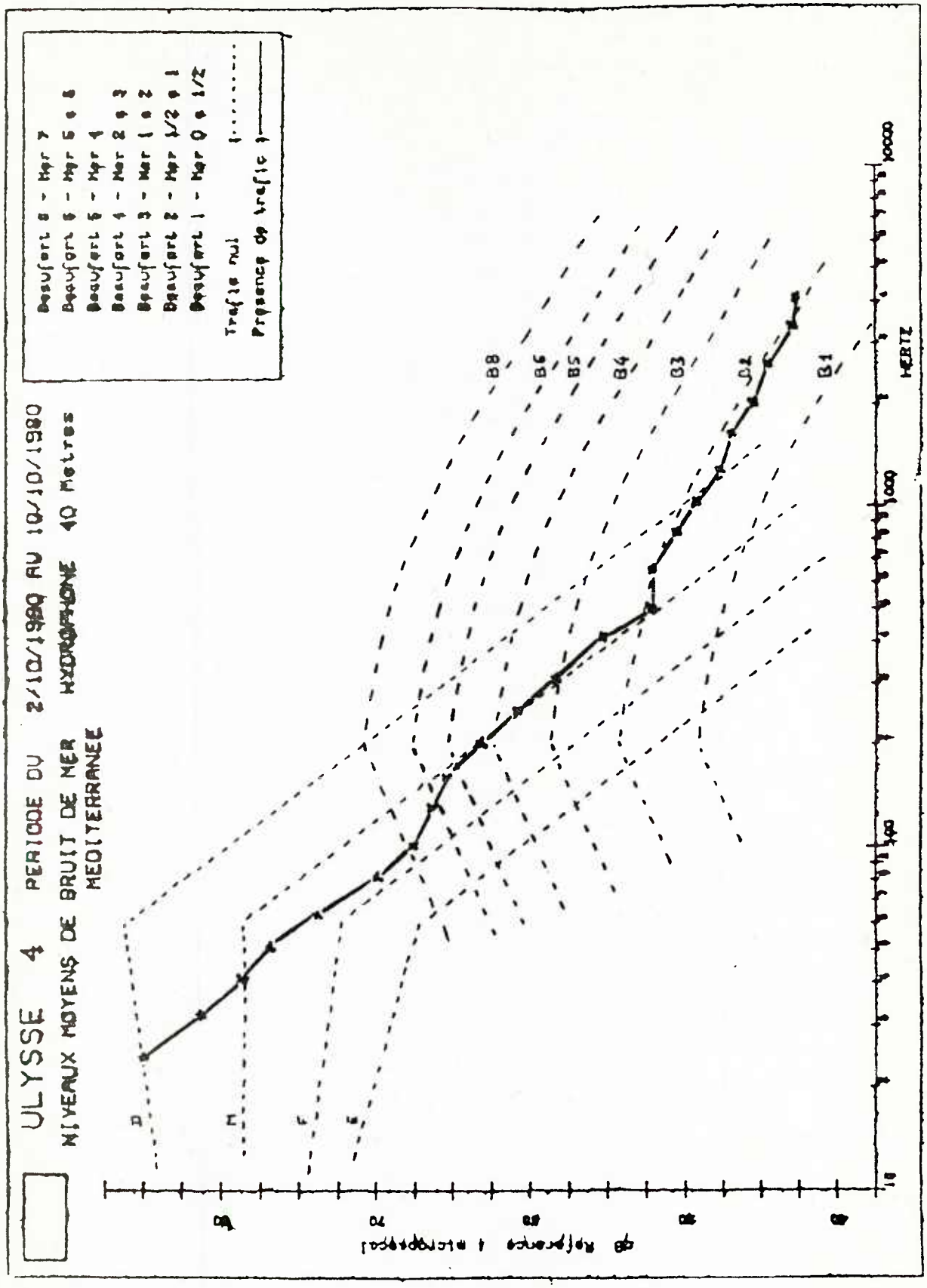
ULYSSE 4 PERIODE DU 2/10/1980 AU 10/10/1980
NIVEAUX MOYENS DE BRUIT DE MER HYDROPHONE 40 Metres
MEDITERRANEE
Beaufort 8 - Mer 7
Beaufort 6 - Mer 5 e 6
Beaufort 5 - Mer 4
Beaufort 4 - Mer 2 e 3
Beaufort 3 - Mer 1 e 2
Beaufort 2 - Mer 1/2 e 1
Beaufort 1 - Mer 0 e 1/2
Trafic nul
Presence de trafic
B8
B6
B5
B4
B3
B2
B1
HERTZ
dB référence 1 micropascal

FIG. 8

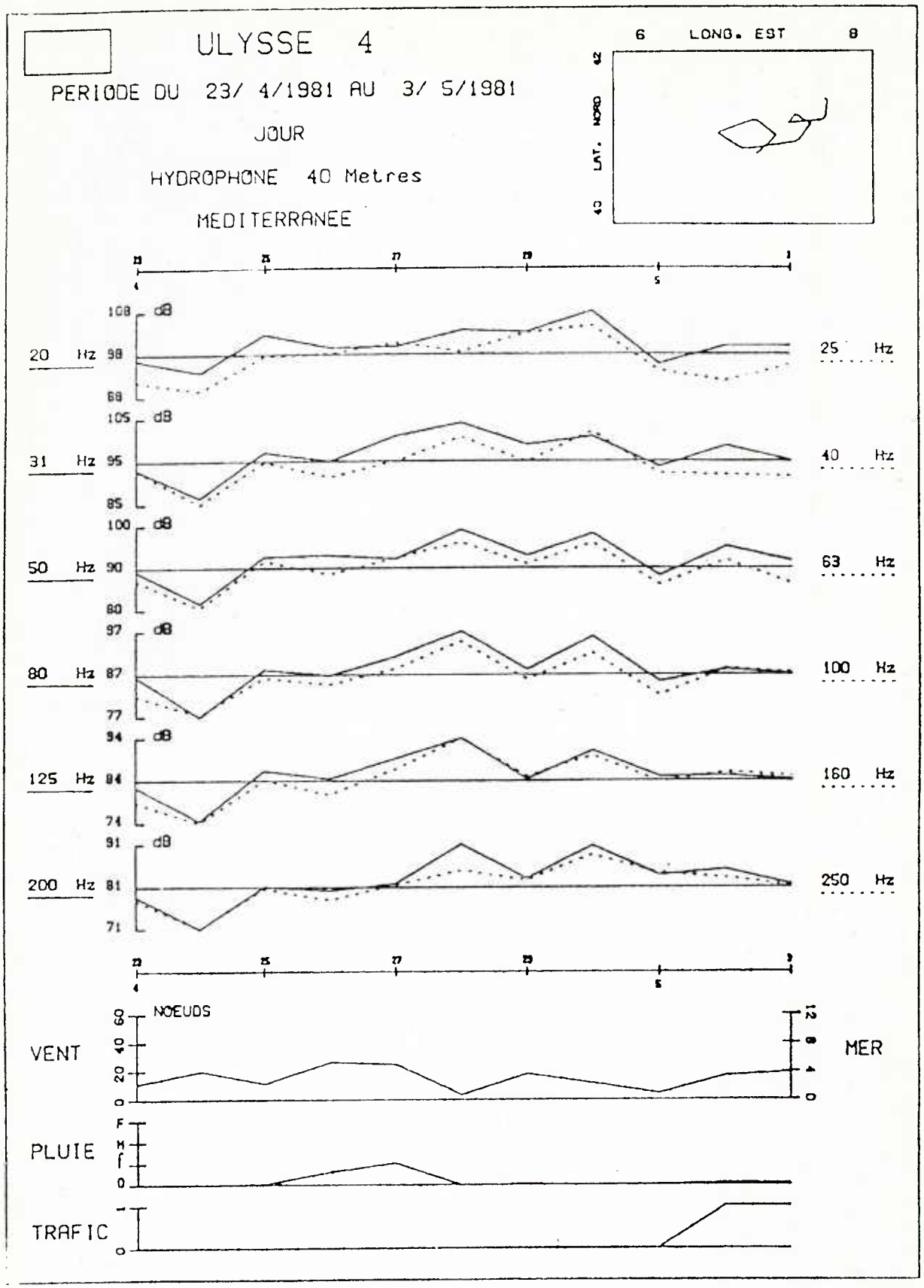
ULYSSE 4
PERIODE DU 23/ 4/1981 AU 3/ 5/1981
JOUR
HYDROPHONE 40 Metres
MEDITERRANEE
6 LONG. EST 8
LAT.
20 Hz
25 Hz
31 Hz
40 Hz
50 Hz
63 Hz
80 Hz
100 Hz
125 Hz
160 Hz
200 Hz
250 Hz
dB
NOEUDS
VENT
MER
PLUIE
TRAFIC

FIG. 9

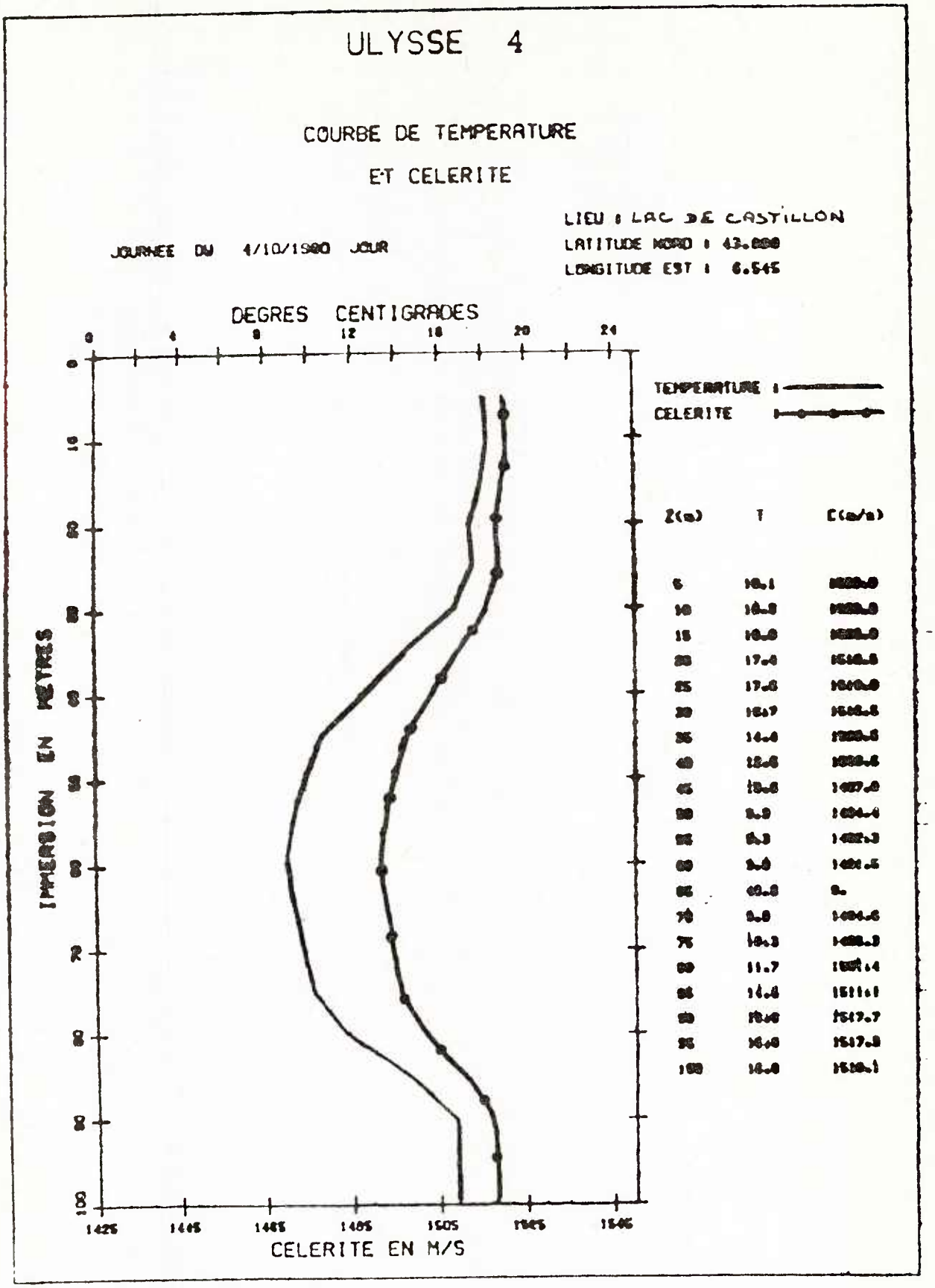
ULYSSE 4
COURBE DE TEMPERATURE
ET CELERITE
LIEU : LAC DE CASTILLON
LATITUDE NORD : 43.000
LONGITUDE EST : 6.545
JOURNEE DU 4/10/1980 JOUR
DEGRES CENTIGRADES
0
4
8
12
16
20
24
TEMPERATURE :
CELERITE :
Z(m)
T
C(m/s)
IMMERSION EN METRES
0
10
20
30
40
50
60
70
80
90
100
1425
1445
1465
1485
1505
1525
1545
CELERITE EN M/S

FIG. 10

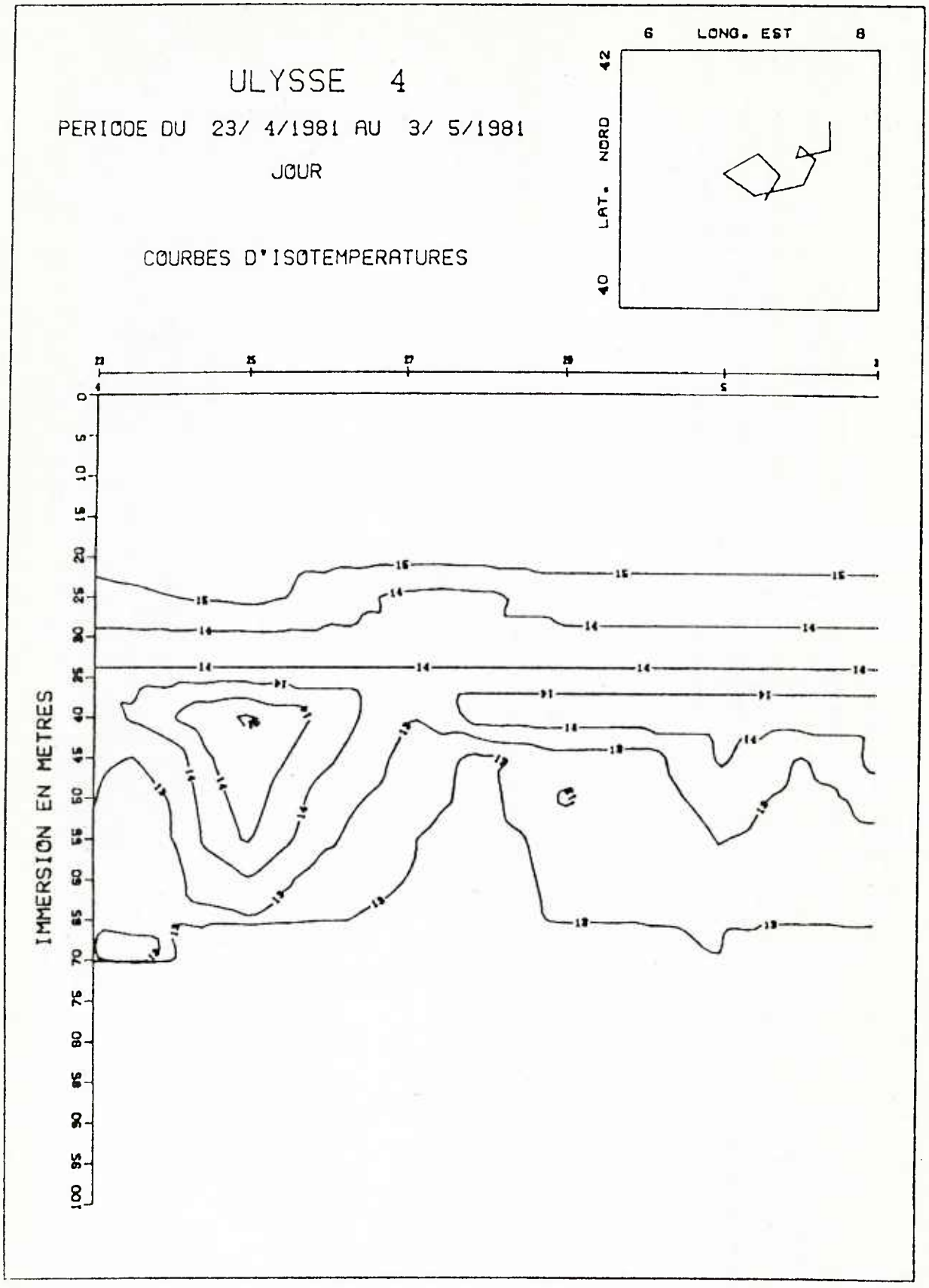
ULYSSE 4
PERIODE DU 23/ 4/1981 AU 3/ 5/1981
JOUR
COURBES D'ISOTEMPERATURES
6 LONG. EST 8
42
LAT. NORD
40
IMMERSION EN METRES

FIG. 11

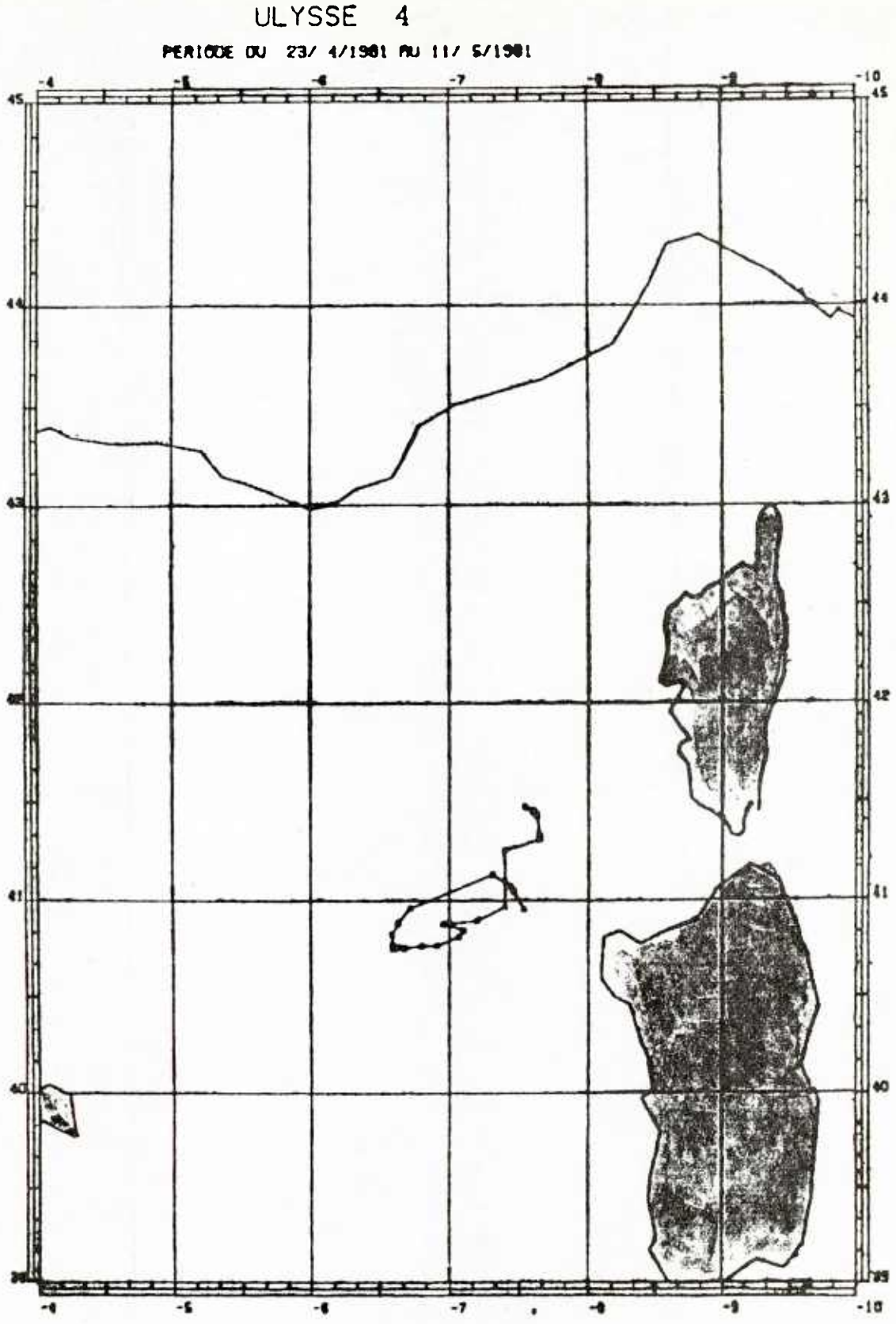

FIG. 12

ARCTIC AMBIENT NOISE STATISTICAL MEASUREMENT RESULTS AND THEIR IMPLICATIONS TO SONAR PERFORMANCE IMPROVEMENTS

by

Roger F. Dwyer
Naval Underwater Systems Center
New London, CT 06320 U.S.A.

ABSTRACT

Recent analyses of FRAM II arctic data have shown that under ice ambient noise can be at times highly impulsive and non-Gaussian. The analyses included time domain statistical measurements which were consistent with previously reported results of experiments made within the Canadian Arctic Archipelago. New findings of frequency domain estimates of complex skew and kurtosis and cumulative distribution functions, measured in 2, 6, and 10 Hz resolution cells at the output of a discrete Fourier transform, also indicate the existence of strong non-Gaussian noise. It is known that the ability to detect and estimate signals contaminated with non-Gaussian noise using conventional processing is degraded compared with optimum techniques which utilize knowledge of the noise statistics. The FRAM II data results suggest that sonar performance can be improved in the arctic environment by optimum signal processing methods.

INTRODUCTION

This paper describes the results of a statistical analysis study of FRAM II arctic under ice ambient noise data (1). The specific data that were analysed were recorded on the 23rd and 24th of April, 1980, from a pack ice camp in the Arctic Ocean, located at 86° N latitude, 25° W longitude.

The measurement system consisted of a broadband omni-directional hydrophone, suspended to a depth of 91 m from a sonobuoy located in a lead. Under the influence of arctic currents, wind and neighboring floes the pack ice was slowly moving. This movement caused rifting and cracking of ice which occurred throughout the experiments and represented a structured acoustic noise source. Both impulsive and narrowband non-Gaussian noise were identified in the data and were probably created by tensile cracks and rubbing ice masses. The data collected by A. R. Milne and J. H. Ganton were obtained in the Canadian Arctic Archipelago region under stationary shore fast ice. In this region, the mechanism for impulsvie and non-Gaussian noise is due to tensile stresses caused by rapid reduction in air temperatures (2). Noise from the pack ice, on the other hand, is due to the friction between interacting and colliding ice floes and, probably, to tensile stresses.

In order to better understand the statistical properties of under ice ambient noise, we essentially repeated Milne's time domain experimental measurements

(albeit with different bandwidths) and deduced similar conclusions on the non-Gaussian nature of under ice ambient noise. Moreover by statistically examining the discrete frequency components, we found that they were also non-Gaussian due to ice dynamics. Specifically, the skew, kurtosis, and cumulative distribution function (cdf) of the data were estimated.

In the time domain, the statistics were estimated in 100, 350, and 2500 Hz bands. At times, the statistical estimates in all bands deviated from Gaussian noise significantly, and were consistent with previously reported results of experiments made within the Canadian Arctic Archipelago. The estimated energy of FRAM II data predicted detection thresholds 3 to 10 dB higher than would be expected from purely Gaussian phenomena.

Spectrum levels and spectrograms were also estimated. The spectrograms depicted dynamic frequency components which appear, from aural information that sounded like squeaks, to be correlated with ice dynamics. Comparisons of broadband spectrum level estimates at different times, indicate non-stationary frequency domain components which also appear to be correlated with ice dynamics. Since it was suspected that ice dynamics generate narrow-band non-Gaussian noise, statistical estimates of frequency domain components were also measured. These frequency domain statistical measurements represent new techniques for estimating environmental noise phenomena. The complex skew, kurtosis, and cdf were measured in 1, 2, 6, and 10 Hz resolution cells at the output of a fast Fourier transform (FFT) with processing times from 2 to 14 minutes. These new findings indicate the existence of strong non-Gaussian noise in the frequency domain.

DESCRIPTION OF EXPERIMENT

The FRAM II under ice ambient noise data, to be discussed, were collected in the spring of 1980 as part of a multi-institutional arctic research program sponsored by the office of Naval Research. Only the single channel wideband recordings will be discussed here. Reference 1 summarizes the data collected for the other scientific experiments.

Over 30 hours of analog data from an omni-directional hydrophone suspended to a depth of 91 m from a sonobuoy deployed in a lead were recorded. The data were radio-linked to a receiver, filtered in a 10 to 5 kHz band and recorded on a 4-channel Tandberg analog recorder. About 2 hours of this data set were subsequently processed and a representative sample is presented here. However, the FRAM II log indicates that there are periods when the ice actively lessened and periods of severe ice noise. Neither of these two extremes are presented. Rather the data which falls between these two extremes are presented. In this way we believe the results more closely reflect the average conditions prevailing during the experiments. Even so, the data sample chosen still shows variability and nonstationarity in the measured parameters.

The statistical results of the time domain analysis will be discussed first, then we will present the statistical results of the frequency domain analysis. However in order to introduce and possibly anticipate the results to follow

we present in Fig. 1 an example of nonstationary under ice ambient noise. After filtering through a 2500 Hz lowpass filter and then digitizing the data at a 10 kHz rate, we compared its spectrum for two time periods. The top curve in Fig. 1 represents the average spectrum using 100 consecutive 1024 point FFT estimates, which is equivalent to about 10 seconds of data. The same procedure was used for the bottom curve except that the estimates were made 3 minutes later. The horizontal scale represents normalized frequency which conveniently gives the FFT bin locations. To convert to frequency simply multiply by the resolution which is approximately 10 in this case. The important features of Fig. 1 are the change in spectrum shape over time especially at some frequencies, suggesting nonstationary discrete noise components; and the large dc levels. We shall address the dc level in the next figure.

TIME DOMAIN RESULTS

For the time domain analysis we estimated the first four statistical moments, namely the mean, variance, skew, and kurtosis, and the cumulative distribution functions (cdf) in bandwidths of 100, 350, and 2500 Hz. The data were filtered, sampled, and grouped into records of 1024 samples each. The statistical moments were then estimated for each record. Over time intervals consisting of hundreds of records the cdf of the energy (square of the data samples) was estimated and shown for the most part to be non-Gaussian but with nonstationary distribution functions over successive intervals. Figures 2 through 5 represent the time domain results of the FRAM II data for a particular time window. Additional FRAM II data analyses results are given in Ref. 3.

Figure 2 shows the statistical moments for the time domain data which were filtered through a 2500 Hz lowpass filter and then sampled at a 10 kHz rate. Therefore each record represents a time interval of about .1 seconds giving an overall data length of 10 minutes. The graph on the top left shows that the mean is not zero. This bias which caused the large dc level in Fig. 1 was due to the carrier frequency of the tape recorder being slightly misaligned. In subsequent processing we subtracted out this bias. Some other important observations about this data are the variability of the variance over time and the significant deviation from the Gaussian assumption based on the skew and kurtosis estimates. In order to assess which frequencies were dominating the variance in the band we processed the data in smaller bandwidths of 100-200 Hz, 200-300 Hz, 300-400 Hz, 400-750 Hz, 750-1100 Hz, and 1100-1450 Hz. The 300-400 Hz band will be discussed later in detail. We found that the higher frequency bands (i.e., 750-1100 Hz and 1100-1450 Hz) were contributing to the variability of the variance.

The kurtosis is especially important because it indicates deviations from the Gaussian distribution by values being greater or less than 3. The values greater than 3 pertain to distributions which are more peaked than the Gaussian distribution whereas values less than 3 correspond to distributions which are less peaked. For example, a purely sinusoidal signal, with uniformly distributed phase, has a kurtosis of 1.5. None of the records in Fig. 2 have kurtosis values of 1.5, although some are near 2.

Next we will discuss the estimated energy cdf for two separate data blocks consisting of 300 records (approximately 300,000 samples) each. The data blocks start at the first and 1800th record, respectively, as shown in Fig. 2.

The estimated time domain energy cdf is shown in Fig. 3. Each sample was first squared and then the cdf was estimated for the 300 records, which represent a time interval of about 30 seconds for each block. The vertical axis is plotted as the logarithm of the excedance probability. The horizontal scale is plotted as the logarithm of the energy normalized by the variance of the original data. In the figure the solid curve represents the energy cdf of a known Gaussian noise source that was digitized and processed exactly as the data. The curves b and c represent the data for the first and second block, respectively. The significance of these plots can be appreciated by a simple example.

Suppose we want to set a threshold in an energy detector on a per sample basis so that the false alarm rate is .0001. From the figure, we would have to set the threshold 3-4 dB higher for curve b, and 9-10 dB higher for curve c, compared to what the threshold would be set at for purely Gaussian noise. These results, of course, would change depending upon the detection integration time for any particular application.

The first four statistical moments of another data set are given in Fig. 4. This data was first filtered by a 100 Hz bandpass filter centered at 350 Hz, sampled at a 2 kHz rate and processed in records of 1024 samples each, giving a time interval per record of approximately .5 seconds. The important observations in Fig. 4 are that the variability in the variance is greatly reduced, compared with Fig. 2, however many records still deviate from a Gaussian distribution based on the kurtosis estimate. We also calculated the energy cdf for this band in sub-intervals of approximately 2.4 minutes each. Over 14.5 minutes of data were used and we therefore obtained 6 energy cdf estimates. These estimates were nonstationary in that each estimate deviated from a Gaussian distribution.

We conclude, therefore, at least for this data set, that the under ice ambient noise in the time domain is impulsive and non-Gaussian as measured by the skew, kurtosis, and cdf estimates, and it is also non-stationary in that the cdf estimates change over time intervals on the order of minutes.

FREQUENCY DOMAIN RESULTS

An important aspect of our study of under ice ambient noise was an evaluation of the statistics in the frequency domain. Usually, the statistics of acoustic noise in the frequency domain are assumed Gaussian. As we shall show, this is not necessarily the case in the arctic. To understand the frequency domain properties of under ice ambient noise we processed the data as a spectrogram (power spectrum vs time). In Fig. 5 we show the results of a spectrogram processed with a 2 Hz resolution. The total time in the figure is about 2.5 minutes. We can see large but dynamic tonals in the data occurring over the time interval. These events sounded like squeaks and appear to be due to ice dynamics. Another different data set, not shown here, of approximately 45 minutes in duration was analyzed by listening to its aural character, while visually observing its spectrogram. Throughout this

data set we observed dynamic tonals with accompanying squeaks occurring randomly over the interval and sometimes observed high level broadband noise which sounded like ice rubbing.

To better appreciate the significance of this data we measured the statistics at the output of a FFT, for each bin, for both its real and imaginary parts. Figure 6 shows a comparison of the power spectral density (PSD) (top curve), real skew (middle curve) and real kurtosis (bottom curve) for the under ice data which has been processed with a 10 Hz resolution and averaged over 1000 consecutive FFT's giving a total time interval of 1.7 minutes. The data clearly indicates non-Gaussian noise over a wide bandwidth based on the frequency domain skew and kurtosis. However, the lower frequencies (i.e., below about 300 Hz) appear to be Gaussian. Under ice ambient noise data at other time periods show low frequency components also deviating from the Gaussian assumption based on the skew and kurtosis.

Over a relatively flat portion of the band as seen in the PSD estimate of Fig. 6 we estimated the amplitude cdf for both real and imaginary parts using the 1000 consecutive FFT's. The total number of bins used over the 1.7 minutes in the estimates were approximately 200,000. The vertical axis in Fig. 7 is plotted as the logarithm of the excedance probability and the horizontal scale represents the amplitude level normalized by the corresponding standard deviation. The dashed curve in the figure is the result of a known Gaussian noise source that has been processed in exactly the same manner as the data. The results clearly show the significant deviation in the data from a Gaussian distribution in the frequency domain. We have also processed other under ice ambient noise data in 6 and 2 Hz resolutions and obtained similar results.

The frequency domain results for the 300-400 Hz band as discussed in the previous section is shown in Fig. 8. Since the sampling rate was 2 kHz the resolution for a 1024 point FFT is 2 Hz. A total of 750 consecutive FFT's were processed giving an overall time interval of 6.25 minutes. We estimated the PSD and the real and imaginary skew and kurtosis over the 750 consecutive FFT's. Only the real part of the skew and kurtosis estimates are shown in Fig. 8. The results as seen in the figure show that many frequency locations deviate from a Gaussian distribution based on the frequency domain skew and kurtosis estimates. In addition a 60 Hz tonal and some of its harmonics are present in the PSD estimate in Fig. 8. The corresponding frequency domain kurtosis estimates show values which are significantly less than 3. A theoretical discussion explaining these results for a signal propagation in a medium with fading or multipath effects is given in Ref. 4. Essentially, we found that for a purely sinusoidal radiated signal with uniformly distributed phase propagated in a medium without fading or multipath effects the frequency domain kurtosis estimate would be 1.5 under high signal-to-noise ratio conditions. The kurtosis value could be greater than 1.5 depending upon the fading environment. For non-sinusoidal radiated signals the frequency domain kurtosis values would increase even more over the values obtained for the sinusoidal case. We have also estimated the amplitude cdf for the real and imaginary parts of this data and obtained similar results to the curves shown in Fig. 7. That is, for a relatively flat portion of the PSD estimate in Fig. 8, the estimated cdf deviated significantly from the Gaussian distribution. The total number of bins used in the estimates for both the real and imaginary parts were 27,000.

Our last figure is concerned with the frequency domain envelope distribution. These and the previous results of the FRAM II data are important for designing optimum frequency domain processing methods. Figure 9 shows a plot of the envelope distribution at the output of a FFT at three frequencies and for three different resolutions. We considered FFT's with 10, 6, and 2 Hz resolution and with time-resolution products (TRP) of 1000, 1000, and 750 respectively. The vertical scale in the figure represents the envelope (normalized by its standard deviation) in dB and the horizontal axis is the excedance probability. In order to better visualize the tail behavior of the envelope distribution we included a small number of adjacent bins in the estimate. These estimates followed approximately the curves shown in Fig. 9. In this way we were able to extend the tail region and observe its trend. The solid line in the figure represents a Rayleigh distribution. As can be seen the data deviates from the Rayleigh distribution for all three cases considered. This suggests the possibility of modeling the envelope distribution of the FRAM II data in the frequency domain.

SUMMARY

We have found that the single channel FRAM II arctic data were highly non-Gaussian in both the time and frequency domains. The time domain statistical results were similar to the results obtained by Milne and Ganton who performed measurements in the Canadian Arctic Archipelago under shore fast ice conditions. New results obtained in this study pertain to the statistics in the frequency domain. We initially processed the under ice data as a spectrogram and then estimated statistical parameters at the output of a FFT. The results of the first four statistical moments and cdf estimates strongly indicate the presence of non-Gaussian noise in the frequency domain.

REFERENCES

1. F. R. DiNapoli, P. N. Mikhalevsky, W. Roderick, S. Jackson, E. Hug, and D. Viccione, "Tristen/FRAM II Cruise Report East Arctic, April 1980," NUSC TD 6457, 13 April 1981.

2. A. R. Milne and J. H. Ganton, "Ambient Noise Under Arctic-Sea Ice," J. Acoust. So. Am. Vol. 36, No. 5, May 1964.

3. R. Dwyer, "FRAM II Single Channel Ambient Noise Statistics," NUSC TD 6583, 25 November 1981.

4. R. Dwyer, "A Statistical Frequency Domain Signal Processing Method," NUSC Reprint Report 6687, 22 March 1982. Also to be published in the Proceedings of the 16-th Annual Conference on Information Sciences and Systems," Princeton University, 17, 18, and 19 March 1982.

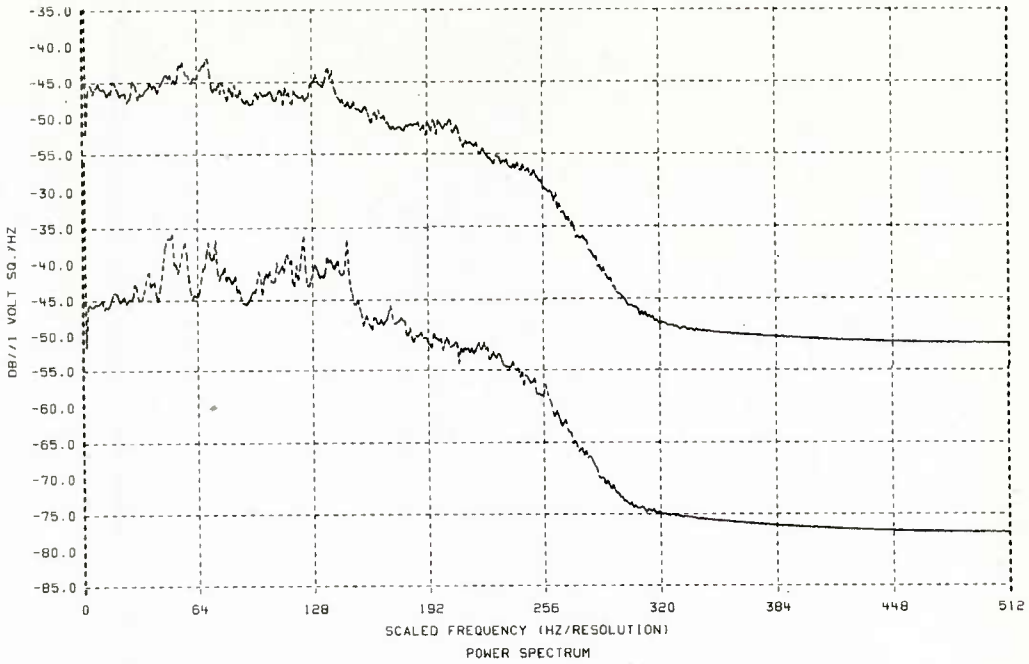

FIG. 1 SPECTRUM OF UNDER ICE NOISE FOR TWO DIFFERENT TIME PERIODS

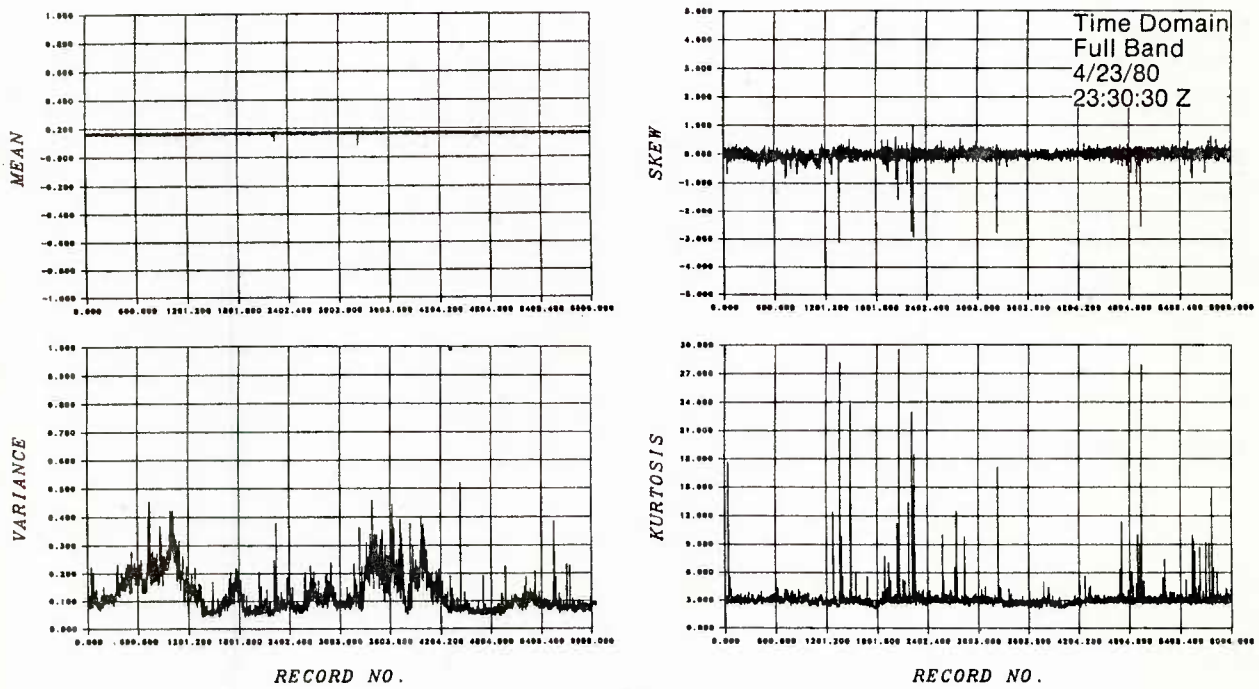

FIG. 2 TIME DOMAIN STATISTICAL MOMENTS FOR 2500 Hz BAND

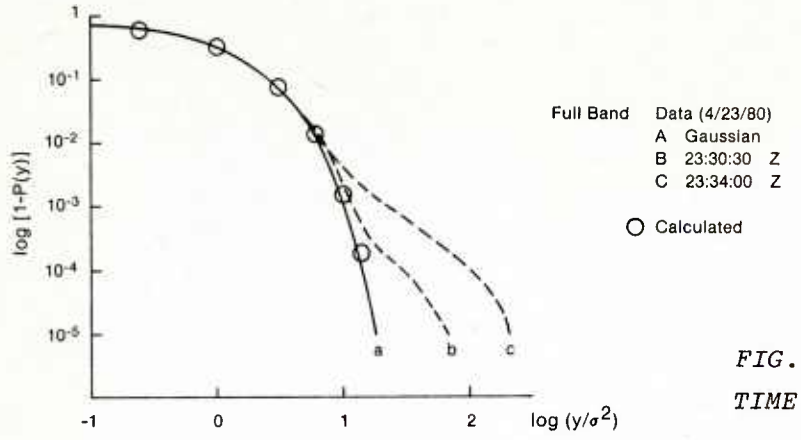

FIG. 3
TIME DOMAIN ENERGY DISTRIBUTION

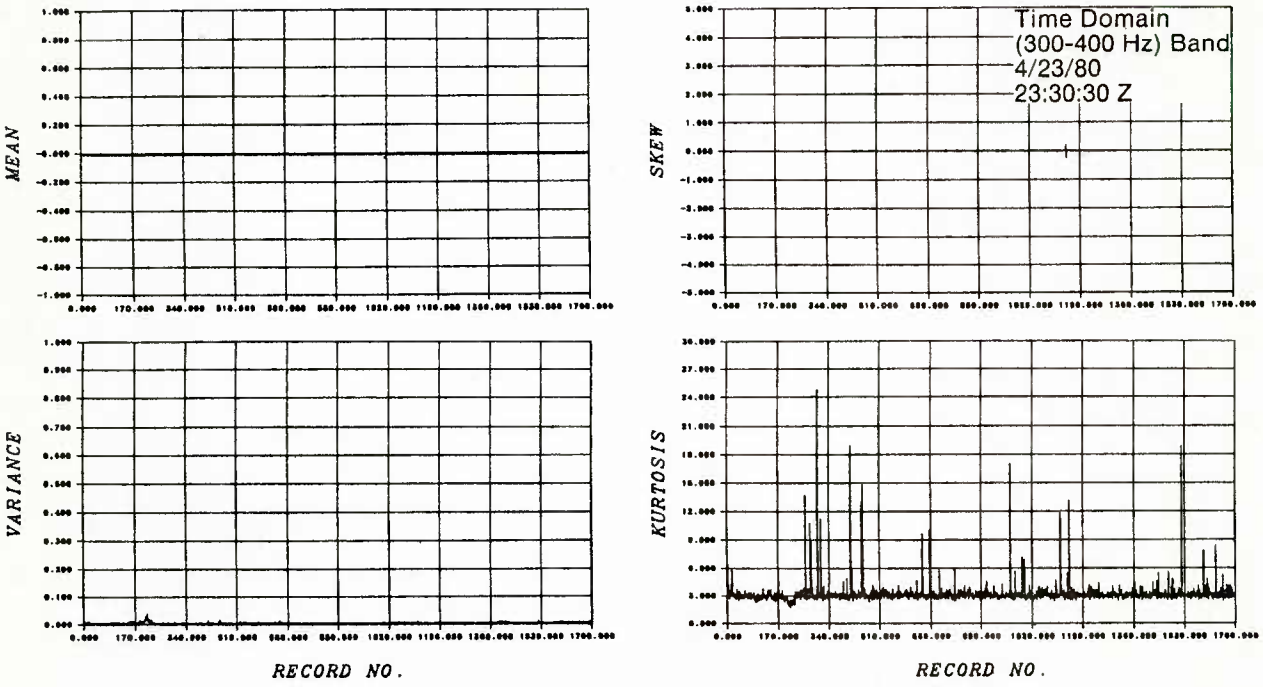

FIG. 4 TIME DOMAIN STATISTICAL MOMENTS FOR 300-400 Hz BAND

FIG. 5
SPECTOGRAM OF 2500 Hz BAND

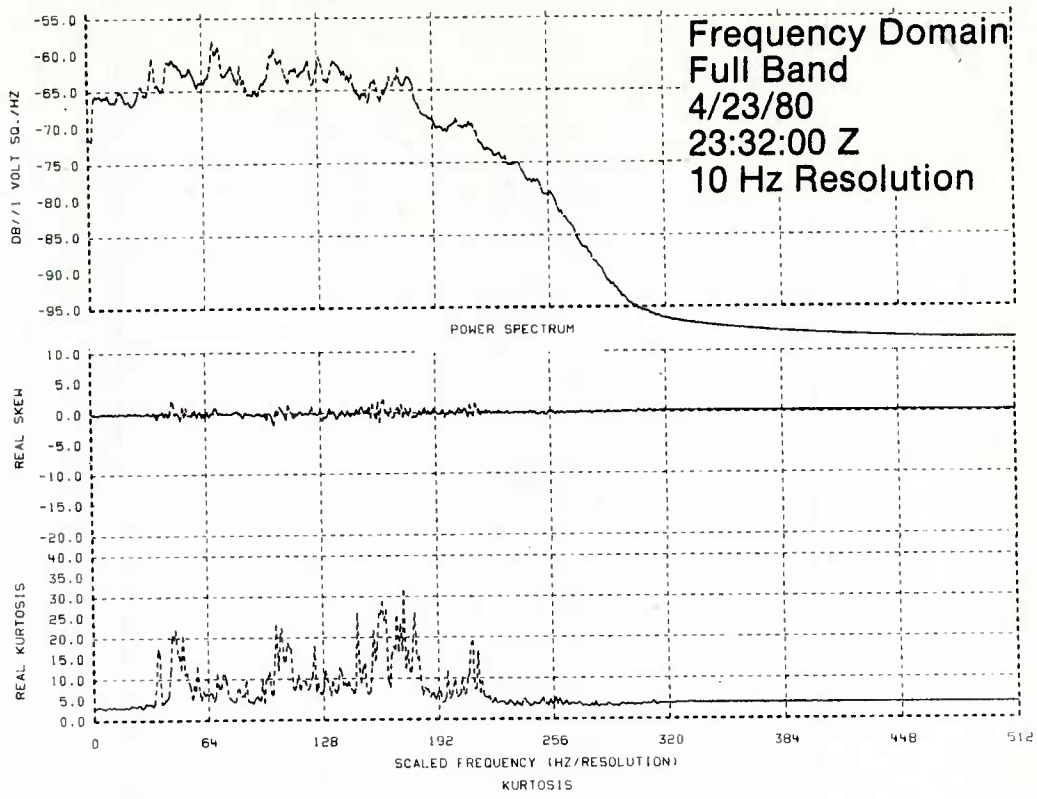

FIG. 6 FREQUENCY DOMAIN STATISTICAL MOMENTS (REAL PART)

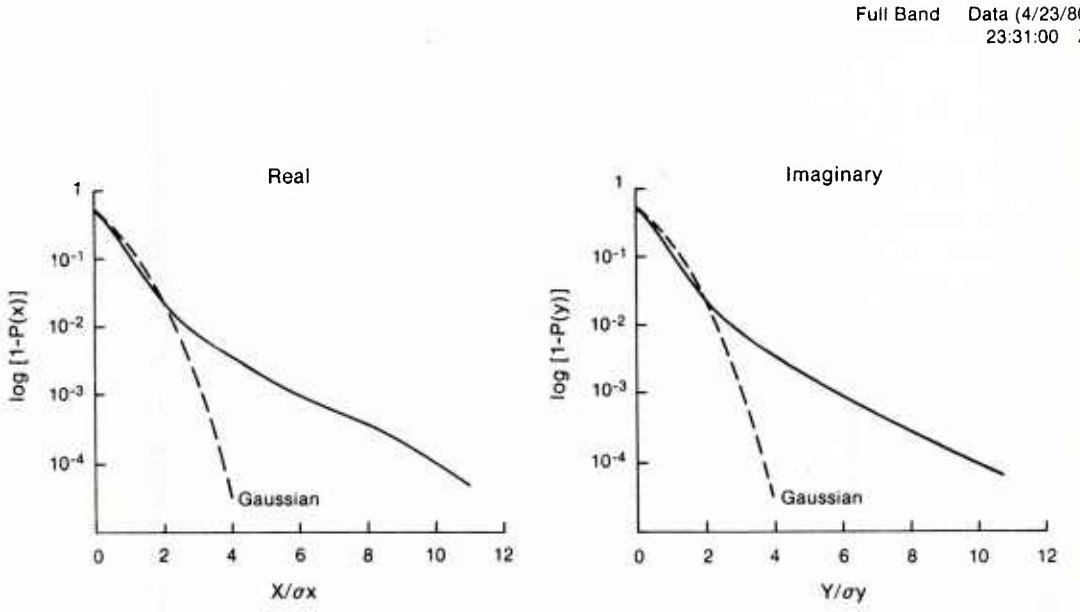

FIG. 7 FREQUENCY DOMAIN AMPLITUDE DISTRIBUTION

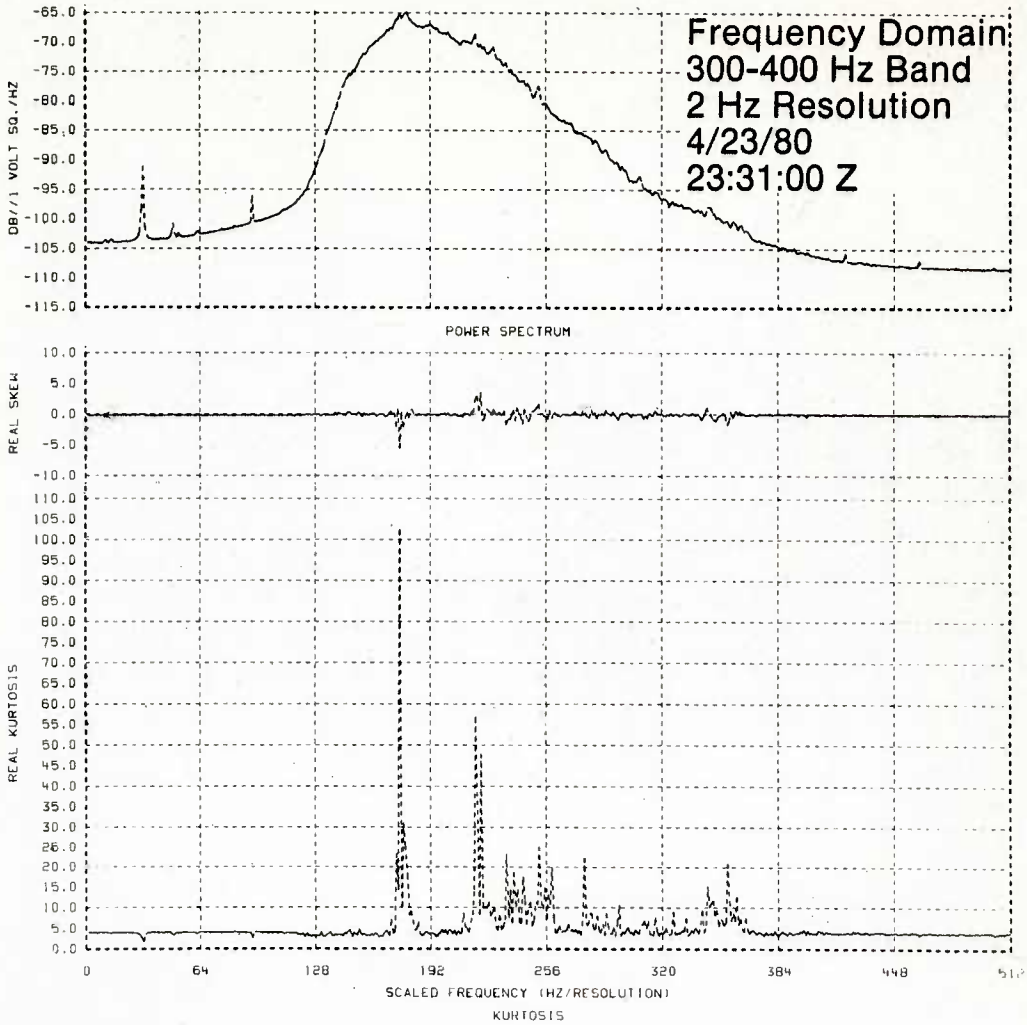

FIG. 8 FREQUENCY DOMAIN STATISTICAL MOMENTS FOR 2 Hz RESOLUTION

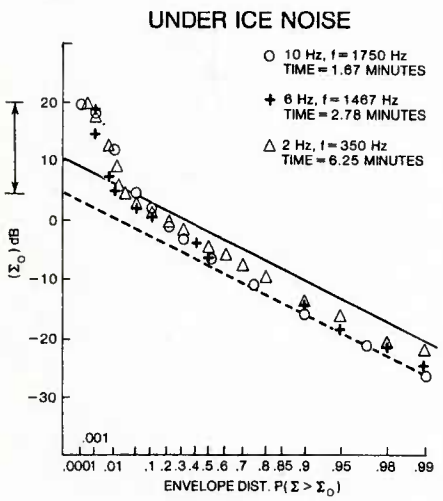

FIG. 9
FREQUENCY DOMAIN ENVELOPE DISTRIBUTION

ACOUSTIC AMBIENT NOISE IN THE BARENTS SEA

by

Øivind Grenness
NDRE
Horten, NORWAY

ABSTRACT

Recorded observations of acoustic ambient noise in the Western Barents Sea are presented. The observations were made in a position approximately 100 km North of North Cape in Norway, with the hydrophone on the bottom - approximately 370 m deep. Noise was recorded broad-band and in 15 successive third-octave frequency bands with center frequencies from 12,5 to 315 Hz. Noise samples of 3 minutes duration were taken approximately every hour, continuously throughout periods up to 18 months. Time series and spectra are presented. At the low frequencies very large variations are observed, and which are better correlated with the wind than the high frequencies are. Also, very low levels have been observed at the lowest frequencies, which may be of considerable military significance. The observations and auxiliary data have allowed wind-dependent spectra of ambient noise to be established down to 12,5 Hz.

INTRODUCTION

The observations were made in two periods between September 1969 and April 1982, the first one of 18 months duration and the second of 5. The observations were made on essentially a continuous basis, every hour, 24 hours per day. The continuity of observation was at times interrupted - as a consequence of power failures to the shore installation, or when the shore installation was operated for other purposes than these measurements. The effect of short interruptions, typically of 2 to 4 hours duration, is disregarded in the analysis.

The only interruption of consideration, and which is evident in the time series, is the period between 12. December 1968 and 4. February 1969.

The second observation period refer to a slightly different position, but at the same depth and in the same general area. These observations were recorded on board the research vessel H U SVERDRUP, moored approximately 2500 m away from a radio-telemetry buoy.

The results are presented in two basic forms, frequency spectra and time series. The frequency spectra appear to have a simple basic shape, whereas the time-series are of a more complicated structure.

The data are presented as Spectrum Levels - re. 1 $\mu pa/\sqrt{Hz}$, using the statistical median value. In addition, the Quartile Spreading in the cumulative distribution is presented. The statistics is based on time intervals of one month, allowing analysis of seasonal changes.

SOURCES

It is believed that the observations are dominated by a varying contribution from the following three sources:

- distant ship traffic and fishing activity,
- wind and surface wave action,
- whales

However, it is known that some of the observations were influenced by local traffic noise and/or local fishing activity to such a degree that the noise could not be considered as the wanted "natural ambient noise".

These observations were not accepted for the analysis discussed here, but were discarded - and their effect upon the statistics have been disregarded. After removal from the analysis of local, known or identifiable source activity - some 600 observations remained for each monthly interval.

OBSERVATIONS

The 18 month long series of median monthly spectra is shown in Fig. 1, with each successive month staggered vertically. Traffic noise appear to be the dominating effect, with spectrum levels peaking around 80 dB in the frequency region between 50 and 100 Hz. With few exceptions it is observed that the levels are quite similar from one year to the next for those months where two years are represented. When they differ, they do so in consistence with wind observations from Fruholmen lighthouse - the nearest weather observation station along the norwegian coast.

The low frequency peak centered at 20 and 25 Hz is believed to have its origin in the activity of a bio-acoustic sound source, probably whales. This "whale effect" is observed only during the winter months, peaking in February and March.

Fig. 2 is a time series for 4 selected frequencies: the lowest of 12,5 Hz, the highest one - 315 Hz, then 100 Hz representing the central and traffic-noise dominated region, and 25 Hz typical of the "whale effect". From Fig. 2, and better even - from Fig. 6 and 7, the seasonal trends can be observed. The effect is obvious at 25 Hz, as a consequence of the whale effect. It is evident but not quite consistent at the highest frequency. At the lowest frequency the seasonal effect is quite pronounced, whereas at the central frequency of 100 Hz it is hardly observable.

Fig 3 illustrates details of the whale sounds. The sounds are frequency modulated, of 20 - 25 seconds duration - starting at approximately 27 Hz and tapering off near 20 Hz. The sounds repeat at a fixed pulse rate - some pulses may be absent a few times and reappear "almost perfectly on time". Detailed analysis of the pulse envelope has shown that it remains constant in shape for a considerable period of time. This pulse envelope may perhaps serve as an "acoustical fingerprint" - identifying an individual whale.

No systematic whale observations have been made in this region at the same time as the whale sounds were recorded, but is is known that the "Vaage whale" - also called "Minke" migrate near this area during the winter months, on their way between the Eastern Barents Sea and the East coast of the Unites States.

Fig 5. is an example of the statistical distribution for a selected frequency. A typical summer month - September, and a winter month - January shows an approximately Gaussian distribution in summer and a bimodal distribution in winter.

SMOOTHED VALUES

With the purpose to obtain a better resolution of the variations of the values it became of interest to establish a reference spectrum - and subtract this from the actually observed noise levels, referring noise levels and spectra to this "Minimum Reference Spectrum" (MRS)

The MRS is for this purpose defined as the spectrum of the lowest observation ever made for the various frequencies. It is not an actually observed spectrum since the levels used were not necessarily observed simultaneously. It does however serve the useful dual purpose as:

- The lower limit of the expected values under the most favourable conditions,

- A means of removing from the actually observed spectra, the inherent spectrum - a normalizing process. This will increase the contrast of other variations.

Incidentially, most of these minimum values were observed during the very quiet month of September 1969.

Fig. 6 is a contour representation of the monthly median spectrum levels and their time series. The values are now referred to the MRS defined above. The levels have been smoothed in order to suppress any remaining fine structure and emphasize the dominating spectral trends and time variations. Similarly - Fig. 7 is a smoothed contour representation of the monthly Quartile Spreadings and their time series.

Levels at the lowest and at the highest frequencies show similar patterns in time, correlated with the pattern for the spreading at the lowest frequencies and the pattern for the wind force observed at Fruholmen.

The contrast of the whale sounds is quite pronounced, building up gradually from October/November - peaking in February/March and falling off rapidly during the month of April. It should be noticed that the quartile spreading does not reflect any "whale effect".

On the basis of the noise levels at the high and the low frequencies, their variation and correlation with the wind force levels, it appears reasonable to divide the year into two seasons: a summer season from May through September, a winter season from November through March - with April and October as transition months. It is observed that whereas April of 1969 was a very "noisy" month - and windy, April of 1970 was extremely quiet.

Fig. 8 gives curves, averaged over all months in each season, showing the difference between summer and winter.

THE NOISE - WIND RELATIONSHIP

Since long-term simultaneous wind observations from the hydrophone position were not available, the noise-wind relationship had to be established by another, indirect method. The noise levels at different frequencies were cross-correlated through known - or suspected periods of variable winds at the hydrophone position. Such periods, as observed from wind data from Fruholmen lighthouse, were chosen when the noise observations showed a smooth and systematic variation over the entire frequency range.

This method permit a family of ambient noise spectra to be established for different wind force levels - during such periods of varying winds. This correlation is however too weak to be useful in the central frequency region between 50 and 150 Hz, where the traffic sources dominate.

On a few occations simultaneous observations were available when the research vessel was moored close to the hydrophone position. With these auxiliary measurements, unfortunately only during relatively brief periods, it becomes possible to label the observed noise levels with the corresponding wind force. Fig. 9 shows the relationship established in this way.

CONCLUSIONS

1. It appears reasonable to simplify the time variations observed to two seasons, with the months of April and October as transition periods.

2. The summer season is characterized by very low ambient noise levels, especially at the lower frequencies - and by less variation than in the winter season.

3. The winter season, especially in February and March, is characterized by intense "whale effects".

4. The spectra peak between 50 Hz and 100 Hz, ship traffic is believed to be the major source - masking all wind effects except the extreme ones. The variation has a minimum between 120 Hz and 200 Hz, with a Quartile Spreading between 3 and 4 dB, regardless of season.

5. Noise levels are related to the wind, at the high frequency end in reasonable agreement with the Knudsen/Wenz curves. The response to wind effects appear considerably stronger at the low frequencies than at the high ones.

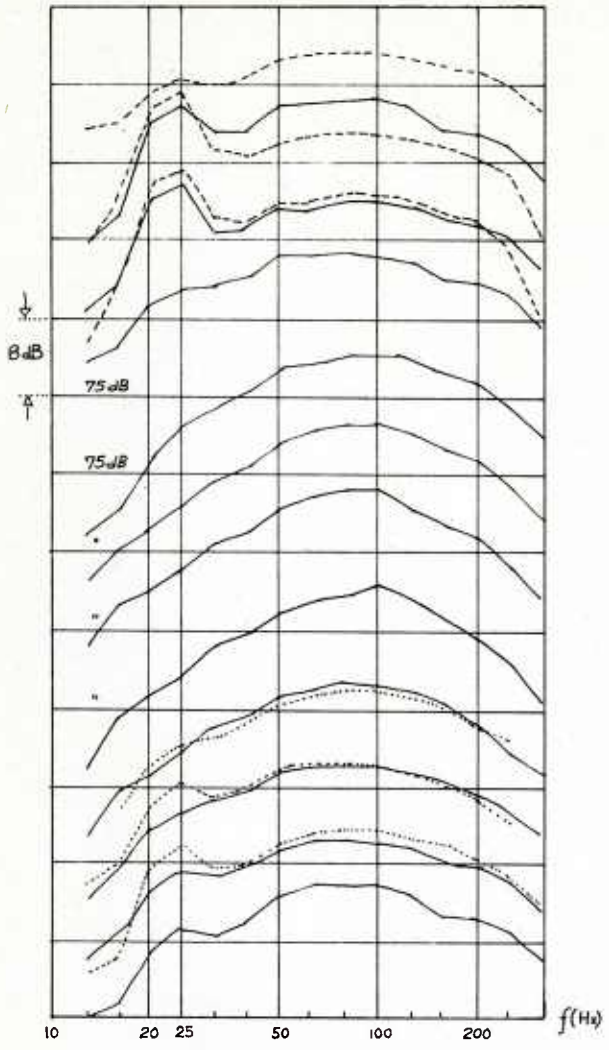
8 dB
7.5 dB
7.5 dB
10
20
25
50
100
200
f(Hz)

FIG. 1

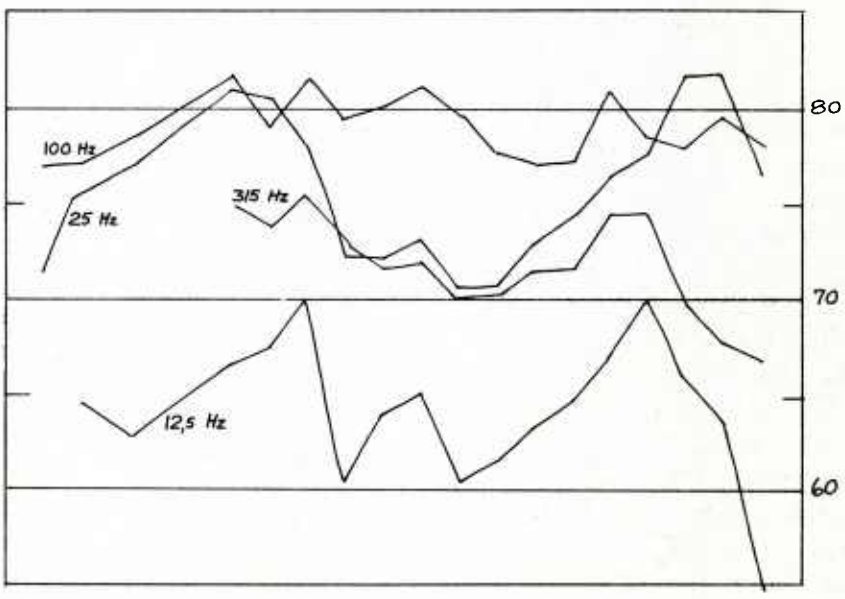
100 Hz
25 Hz
3.15 Hz
12,5 Hz
80
70
60

FIG. 2

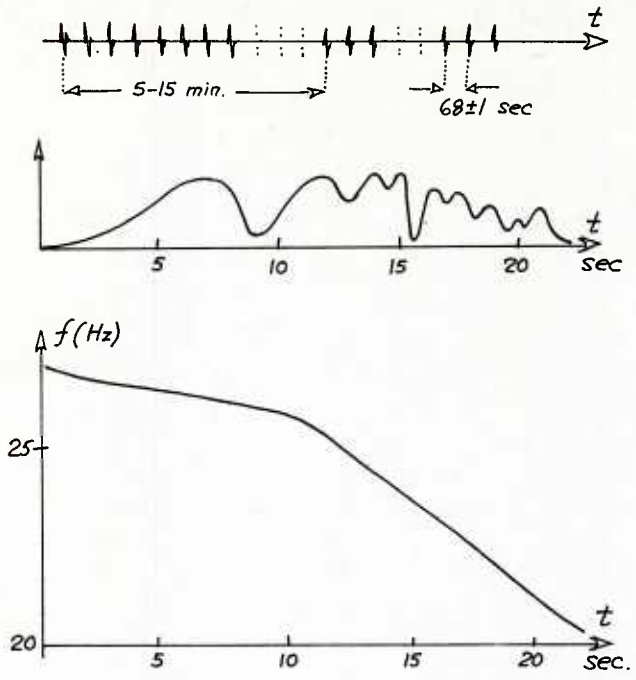
t
5-15 min.
68±1 sec
t
5
10
15
20
sec
f(Hz)
25
20
t
5
10
15
20
sec.

FIG. 3

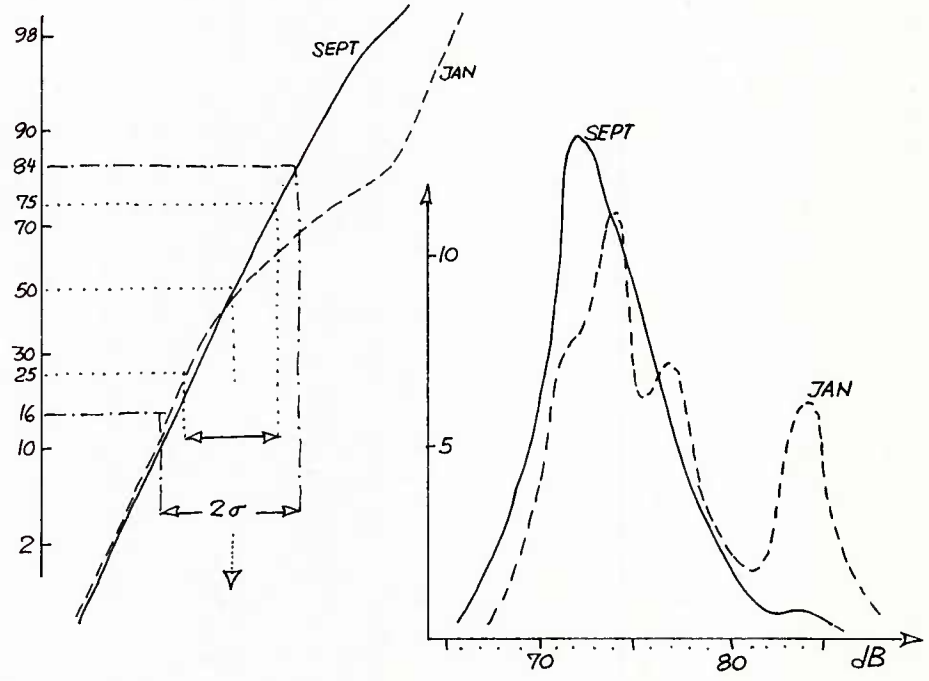
98
90
84
75
70
50
30
25
16
10
2
SEPT
JAN
2σ
SEPT
JAN
10
5
70
80
dB

FIG. 5

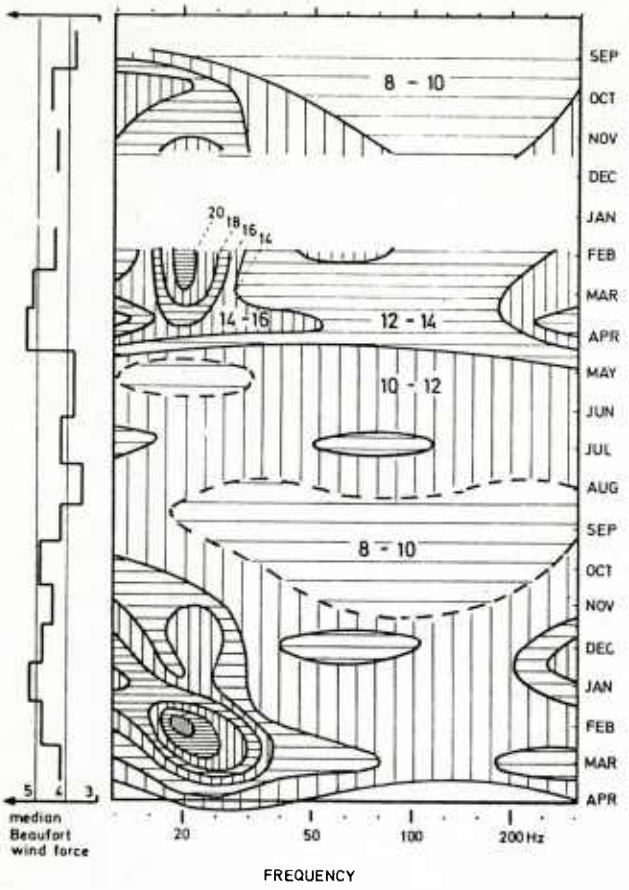

MONTHLY MEDIANS IN
dB ABOVE "MRS"

FIG. 6

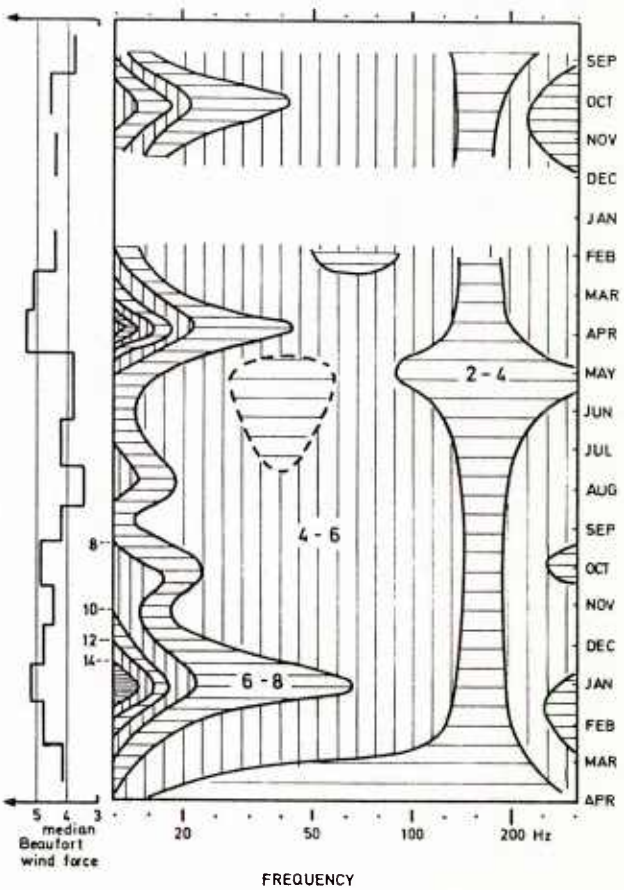

QUARTILE SPREADING
IN dB (75% - 25%)

FIG. 7

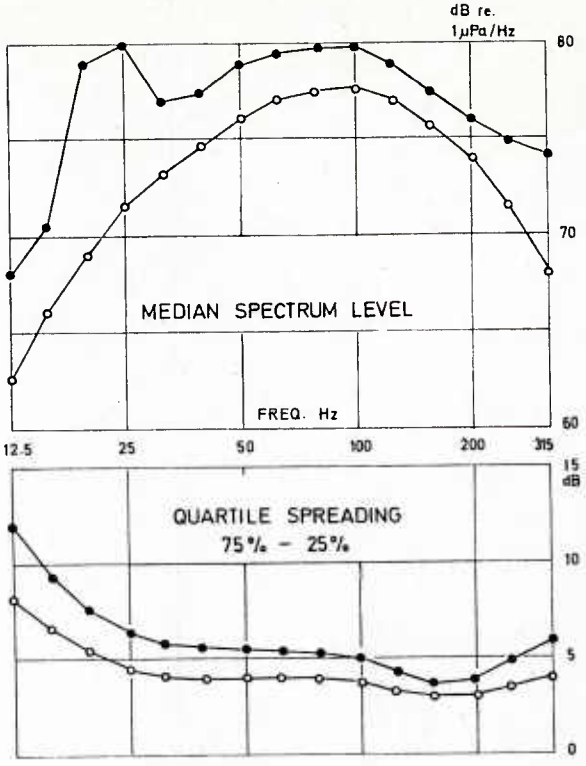
dB re.
1µPa/Hz
80
70
60
MEDIAN SPECTRUM LEVEL
FREQ. Hz
12.5
25
50
100
200
315
15
dB
10
5
0
QUARTILE SPREADING
75% - 25%
BARENTS SEA
DEPTH 350 m
SEPT. 1968 - APRIL 1970
WINTER : NOV. - MARCH
SUMMER: MAY - SEPT

FIG. 8

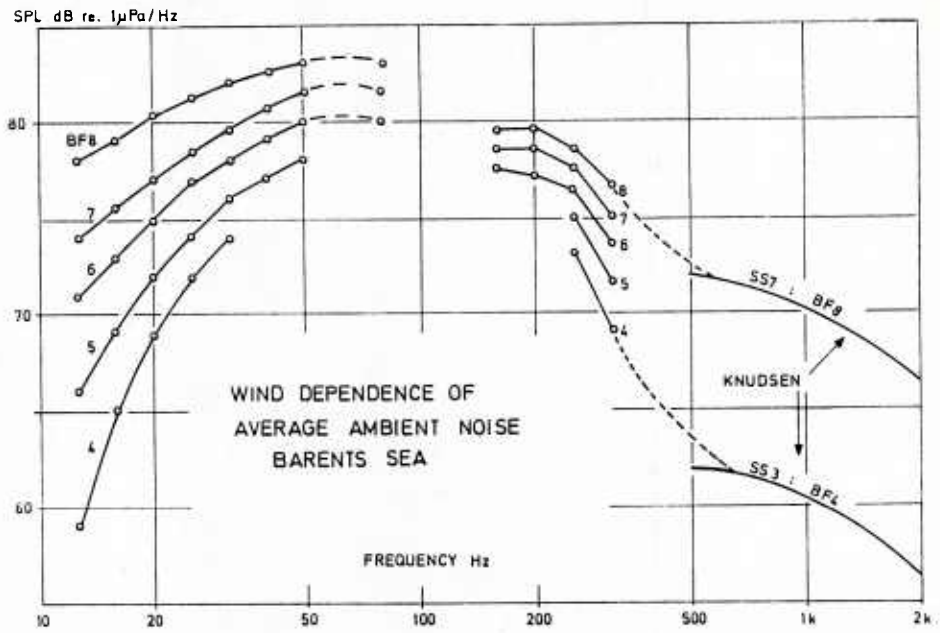
SPL dB re. 1µPa/Hz
80
70
60
BF8
7
6
5
4
8
7
6
5
4
SS7 : BF8
KNUDSEN
SS3 : BF4
WIND DEPENDENCE OF
AVERAGE AMBIENT NOISE
BARENTS SEA
FREQUENCY Hz
10
20
50
100
200
500
1k
2k

FIG. 9

DEPTH DEPENDENCE OF DIRECTIONALITY OF AMBIENT NOISE IN THE NORTH PACIFIC: EXPERIMENTAL DATA AND EQUIPMENT DESIGN

by

Robert C. Tyce
Marine Physical Laboratory
of the Scripps Institution of Oceanography
University of California
San Diego, California 92152

ABSTRACT

Ambient ocean noise studies have been part of the research program of the Marine Physical Lab (MPL) for many years. In recent years this work has included several studies of the depth dependence of vertical directionality of low frequency ambient noise utilizing the research platform FLIP, as well as development of a capability for measurement of depth dependence of the horizontal directionality of ambient noise. A long vertical array of hydrophones has been used from FLIP to measure the vertical directionality of ambient noise in the frequency range from 10 to 400 Hz, and in water depths of more than 4300 meters. The array was positioned at several depths within the water column, ranging from near the surface to near the bottom, at a site approximately 350 miles west of San Diego. For frequencies below about 150 Hz, the noise is concentrated in a near horizontal direction. In the upper part of the water column the measured -3dB points for the noise occur around 13 deg. from horizontal, with noise levels more than 30dB lower outside this angular sector. The width of this angular sector tends to decrease with increasing depth, down to about plus or minus 4 degrees from horizontal near the bottom. Between 150 and 300 Hz a transition occurs from most of the noise arriving from near horizontal directions, to more of the noise arriving from near vertical directions, with several more dB arriving from above than below. A capability for measuring depth dependence of horizontal directionality of noise has also been in development at MPL. Using a long horizontal array attached to FLIP at one end and a buoyant anchor line crawler at the other, depth dependent measurements are possible. The present test array will employ 20 Motorola 68000 microprocessor controlled telemetry units to aid in preprocessing the inputs from 200 hydrophones in a 1500 meter long array, including sub-array beamforming and correction for array deformation.

INTRODUCTION

Research on the depth and directional dependences of ambient noise has been part of the work at the Marine Physical Laboratory for many years (Morris, 1978, Anderson, 1979). During May of 1978 and April of 1979, ambient noise experiments were conducted by MPL, with the aim of measuring the depth dependence of the vertical directionality of low frequency ambient noise. The first experiment concentrated on the frequency range from 10 to 50Hz and the second from 50 to 300Hz.

These experiments involved the use of a modular vertical array deployed in two different configurations from Flip while moored in 4300m of water. The location for these experiments was a deep water site approximately 350 nautical miles west of San Diego, clear of obstructing bottom topography.

The data from these experiments have been analysed with the objective of determining the depth dependence of the directionality of low frequency ambient noise in this deep water, depth excess environment. Some of the results from these analyses are presented in this paper, with more detailed statistical analyses of the data continuing.

The equipment involved in these experiments was developed under the Long Range Acoustic Propagation Program. It has been in use by MPL for many years as has FLIP, the stable support platform for this array. Addition ambient noise related equipment has also been developed at MPL in recent years, as illustrated in figure 1. This includes a light weight modular hydrophone array for horizontal and vertical work, a remotely controlled line crawler for array depth control, and a long horizontal array which is still under development.

VERTICAL NOISE MEASUREMENTS

Vertical Array Instrumentation

The hydrophone array for our vertical directionality work consists of 20 hydrophone/telemetry assemblies connected by pre-cut lengths of 1 cm diameter double armored coaxial cable. The assemblies consist of ceramic cylinders suspended inside metal cages, along with the telemetry packages. The telemetry for this array consists of 20 FM frequency division multiplexed channels spaced between 50 and 620 kHz, supporting a signal bandwidth from 5 to 2000 Hz. The FM signals are transmitted over the suspending armored coaxial cable deployed from the winch aboard FLIP.

Shipboard the FM telemetry signals are demodulated and supplied to an analog to digital converter for logging on 9 track digital magnetic tape.

This vertical array was developed for use from FLIP, the stable research platform developed by MPL in 1962. For these noise experiments, FLIP was put in a three point mooring, using 5500 m of synthetic mooring line and 44,000 kg of anchor per leg. In such a configuration the platform noise and motion is generally insignificant.

Experiments

Utilizing the modular vertical array from FLIP, deep water noise directionality measurements were made during May, 1978 and April 1979. During 1978, under the direction of Dr. Gerald Morris, the array was assembled with 28 m spacing between hydrophones, and data collected for 5 to 50 Hz, with 200 Hz sampling. The array was positioned at 5 different depths spanning the water column.

During April, 1979, the array was assembled with 5 m and 2.5 m spacing between hydrophones and data collected for 50 to 400 Hz, with 1 kHz sampling. The array was positioned with its center at the same 5 depths as in the prior experiment. These deployments are illustrated on the sound velocity profiles of figure 2, and the deployment histories of figures 3 and 4. During both experiments XBT's were taken, wind speed was recorded, and local ship traffic monitored by means of radar.

During the lower frequency experiment the wind varied between 5 and 30 knots, with little apparent effect on these 5 to 50 Hz data. During the second experiment the local wind was relatively constant over the 5 day measurment period, holding between 20 and 28 knots, with local surface generated noise a likely source of significant noise in this 50 to 400 Hz experiment.

Data Processing

Data from these cruises have been processed in a variety of ways. Since the individual hydrophone data were digitized and preserved on tape, many options are possible. In general an array processor and fast Fourier transform (FFT) methods were utilized to analyze the data. Individual hydrophone data have been plotted for selected frequencies to monitor data quality and interference from local ship traffic. A typical single hydrophone noise spectrum from the 10 to 50 Hz data is illustrated in figure 5. Here the spectrum below 10 Hz is thought to represent experimental flow and strumming noise rather than ambient noise. These data represent the average of 32, 512 point FFT's,

representing approximately 1 1/2 minutes of data.

To determine vertical noise directionality, FFT frequency domain beamforming techniques (Williams, 1968) were utilized to produce plots of directionality versus frequency, of directionality versus time for selected frequencies, and of intensity versus time for selected beams. Figure 6 illustrates a calibration plot for the beam forming. Here white noise was introduced at the FM demodulator outputs to the computer analog converter. This white noise was beam formed through double FFT's, with Hamming weighting applied to the hydrophone data before beamforming to suppress side lobes. Note that the side lobes are in fact down 30 dB or more for this synthetic noise data. The 22 Hz anomaly is thought to represent power line harmonic noise.

Sample Results

Samples of vertical noise directionality measurements between 10 and 50 Hz are presented in figures 7 through 11 for the five depths. These data represent 32 accumulations of 512 point FFT's in time, involving about 1 1/2 minutes of data.

Figure 6 represents near surface data, where the low frequency noise here is thought to be FLIP machinery noise. Figure 7 represent sound channel depth data, with the noise concentrated within 13 deg from horizontal. In these figures "0" is horizontal, plus 90 is up and minus 90 is down.

Subsequent figures represent midwater, critical, and near bottom depths, with the width of the horizontal noise lobe steadily decreasing to within 4 deg from horizontal.

This same sort of vertical noise directionality is observed in the higher frequency measurements, with the gradual addition of more localized surface noise as illustrated by figures 12 through 14 (here the angular resolution is reduced due to the shorter array length). At 150 Hz the noise from elevated angles is notably greater than that observed from depressed angles, and is comparable to horizontal noise levels above 200 Hz, with little depth dependence (fig. 14). Of course the wind speed was consistantly 20 to 28 knots during these higher frequency measurements, presumably lowering the frequency where wind generated surface noise sources dominate over distant shipping noise.

The data presented above represent selected samples of a large data set. The examples shown are relatively typical of times when there were no ships within the 25 mile range of FLIP's radar. Figure 15 shows 40 Hz directionality data for a 20 minute period, illustrating the kind of variability typically observed in this pattern. Here the array was at the sound channel axis. Figure 16 shows an earlier 20

minute sample where the directionality pattern is clearly altered by the presence of local ship traffic.

Plots of noise power for selected beams during the times of the previous two figures are shown in figures 17 and 18. For the distant ship pattern the variability observed is similar for all the selected beams (fig. 17). With local ship traffic, the higher angle beams show notably more variability, as one might expect (fig. 18).

The sample vertical directionality results presented above represent work preliminary to more detailed statistical analyses of these data sets. This is clearly necessary in order obtain a more generalized interpretation of these data, particularly regarding the stability, stationarity, and variability of vertical directionality. While these data are voluminous, they do represent only a fews days of data from a single location in the northeast Pacific ocean, concerning phenomena which clearly should be variable and even cyclical over much longer time scales. Only long term measurements of directionality statistics, with considerable data compression, can provide a complete description of ambient noise directionality.

NEW EQUIPMENT DEVELOPMENT

Lightweight Modular Array

As part of ambient noise and related research work a number of newer capabilities have been developed at MPL. One of these is a lightweight modular array based on the FM frequency division multiplex telemetry of our vertical array This array was designed to utilize existing FM demodulators, and to be capable of deployment in vertical or horizontal orientations.

During vertical deployments of our older array, measurements have shown very little displacement from a straight line. But for horizontal deployments this is generally not expected to be the case. As a result array deformation measurments are required for horizontal array work, and the newer array incorporates circuitry for doing array navigation. This involves a transponder reply receiver in each telemetry channel, which permits the use of our normal 12 kHz acoustic transponders for array localization.

In its initial application in 1981, this array was configured as a horizontal, near bottom array 500 m long with 20 channels. The array consisted of telemetry packages and coaxial cabling inside a loose net of synthetic Kevlar fibre strength member. The netted Kevlar technique is one developed by R. Swenson at NORDA (Swenson et al., 1979), and has the advantage of modular installation of components and

light weight both in air and in water. This particular fibre net was about 3 cm in diameter when stretched, with a fuzzy fairing to reduce strumming.

Residual Noise Program

Another substantial ambient noise measurement program has been ongoing at MPL for the past few years. This program has the aim of measuring horizontal directionality of ambient noise with enough resolution to observe the predicted occasional holes in the ship noise pattern. The objective here is not simply to observe the characteristics of ship related noise at high resolution, but to measure the residual ambient noise field in the absence of ships.

The nature of this residue is difficult to predict with certainty, but is probably a mixture of a number of sources. Potential sources include local sea surface noise, distant storm noise, secondary ship noise echoes from bottom topography, ocean boundary noises such a breaking waves, and even geological noise sources. Regardless of source, it is this residual noise field that will eventually limit the performance of truly high relolution sonar systems operating at low frequencies.

Such an effort requires a very quiet support ship and a long, well filled array. Here the objective is to have an array with 1 deg or better resolution at frequencies below 200 Hz, with extremely good side lobe rejection. In addition a variable depth capability is desirable to permit studies of depth dependence. Since a long array is hard to keep straight, a system for measuring array deformation and correcting its effects is necessary.

The approach to this problem is illustrated in figure 1. Utilizing FLIP in a mooring as a very quiet support ship, a long horizontal array can be deployed and controlled in depth with the aid of a remotely controlled line crawler.

Line Crawler Depth Control

Such a remotely controlled line crawler was built at MPL and is shown in figure 19. This device was designed to operate over a long coaxial cable, crawling down a synthetic anchor line under remote control. This device was utilized to deploy a short test array from FLIP over 4,300 m of 1 cm diameter armored coaxial cable. This particular device was designed to support up to 11,000 kg of buoyancy. A smaller version of this device with separate flotation is anticipated for future work. Here the aim is to straighten an array through application of up to 4500 kg of tension.

Array Design

For operating frequencies between approximately 50 and 200 Hz a test array of 200 hydrophones spanning 1500 m was deemed appropriate. The initial concept was to connect groups of hydrophones together into sub groups, restricting operation to near broadside as in the oil industry, in order to reduce data acquisition requirements.

Figure 20 shows the beam pattern analysis for an array composed of 39 overlapping sub arrays of 10 hydrophones, where the 10 hydrophones are added without weighting and the sub arrays are added with hamming weighting. When this array is steered 3 deg off axis the side lobes show a considerable increase, as shown in figure 21. Greater steering angles produce greater side lobes. Array deformation, inevitable in a long array due to currents and buoyancy, will also result in unacceptable beam pattern side lobes for such a beam forming approach.

Steering and amplitude shading of sub arrays can result in reduced side lobes and corrections for array deformations. Figure 22 shows beam pattern analysis for an array of 39 overlapped sub arrays where both the main and sub arrays are weighted and steered to an angle of 10 deg from broadside. Clearly side lobes are not a problem with such an approach.

To impliment such an approach, a microprocessor based digital telemtry package has been under development at MPL. Utilizing Motorola 68000 processors for their multiply/divide speed, these units are intended to process the analog inputs from 10 hydrophones into a time shared digital data stream. The processors are expected to provide amplitude shading and steering corrections as directed from the surface via a low speed data link. They are also expected to process reception of 12 kHz acoustic navigation transponder replies to permit array deformation measurements.

Development and testing of these new telemetry units is expected to be completed during the current year. They will then be integrated into a 1500 m long, 200 hydrophone test array for use in ambient noise studies from FLIP. This array will utilize 3 cm diameter oil filled hose sections 75 m long to house hydrophones and preamplifiers and to provide buoyancy. Telemetry packages and hose assemblies will be contained within faired braided Kevlar netting with a break strength of 44,000 kg.

REFERENCES

Anderson, V. C.,"Variation of the Vertical Directionality of

Noise with Depth in the North Pacific",Jour. Acoust. Soc. Am.65(6), June 1979

Morris, G.B.,"Depth dependence of ambient noise in the northeastern Pacific Ocean",Jour.Acoust.Soc.Am 64(2), Aug. 1978

Swenson, R.C., Gholson, N. H., and Rumpf, R. R., "VEKA/FLIP Variable Depth Horizontal/Vertical Array", Marine Tech. Soc. Jour. 14(1) Feb. 1980

Williams, J. R., "Fast Beam-Forming Algorithm", Jour. Acoust. Soc. Am. 44(5), 1968

ACKNOWLEDGMENTS

The results presented here represent the work of a large number of people at the Marine Physical Laboratory. Much of the vertical array work represents the efforts of Dr. G. B. Morris before his relocation to NORDA. The Captains and crews of the research platform FLIP and support tugs deserve special mention for their assistance. The support for this work was provided by the Office Of Naval Research and the Naval Ocean Research and Development Activity.

AMBIENT NOISE EXPERIMENTS

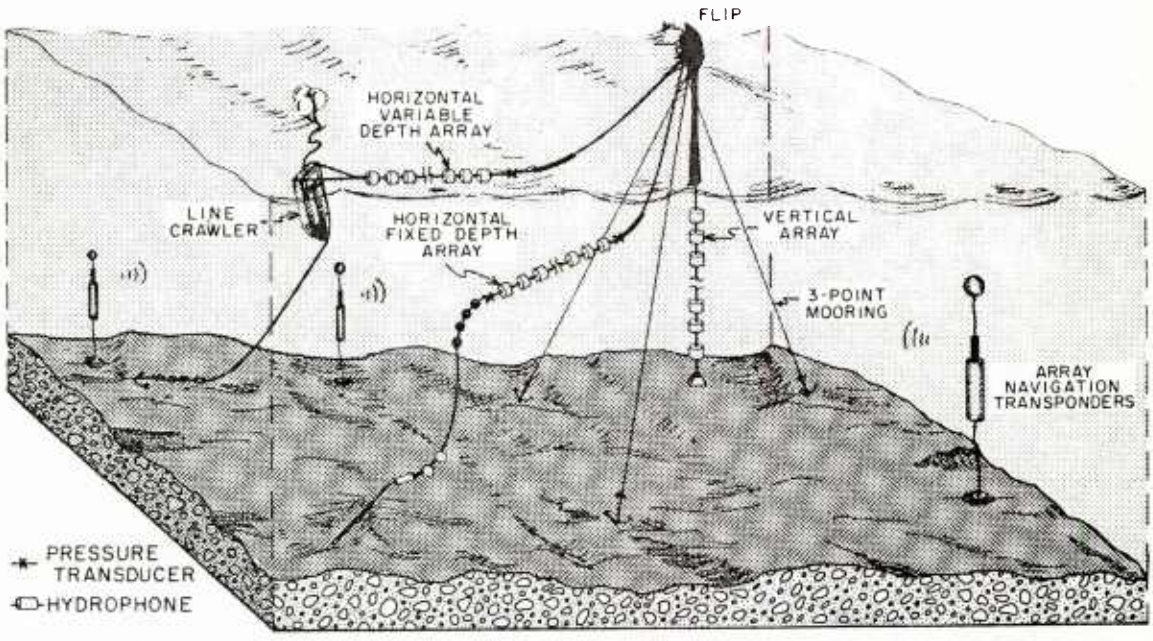

FIG. 1

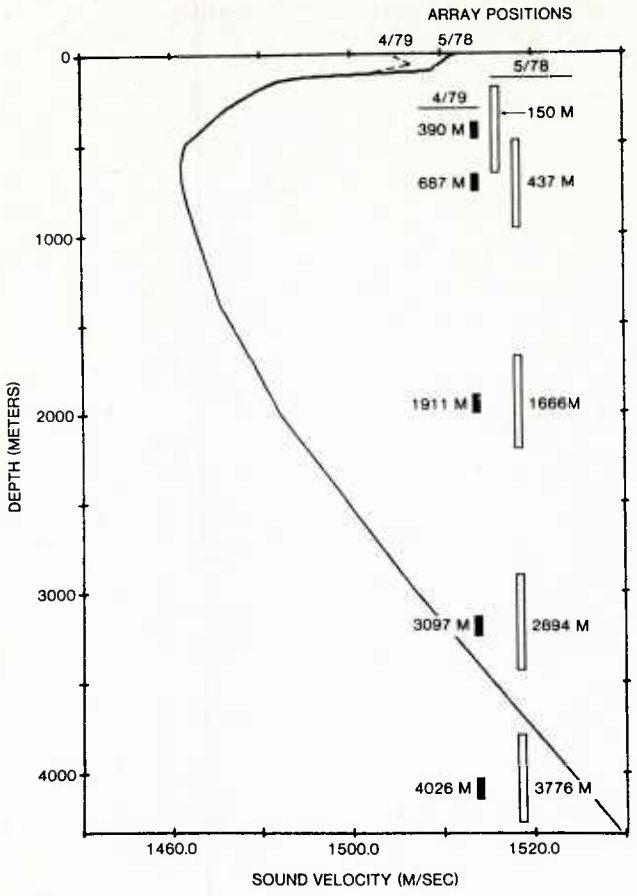
ARRAY POSITIONS
4/79
5/78
5/78
4/79
150 M
390 M
687 M
437 M
1911 M
1666M
3097 M
2894 M
4026 M
3776 M
DEPTH (METERS)
0
1000
2000
3000
4000
1460.0
1500.0
1520.0
SOUND VELOCITY (M/SEC)

FIG. 2

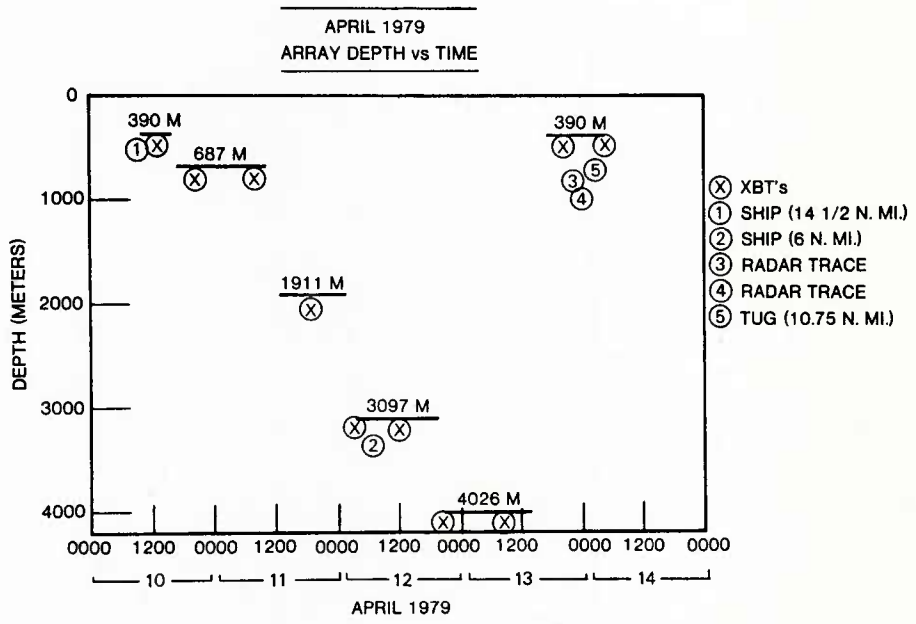
APRIL 1979
ARRAY DEPTH vs TIME
390 M
687 M
1911 M
3097 M
4026 M
390 M
DEPTH (METERS)
0
1000
2000
3000
4000
0000 1200 0000 1200 0000 1200 0000 1200 0000 1200 0000
10
11
12
13
14
APRIL 1979
XBT's
SHIP (14 1/2 N. MI.)
SHIP (6 N. MI.)
RADAR TRACE
RADAR TRACE
TUG (10.75 N. MI.)

FIG. 3

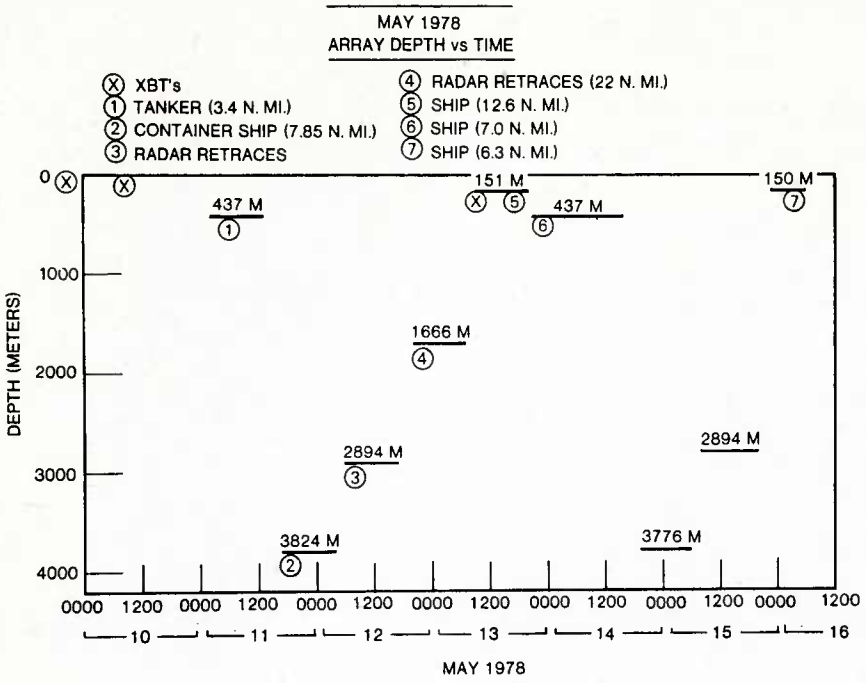
MAY 1978
ARRAY DEPTH vs TIME
X XBT's
1 TANKER (3.4 N. MI.)
2 CONTAINER SHIP (7.85 N. MI.)
3 RADAR RETRACES
4 RADAR RETRACES (22 N. MI.)
5 SHIP (12.6 N. MI.)
6 SHIP (7.0 N. MI.)
7 SHIP (6.3 N. MI.)
DEPTH (METERS)
0
1000
2000
3000
4000
437 M
151 M
437 M
150 M
1666 M
2894 M
2894 M
3824 M
3776 M
0000 1200 0000 1200 0000 1200 0000 1200 0000 1200 0000 1200 0000 1200
10 11 12 13 14 15 16
MAY 1978

FIG. 4

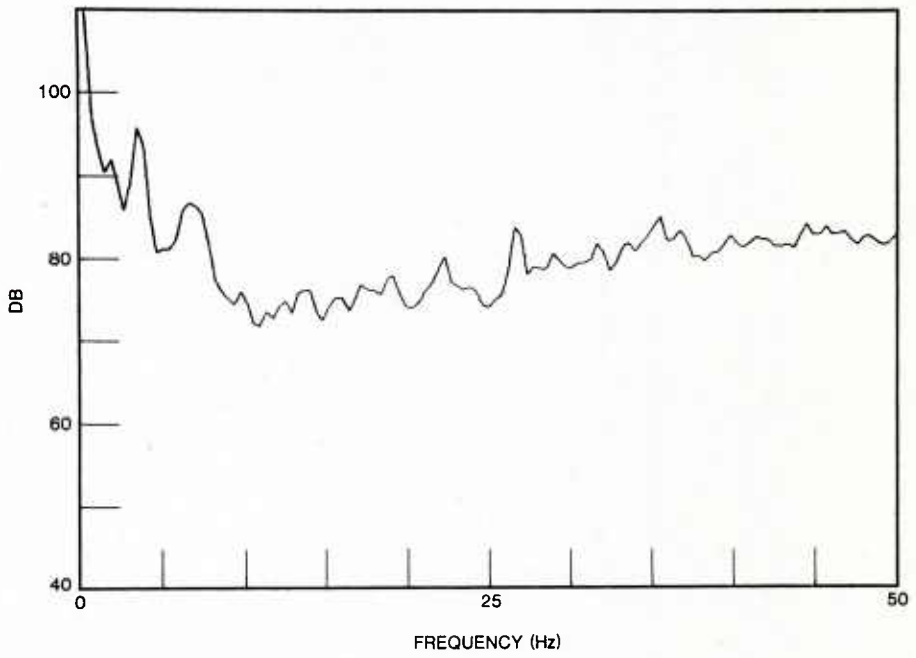
100
80
60
40
DB
0
25
50
FREQUENCY (Hz)

FIG. 5

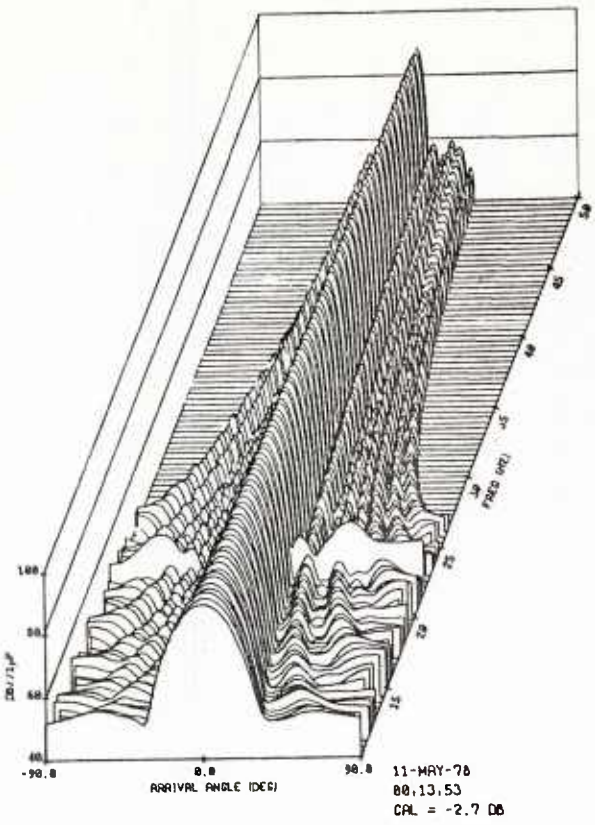

FIG. 6

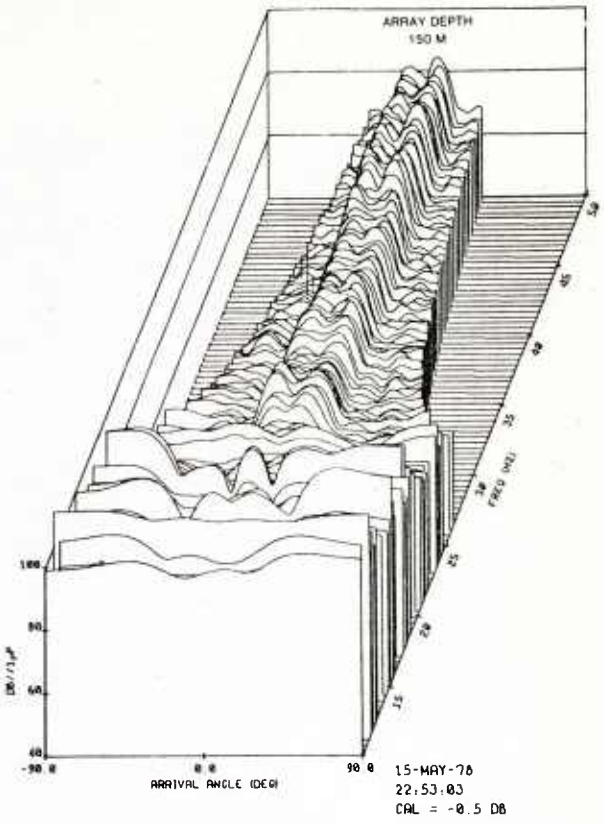

FIG. 7

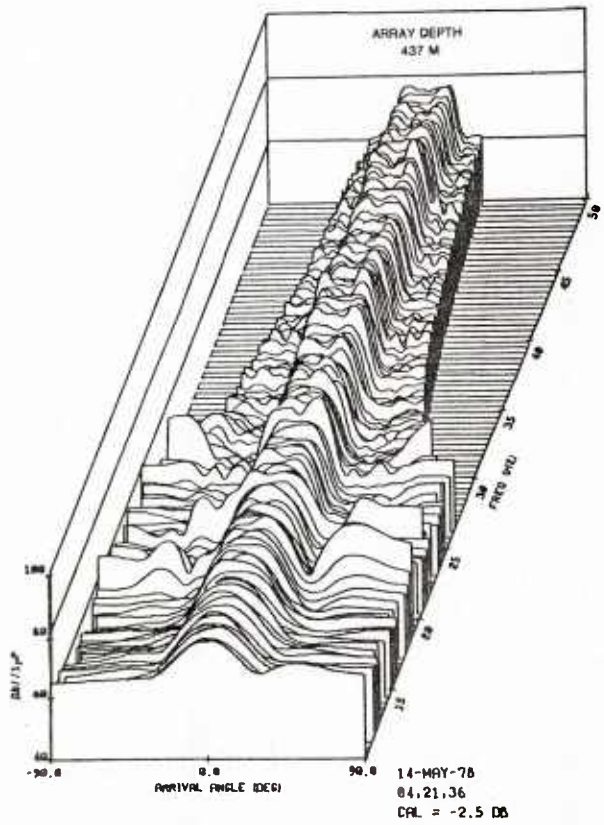

FIG. 8

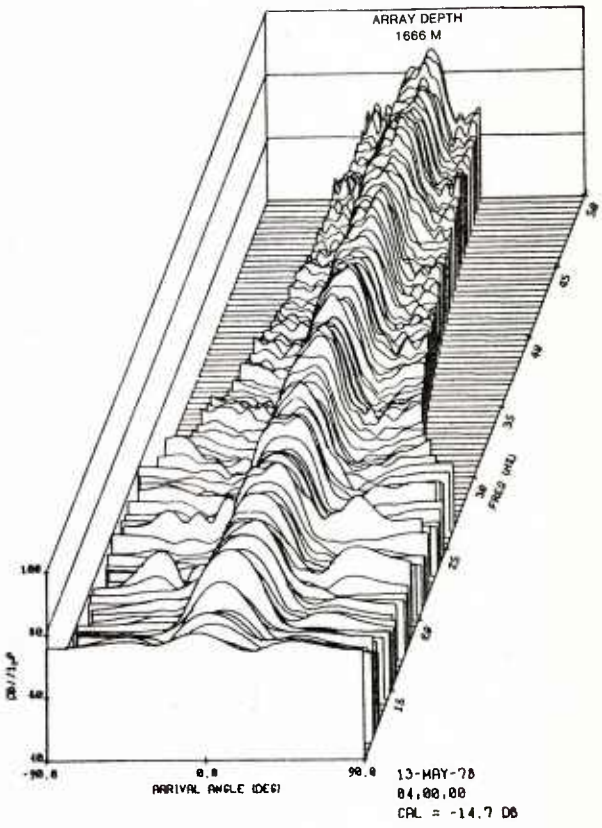

FIG. 9

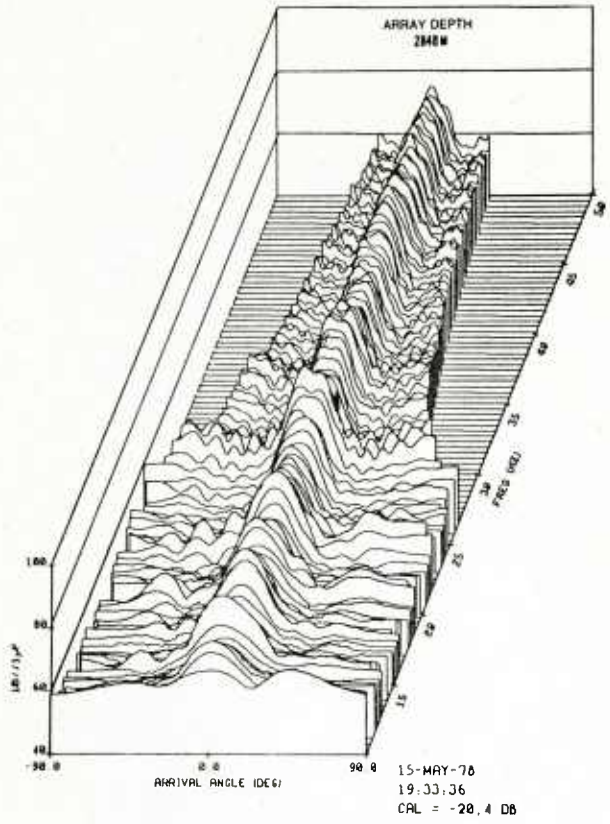

FIG. 10

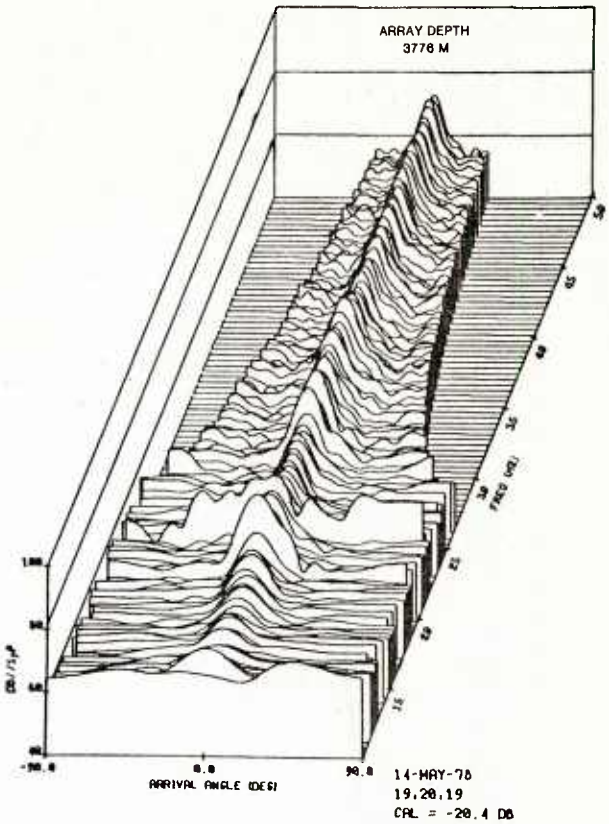

FIG. 11

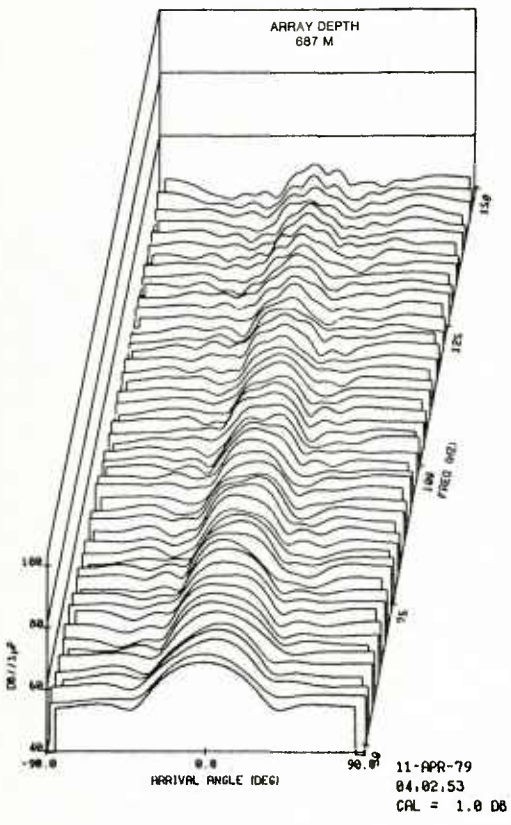

FIG. 12

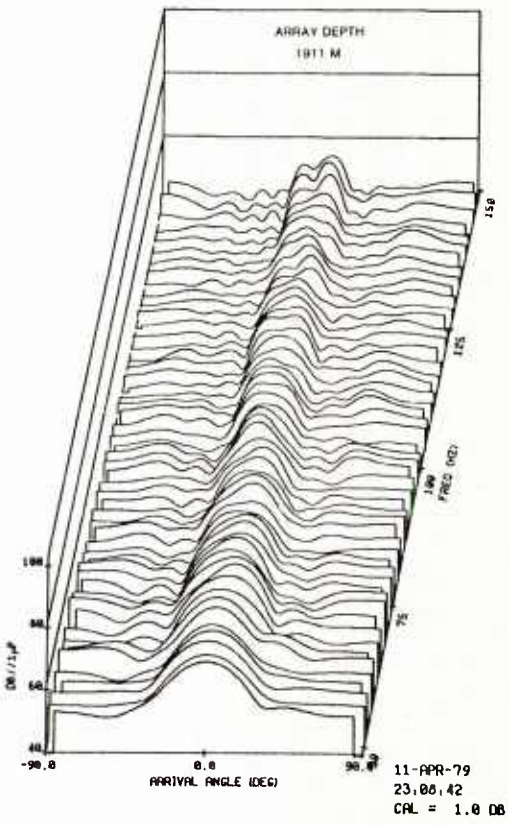

FIG. 13

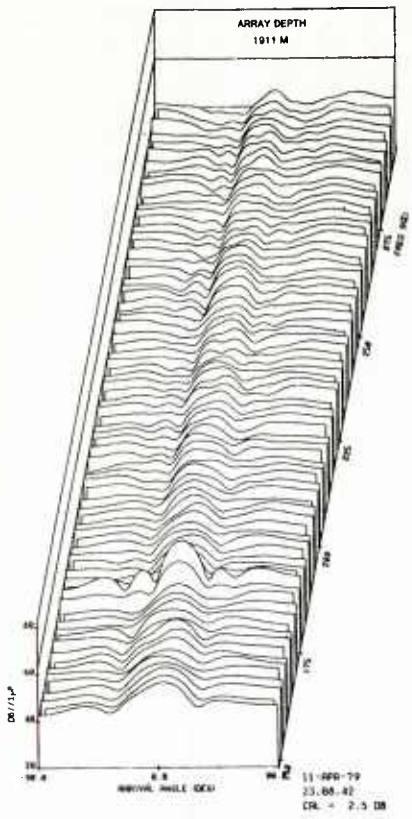

FIG. 14

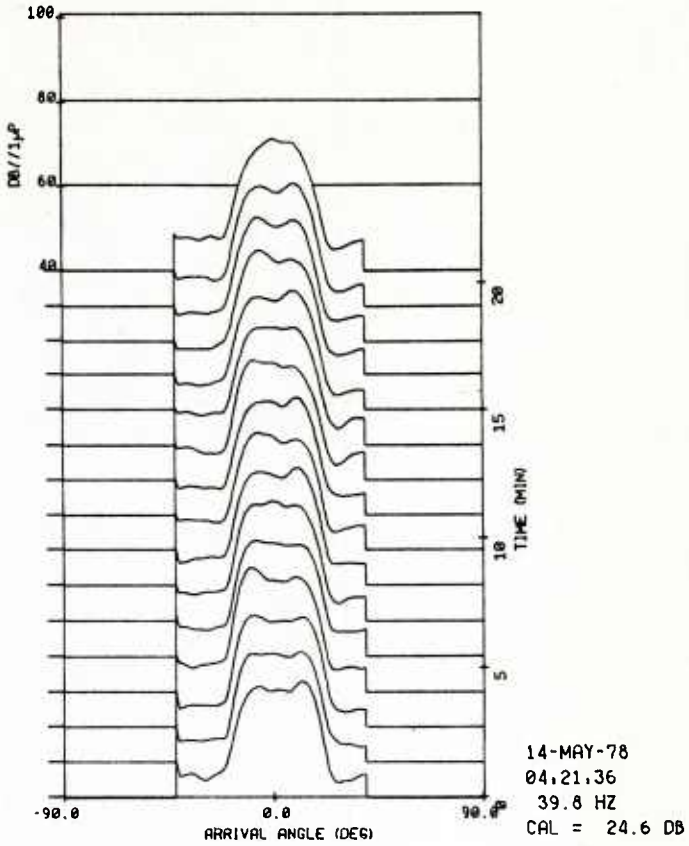

FIG. 15

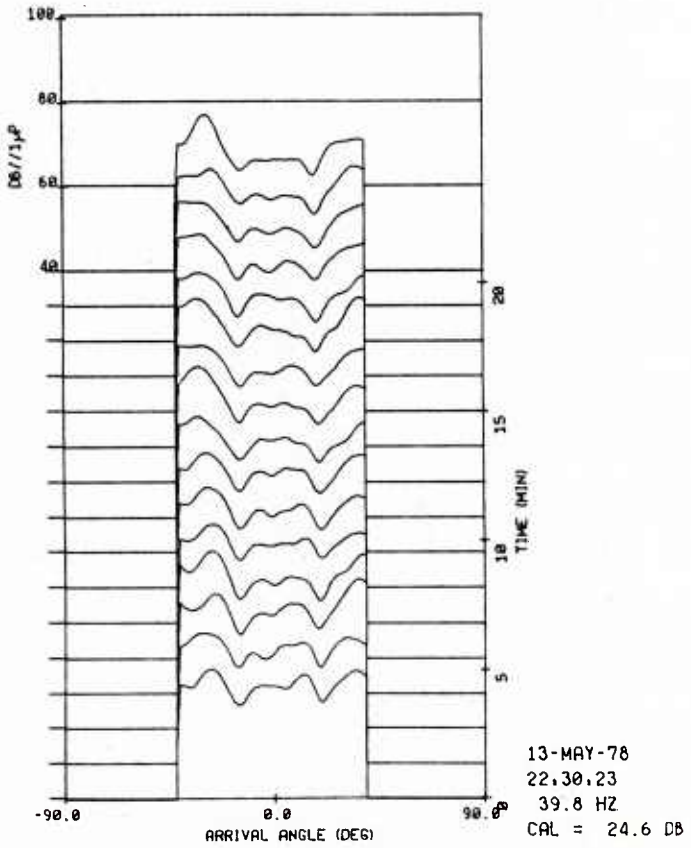

FIG. 16

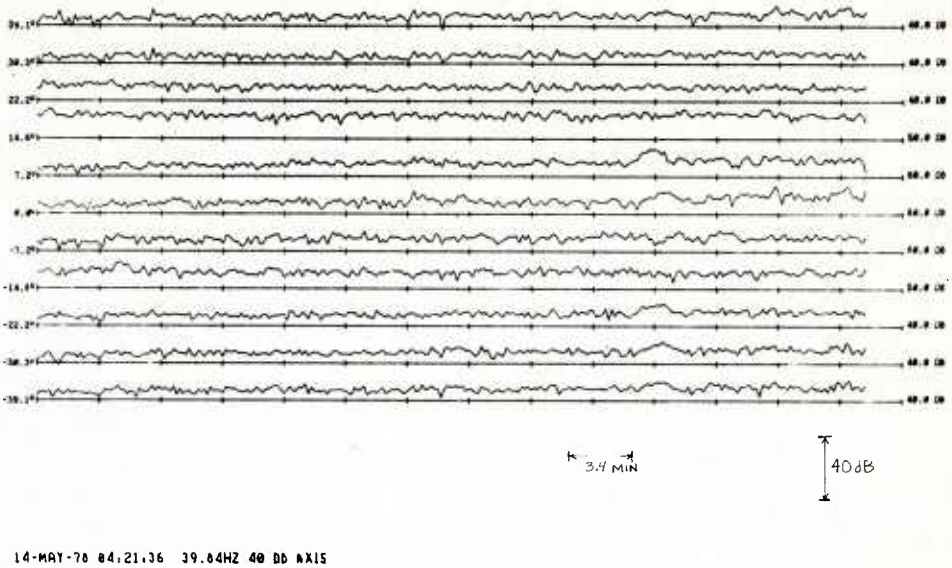
3.4 MIN
40dB
14-MAY-78 04:21:36 39.84HZ 40 DB AXIS

FIG. 17

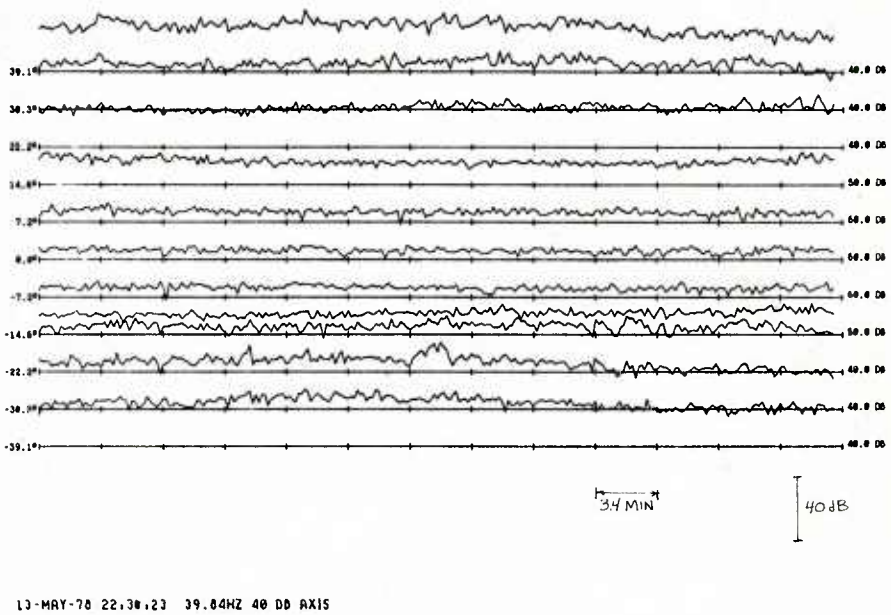
3.4 MIN
40dB
13-MAY-78 22:38:23 39.84HZ 40 DB AXIS

FIG. 18

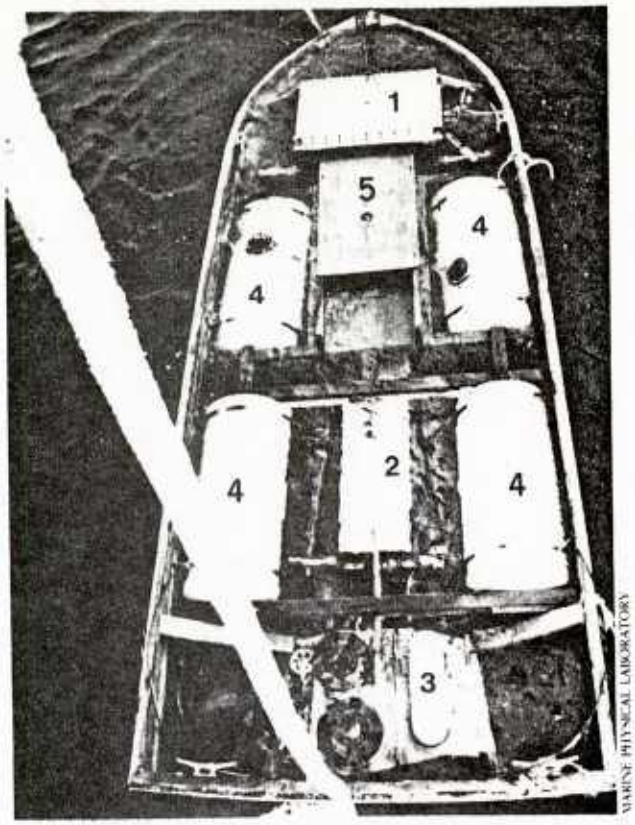

Line crawler prior to descending on mooring line. Power and control are supplied through an armored coaxial cable not visible. 1) control electronics, 2) electrohydraulic converter (motor/pump), 3) traction unit/drive sheaves, 4) buoyancy modules, 5) hydraulic compensator.

FIG. 19

MAIN ARRAY	SUB ARRAY	PLOT PARAMETERS
39 SUB ARRAYS	10 'PHONES	FILE NAME: LB0AA0
2.5 LAMBDA SPACING	0.5 LAMBDA SPACING	10 DB/RADIAL DIV.
HAMM WEIGHTING	EQUAL WEIGHTING	0 TO 180 DEGREES DISPLAYED
BEAM FORMED	BEAM FORMED	10 DEGREES PER ANGULAR DIV.
0 DEGREES OFF AXIS	0 DEGREES OFF AXIS	

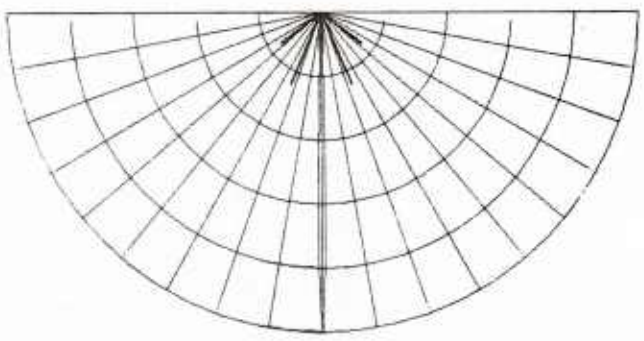

LB0AA0

FIG. 20

TYCE: Depth dependence of noise in the North Pacific

MAIN ARRAY	SUB ARRAY	PLOT PARAMETERS
39 SUB ARRAYS	10 'PHONES	FILE NAME: LB3AA0
2.5 LAMBDA SPACING	0.5 LAMBDA SPACING	10 DB/RADIAL DIV.
HAMM WEIGHTING	EQUAL WEIGHTING	0 TO 180 DEGREES DISPLAYED
BEAM FORMED	BEAM FORMED	10 DEGREES PER ANGULAR DIV.
3 DEGREES OFF AXIS	0 DEGREES OFF AXIS	

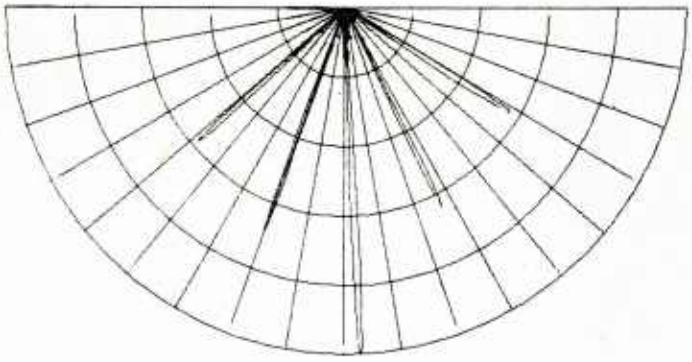

FIG. 21

LB3AA0

MAIN ARRAY	SUB ARRAY	PLOT PARAMETERS
39 SUB ARRAYS	10 'PHONES	FILE NAME: LBAABA
2.5 LAMBDA SPACING	0.5 LAMBDA SPACING	10 DB/RADIAL DIV.
HAMM WEIGHTING	HAMM WEIGHTING	0 TO 180 DEGREES DISPLAYED
BEAM FORMED	BEAM FORMED	10 DEGREES PER ANGULAR DIV.
10 DEGREES OFF AXIS	10 DEGREES OFF AXIS	

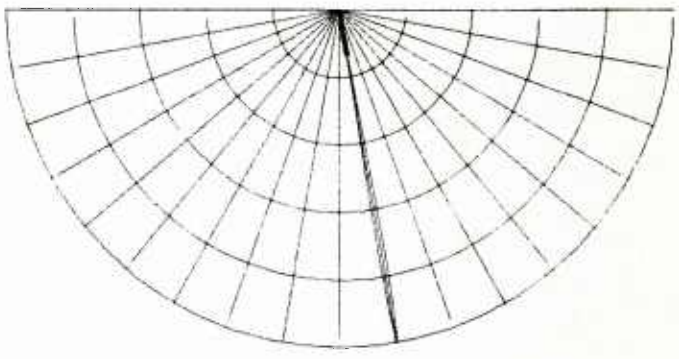

FIG. 22

LBAABA

AMBIENT NOISE LEVELS IN THE NORTHEAST PACIFIC OCEAN AS MEASURED BY AIRCRAFT-DROPPED SONOBUOYS

by

Robert H. Bourke
Scott Polar Research Institute
Cambridge, England.

Thomas H. Holt and Calvin R. Dunlap
Naval Postgraduate School,
Monterey, CA.

ABSTRACT

Ambient noise measurements obtained from sonobuoys air-dropped by U.S.Navy P-3 aircraft during operations over the northeastern Pacific Ocean from January 1978 to December 1980 have been analysed for spatial and temporal trends. Annual, seasonal, and latitudinal means and variability were established as well as event analysis for depth dependence and variability at shorter time scales ranging from weeks to hours. Observations were obtained at six frequencies (50 to 1700 Hz) and grouped in 5^{o} latitude bands extending from 20^{o}N to 55^{o}N. Mean noise levels increased by 1 to 2 dB from 25^{o}N to 45^{o}N, while at mid-latitude a 5 dB seasonal variation (summer louder) was noted. Variability in noise levels of 5 to 6 dB were observed for each season. Fluctuations at 50 Hz were associated with the seasonal migration of the North Pacific shipping routes. The presence of near-by shipping was also noted to severely contaminate (although unknowingly) reported ambient noise levels. The differences in level between deep and shallow buoys were ascribed to upper-ocean related differences in acoustic paths.

INTRODUCTION

When P-3 aircraft conduct ASW operations, they routinely drop ambient noise buoys to measure the background noise level of the ocean in the area of the operation. This term, more than any other in the sonar equation, governs the success of their acoustic range predictions. Air crews depart with a forecast of the ambient noise but generally find it necessary to expend an SSQ-41B or SSQ-57A sonobuoy to obtain a real-time measure of the noise field. Levels are read from a meter at six frequencies and the values recorded into a log. These are later entered into a summary report and filed at a central location such as COMTHIRDFLT.

The Environmental Acoustics Group at the Naval Postgraduate School recently acquired three years of sonobuoy ambient noise data from

throughout the northeast Pacific Ocean. 1130 observations from an area encompasssed by 175°E to 135°W and 20°N to 55°N (Fig. 1) were transcribed by hand from post-mission summary reports; 150 observations in 1978, 367 in 1979, and 613 in 1980. The large increase in the latter part of 1979 and throughout 1980 was due to renewed interest by THIRDFLT tacticians in this essentially forgotten data source.

The data were analyzed for mean and seasonal (quarterly) trends. Spatial trends were obtained by grouping the data into 5° latitude bands. The data were unevenly distributed in both space and time with 65% of the observations made during the summer and fall and 75% between 30°N and 45°N.

In addition to mean trends, analysis was also conducted on the variability of the noise field. Other analyses investigated depth dependence, noise levels under extreme environmental conditions, effects of ocean fronts, and the seasonal shift of shipping routes. Comparisons were made with other data from the area and with other sonobuoy data.

DATA SOURCE

Two sonobuoys are currently in use in the fleet which can measure the ambient noise of the ocean, the SSQ-57A and the SSQ-41B. The SSQ-57A is a calibrated buoy which has a frequency range of 10 to 20000 Hz and can be set to operate at a depth of 60 or 300 ft (18 or 91 m). The SSQ-41B has a range of 10 to 10000 Hz and depth settings of 60, 400, and 1000 ft (18, 122, and 305 m). The SSQ-57A is nominally more accurate but both buoys have been shown to have an accuracy of $\pm$ 2 dB (NAVAIRSYSCOM, 1973).

The ambient noise meter indicates the noise level at 50, 100, 200, 440, 1000, and 1700 Hz. Signals are corrected to an ideal 1 Hz bandwidth and visually displayed on a meter with an accuracy of $\pm$ 1 dB. Maximum, mean, and minimum values are recorded in the flight log by the operator. Several sets of readings at each frequency are normally obtained depending on the length of time the aircraft remains within VHF range of the buoy. Ten minutes is a typical sample time. A degree of operator proficiency is required to discern apparent anomalous readings caused by near-by shipping, buoy motion during high sea states, or equipment malfunction.

The predominant environmental constraint on buoy performance is loss of RF signal due to antenna washover in sea states greater than 4 or 5. Hence, there is a bias in the data towards low to moderate wave conditions.

MEAN STATISTICS

Mean annual and seasonal spectrum levels are shown in Fig. 2. The shipping-dependent portion of the spectrum, below 200 Hz, has a slope of -7 dB/octave and displays minimal seasonal variability. Frequencies above 200 Hz, the wind-dependent part of the spectrum, exhibit a slope of -4 dB/octave and considerable seasonality. The fall and winter seasons are about 2 dB louder than the mean while spring and summer are 2 to 3 dB quieter. Fig. 3 shows the seasonal spectral envelope plotted against a modified Wenz curve (DIRNAVOCEANMET, 1976). The sonobuoy data appear somewhat louder at 50 and 100 Hz being aligned with the "average ship traffic in shallow water" curve. This may reflect the difference between past measuring systems, mostly arrays at deeper depths, or changes in shipping densities since the Wenz curves were derived, or perhaps sonobuoy measurements made predominantly near shipping lanes. Above 440 Hz the data are aligned with the 1 to 2 ft wave height curve which appears appropriate for a mean curve and for sonobuoys which generally are not deployed in high sea states.

A plot of the mean noise level within each 5° latitude band (Fig. 4) shows that at all frequencies there is a 2 to 3 dB increase from low (30°N) to high (50°N) latitude. This trend was also observed in the "Church" series of measurements in the Pacific, for frequencies below 200 Hz, except that the latitudinal increase was larger, from 2 to 16 dB (Wagstaff, 1978; Raisbeck et al.,1978).

There appear to be two distinct breaks in the slope of the curves of Fig. 4, one between 25° and 30°N and the other between 45° and 50°N. These are nicely associated with the positions of the Subarctic and Subtropic Fronts which act as boundaries separating water masses with distinct temperature, salinity, and sound speed profiles. The fronts undergo a seasonal migration, moving northward in summer, as well as a seasonal variation in frontal strength (horizontal property gradient), winter stronger. These seasonal changes are somewhat reflected in the seasonal latitidinal noise level plots. However, one can not separate out the impact due to the presence of these fronts from other possibly more dominant features such as seasonal wind patterns, seasonal migration of shipping routes, or seasonal changes in mixed layer depth.

Quarterly time series plots of ambient noise were constructed for each latitude band to observe cyclic trends over the 3-year measurement period. Fig. 5 is an example of a plot for the 40° to 45°N band. A strong annual periodicity is observed for frequencies 200 Hz and greater, a trend noted for all other latitude bands. This trend is obviously in response to the annual cycle in wind forcing. In general, fall and winter levels are about 5 dB greater than summer levels. This is in agreement with the findings of Wenz (1969). He also noted that for the more southerly latitudes maximum

noise levels occur later in spring, a condition found in our data for latitudes below 25°N.

The shipping-dependent frequencies, 50 and 100 Hz, exhibit a weak annual cycle which, unlike the wind-dependent part of the spectrum, is phase shifted with latitude (Fig. 6). This is evidently a response to the seasonal migration in shipping routes, to be discussed later. The pattern is more clearly seen in 1980 where more data exist but inter-annual variability in storm intensity causes a non-steady pattern.

NOISE VARIBILITY

The variability or degree of fluctuation of the noise field is often a parameter which leads to success or frustration in assessing the performance of a sonar system. The fluctuation statistics, as expressed by the standard deviation, for mean noise levels at 50 and 1000 Hz are shown in Figs. 7 and 8. Both frequencies indicate a mean standard deviation of about 5 to 6 dB with no obvious latitudinal trend. At 1000 Hz a slight annual cycle is noted especially at 35° to 40°N and 45° to 50°N where fall/winter values are about 2 dB greater than summer values. The standard deviation also appears to be independent of frequency as observed in Fig. 9. This is in agreement with the findings of Bannister et al. (1979). Fig. 9 also indicates greater noise fluctuation for the more southerly latitude bands, a feature attributable to the lower wind speeds of this region.

In addition to characterizing the mean and seasonal fluctuations, it was possible to analyze the data for shorter-term fluctuations. During 29 individual flights, recordings were made on four or more separate buoys over time periods of 1 to 8 hours. These indicated standard deviations of 2 to 3 dB, much lower than the annual or seasonal mean fluctuations (Fig. 10). When compared with the regional groupings of Bannister et al. (1979), the data are aligned with their curve for local multiple-ship dominated areas for which the standard deviation is virtually independent of frequency.

DEPTH DEPENDENCE

Within the entire data set there were 27 flights wherein both shallow (60 ft) and deep (300 or 1000 ft) buoys were dropped. At 50, 100, and 200 Hz the deeper buoys were louder than the shallower ones. The maximum difference was at 50 Hz (1.8 dB) and decreased to near zero at 440 Hz. At 1000 and 1700 Hz the shallower buoys were slightly noiser, averaging about 0.75 dB greater (Fig. 11). These values and trends are quite similar to those reported by Hammond (1975) who also employed sonobuoys in his study conducted off Bermuda.

The above results are consistant with past findings which have shown that for shipping-related noise the deeper hydrophones, which generally are below the mixed layer, couple better with the distant-shipping noise traveling within the SOFAR channel (Arase and Arase, 1967). Although no latitudinal analysis was conducted, it should be pointed out that deep buoys dropped in areas above 45°N are often on or near the SOFAR channel axis. For shallow buoys the contribution from distant shipping is frequently "cut off", especially during summer, due to the inability to trap low-frequency signals in the relatively thin duct formed by the mixed layer. Hence, shallow buoys are more sensitive to higher frequency, wind-dependent noise sources which are a near-surface phenomenon arriving from near-vertical angles.

OTHER ENVIRONMENTAL EFFECTS

The summary sheet from which the data were transcribed sometimes includes notations concerning unusual weather events. During one such flight a rain squall was noted in the vicinity of the sonobuoy field but comments concerning distance to the storm and storm intensity were not reported. Noise levels during this event were 5 to 6 dB greater than the mean noise values of this study. However, when compared with the "rain squall" line shown on the modified Wenz curve (Fig. 12), the values were 10 to 15 dB lower for frequencies above 400 Hz. The rain squall evidently did not pass directly over the sonobuoy at the time the measurements were being recorded. At 200 Hz there is agreement between the two curves, mostlikely due to the increased noise level from distant shipping.

There were several occurrences when measurements were made under conditions of relatively high sea states. Those for which wave heights in excess of 10 ft (3 m) were noted were grouped and plotted in Fig. 12. These values are 1 to 3 dB louder than the rain squall noise. The comparison with the 8 to 13 ft wave height Wenz curve is remarkably good.

Inadvertantly, a ship may wander through an ASW operating area passing close aboard to a buoy. This unwanted signal can considerably raise the noise level at all measured frequencies (Polin, 1970). During one evolution a large ship passed within 6 n mi (11 km) of the ambient noise buoy raising the noise level 5 to 10 dB above that predicted for individual ships by the modified Wenz curve (Fig. 12). Higher frequency harmonics, usually not seen when shipping is truely distant (removed by attenuation), are evidently present and flood the wihd-dependent spectrum as well.

SHIPPING ROUTES

It was noted earlier that a seasonal latitudinal dependence was observed in the shipping-dependent portion of the spectrum. This is probably in response to the seasonal migration of shipping routes, a seasonal shift to avoid storms. Soloman et al. (1977) have constructed an idealized envelope of seasonal shipping patterns (Fig. 13) for the North Pacific Ocean. Below 40°N the number of ships and shipping noise should increase during winter over summertime values. Above 45°N shipping density and shipping noise should increase during summer. Between 40° and 45°N levels should be most intense during spring and fall.

Fig. 6 (45° to 50°N) shows that indeed during the spring and summer months there is a relative increase in the noise level at 50 Hz. Fig. 5 (40° to 45°N) shows a pattern of alternating highs during fall and spring. Fig. 6 (35° to 40°N) shows relative peaks during fall/winter. In none of these figures is the seasonal pattern at 50 Hz coupled with the pattern for the higher, predominantly wind-dependent frequencies.

The pattern displayed in the above figures is not perfect (noisy) as the inter-annual variability in storm intensity and location is large. For example, at higher latitudes (45° to 50°N) the springtime storm activity might be less severe permitting shipping to migrate farther north than usual. The peak during spring 1980 (Fig. 6) may be a manifestation of this feature.

CONCLUSION

Ambient noise as measured by routinely dropped sonobuoys has been shown to provide an accurate assessment of the noise field under a wide variety of environmental conditions. It is a readily available data source that can be used to provide timely, wide-area input to ambient noise prediction models. A renewed effort should be made to collect and incorporate such data in operational models.

REFERENCES

Arase, E. M. and T. Arase, "Ambient Sea Noise in the Deep Ocean and Shallow Ocean," J. Acoust. Soc. Am. **42**:73-77(1967).

Bannister,R. W., R. N. Denham, K. M. Guthrie, D. G. Browning, and A. J. Perrone, "Variability of Low-Frequency Ambient Sea Noise," J. Acoust. Soc. Am. **65**: 1156-1163(1979).

Director, Naval Oceanography and Meteorology, "ASW Oceanographic and Acoustic Support Products Manual, Vol. 1," DIRNAVOCEANMET INST C3160.4(1976).

Hammond, D. F., "Near Surface Ambient Noise Measurements (Phase I-Westlant) (U)," Naval Air Development Center Report, NADC-75139-20, September

1975 (Confidential).

Naval Air Systems Command (NAVAIRSYSCOM), "Ambient Sea Noise Indicator Assembly ID-1872/A Maintenence Instructions (Intermediate) Illustrated Parts Breakdown," NAVAIRSYSCOM Tech. Man. 16-35101872-1, February 1973.

Polin B., "A Statistical Investigation of Low Frequency Ocean Ambient Noise (U)," Naval Air Development Center Report, NADC-SD-7095, December 1970 (Confidential).

Raisbeck, G. and others, "Church Stroke One Environmental Acoustics Summary (U)," Long Range Acoustic Propagation Project Report S78-021, March 1978 (Secret).

Solomon, L. P., A. E. Barnes, and C. R. Lunsford, "Ocean Route Envelopes," Planning Systems, Inc., McLean, Va. (1977).

Wagstaff, R. A., "Horizontal Directionality of Ambient Noise During the Church Opal Exercise (U)," Naval Ocean Systems Center Report TR 394, October 1978 (Secret).

Wenz, G. M., "Low Frequency Deep-Water Ambient Noise Along the Pacific Coast of the United States (U)," JUA(USN), **19**:423-444 (1969) (Confidential).

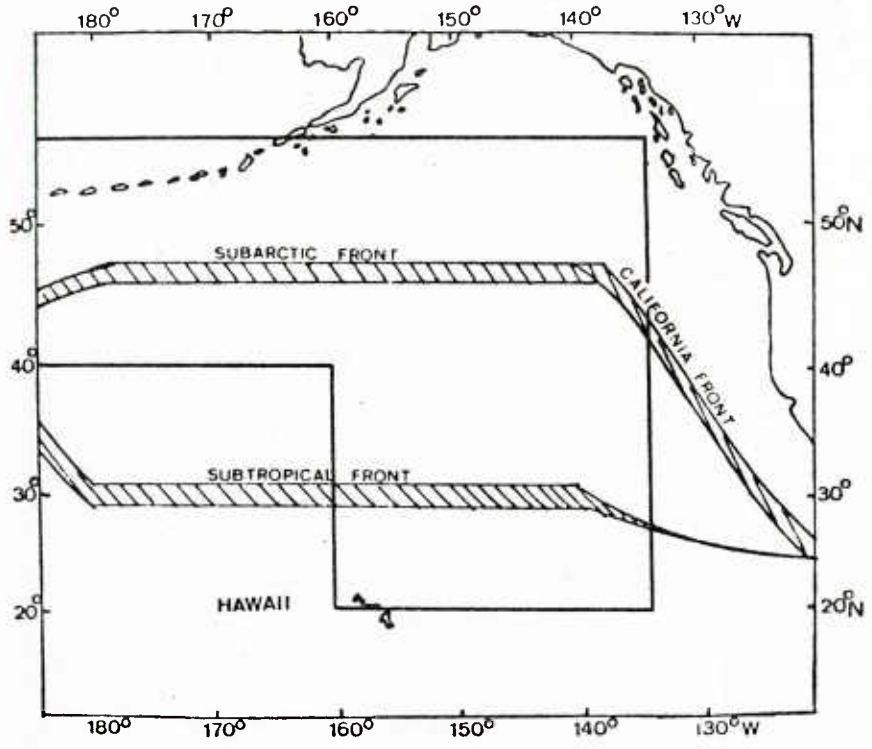

FIG. 1 AMBIENT NOISE STUDY AREA IN THE NORTHEAST PACIFIC OCEAN. THE MEAN POSITION OF THE OCEANIC FRONTS TRAVERSING THIS AREA ARE DEPICTED IN THE HATCHED AREAS

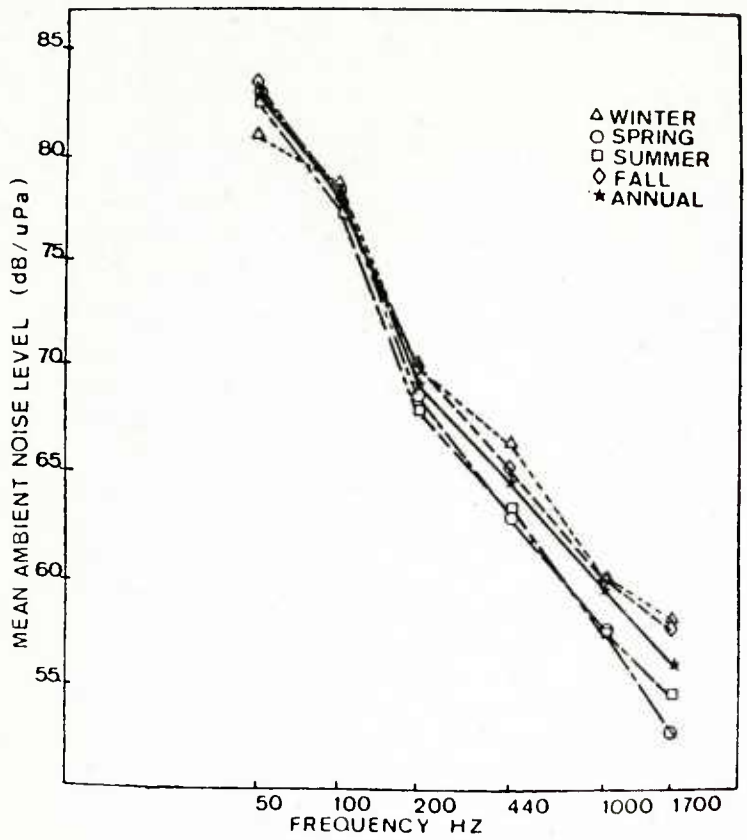

FIG. 2 MEAN ANNUAL AND SEASONAL SPECTRUM LEVELS

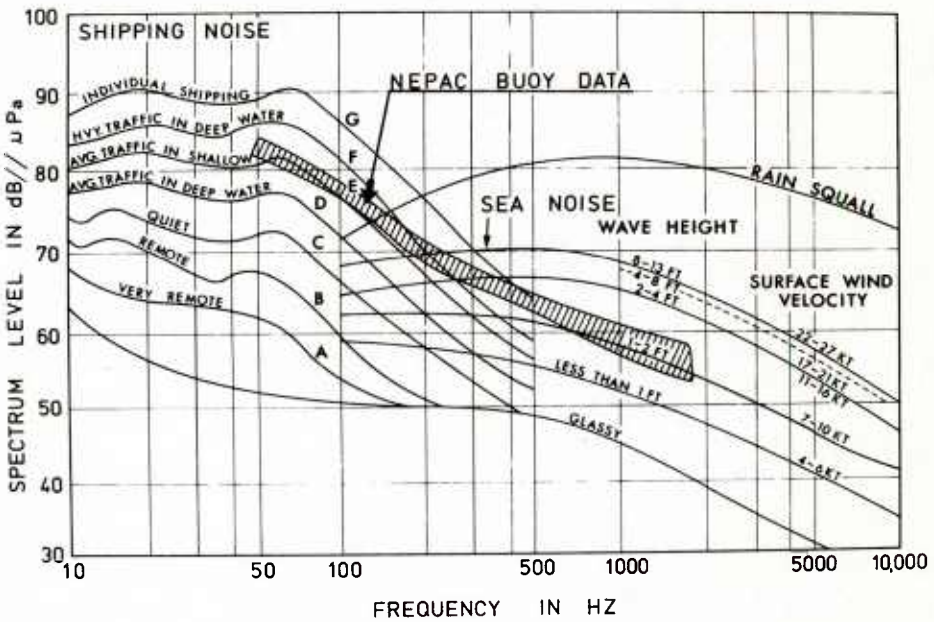

FIG. 3 ENVELOPE OF THE MEAN SEASONAL SPECTRUM COMPARED WITH THE MODIFIED WENZ CURVES (after DIRNAVOCEANMET, 1976)

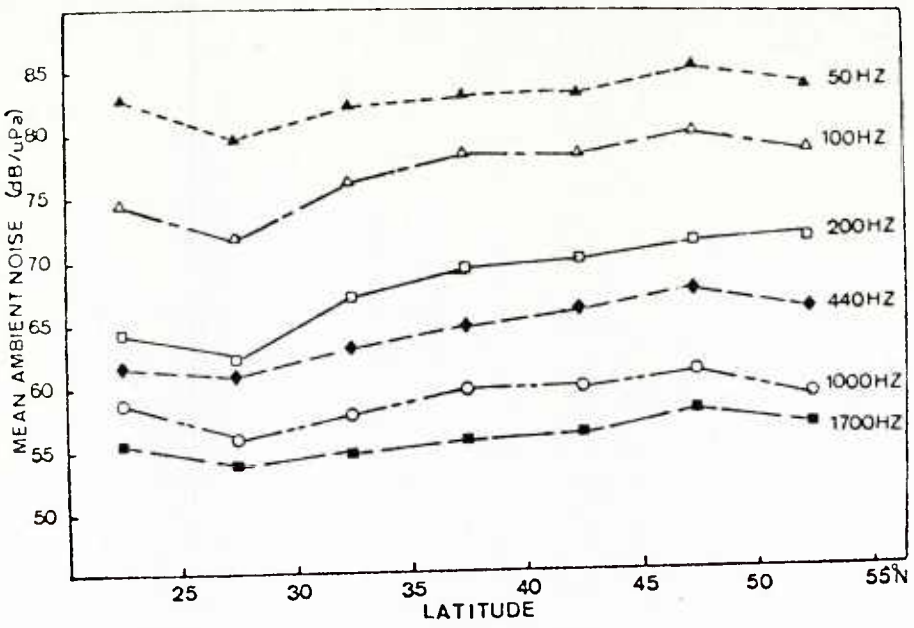

FIG. 4 MEAN ANNUAL NOISE LEVEL WITHIN EACH 5° LATITUDE BAND

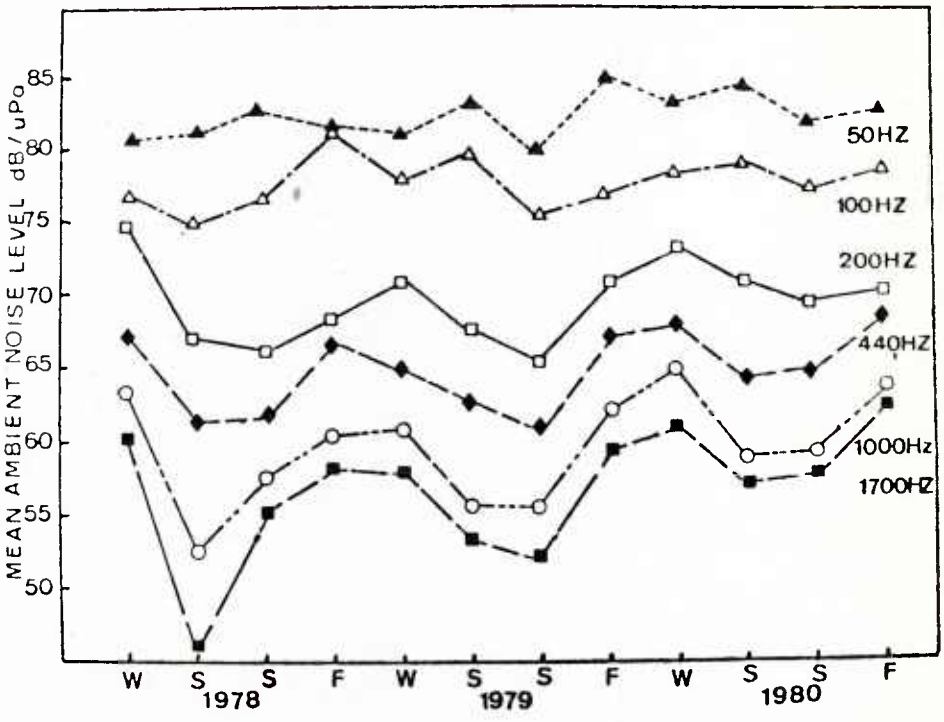

FIG. 5 MEAN QUARTERLY NOISE LEVELS OVER THE 3-YEAR MEASUREMENT PERIOD FOR THE 40°-45°N LATITUDE BAND

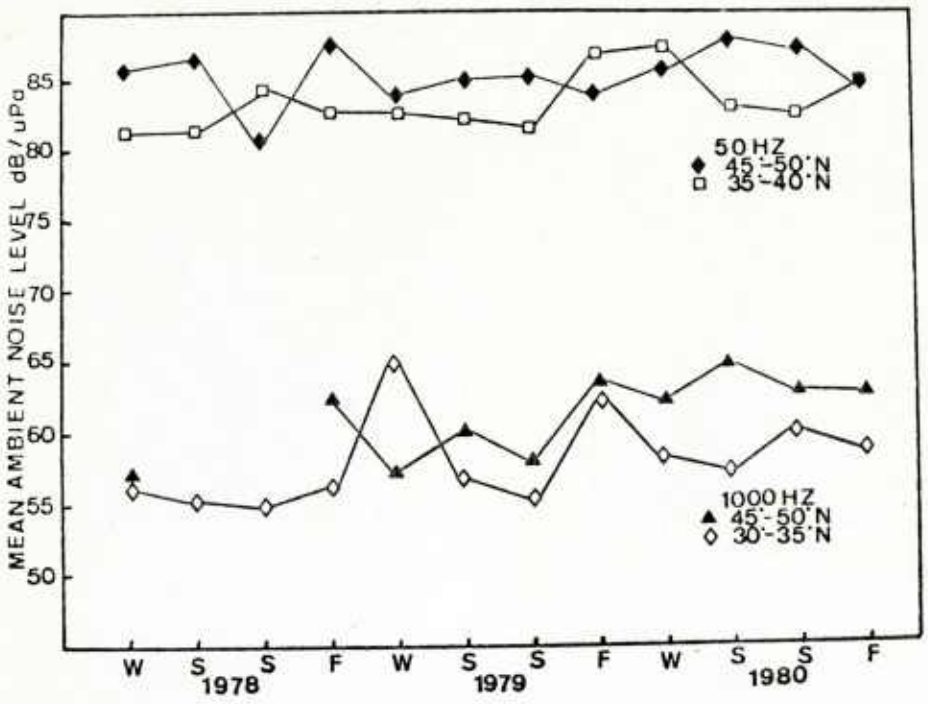

FIG. 6 MEAN QUARTERLY NOISE LEVEL FOR 50 and 1000 Hz FOR A NORTHERLY AND A SOUTHERLY LATITUDE BAND

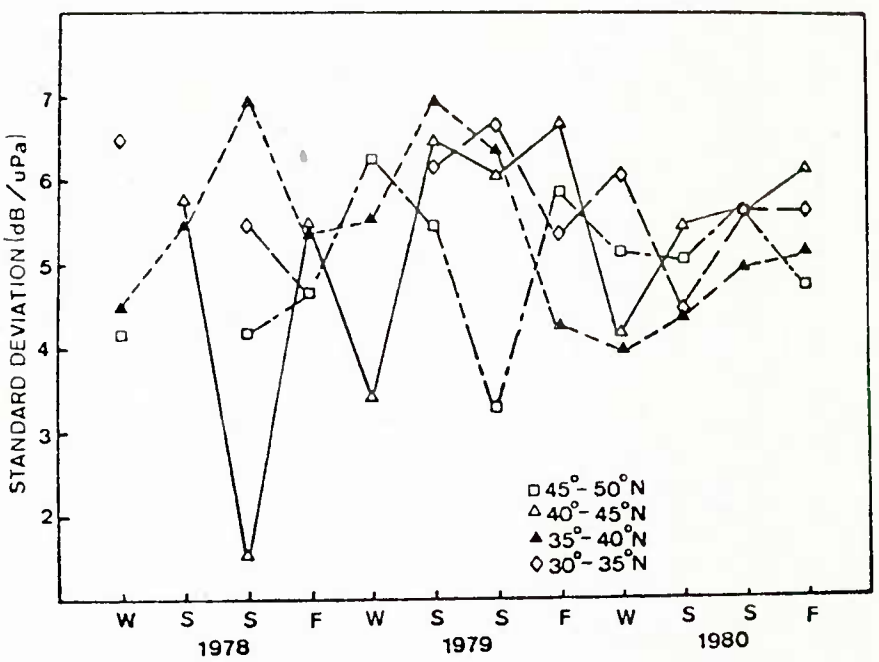

FIG. 7 STANDARD DEVIATION OF THE MEAN SEASONAL AMBIENT NOISE LEVEL AT 50 Hz FROM 30° to 50°N

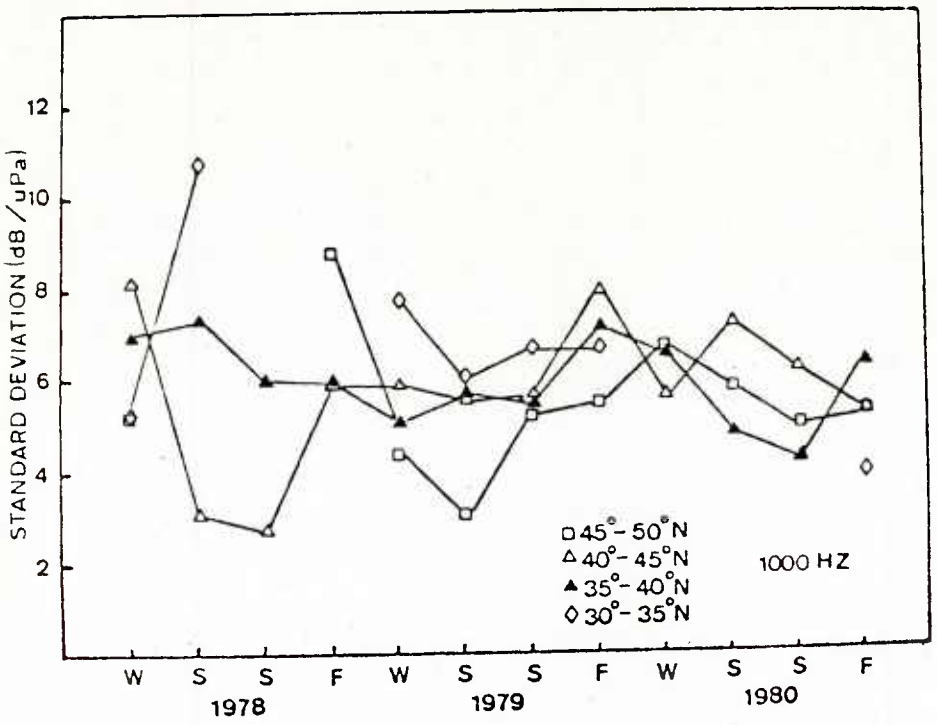

FIG. 8 STANDARD DEVIATION OF THE MEAN AMBIENT NOISE LEVEL AT 1000 Hz FROM 30° TO 50°N

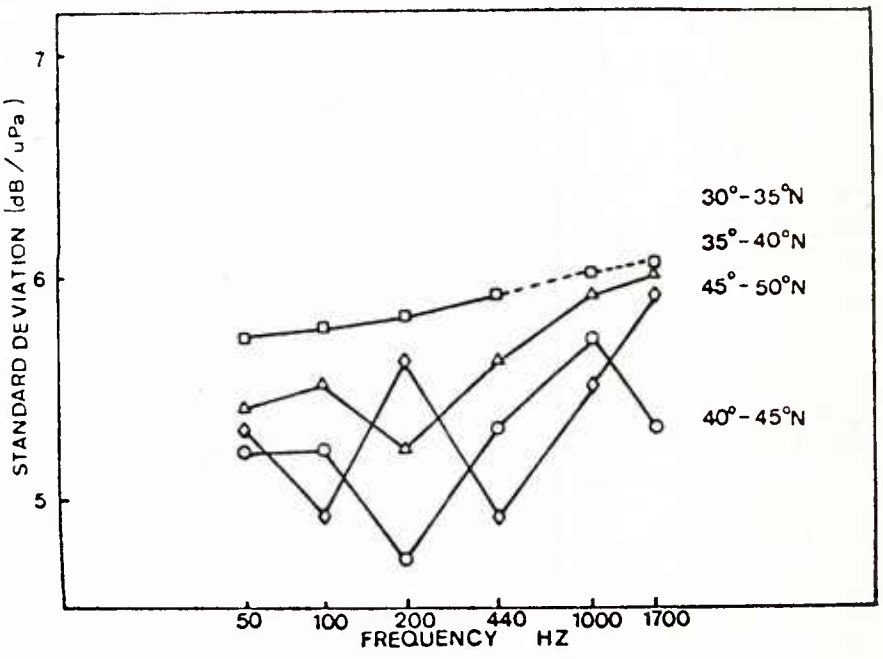

FIG. 9 STANDARD DEVIATION OF THE MEAN AMBIENT NOISE LEVEL FOR FOUR LATITUDE BANDS SHOWING ITS RELATIVE INVARIANCE WITH FREQUENCY

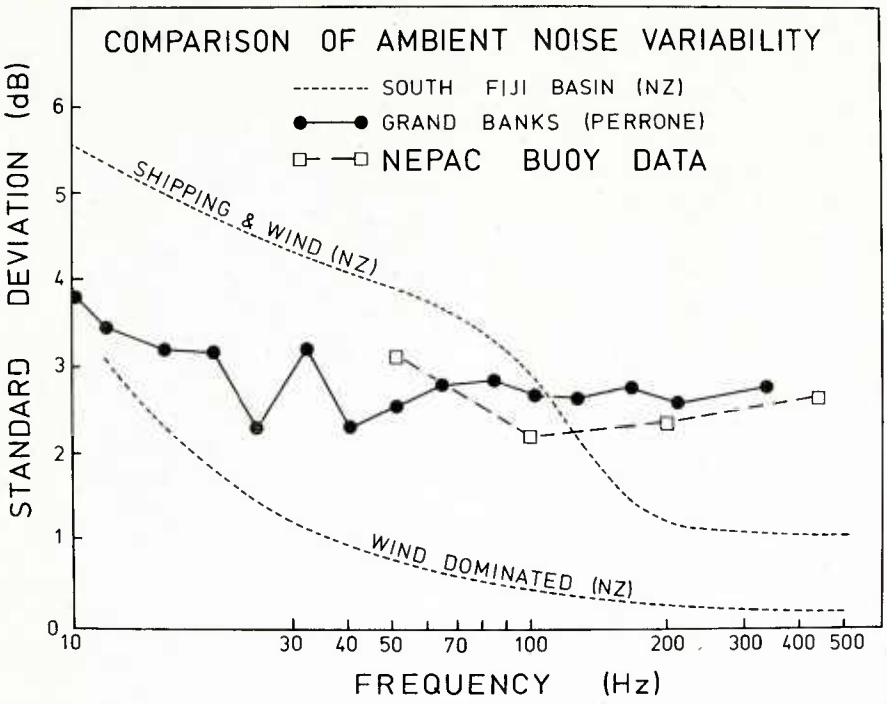

FIG. 10 STANDARD DEVIATION FROM 29 SHORT-TERM MEASUREMENTS COMPARED WITH THE REGIONAL GROUPINGS OF BANNISTER et al (1979)

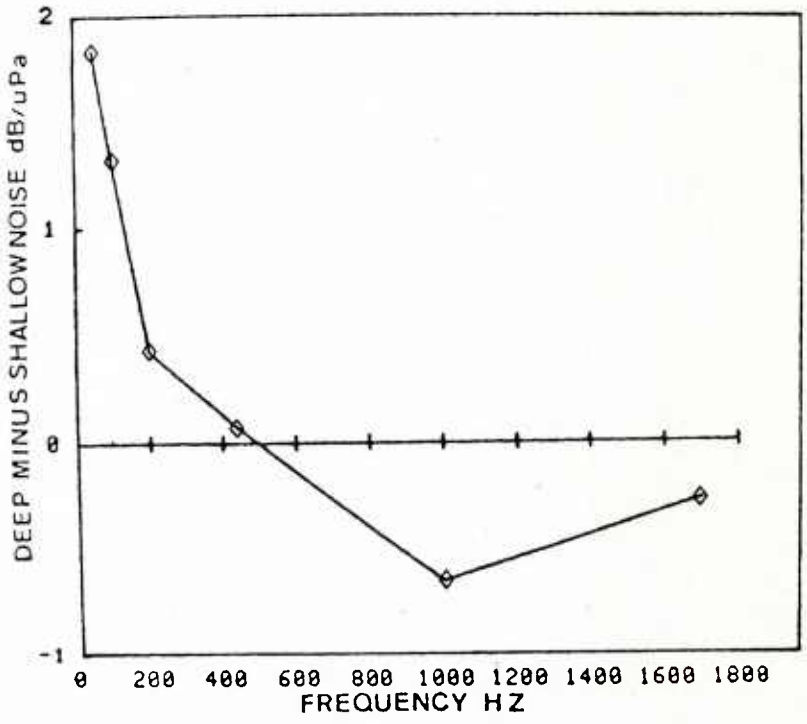

FIG. 11 COMPARISON OF SPECTRUM LEVELS FOR DEEP AND SHALLOW BUOYS

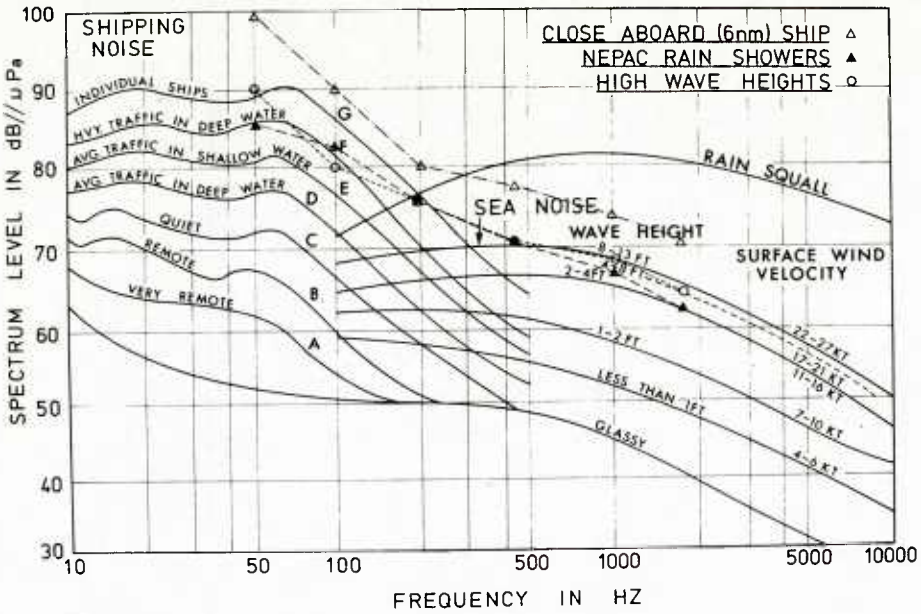

FIG. 12 AMBIENT NOISE SPECTRUM DURING A RAIN SHOWER, DURING HIGH SEA STATES, AND WHEN A SHIP PASSED CLOSE ABOARD

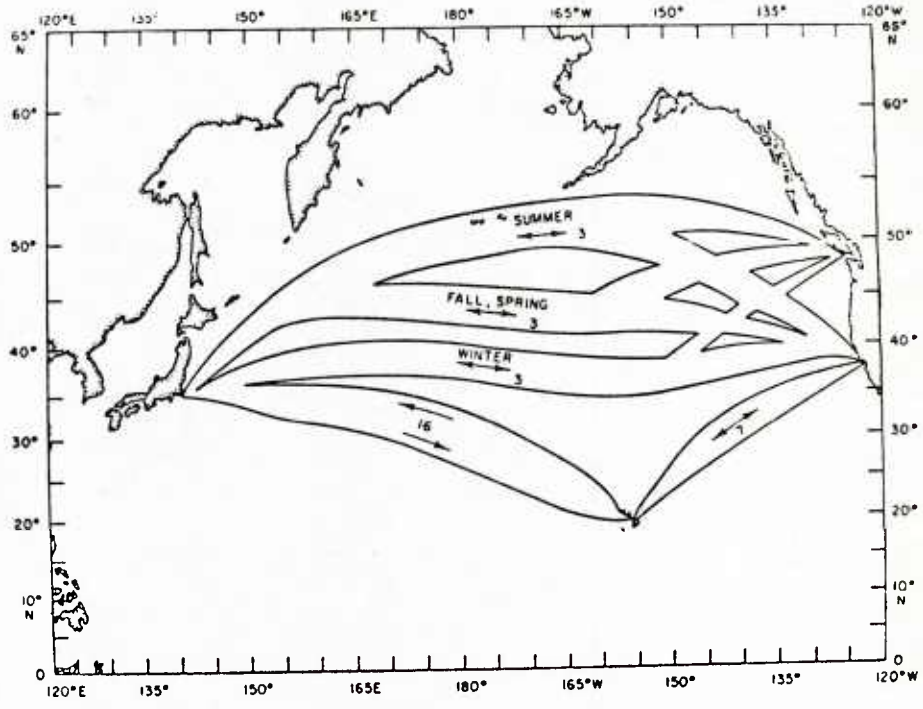

FIG. 13 SEASONAL SHIPPING ROUTES IN THE NORTH PACIFIC OCEAN (from Solomon et al, 1977)

A REAL-TIME SYSTEM FOR TOWED-ARRAY CALIBRATION AND PERFORMANCE ANALYSIS, OR HOW TO GET 50 dB SIDELOBES FROM A TOWED ARRAY

by

J.L. Berrou, O.Z. Bluy and R.A. Wagstaff
SACLANT ASW Research Centre
19026 La Spezia, Italy

ABSTRACT

Sidelobe suppression levels of 30 dB for a towed array are generally considered excellent; values above that are considered exceptional or unachievable. However, 40 to 50 dB suppression levels have been achieved and maintained throughout most of the measurements conducted within the last two years with SACLANTCEN's towed array and can be considered the norm rather than the exception. The key to achieving and maintaining this high level of performance is to keep the system free from faults and properly groomed. The techniques by which degraded performance is detected in real-time are discussed and illustrated by examples from past measurements. When the faults were repaired, the system performance returned to its usual high level. Similar techniques could be implemented by other researchers, with high expectations of receiving similar performance from their towed-array sonars.

INTRODUCTION

Sidelobe suppression levels of 30 dB for a towed array are generally considered to be excellent and 40 dB or above are considered the exception or unachievable. However, experience with SACLANTCEN's towed array demonstrates that it is possible for performance to be sufficiently high that sidelobe suppression levels of 40 to 50 dB can be the norm rather than the exception. This has been achieved and maintained throughout most of the ambient-noise measurements conducted by SACLANTCEN's Ambient Noise Group during six measurement exercises within the last two years.

There is nothing particularly special or unique about the Centre's towed array sonar system that achieved this high-level performance. If kept in perfect condition this sonar, like many others in use today, is capable of achieving and maintaining such performance. The key is to keep these systems free from faults and properly groomed. There is nothing new in the idea that good array grooming leads to improved performance. Achieving 40 to 50 dB sidelobe suppression continuously and the techniques that make this feasible in real-time, however, are new. The reality of such performance and the techniques for detecting degraded performance are discussed and illustrated by examples of faults that occurred during measurements.

1 BACKGROUND

In the past two years a towed array has been used extensively at SACLANTCEN. Six major measurement exercises have been conducted in the Mediterranean and in the eastern North Atlantic to measure ambient noise directionality and beam-noise statistics. A schematic of the system used for the series of measurements is shown in Fig. 1. Descriptions of the measurement techniques and the data analysis products are given in <1-3>. A summary of the measurements is given in <4>.

Experience prior to this series of measurements had suggested that it is vital to monitor the data from towed arrays in real-time. The towed-array sonar is a very complex system that, like any other sonar system, is subject to electrical and mechanical faults. It is even more vulnerable to degradation than other "conventional" sonars because it is not constrained to remain either linear or horizontal; deviations from either can degrade the system performance, even though it might be electrically and mechanically sound.

Because of the high potential for degraded performance by the towed array, techniques were developed to measure the system's performance and to assess the quality of the acoustic data. The techniques became more versatile and inclusive as experience was gained. This resulted in the present onboard analysis system, which can not only monitor the performance of the sonar system but is actually an onboard relative-phase-and-amplitude calibration system. In addition, the quality-assessment products generated by the system provide clues to faults that cause degraded performance. Once degraded performance is discovered it is usually not long before the fault is found and corrected. The measurements can usually be continued with a near-perfect system.

There were two discoveries that greatly enhanced the capabilities of the towed-array sonar analysis system. The first was that the towship could actually be used as a broadband sound-source to check the system. When the active rudder is idling it makes a terrible racket, up to 30 dB above the normal towship noise. It is thus an excellent source that is always available for a complete acoustic check of the system without the usual deployment problems of towed sources.

The second important discovery was that the virtual beams can be used to help judge the quality of the data and to assess the array performance because they provide information that is not otherwise available. These virtual beams are the beams that correspond to phase shifts or time delays greater than those corresponding to an endfire beam. They are produced by the FFT beamformer at all frequencies below design frequency. There are at least three ways in which the virtual beams can receive energy.

a. Virtual beams, like real beams, have sidelobes that extend into real space. If the sidelobe rejection of the beamformer is poor, strong sources from acoustic space can "leak" acoustic energy into the virtual beams.

b. There could be energy propagation in the array at a speed lower than the speed of sound in the sea. This energy would appear on one virtual beam.

c. There is energy on the hydrophones that is not coherent from one hydrophone to another. This energy may be of acoustic (flow noise), electronic, or mechanical (shock, vibration) origin. These incoherent noises are spread among all the beams, real and virtual. However, they are most easily spotted in the virtual domain because there is normally less energy there to mask them.

The energy in the virtual beams can therefore be invaluable for quality checking and "grooming" the towed-array system. A more complete description of virtual beams and their use for system performance assessment is given in <6>.

2 APPROACH

The usual procedure for assessing the performance of the towed-array system is to collect time-series of beam levels from all beams produced by the FFT beamformer. Approximately 50 spectral samples per beam per frequency analyzed are considered adequate. Inverse FFTs are used to convey the beam data to analogous time-series of hydrophone data for all hydrophones of the array. Time-series of the phase relative to that of an "average hydrophone" are obtained from the hydrophone data. The following statistics are calculated from these three types of time-series data.

- Percentile levels of 10, 25, 50 (median), 75 and 90
- Average power levels
- Geometric mean power levels (dB average)
- Standard deviation of the decibel or phase-angle time-series
- Percentile deviation of the phase angles, which is the quartile spread normalized to give the same value as the standard deviation for a gaussian distribution
- Spearman's rank correlation coefficients and associated confidence levels for beams correlated with all other beams.

The above statistics are used to generate plots of:

- Beam level versus beam number or azimuth angle
- Hydrophone level versus hydrophone number
- Phase angle versus hydrophone number
- Spearman's rank correlation matrix

The combination of the towship noise and the virtual beams provides a very powerful tool to debug and calibrate the whole system. The statistical outputs used for checking data quality are:

- Hydrophone amplitude plots, which show power average, dB average, median and dB standard deviation of hydrophone power series

versus hydrophone number. These can be used to detect anomalous behaviour of hydrophone channels.

- Hydrophone phase plots, which show the average, median, standard deviation and percentile deviation for the phases of the hydrophones relative to an "average" hydrophone, after removing the theoretical time shift for each hydrophone
- Beam level plots, which show power average, dB average, median, standard deviation and (power average - dB average) of the beam power series versus beam number. These give a measure of the sidelobe suppression on the self noise and can be used to detect actifacts in the beamformed outputs.
- Beam polar plots, which show median beam versus beam heading for real beams
- Spearman's rank correlation matrixes, examples of which are given as parts of Figs. 7, 10 and 11.

The top half gives 100 times the Spearman's rank correlation coefficient, which measures the correlations of the beam power time series for each set of two beams. Below the diagonal are the corresponding confidence levels, which are zeroed when the confidence level is low, and printed only if the confidence level is high enough that the beams are correlated.

3 THE TOWSHIP AS A NOISE SOURCE

The MARIA PAOLINA G., SACLANTCEN's research vessel, is neither particularly quiet nor noisy in normal operation, but has an active rudder that is very noisy when idling. The active rudder, consisting of an electric motor with a variable-pitch screw mounted on the ship's rudder, is used to manoeuvre the ship at low speeds. When idling, it rotates at high speed at zero pitch, generating cavitation and mechanical noise. The noise it creates is at medium frequencies; that is, around 500 Hz to 2 kHz. At lower frequencies, the source is so close to the surface that the Lloyd mirror effect reduces its output greatly.

The noise from the towship noise does not propagate to the array through a single path, as shown in Fig. 2 for deep and shallow water. In deep water, the direct path is usually dominant. In shallow water this is not so and many paths contribute significantly, the dominant one being usually the first bottom-reflected path. The total energy received on the forward endfire beam is greater by 15 to 12 dB in shallow water, and more beams receive the towship noise. Figure 3 gives the noise levels on the forward endfire beam for the ship in normal operation and with the active rudder idling, both for deep and shallow water. It shows that the active rudder can indeed be used as a good beacon to calibrate the system, as its level is well above the range of ambient noise levels, at least at high frequencies.

When such a single dominant beacon is available, the hydrophones all see the same signal, and a relative calibration can be performed. The active rudder has therefore been used as such a beacon at the beginning and end of each measurement, and also at any other time when the system quality needed to be checked. These array-performance tests delay the normal measurement by 15 minutes; they do not require any change in the acquisition or processing system.

4 RESULTS AND DISCUSSION

Figure 4 shows the hydrophone amplitude plots for three different types of averaging power average (upper dotted), dB average (lower dotted), and median (solid) at 750 Hz, for two situations.

The right side corresponds to a shallow-water measurement and shows excellent balance among the successive 40 hydrophones. The absolute level is high and the standard deviation (bottom curve) is the same for all the hydrophones. Apart from hydrophone N° 5 which has 1 dB more sensitivity than the others, the hydrophone plot looks almost perfect. The high level of the standard deviation is an artifact due to the randomness of the source level. The active rudder is very close to the surface and has a daisy directivity pattern caused by the surface. This pattern rotates with the sea surface and gives a very irregular level at the array. The left side shows the hydrophone plots in a deep-water location at the same frequency. Three hydrophones were malfunctioning due to bad contacts in the connectors of the array, and the performance was seriously degraded, as will be shown later.

In deep water, when a single path is predominant, the hydrophones can be calibrated in phase as well as in amplitude. The phase calibration is a bit delicate because the source is close to endfire and a phase unwrapping must be performed before doing any statistical analysis of the phases; in Fig. 5 the plot shows the average (dotted) and the median (continuous) phases of each hydrophone relative to a "reference" hydrophone. The "reference" hydrophone is not a physical one, but rather an "average hydrophone" for each acquisition. The right side shows a good array, with phase variations of 1° to 3° for the different hydrophones. This may be due to inexact positions of the hydrophones in the array, as the phase calculation assumes them to be exactly equidistant. A 3° degree phase error at 750 Hz corresponds to an error in position of 2 cm. The bottom curves show the phase standard deviation (dotted) and percentile deviation (continuous) of the phase with a 30° offset. If the phase had a gaussian distribution, the standard deviation and percentile deviation would be the same. Note that the bottom curves of the graph show that the phase distribution of the 50 successive measurements is not gaussian, as the PCDEV (standard deviation estimated from percentiles) is smaller than the standard deviation estimated by conventional methods.

The left side shows the same phase plot when hydrophones 6 and 9 had been interchanged by mistake. If the phase calibration is done, it will immediately spot such an error. However, the phase calibration is possible only when the signal is coming through a single path and is dominant on every hydrophone with a reasonable signal-to noise-ratio. The phase measurement shown here was for a beacon 15 dB above the omnidirectional noise level.

When the signal from the beacon reaches the array with multipath structure, the phase plots may not make any sense. The quality of the array can still be assessed by using the beam level plots. Figure 6 shows the beam level plots for two situations. Again, power, median, and dB averages are plotted together to help spot any abnormal distribution. On the right is the beam level plot for a near perfect array in deep water. Beam 17 is forward endfire, which receives the direct arrival from the towship. The bottom-bounce arrival is on beams 29 and 30. The virtual beams, 1 to 16

and 48 to 64 , receive the towship on their sidelobes and show the excellent sidelobe rejection of the array. The plot on the left shows a malfunctioning array. It corresponds to the left plot of Fig. 4 which had three bad hydrophones. The sidelobe rejection is not as good as is the previous example. The similar levels of virtual and real beams suggest that the system is seeing the towship on all beams, and does not see the ambient noise at all.

Figure 7 shows the median beam plots and the rank correlation matrixes for two active-rudder tests. The upper matrix corresponds to the continuous curve; they show that the sidelobe rejection is only about 25 to 30 dB. This curve corresponds to the case where hydrophones 6 and 9 had been interchanged. After correction, the lower matrix shows no correlation of the beams corresponding to real space. They really measure ambient noise, without being corrupted by towship noise. The virtual beams are still correlated with the beam towards the towship, but their levels are well below the ambient noise, as can be seen on the dotted curve. The sidelobe rejection capability of the array at that frequency is 45 to 50 dB.

In the example of Fig. 7, the error was found and the performance of the array fully restored. When the array is damaged, repair would sometimes take too much time and it is necessary to decide whether to continue. The virtual beams can be used to evaluate the degree of the degradation. If the performance of the array is not sufficient to ensure good data quality, then the bad channels can be replaced by a combination of their neighbours, providing sufficient, if not optimum performance. This is illustrated in Fig. 8. The phone plots showed two bad channels, 14 and 37. Channel 14 was dead due to a bad contact in one of the vibration-isolation modules in the array. Repair would have taken at least one day of work at sea, and would have precluded measurement at that site. The resulting beam plot appears at the centre and shows only 20 dB of sidelobe rejection, not enough to destroy the measurement, but marginal for the rest of the experiment, as any closeby source would blow up the entire field. Hydrophone 14 was therefore replaced by the average of 13 and 15, and the beam plot on the right resulted, showing 35 dB sidelobe suppression, adequate for continued measurement.

In shallow water, the phase is difficult to measure directly, because the towship noise reaches the array through many paths and the phase plots are often scrambled. An indirect estimation of the phase quality can still be performed by measuring the dynamic range of the beams. Figure 9 shows the beam plots for an active-rudder test in shallow water. Sound from the towship reaches the array through many paths, as evident on the polar plot (the forward beams are contaminated by the towship). The linear plot on the left shows the virtual beams to be down by 45 dB. If the sidelobe rejection of the system is 45 dB, it must have good phase match between channels.

While good sidelobe rejection is necessary it is not the only criterion by which to judge data quality. The system must also have low self-noise. This self-noise comes from two sources. One is the towship, whose noise is coherent, and can be cancelled by the spatial transient elimination techniques described in <1,2,7>. The other is the array self-noise, which can be of electrical or mechanical origin, and the flow noise. This type of noise is usually incoherent from hydrophone to hydrophone and is spread evenly among the different beams by the FFT beamformer. Thus the noises from the different channels always sum in energy; however they are delayed

before the summation. To estimate this self-noise in the presence of noise of acoustic origin is trivial if the virtual beams are available, and if the sidelobe suppression of the system is sufficient. Figure 10 illustrates such a situation. The sidelobe-suppression capability of the system is over 40 dB and the Spearman's rank correlation matrix shows no correlation between beams. The level of the virtual beams looks reasonably flat and is free from contaminations from the acoustic space. The energy present on the virtual beams is the system's incoherent noise, which is electronic noise at that frequency. Figure 11 shows a different case. The rank correlation matrix shows a high level of correlation between all the virtual beams. The beam level plots show the power average level of the virtual beams to be 10 to 12 dB higher than the median and dB-average levels. This was due to mechanical impulse noise occurring randomly on the hydrophones, probably due to lack of oil in the array and oscillations caused by rough sea conditions.

The virtual-beam noise levels at low frequency can be used to monitor and measure flow-noise. The array used by SACLANTCEN is electronically noisy at low frequencies because it has prewhitening high-pass filters. At 4 kn, the electronic noise is dominant at all frequencies, but at 8 kn, the flow-noise component begins to be clearly apparent, as shown in Fig. 12. The noise measurements were all conducted at 4 to 5 kn to minimize the flow noise. At 300 Hz, the 50 dB level is below sea-state 0 noise, and the virtual beams permit measurement of the flow noise during ambient-noise measurements in 20 to 25 kn winds (Force 6).

The excellent quality of the towed-array system has demonstrated a curious artifact, as shown in Fig. 13. At 1460 Hz, during the active-rudder test, there is always a target following the towship, 25 dB down in level at 114° relative to the towship. This is believed to be due to part of the towship noise being guided in the array. In tests at other nearby frequencies the relative level stayed constant while the direction slightly rotated, indicating it could be caused by a grating lobe for a sound speed of 940 m/s in the array. At lower frequencies no such phenomenon has been observed, but the waveguide effect, if real, would obviously vary with the ratio of the wavelength to the array diameter. In this array no measure was taken to attenuate acoustic propagation in the filling liquid.

CONCLUSIONS AND RECOMMENDATIONS FOR FUTURE WORK

The real-time calibration and test system integrated in the ambient-noise measurement system has proven very useful during the six major noise measurement exercises conducted in the last 20 months. Without it, it would have been impossible to keep the array in good working condition. The constant monitoring also gave a very high confidence level in the data collected during these noise measurements. A new system is being prepared, which will expand the eight frequency measurements to 256 frequencies on a frequency/wavenumber display, with automatic tests in the system to give warnings when the data have anomalies. Users of towed-array systems might wish to integrate similar tests in their systems in order to monitor the quality of their data.

REFERENCES

1. WAGSTAFF, R.A. Onboard acoustic data processing for the statistical analysis of array beam-noise, SACLANTCEN SM-144. La Spezia, Italy, SACLANT ASW Research Centre, 1980. [AD A095 112]

2. WAGSTAFF, R.A. Iterative techniques for ambient noise horizontal directionality estimation from towed array data. Journal Acoustical Society America 63, 1978: 863-869.

3. WAGSTAFF, R.A. Horizontal directionality estimation considering array tilt and noise field vertical arrival structure. Journal Acoustical Society America 67, 1980: 1287-1294.

4. WAGSTAFF, R.A., BLUY, O.Z., and BERROU, J.L. Ambient noise and beam noise statistics in the Mediterranean and Northeast Atlantic: a summary of towed-array measurements by SACLANTCEN. In WAGSTAFF, R.A. and BLUY, O.Z. eds., Undersea Ambient Noise, Proceedings of a conference held at SACLANTCEN, 11-14 May 1982, SACLANTCEN CP-31, NATO CONFIDENTIAL. La Spezia, Italy, SACLANT ASW Research Centre, 1982.

5. WAGSTAFF, R.A., BERROU, J.L. and COTARAS, F.D. Use of the towship for assessing towed array performance and analysing data quality. To be published in Journal Acoustical Society America (July 82).

6. BERROU, J.L. and WAGSTAFF, R.A. Virtual beams from a FFT beamformer and their use to assess the quality of a towed array system. Presented at ICASSP Conference in Paris, 3-5 May 1982.

7. WAGSTAFF, R.A. and BERROU, J.L. Is power averaging the best estimator for undersea acoustic measurements. Present volume: page 17-1.

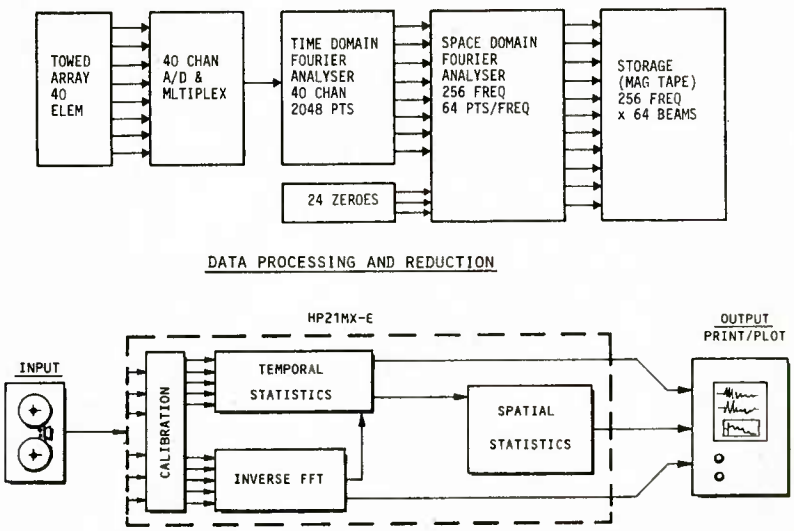

FIG. 1 THE DATA-ACQUISITION, PROCESSING, AND ANALYSIS SYSTEM

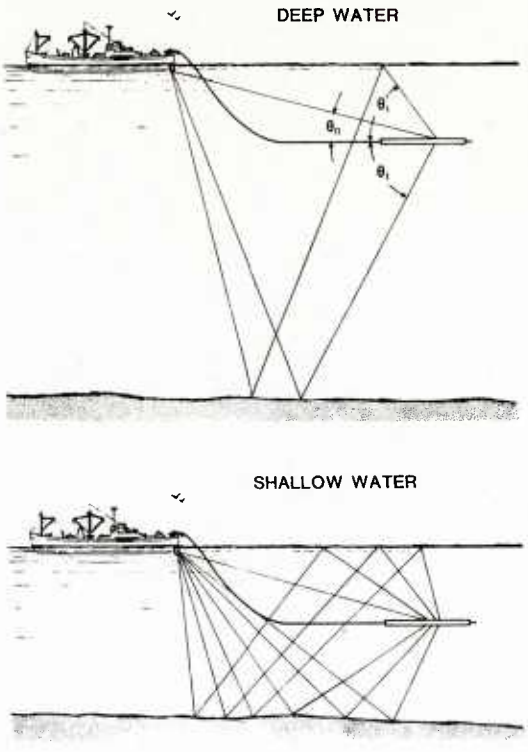

FIG. 2 THE TOWSHIP-NOISE PROBLEM: ARRIVAL ANGLES OF TOWSHIP NOISE AT THE ARRAY

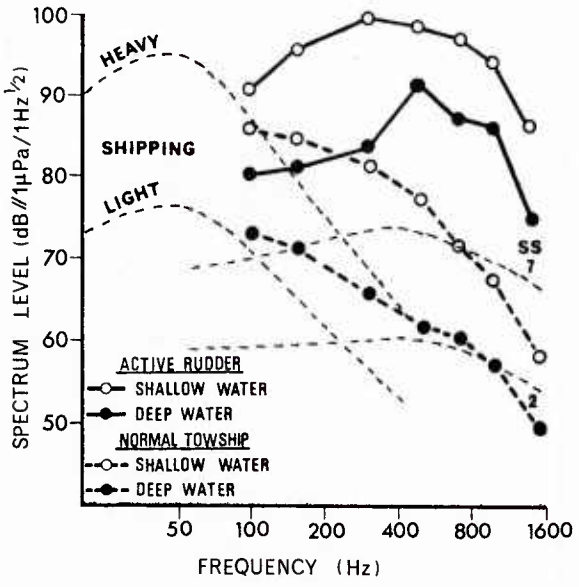

FIG. 3 TOWSHIP NOISE LEVELS IN NORMAL OPERATION, AND WITH THE ACTIVE RUDDER IDLING, IN DEEP AND SHALLOW WATER

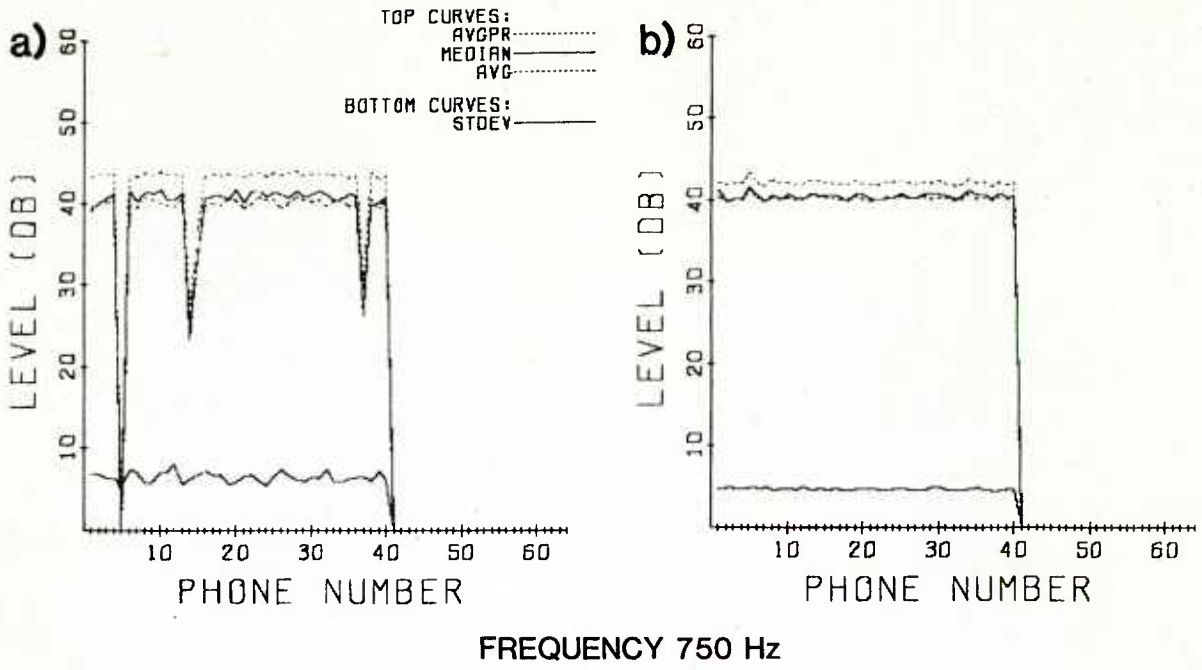

FIG. 4 HYDROPHONE LEVEL PLOTS AT 750 Hz
a) Array with 3 bad channels
b) Properly functioning array

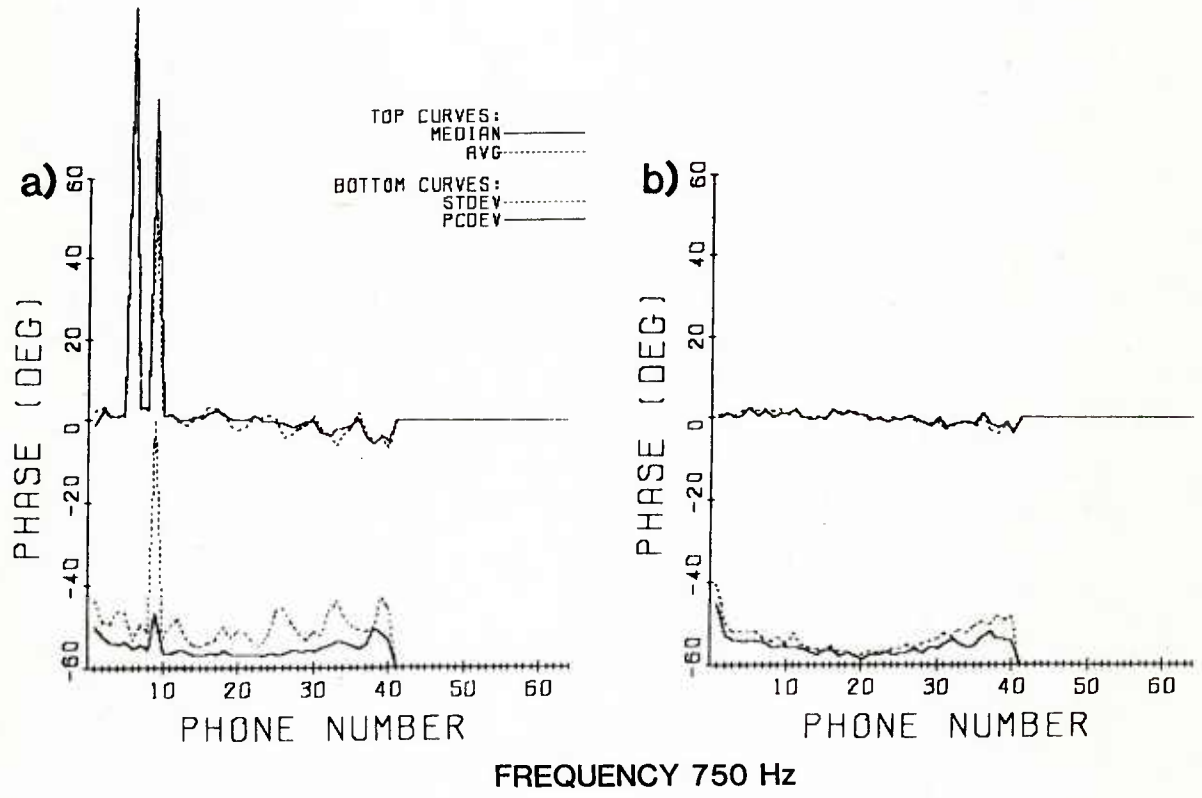

FIG. 5 HYDROPHONE PHASE PLOTS AT 750 Hz
a) Array with channels 6 and 9 interchanged
b) Properly connected channels

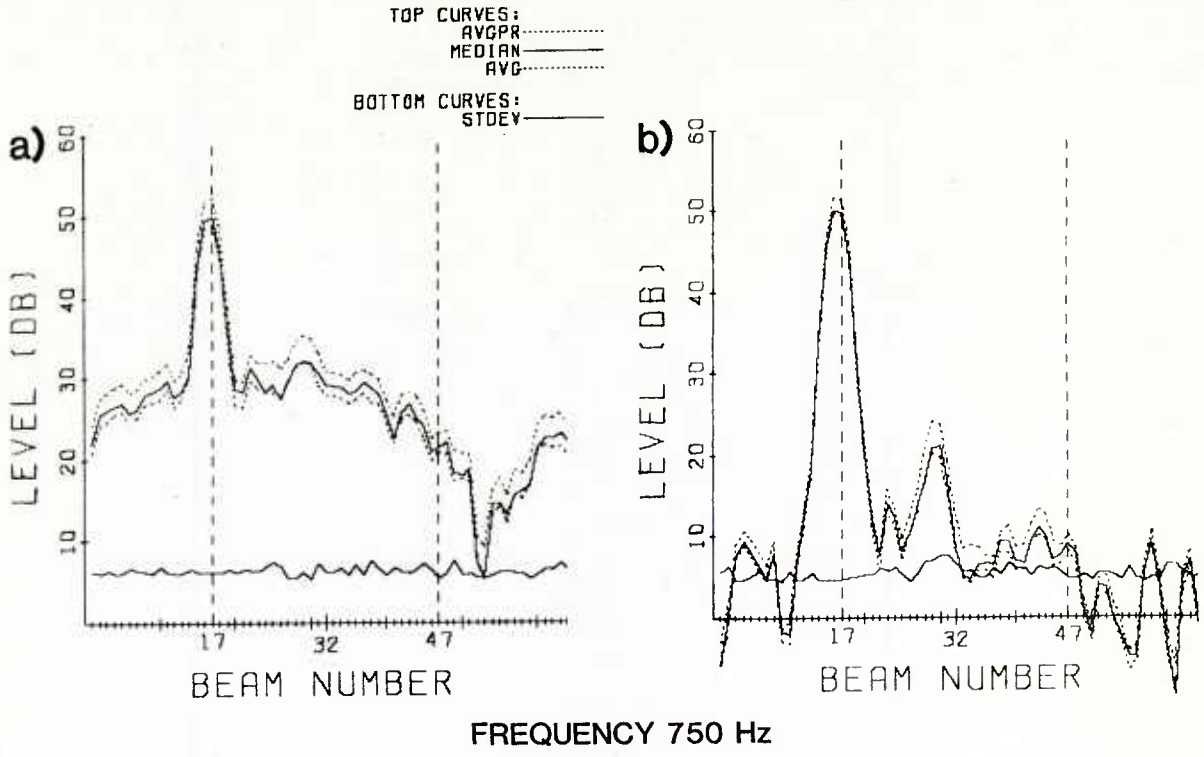

FIG. 6 BEAM LEVEL PLOTS
a) Array with 3 bad hydrophones
b) Properly functioning array

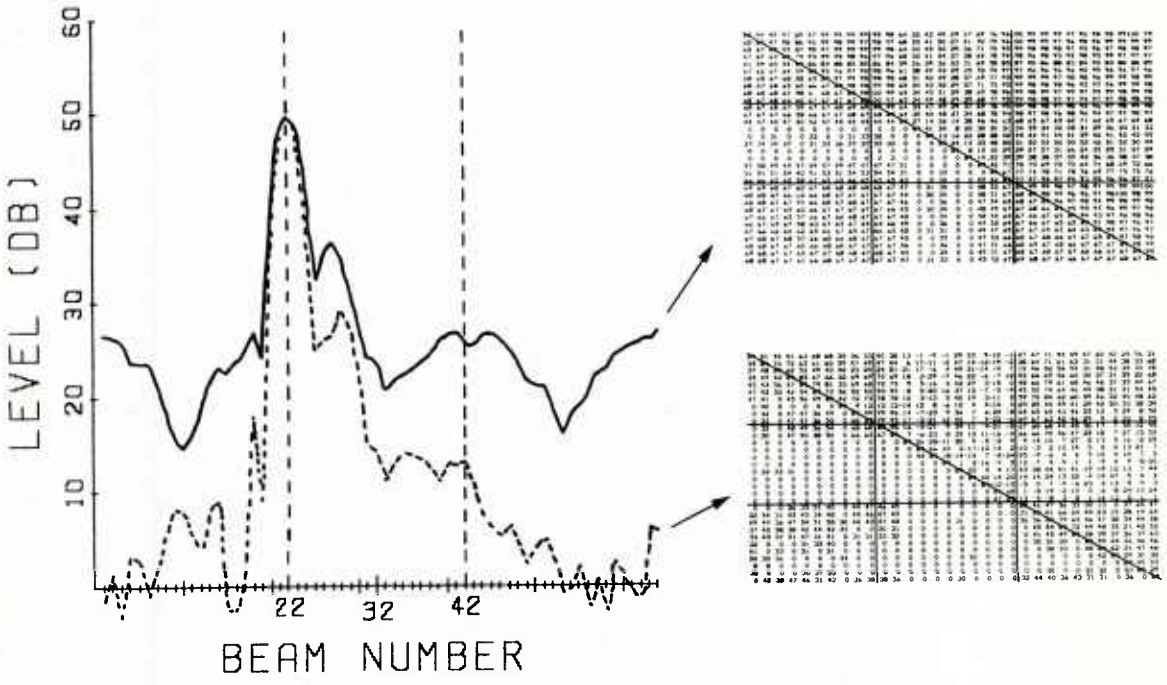

FIG. 7 BEAM LEVEL vs BEAM NUMBER PLOTS AND RANK CORRELATION MATRIXES FOR THE TWO CASES OF FIG. 5
Top curve and matrix: Channels 6 and 9 interchanged
Bottom curve and matrix: Array after correction

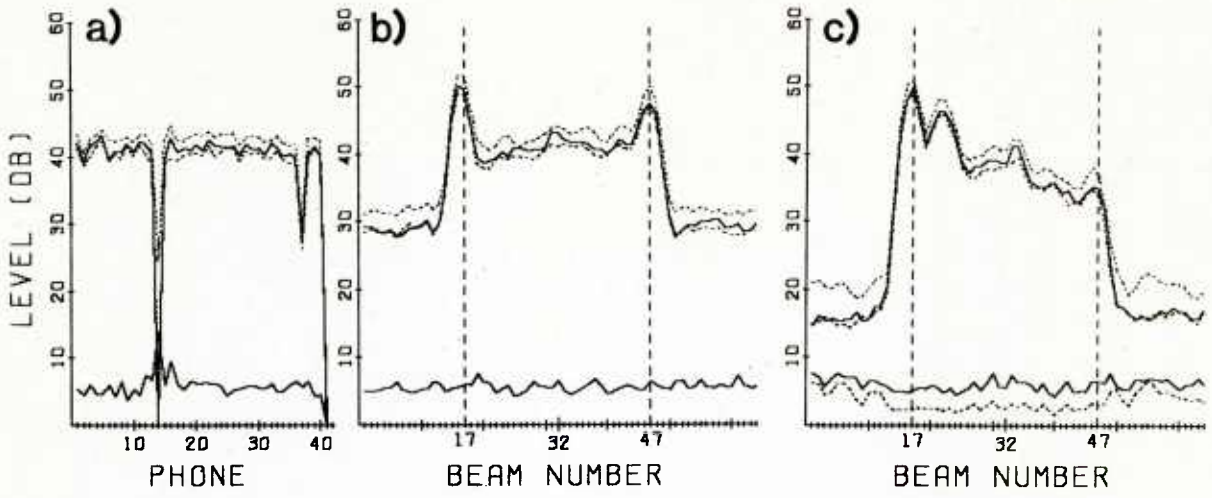

FIG. 8 PHONE LEVEL AND BEAM LEVEL PLOTS
a) Hydrophone plot showing malfunctioning channels 14 and 37
b) Corresponding beam plots
c) Beam plot after replacement of channel 14 by the average of 13 and 15

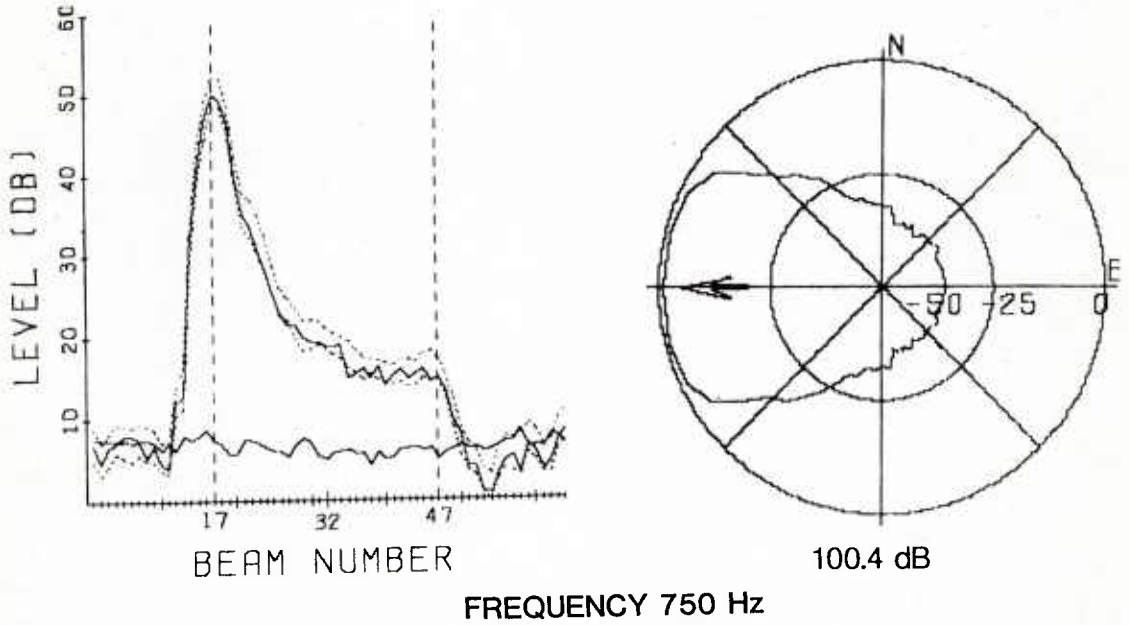

FIG. 9 BEAM LEVEL PLOTS FOR AN ACTIVE-RUDDER TEST IN SHALLOW WATER
a) Beam level vs beam number plot
b) Polar beam level plot

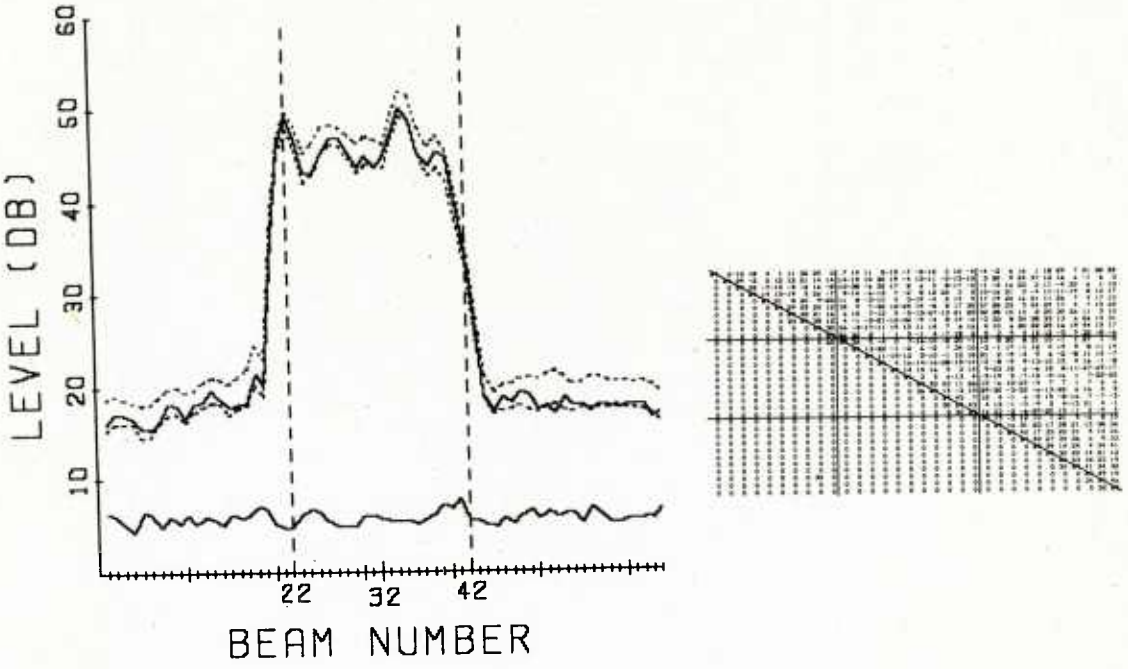

FIG. 10 BEAM LEVEL PLOT AND SPEARMAN'S RANK CORRELATION MATRIX FOR A MEASUREMENT AT 480 Hz, SHOWING ELECTRONIC NOISE ON THE VIRTUAL BEAMS

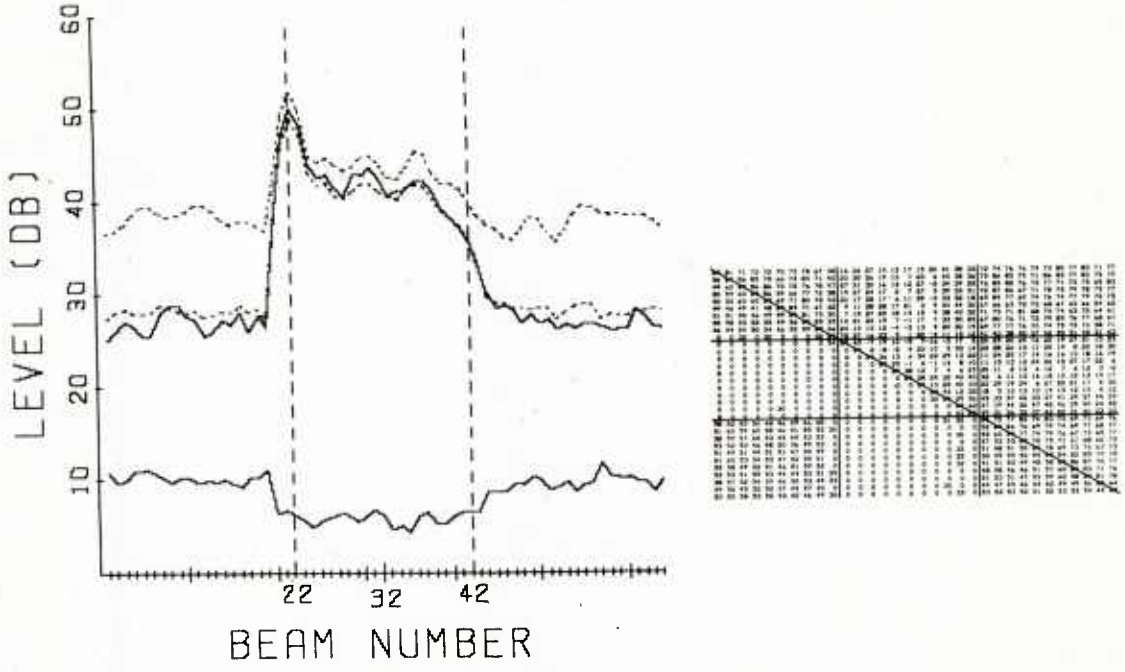

FIG. 11 BEAM LEVEL PLOT AND SPEARMAN'S RANK CORRELATION MATRIX FOR A MEASUREMENT AT 480 Hz, SHOWING THE EFFECTS OF RANDOM MECHANICAL HYDROPHONE IMPULSE NOISE ON THE VIRTUAL BEAMS

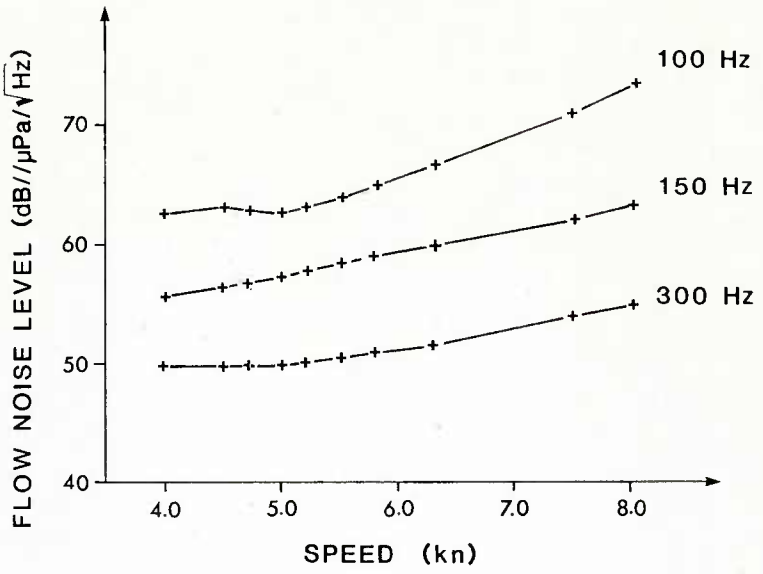

FIG. 12 SELF-NOISE LEVEL VERSUS TOW SPEED AT 100 Hz, 150 Hz AND 300 Hz

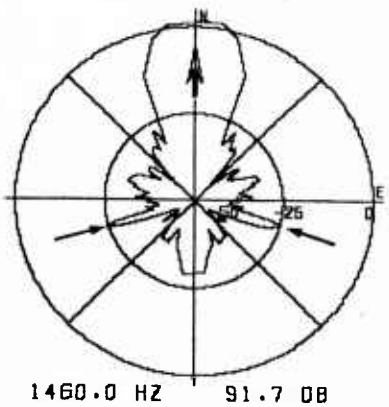

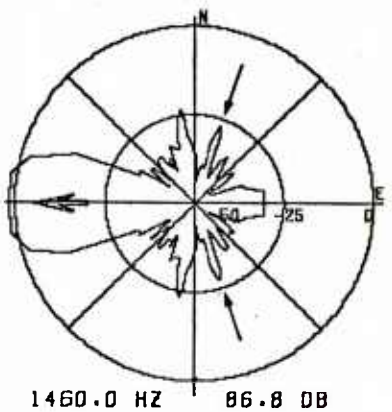

FIG. 13 POLAR BEAM LEVEL PLOTS FOR TWO ACTIVE-RUDDER TESTS AT 1460 Hz, SHOWING AN ARTIFACT AT 114° FROM FORWARD ENDFIRE

NOTES ON THE INTERPRETATION OF AMBIENT NOISE STATISTICS

by

Raymond C. Cavanagh
Planning Systems Incorporated
McLean, VA 22102, USA

ABSTRACT

Interpretation of statements about the character of ambient sea noise, as well as schemes to measure or model noise, are sensitive to the context or underlying view of what is essentially a stochastic process. A framework is proposed to aid in establishing and articulating a non-trivial context or view. For low to mid frequencies, the framework consists of individual types of noise components (background ship noise, wind noise, transient noises), each with rough estimates of fluctuation rates and statistical distributions for time scales from seconds to years. Estimates of the dependence of fluctuation properties on frequency, beamwidth, etc., are made whenever possible. Within such a framework, statements about noise properties can be much more readily interpreted, as illustrated through examples derived from ambient noise modeling and measurement problems.

1. INTRODUCTION

This discussion was motivated by reactions to and thoughts about the following kinds of statements:

> "The probability density function for the ambient noise level is approximately Gaussian with a mean of 82 dB and a standard deviation of 4 dB."
>
> "What sampling strategy should be used in measuring noise? How long must I look? How much time between uncorrelated samples... or independent samples?"
>
> "Ambient noise is a stationary random process."
>
> "Ambient noise is a non-stationary random process."
>
> "Ambient noise is easy to predict"... or... "impossible to predict."

The one thing which these statements have in common is that they all depend on how one views the noise field and its characteristics. None can be addressed or meaningfully interpreted without a detailed description about the case in question, the scales of interest,..., in short, the entire background for each. They are really statements taken "out of context." Unfortunately, that context is often difficult to establish and even more difficult to articulate.

For example, consider the first statement above. To make it useful, we need to know more. What is the bandwidth and processing and integration time and sampling rate for which the density is to apply? Based on theory or derived from measurements? Over what ensemble is the population? Time, and how much time? Over space or depth? Are the statistics calculated from intensities or dB's, histograms or moments or percentiles? And so on.

Related to the preceding is a general observation that in attempting to understand or summarize or explain or model ambient noise, we search for trends, persistence, cyclical events, ..., i.e., for properties which are prevailing and perhaps even predictable. How that search is conducted seems to depend greatly on the investigator's particular views and beliefs about the mechanisms which cause the noise and its variability, about the types of ensembling which make sense, and about the underlying stochastic nature of noise processes.

For both the interpretation of statements about noise properties and for activities related to modeling and measuring noise, my point is that the result will most often be very sensitive to the particular context or underlying statistical view. Noise is not unique in this respect for underwater sound, of course. Transmission loss fluctuations (but not necessarily mean values), reverberation, and scattering processes fall into the same category. For noise (especially low-frequency noise) and the others mentioned, there is an inherent randomness induced by physical mechanisms which themselves are difficult or impossible to view as deterministic: surface ship sources, scattering surfaces, volume inhomogeneities, etc. Hence, the need for statistical descriptions and careful delineation of the scales and ensembles involved.

Instead of developing a definitive context or view which covers all cases (this may be feasible, but also probably degenerate), I propose below a rough framework within which a subset of the cases can be considered. It is based on a model (of sorts) and incorporates the findings and hypotheses of a number of investigators who have, over the years, spent a lot of time thinking about noise. This framework is certainly not a unique candidate, but I hope it will serve to illustrate my point and to suggest to you (as you agree or disagree with my approach) ways to refine your particular view of ambient noise processes.

2. A FRAMEWORK

Some Details

In most practical applications, the received noise pressure p is filtered and/or quadrature demodulated, yielding samples of the complex pressure envelope associated with a nominal "carrier" frequency. With multiple hydrophone arrays, time-delay beamforming before or frequency-domain beamforming following the filtering process may be performed. The output in any case will be labeled E and represent the complex quadrature components (envelope) of the single-phone or beam output. Integration time to produce E depends on filter bandwidth (or coherent quadrature interval), but is typically on the order of fractions of a second to a few minutes. The squared modulus $|E|^2$ of E is the power spectrum estimate for the frequency band under consideration. Averaging of sequential samples of $|E|^2$ is then usually performed to yield the short-term average pressure-squared (re. the band) or more commonly (depending on normalization) a power spectral density or spectrum level or intensity estimate. I will use intensity, label it I, and presume that the averaging interval is on the order of a few seconds to a few minutes, usually long enough to make the time-bandwidth product large. Finally, let L=10log I, the "level" in dB's.

The quantities p, E, and I are all functions of time, and represent, in order, successively more processing or averaging.

Noise Components

To help make our problem tractable, I limit the frequency regime of interest from 10 or 20 Hz to a few thousand hertz. Following general agreement within the community (Wenz [1962], and many others), the important components of noise come in two classes: a "prevailing" background of ship-traffic and wind-related noise and a class of "transient" noises caused by nearby or particularly loud (identifiable) ships, by biological sources, by hurricanes or typhoons, rain storms, or seismic prospecting and oil rigs. The controversial aspect of this breakdown is the rule by which noises are classified as transient--the same problem as is always encountered in "cleaning" the noise or distinguishing "interference."

The proposed framework is now built upon these components, but with additional information about how they might be expected to behave.

Background Shipping Noise

Over short periods of time (minutes), p and E will reflect the detailed spectral content of the field--including tonals and detailed source instabilities. In the absence of tonals and with time-bandwidth product (T•W) small, successive samples of E will be uncorrelated, and E will usually resemble a zero-mean Gaussian process (see, e.g., Jobst and Adams [1977]). When tonals dominate, samples will correlate over longer time periods and may modify the distribution.

Over scales of minutes to an hour or more, the behavior of I is expected to follow Dyer's model: the fluctuation rate is determined by superimposed frequency-dependent multipath interference fields and the probability distribution will be approximated by that for the sum of gamma or non-central gamma variables, where the sum depends on the number of ships. As more ships (or ship lines) contribute, the distribution changes form from the skewed-to-the-right gamma with 2 degrees of freedom (2 df) to a nearly Gaussian form. In decibel units, the distributions become tighter and variances are reduced from 25 or 30 dB to a few dB. The number of contributing ships will, of course, depend on array response, frequency, the ocean environment, etc. (see Dyer [1973], O'Connor [1973]).

Over periods from an hour or less to days, the temporal variation of I will show effects of ships encountering convergence zone (CZ) ranges, passing through array beams, approaching the continental shelf, etc. Both measurements and models show a superposition of fluctuation components with periods ranging from an hour or two to days, and not particularly sensitive to frequency or number of components. The more ships contributing, the tighter the distribution. The stronger and more distinct the CZ's, the greater the variance (often observed in the depth dependence of the variance as the surface and critical depths are approached, e.g., Daubin [1977]. Decorrelation times (for I or L) of 2 to 10 hours are common, as are standard deviations (for L) of 2 to 5 dB (see, e.g., Perrone and King [1975] and Bannister, et al., [1979]).

Over periods of days to weeks, the behavior of I shows the effects of gross changes in shipping patterns, the transmission environment, etc. Over a year, the seasonally averaged ship noise tends to be 5 or so dB louder in the winter than summer, because of more favorable transmission.

The important aspects of this view of ship noise might be summarized in a non-physical but useful plot (Figure 1) of the modulus-squared of the Fourier transform of L (or I, if you prefer) for a hypothetical multi-year time series. The variance corresponding to a set of fluctuation periods is proportional to the integral over that part of the spectrum plot.

Background Wind Noise

For the scale appropriate to E, wind noise is expected to be zero-mean, Gaussian, and white over any small frequency band.

Fluctuation power for L (or I) is expected to be controlled by that of the local windspeed--with dominant periods from 20-40 hours and more, but little power below 20 hours, as shown in Fig. 2. The corresponding decorrelation time is accordingly near 20 to 40 hours, and the observed level L is likely to vary only a dB or two over a day or more (see Perrone and King [1975]). Seasonal variability is generally large, and dominated by local wind variations rather than long-range propagation conditions. The probability density function for L will follow that of the logarithm of the windspeed--and be sensitive to the temporal or spatial ensemble interval.

Finally, local wind noise, in the band of interest here, seems to provide a lower limit on the noise level L. When all other contributions are weak, even when the windspeed is small, this steady component will be observed.

Transient Noise

Turn next to a common source of transient noise: a nearby or especially loud or otherwise identifiable ship (e.g., the only ship in the basin or on a beam). It is a transient because it overwhelms other noise components and exhibits the structure of the transmission-loss (TL) field as the source moves in range with time. That structure is modified by aspect, speed, entry and exit of beams, etc.

Over short time periods, E may look very much like a background component, depending on stability of the source and relative speed and frequency. For time intervals beyond minutes, however, E and I (or L) will show the quasi-periodic nature of the TL--with fluctuation periods from minutes to hours (depending again on frequency, relative speed, range, etc.) and a distribution function like that of the observed TL curve.

The occurrence of such transient events in a region can usually be summarized statistically in terms of chances of ships coming nearby or being loud or whatever.

Typhoons, hurricanes, whales, seismic exploration sources, and other such "non-prevailing" sources of noise are viewed in much the same way as the nearby ship. Their influence may persist for long time periods; their statistical properties are unlike those of the persistent background and treated on an individual basis. Almost any spectral plot for L is possible, in contrast to the structured forms of Figs. 1 and 2.

Summary

The proposed approach is to view noise as a sum of components, some background components and others transients. For each time scale, the expected fluctuation rates are identified and corresponding variances and distribution functions estimated. The dependence of the rates and variances on frequency, beamwidth, etc., is also estimated whenever possible. With such a rough framework in mind, there is a chance that statements of the type given in the Introduction can be sensibly interpreted.

3. INTERPRETATION OF STATEMENTS ABOUT NOISE STATISTICS

One-Dimensional Density Functions

In light of the expected temporal fluctuation scales of all components of noise, the one-dimensional density function (or moments or percentiles) is of little value without careful specification of the quantity under study

(p or E or I or L, with integration time) and the fluctuation components over which the density is supposed to apply.

In the case of either wind or ship noise, the temporal variance of I should be very sensitive to the ensemble. It will increase substantially as the observation time increases from minutes to hours to days. This is evident from Figs. 1 and 2. Sampling strategies for measuring noise should be based on such a picture, and should endeavor to yield not only the density functions, but the fluctuation rates as well. After all, experience shows that "uncorrelated" samples are usually spaced 2 to 50 hours apart, depending on dominant source.

Model predictions of one-dimensional statistics present even greater interpretation problems. A popular one (Jennette, et al. [1977]) models ship counts in 1°x1° cells as Poisson variables, with the environment as static. The resulting density function and statistics for I are thus over an ensemble of all possible ship distributions. No temporal properties are predicted, and it is a challenge to figure out how to interpret the prediction. Over what time period would ships move around enough to approach the Poisson ensemble? Would not the environment be subject to significant variation over that time? The prediction is useful for predicting the noise for any single sample--but of no use in estimating how it will vary from that value over an hour or day or week.

Stationarity and Decorrelation Times

I have implicitly assumed noise to be a stationary process--broken down in terms of Fourier components. True stationarity is a mathematical ideal, and any finite-length time series can be embedded in a stationary process. Do the local (over limited time intervals) statistics change with time? Of course they do. There are low-frequency (stationary) trends to be observed in all types of ambient noise processes. Although certainly not a complete description, the spectral components of I or L or E (c.f. Figs. 1 and 2) give significant information about how these variables change with time, about the low- and mid- and high-frequency trends, about lengths of time over which statistics should be slowly varying, etc.

As a coarse rule of thumb, the decorrelation time for the quantity of interest (time beyond which the autocorrelation function is small) is approximately the lowest significant period appearing in that quantity's power spectrum. For nearly white noise, E's spectrum will look flat from DC all the way out to the sampling frequency (reciprocal of integration time). The decorrelation time is the integration time. However, if $|E|^2$ is averaged for a few minutes to yield I, a new spectrum applies. Components of I with periods of minutes do decorrelate in minutes, but have little fluctuation power. At this scale, components of I (or L) with two-hour (or four or eight or thirty-two, depending on dominant noise source) periods dominate--so that decorrelation times occur at the smallest of these periods.

While level-crossing properties (e.g., the distribution of time interval lengths for which the noise remains below a given level) and other multi-

dimensional statistics are not available from a model which specifies only the autocorrelation function and one- or two-dimensional densities, I emphasize the value of such a model for estimating the important scales of variability, for interpreting predicted and measured noise statistics, and for designing experiments.

Predictability of Noise

The final example is a complex and important one. The statement concerns the predictability of ambient noise. In terms of the framework described above, I deal with one component at a time and worry about whether it is possible now or will ever be possible to predict features viewed here as important.

Background Wind Noise. Given wind speeds, which are pretty readily available, wind-generated noise properties should be easy to predict, and experience supports that conclusion. Empirical source levels and directivities, combined with simple propagation models usually suffice to yield good estimates of the features of E and L, both omni and directional. Some problem areas remain. There are measurements in some geographic regions (e.g., shallow water) which challenge explanation. The source mechanism for mid-frequency (50-1000 Hz) wind-noise is not yet known for sure, nor is the directivity of the source modelable in detail (so that the importance of surface-ducted wind noise is not clear). Finally, the treatment of noise caused by storms, especially distant storms, is currently the subject of considerable attention.

Background Ship Noise. Experience has shown that when many ships contribute and the environment in the neighborhood of the receiver is not too complicated, then the long-term average level (e.g., month) of the ship-noise component, as well as fluctuation scales and probability densities for L, can be estimated within a few dB. Otherwise, our prediction capability is poor. This is consistent with our current knowledge about ship source characteristics/locations, the details of TL, and the fluctuation scales of L. As less and less averaging over sources and time is performed, more uncertainty arises.

Propagation complexities tend to confound predictability at all scales. For example, as the receiver approaches the bottom (mode stripping) or the bottom approaches the receiver (topographic stripping, shallow water), the distant ship noise is reduced--but the rate and amount of reduction is very sensitive to the frequency and local bottom. As ship contributions diminish, the fluctuations change, and in the limit transient sources may dominate. Knowledge of the average level may give the only clue about the fluctuations.

I also cannot pass up the opportunity to relate noise depth dependence with vertical directionality: if one is known (on average), then in many cases the other is also. If neither is known, then the importance of ships over slopes and shoaling channel axes is uncertain. Azimuthal directionality is also then not easy to estimate. Because of gaps in knowledge

about both ship and TL properties, these characteristics of the noise field, at every scale, are generally unpredictable today; models rely on measurements in these cases (Wagstaff [1981], Cavanagh and Renner [1979] and [1980]).

Transient Noise. As reflected in the framework, the transient noise components are the most difficult to characterize, and hence to predict. Only at the grossest statistical level can transient ship noise be predicted. The principal deficiency here for all transient sources is typically the absence of knowledge about source location, emission properties, and sensitivity to the local environment.

4. FINAL REMARKS

A rough framework upon which to view statements about ambient noise properties has been proposed, and examples of its use discussed. The approach uses information about noise presented over the years by such investigators as Wenz, Dyer, Daubin, Perrone and King, Jobst, Adams, Bannister, et al. While neither rigorous nor complete nor unique, the view has proved useful to me in its formative stage. I suggest that any person actively engaged in noise R&D, be it model or data related, can benefit from a review and regular refinement of his particular framework for thinking about noise.

REFERENCES

1. Bannister, R.W., et al., "Variability of Low-Frequency Ambient Sea Noise," J. Acoust. Soc. Am. 65, 1156-1163 1979 .

2. Cavanagh, R.C. and Renner, W.W., "A Modified Noise Directionality Model for VLA Applications of ASRAP," Science Applications Inc., Rept. 81-322-WA, McLean, Virginia 1979 .

3. Cavanagh, R.C. and Renner, W.W., "Vertical Directionality and Depth Dependence of Averaged Acoustic Signals and Noise," J. Acoust. Soc. Am. 68, 1467-1474 1980 .

4. Daubin, S.C., "Statistical Analysis of Ship-Generated Noise," International Workshop on Low-Frequency Propagation and Noise," Maury Center Publications, Department of the Navy, Washington, 1977 .

5. Dyer, I., "Statistics of Distant Shipping Noise," J. Acoust. Soc. Am. 53, 564-570 1973 .

6. Jennette, R.L., Sander, E.L., Pitts, L.E., "The USI Noise Model, Version I, Vol. 1, Physics Documentation," USI-APL-R-8, April 1977 .

7. Jobst, W.J. and Adams, S.L., "Statistical Analysis of Ambient Noise," J. Acoust. Soc. Am. 62, 63-71 1977 .

8. O'Connor, J.C., "Statistics of Sea Noise," MIT Thesis 1973 .

9. Perrone, A.J. and King, L.A. "Analysis Technique for Classifying Wind- and Ship-Generated Noise Characteristics," J. Acoust. Soc. Am. 58, 1186-1189 1975 .

10. Wagstaff, R.A., "Low-frequency Ambient Noise in the Deep Sound Channel-The Missing Component," J. Acoust. Soc. Am. 69, 1009-1014 1981 .

11. Wenz, G.M., "Acoustic Ambient Noise in the Ocean," J. Acoust. Soc. Am. 34, 1936-1956 1962 .

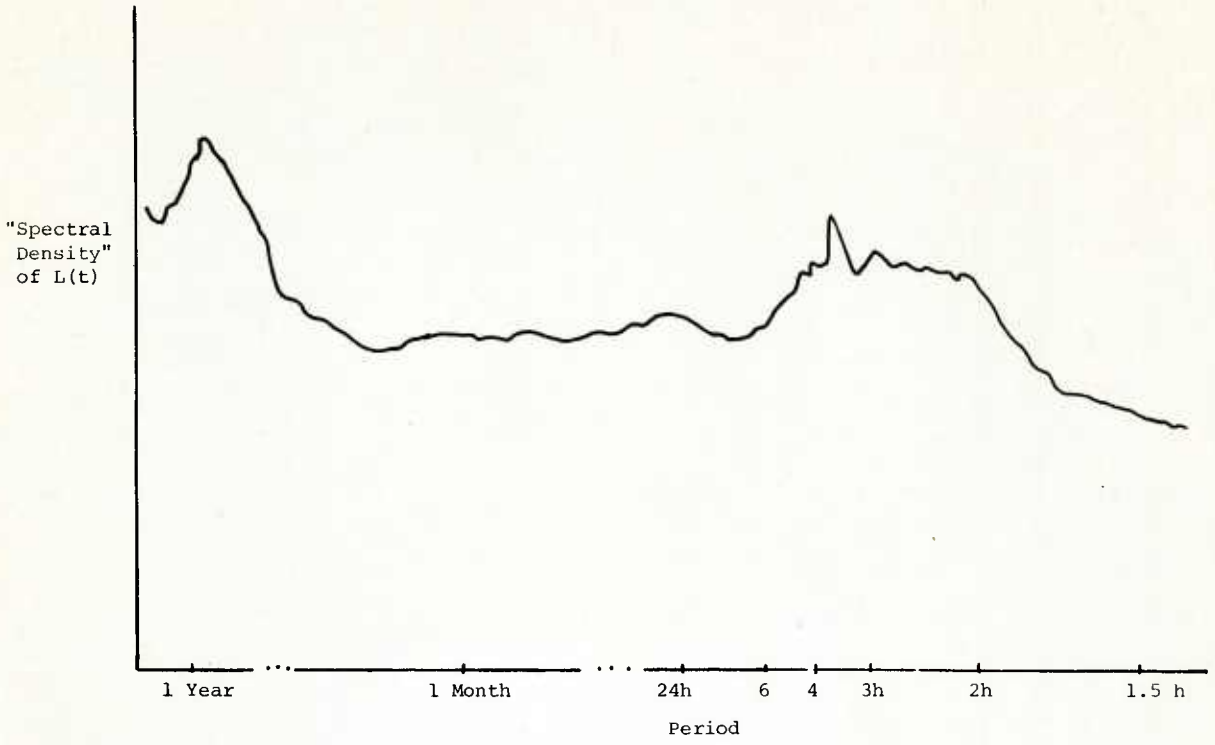

FIG. 1 SPECTRAL COMPONENTS OF SHIP NOISE TIME SERIES

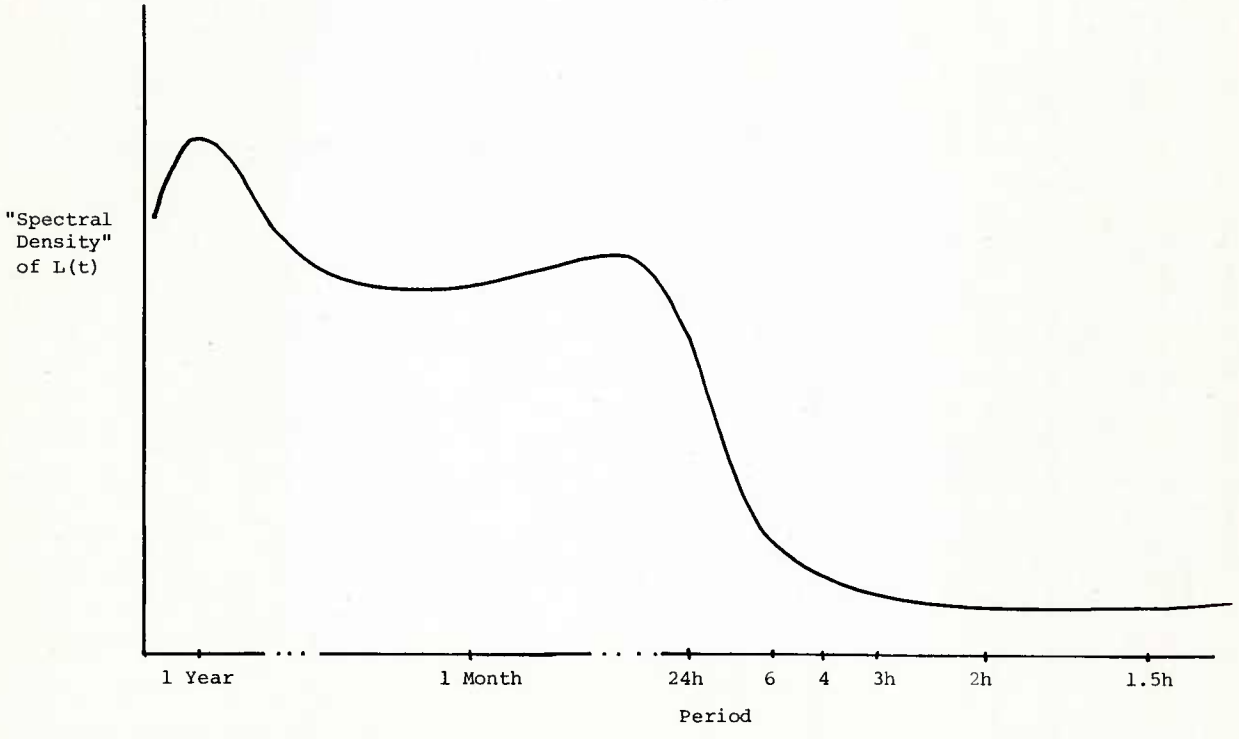

FIG. 2 SPECTRAL COMPONENTS OF WIND NOISE TIME SERIES

INITIAL DISTRIBUTION

	Copies
MINISTRIES OF DEFENCE	
MOD Belgium	2
DND Canada	10
CHOD Denmark	8
MOD France	8
MOD Germany	15
MOD Greece	11
MOD Italy	10
MOD Netherlands	12
CHOD Norway	10
MOD Portugal	5
MOD Turkey	5
MOD U.K.	16
SECDEF U.S.	55
NATO AUTHORITIES	
Defence Planning Committe	3
NAMILCOM	2
SACLANT	10
SACLANTREPEUR	1
CINCWESTLANT/COMOCEANLANT	1
COMIBERLANT	1
CINCEASTLANT	1
COMSUBACLANT	1
COMMAIREASTLANT	1
SACEUR	2
CINCNORTH	1
CINCSOUTH	1
COMNAVSOUTH	1
COMSTRIKFORSOUTH	1
COMEDCENT	1
COMMARAIRMED	1
CINCHAN	1

	Copies
SCNR FOR SACLANTCEN	
SCNR Belgium	1
SCNR Canada	1
SCNR Denmark	1
SCNR Germany	1
SCNR Greece	1
SCNR Italy	1
SCNR Netherlands	1
SCNR Norway	1
SCNR Portugal	1
SCNR Turkey	1
SCNR U.K.	1
SCNR U.S.	2
French Delegate	1
SECGEN Rep. SCNR	1
NAMILCOM Rep. SCNR	1
NATIONAL LIAISON OFFICERS	
NLO Canada	1
NLO Denmark	1
NLO Germany	1
[illegible]	1
[illegible]	1
[illegible]	1
[illegible] TO SACLANT	
NLR Belgium	1
NLR Canada	1
NLR Denmark	1
NLR Germany	1
NLR Greece	1
NLR Italy	1
[illegible]erlands	1
[illegible]	1
[illegible]l	1
[illegible]	1
NLR [illegible]	1
NLR US	1
ATTENDESS	100
Total initial distribution	231
SACLANTCEN Library	10
Stock	19
Total number of copies	360